9. SITE 763[1]

Shipboard Scientific Party[2]

HOLE 763A

Date occupied: 5 August 1988

Date departed: 6 August 1988

Time on hole: 1 day, 4 hr, 25 min

Position: 20°35.20′S, 112°12.50′E

Bottom felt (rig floor; m, drill pipe measurement): 1378.9

Distance between rig floor and sea level (m): 11.4

Water depth (drill pipe measurement from sea level, m): 1367.5

Total depth (rig floor; m): 1573.80

Penetration (m): 194.90

Number of cores (including cores with no recovery): 21

Total length of cored section (m): 194.90

Total core recovered (m): 201.88

Core recovery (%): 104

Oldest sediment cored:
Depth (mbsf): 194.90
Nature: foraminifer nannofossil ooze/chalk to nannofossil ooze/chalk with foraminifers
Age: late Eocene
Measured velocity (km/s): 1.6

HOLE 763B

Date occupied: 6 August 1988

Date departed: 11 August 1988

Time on hole: 5 days, 30 min

Position: 20°35.19′S, 112°12.52′E

Bottom felt (rig floor; m, drill pipe measurement): 1378.9

Distance between rig floor and sea level (m): 11.4

Water depth (drill pipe measurement from sea level, m): 1367.5

Total depth (rig floor, m): 2032.40

Penetration (m): 653.50

Number of cores (including cores with no recovery): 54

Total length of cored section (m): 463.50

Total core recovered (m): 376.36

Core recovery (%): 81

Oldest sediment cored:
Depth (mbsf): 653.50
Nature: silty claystone and sandy clayey siltstone
Earliest age: Lower Cretaceous (Berriasian)
Latest age: Lower Cretaceous (Valanginian)
Measured velocity (km/s): 1.8

HOLE 763C

Date occupied: 11 August 1988

Date departed: 17 August 1988

Time on hole: 5 days, 15 hrs

Position: 20°35.21′S, 112°12.51′E

Bottom felt (rig floor; m, drill pipe measurement): 1378.9

Distance between rig floor and sea level (m): 11.4

Water depth (drill pipe measurement from sea level, m): 1367.5

Total depth (rig floor, m): 2415.50

Penetration (m): 1036.60

Number of cores (including cores with no recovery): 46

Total length of cored section (m): 401.00

Total core recovered (m): 332.83

Core recovery (%): 83

Oldest sediment cored:
Depth (mbsf): 1036.60
Nature: silty claystone
Age: Lower Cretaceous (middle Berriasian)
Measured velocity (km/s): 2.2

Principal results: Site 763 (20°35.19′S, 112°12.52′E, water depth 1367.5 m; proposed Site EP7V) is located about 84 km south of Site 762 on the western part of central Exmouth Plateau. Because this is a known hydrocarbon area, the safety provisions stipulated that the site be located near industry well Vinck-1 (about 2 km southeast). Sites 762 and 763 provide a transect on the Exmouth Plateau, with Site 762 located distally and Site 763 more proximally to the terrigenous source of sediments being shed from the southern and southeastern hinterlands during the Triassic through early Cretaceous. Extensive seismic data in the area show a thinner Cenozoic and a considerably thicker Cretaceous section at Site 763 than that recovered at Site 762. The major objectives of the Exmouth Plateau transect included documenting Cretaceous depositional sequences, dating Tertiary hiatuses, and testing sequence-stratigraphic and eustatic models.

Site 763 was drilled to a total depth (TD) of 1036.6 mbsf with a relatively high recovery rate of 82%. The cored section ranges from lower Berriasian–Tithonian syn-rift stage prodelta mudstones to eupelagic Quaternary oozes. The upper 141.7 m consist of gray to white Quaternary to lower Miocene foraminifer nannofossil oozes, which are unconformably underlain by 105.4 m of white nannofossil chalk of early Miocene to middle Eocene age. A 30-m.y. hiatus separates the underlying 138.7-m-thick upper Campanian to Turonian green bioturbated chalk with microcycles and *Inoceramus* fragments (Toolonga Calcilutite equivalent). This is followed by 184.3 m of upper Cenomanian to mid-Aptian green-gray calcareous zeolitic claystones rich in glauconite, belemnites, and pyrite (Gearle Siltstone equivalent). A lower Aptian black silty claystone (Muderong Shale equivalent) underlies this unit. Below the pre-Barremian breakup unconformity we cored 414.1 m of silty claystones of shelf margin prodelta origin (Barrow Group equivalent). The upper part of the Barrow Group equivalent consists of 21 m of Valanginian glauconite- and belemnite-rich silty claystones to sandy siltstones, underlain by 27.1 m of poorly recovered sandstones. The lowermost unit down to TD (1036.6 mbsf) con-

[1] Haq, B. U., von Rad, U., et al., 1990. *Proc. ODP, Init. Repts.*, 122: College Station, TX (Ocean Drilling Program).

[2] Shipboard Scientific Party is as given in the list of Participants preceding the contents.

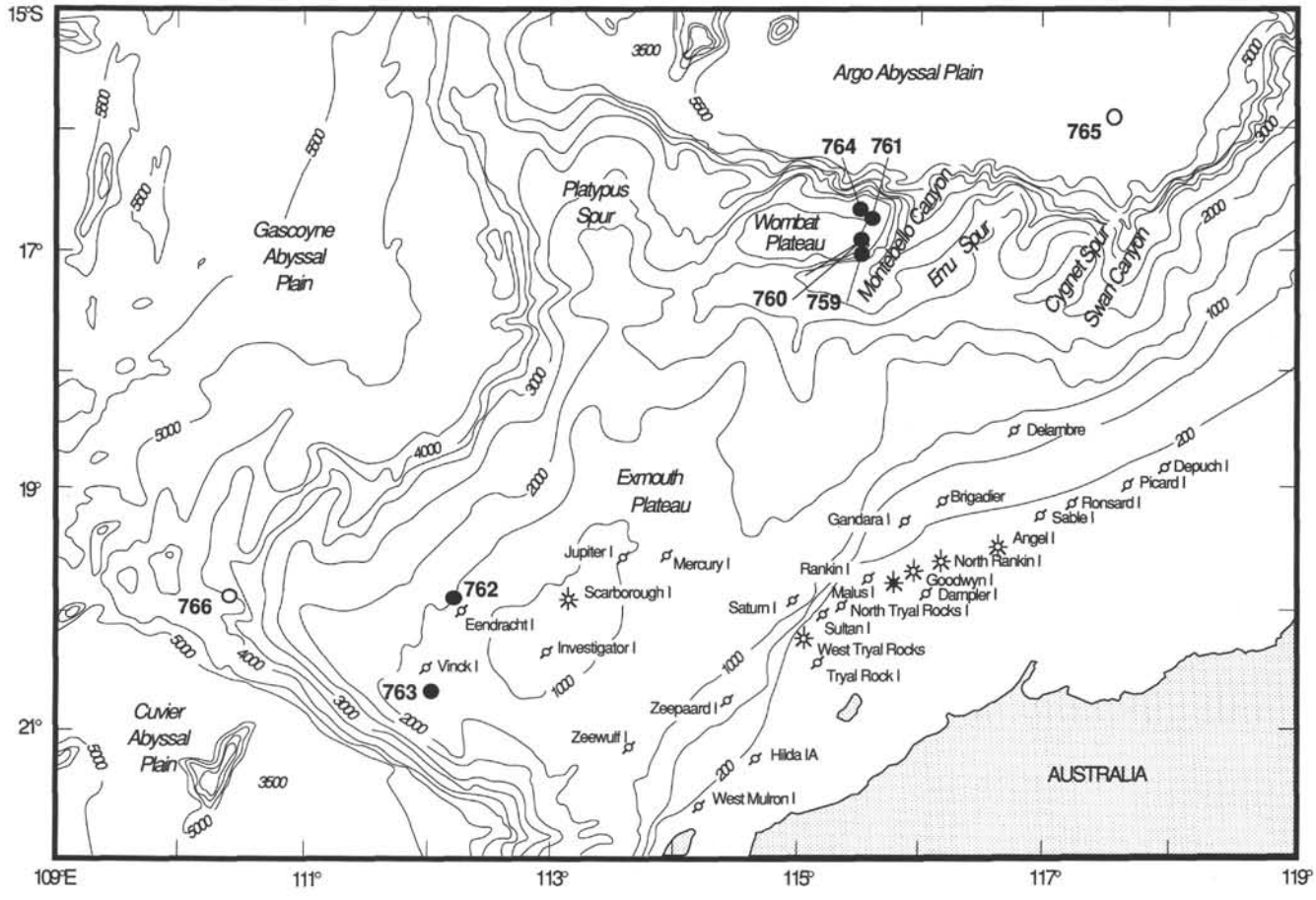

Figure 1. Bathymetric map of Exmouth Plateau region showing location of ODP sites (closed circles = Leg 122 sites, open circles = Leg 123 sites) and commercial wells. Bathymetry is in meters (Exon, unpubl. data).

sists of structureless black to dark gray silty claystones to sandy siltstones with pyrite nodules and siderite concretions.

Highlights of this site include:

1. Recovery of a fairly complete Quaternary to middle Eocene eupelagic carbonate section with excellent nannofossil and foraminiferal content and preservation;
2. Discovery of an unexpected major late Campanian to middle Eocene hiatus that removed the equivalent of 350 m of the record recovered at nearby Site 762 and indicates major remobilization of sediments by erosive bottom currents (caused by tectonic events?) during that time interval;
3. Color cycles in the Campanian to Turonian chalks, recognized on the basis of varying carbonate/clay ratios, possibly caused by Milankovitch-type cycles of about 20,000–60,000 years duration;
4. A well-represented Cenomanian/Turonian boundary blackshale event;
5. A possibly complete, 180-m-thick mid-Aptian to upper Cenomanian hemipelagic "juvenile ocean" facies of bioturbated, zeolitic calcareous claystones with minor limestone;
6. A slowly deposited early Aptian transgressive facies of neritic, glauconite-rich silty claystones with thin-shelled ammonites, overlying the pre-Barremian breakup unconformity;
7. A low sedimentation rate (condensed?) for Valanginian glauconitic claystones rich in belemnites and ammonites, which were most likely deposited during a sea-level rise;
8. A >370-m-thick Berriasian sequence of prograding prodelta claystones, rapidly deposited during the latest rifting stages prior to the Neocomian onset of sea-floor spreading in the adjacent Gascoyne and Cuvier Abyssal Plains;
9. Lithostratigraphy, magnetostratigraphy, and biochronostratigraphy (including dinoflagellates) extending down into the early Berriasian, which along with seismic stratigraphy form an important database for ground-truthing sequence stratigraphic models; and
10. Significant downhole changes in the source and maturation of organic matter (including the nature and abundance of hydrocarbon gases) that correlate with the age and lithology of the various stratigraphic units.

Due to severe bridging problems, especially in the rapidly swelling lower Cretaceous claystones, we could only log the intervals between 690 and 200 mbsf.

BACKGROUND AND OBJECTIVES

Site 763 (proposed Site EP7V) is located on the western part of central Exmouth Plateau (Fig. 1), about 84 km south of Site 762, at a water depth of about 1370 m. Along with Site 762, Site 763 was designed to provide a transect on the Exmouth Plateau, with Site 762 being more distal and Site 763 more proximal to the terrigenous source of sediments shed from the southern hinterlands during the Triassic through early Cretaceous. The background and objectives of this site were therefore very similar to Site 762 (see "Background and Objectives," Site 762 chapter, this volume). The major objectives of Site 763 included documenting the Berriasian to Quaternary depositional sequences and testing sequence-stratigraphic and eustatic models.

Site 763 was planned to be drilled about 2 km southeast of the Vinck-1 industry well to a total depth of 1150 mbsf.

Vinck-1 well-site data and the extensive seismic data in the area indicate a thinner (about 240 m) Cenozoic section than that cored at Site 762. This is underlain by an undifferentiated upper Cretaceous chalk unit to 330 mbsf, followed by the Toolonga Calcilutite equivalent to a depth of 390 mbsf, considered to be Turonian through Campanian in age. The Albian to Cenomanian Gearle Siltstone equivalent unit is much more expanded at Site 763 than at Site 762 and extends to 565 mbsf, as is the underlying Muderong Shale unit, greater than 50 m thick at this site (compared to only 10 m at Site 762). The Hauterivian to Aptian Muderong Shale equivalent strata are unconformably underlain by the thick prodelta sediments of the Valanginian to Berriasian Barrow Group, largely siltstones and claystones that extend from about 610 to 1295 mbsf and are underlain by late Jurassic claystones equivalent to the Dingo Claystone on land. For safety reasons, the maximum depth of penetration was limited to about 145 m above the Dingo Claystone (1150 mbsf), as this unit may be an important seal and barrier to hydrocarbons potentially reservoired in the underlying Triassic sands of the Mungaroo Formation.

OPERATIONS

Hole 763A

Site 763 is located 42 nmi south of Site 762 (Fig. 1). The voyage was made in 6.5 hr, which included a brief site survey. Beacon SN 329 (16 kHz) was dropped at 1505 hr (local time, or LT) 5 August 1899, near 20°35.17′S, 112°12.49′E. An 11-7/16-in. Security S86 bit was selected to begin advanced-piston-corer/extended-core-barrel (APC/XCB) operations. In preparation for a full-size reentry cone, a jet-in test was made. The sea bottom was very soft, and the interpretation of the test results was that 4 joints or about 160 ft (48.8 m) of casing could be jetted-in without difficulty.

The first APC core established the seafloor to be at 1367.5 m. Twenty piston cores were routinely taken to 185.4 mbsf (Table 1), with heat flow measurements and pore-water samples after Cores 122-763A-6H, -10H, and -16H. The maximum core-barrel pullout was 20,000 lbs. Core 122-763A-21H could not be extracted with 140,000 lbs overpull. Washing the bit over the barrel failed. Tension was taken on the core line, and the bit was rotated 7 m over the barrel. The barrel was rescued without damage.

Nearly all of the APC cores were longer than the 9.5-m stroke of the coring assembly (Fig. 2). This is attributed to gas expansion, although gas contents measured by vacutainer and headspace analysis did not begin to increase until below 160 mbsf. Core recovery for Hole 763A was 201.88 m or 103.6%. The hole was abandoned at 1930 hr (LT) on 6 August (Fig. 3).

Hole 763B

The ship was moved 50 m north as a full-size, 16-ft-diameter (4.9 m), reentry cone was to be deployed because of the importance of deep penetration at this hole. The 16-ft-diameter cone was moved into the moonpool area and set on the moonpool doors. Four joints (48.8 m) of 16-in. (41 cm) casing were lowered into the cone. It was necessary to remove the box from the top joint of casing before screwing the box end of the casing hanger onto the casing. We were surprised to discover that the boxes on this particular 16-in. casing were not threaded but welded to the body of the pipe. Therefore, we had to construct a 16-in. cross-over sub by welding a slip-on box from a drive-pipe shoe to a piece of casing that had a pin on the other end. The slip-on box of the cross-over sub was welded to the body of the 16-in. casing and the hanger was screwed onto the pin end. The fabrication took about 3 hr.

Table 1. Coring summary for Site 763.

Core No.	Date (Aug. 1988)	Time (local)	Depth (mbsf)	Cored (m)	Recovered (m)	Recovery (%)
122-763A-						
1H	5	2345	0.0–4.9	4.9	4.90	100.0
2H	6	0010	4.9–14.4	9.5	10.06	105.9
3H	6	0400	14.4–23.9	9.5	9.44	99.3
4H	5	0105	23.9–33.4	9.5	9.27	97.6
5H	6	0130	33.4–42.9	9.5	9.83	103.0
6H	6	0200	42.9–52.4	9.5	9.74	102.0
7H	6	0400	52.4–61.9	9.5	10.07	106.0
8H	6	0430	61.9–71.4	9.5	9.99	105.0
9H	6	0450	71.4–80.9	9.5	9.76	103.0
10H	6	0515	80.9–90.4	9.5	9.76	103.0
11H	6	0700	90.4–99.9	9.5	9.68	102.0
12H	6	0745	99.9–109.4	9.5	9.82	103.0
13H	6	0810	109.4–118.9	9.5	10.03	105.6
14H	6	0840	118.9–128.4	9.5	10.08	106.1
15H	6	0910	128.4–137.9	9.5	10.07	106.0
16H	6	1000	137.9–147.4	9.5	9.67	102.0
17H	6	1150	147.4–156.9	9.5	9.42	99.1
18H	6	1230	156.9–166.4	9.5	9.84	103.0
19H	6	1330	166.4–175.9	9.5	10.59	111.5
20H	6	1400	175.9–185.4	9.5	9.86	104.0
21H	6	1545	185.4–194.9	9.5	10.00	105.2
Coring totals				194.9	201.88	103.6
122-763B-						
1C	8	0035	0.0–190.0	(Wash and drill—190.0 m)		
2X	8	0110	190.0–199.5	9.5	7.65	80.5
3X	8	0140	199.5–209.0	9.5	8.17	86.0
4X	8	0205	209.0–218.5	9.5	4.00	42.1
5X	8	0235	218.5–228.0	9.5	5.82	61.3
6X	8	0300	228.0–237.5	9.5	8.99	94.6
7X	8	0300	237.5–247.0	9.5	2.73	28.7
8X	8	0410	247.0–256.5	9.5	5.80	61.1
9X	8	0450	256.5–266.0	9.5	9.87	103.9
10X	8	0530	266.0–275.5	9.5	9.86	103.8
11X	8	0610	275.5–285.0	9.5	7.76	81.7
12X	8	0645	285.0–294.5	9.5	6.37	67.1
13X	8	0715	294.5–304.0	9.5	9.44	99.4
14X	8	0745	304.0–313.5	9.5	7.90	83.2
15X	8	0810	313.5–323.0	9.5	9.75	102.6
16X	8	0840	323.0–332.5	9.5	8.68	91.4
17X	8	0910	332.5–342.0	9.5	7.59	79.9
18X	8	1000	342.0–351.5	9.5	6.49	68.3
19X	8	1105	351.5–361.0	9.5	9.79	103.1
20X	8	1250	361.0–370.5	9.5	2.18	33.5
21X	8	1430	370.5–380.0	9.5	2.83	29.8
22X	8	1605	380.0–389.5	9.5	2.19	23.1
23X	8	1823	389.5–399.0	9.5	7.56	79.6
24X	8	1950	399.0–408.5	9.5	9.98	105.0
25X	8	2115	408.5–418.0	9.5	9.65	101.6
26X	8	2235	418.0–427.5	9.5	6.81	71.7
27X	9	0025	427.5–437.0	9.5	9.98	105.1
28X	9	0140	437.0–446.5	9.5	10.08	106.1
29X	9	0235	446.5–456.0	9.5	9.92	104.4
30X	9	0400	456.0–465.5	9.5	9.93	104.5
31X	9	0510	465.5–475.0	9.5	9.89	104.1
32X	9	0630	475.0–484.5	9.5	9.87	103.9
33X	9	0740	484.5–494.0	9.5	9.82	103.4
34X	9	0840	494.0–503.5	9.5	9.90	104.2
35X	9	0940	503.5–513.0	9.5	9.69	102.0
36X	9	1045	513.0–522.5	9.5	9.85	103.7
37X	9	1230	522.5–532.0	9.5	8.42	88.6
38X	9	1430	532.0–541.5	9.5	1.57	16.5
39X	9	1615	541.5–551.0	9.5	2.23	23.5
40X	9	1920	551.0–560.5	9.5	3.22	33.9
41X	9	2101	560.5–570.0	9.5	3.13	32.9
42X	9	2235	570.0–579.5	9.5	10.46	110.1
43X	10	0050	579.5–589.0	9.5	4.95	52.1
44X	10	0230	589.0–598.5	9.5	9.88	104.0
45X	10	2035	598.5–608.0	9.5	5.63	59.3
46X	10	2215	608.0–617.5	9.5	10.71	112.7
47X	10	2320	617.5–622.5	5.0	4.78	95.6
48X	11	0025	622.5–627.5	5.0	7.27	145.4
49X	11	0155	627.5–632.5	5.0	6.65	133.0
50X	11	0250	632.5–637.5	5.0	8.15	163.0
51X	11	0350	637.5–642.5	5.0	8.07	161.4
52X	11	0440	642.5–647.5	5.0	0.01	0.2
53X	11	0545	647.5–648.5	1.0	1.89	189.0
54X	11	0700	648.5–653.5	5.0	1.54	30.8
Coring totals Wash and drill = 190.0 m				463.5	376.35	81.2
122-763C-						
1C	12	0815	0.0–385.0	(Wash and drill—385.0 m)		
2R	12	0910	385.0–394.5	9.5	6.81	71.7
3C	12	2025	394.5–645.1	(Wash and drill—250.6 m)		
4R	12	2200	645.1–654.6	9.5	0.61	6.4
5R	12	2240	654.6–660.6	6.0	0.59	9.8
6R	13	0000	660.6–665.6	5.0	3.82	77.8
7R	13	0055	665.6–670.6	5.0	3.00	60.0
8R	13	0145	670.6–675.6	5.0	4.30	86.0

Table 1 (continued).

Core No.	Date (Aug. 1988)	Time (local)	Depth (mbsf)	Cored (m)	Recovered (m)	Recovery (%)
9R	13	0300	675.6–685.1	9.5	8.44	88.8
10R	13	0410	685.1–694.6	9.5	9.67	101.8
11R	13	0500	696.4–704.1	9.5	1.74	18.3
12R	13	0655	704.1–713.6	9.5	3.00	31.5
13R	13	0810	713.6–723.1	9.5	8.56	90.1
14R	13	0915	723.1–732.6	9.5	7.71	81.1
15R	13	1045	732.6–742.1	9.5	5.42	57.1
16R	13	1215	742.1–751.6	9.5	9.40	98.9
17R	13	1400	751.6–761.1	9.5	9.62	101.3
18R	13	1515	761.1–770.6	9.5	9.25	97.4
19R	13	1915	770.6–780.1	9.5	7.78	81.9
20R	13	2105	780.1–789.6	9.5	7.24	76.2
21R	13	2235	789.6–799.1	9.5	8.91	93.8
22R	14	0200	799.1–808.6	9.5	9.82	103.4
23R	14	0155	808.6–818.1	9.5	6.92	72.8
24R	14	0310	818.1–827.6	9.5	9.74	102.5
25R	14	0435	827.6–837.1	9.5	9.69	102.0
26R	14	0605	837.1–846.6	9.5	8.82	92.8
27R	14	0730	846.6–856.1	9.5	9.50	100.0
28R	14	0910	856.1–865.6	9.5	8.84	93.1
29R	14	1020	865.6–875.1	9.5	8.14	85.7
30R	14	1200	875.1–884.6	9.5	8.78	92.4
31R	14	1405	884.6–894.1	9.5	9.87	103.9
32R	14	1616	894.1–903.6	9.5	9.51	100.1
33R	14	1800	903.6–913.1	9.5	7.51	79.1
34R	14	2005	913.1–922.6	9.5	8.77	92.3
35R	14	2210	922.6–932.1	9.5	8.96	94.3
36R	15	0025	932.1–941.6	9.5	8.68	91.4
37R	15	0145	941.6–951.1	9.5	9.50	100.0
38R	15	0330	951.1–960.6	9.5	9.83	103.5
39R	15	0550	960.6–970.1	9.5	8.14	85.7
40R	15	0715	970.1–979.6	9.5	2.81	29.6
41R	15	0900	979.6–989.1	9.5	9.09	95.7
42R	15	1120	989.1–998.6	9.5	7.35	77.4
43R	15	1320	998.6–1008.1	9.5	9.44	99.4
44R	15	1555	1008.1–1017.6	9.5	9.92	104.4
45R	15	1815	1017.6–1027.1	9.5	9.82	103.4
46R	15	2010	1027.1–1036.6	9.5	7.51	79.1
Coring totals				401.0	332.83	83.0
Wash and drill = 635.6 m)						

The casing was jetted-in with only minor difficulty from 0.0–50.5 mbsf. The weight required was 0–10,000 lbs with 20–110 strokes/min (spm). Total jetting-in time, including 3 drill-pipe connections, was 1.75 hr. The total deployment time for the cone was 29 hr, including two round trips (Fig. 3).

We forecasted that the formation would be similar to that cored at Site 762. The operational plan was to use the XCB as far as possible in order to take advantage of its better recovery, then make a round trip with the drill pipe to pick up an RCB coring assembly and core to total depth. An 11-7/16-in. (29.28 cm) Security S86 bit was selected for the XCB. The bottom hole assembly (BHA) was the same one that had been used on previous Leg 122 XCB holes. The bit was drilled with a center bit to 190.0 mbsf (close to the total depth of Hole 763A), at which point we commenced coring.

The amount of headspace gas started to increase and by 350 mbsf was in the range of 10,000 ppm (see "Organic Geochemistry," this chapter). As coring progressed, the visual evidence of gas in the cores increased. Separations in the cores were observed through the transparent liners, which would often collapse when punctured to relieve the pressure, spurting out soft material. In some cases the core material expanded beyond the ends of the core liner, necessitating that we puncture the end caps to prevent them from being forced off.

The large increase in gas content observed at Site 763 would have been sufficient cause to end operations at most ODP holes. However, the electric logs from the offset industry well Vinck-1 indicated that there were no hydrocarbon-bearing, porous reservoirs in this depth range. Furthermore, the shipboard gas chemists had calculated that the amount of gas present in the cores was about one-half the amount needed to saturate the water in the formations, so coring continued.

Subsequently, we noticed a strong hydrogen sulfide (H_2S) gas odor in Core 122-763B-9X (256.5–266.0 mbsf). The highest H_2S concentration measured in the headspace gas analysis was 22 ppm, within the safe working levels, and most of the H_2S gas concentrations were too low to be detected analytically. Personnel on the rig floor were cautioned to position themselves upwind from the core barrel when it was opened, and the door and windows of the lab were opened to provide a free flow of air. The H_2S odor ceased around Core 122-763B-18X, at approximately 315 mbsf. Coring conditions and results were excellent, as the rate of penetration was typically 30 min per core and recovery was usually in excess of 100% (Fig. 4).

At 598.5 mbsf the coring operation was interrupted to run a correlation electric log. This log was planned because of JOIDES Pollution Prevention and Safety Panel concerns. Logs from the offset Vinck-1 well indicated that it contained no porous reservoir sand above 600 mbsf, but below 600 mbsf there were water-filled sands. We were instructed to terminate our hole if it was more than 10 m structurally higher than the Vinck-1 well. The hole was conditioned with a wiper trip, pumping 6,000 strokes of seawater, and 70 barrels of mud. After a tool malfunction, the DIT-E/SDT/NGT/MCD tool string was run from 557.9–365.4 mbsf. The logs were correlated and we concluded that Hole 763B was 12 m structurally lower than Vinck-1.

Cores 122-763B-38X through -41X (532.5–570.0 mbsf) were unusual in that recovery was only about 1/3 that of cores just above and below, but rotating time was 2–3 times longer than that of adjacent cores. The correlation log indicates that this interval of poor recovery may contain fractured limestone.

From Core 122-763B-48X through -55X (622.5–653.5) mbsf, 5-m cores were taken at the request of the co-chief scientists in an attempt to enhance recovery in one of the most scientifically critical parts of the section. Recovery in the 5-m intervals averaged 96%; note however, that the recovery for individual cores ranged from 0.01 to 8.15 m as a result of gas expansion and ship heave. The cores were highly biscuited and disturbed, with as much as 50% of the core consisting of drilling slurry.

A hard drilling streak was encountered in Core 122-763B-55X (653.5–656.5 mbsf). Upon retrieval of the core barrel, we found that the Spring Stop Quick Release had parted and the bottom portion of the barrel had been left in the hole. A wireline run confirmed that the missing barrel was not inside the BHA, and drill-pipe measurement indicated that the fish was at the bottom of the hole in two pieces or bent and crushed. Experience suggested that we were faced with a hopeless fishing job.

After discussion among the co-chiefs and the operations superintendent, the decision was reached that the best use of the remaining time in the leg would be to plug and abandon the hole, and then rotary core an offset hole as deep as possible.

The drill pipe was positioned at the bottom of the hole, and 200 barrels (bbl) of 10.2 pounds per gallon (ppg) mud was circulated into the hole. This volume of mud was sufficient to cover the gassy formations. The drill pipe was then raised to 220 mbsf (near the top of the high gas readings) and a 200-sack cement plug was placed. The drill pipe and BHA were recovered, and Hole 763B was abandoned at 2100 hr (LT), 11 August 1988.

Hole 763C

The ship was moved 30 m south to avoid the 16-ft-diameter (4.9 m) reentry cone, which had now become redundant to our operation. There was not sufficient time remaining in the leg to enjoy the luxury of a bit trip and reentry if we were to reach total depth. An RBI C3 bit was selected. The BHA consisted

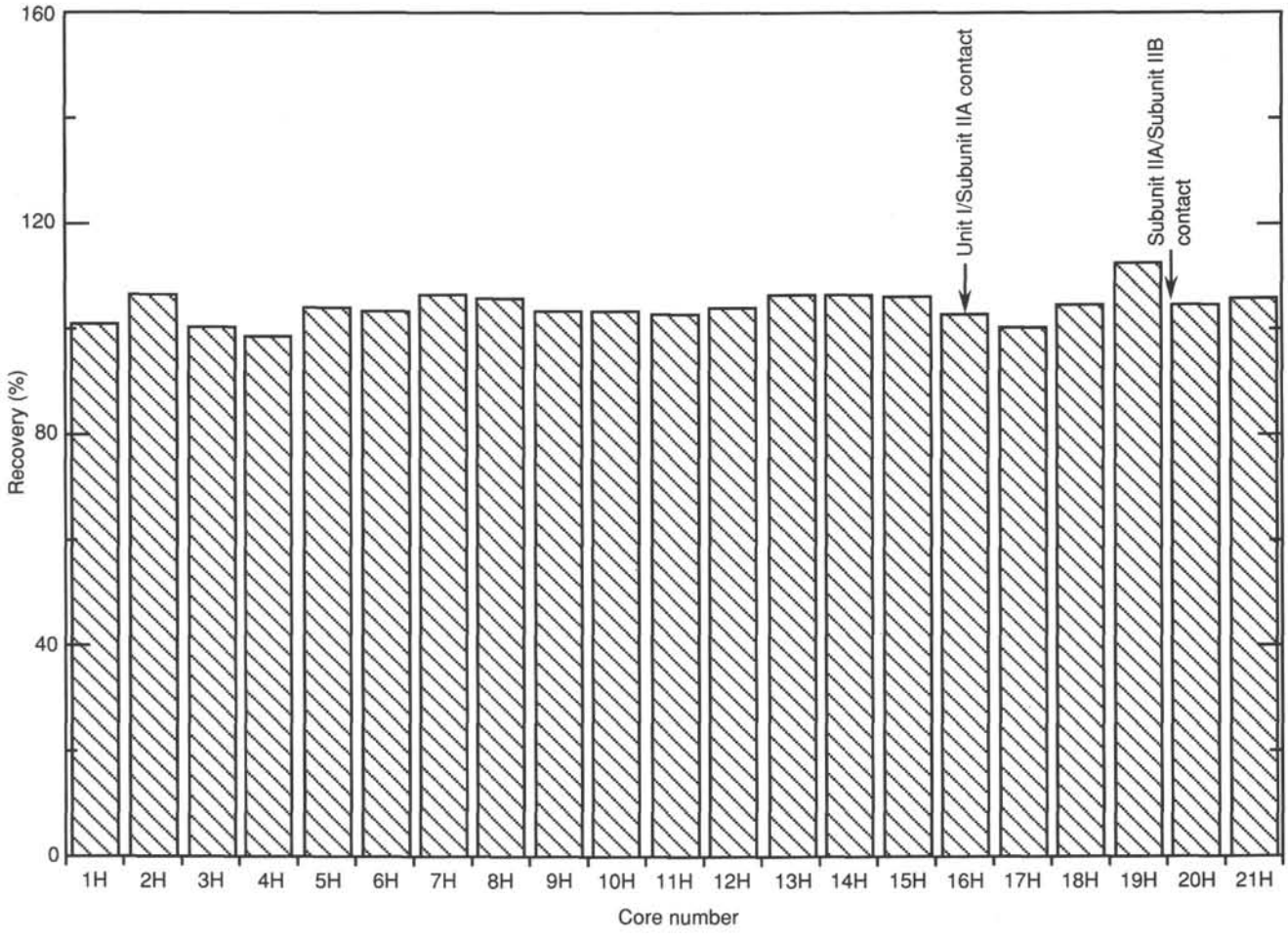

Figure 2. Percent core recovery in Hole 763A, cored with the APC.

of the 9-7/8-in. (25.28 cm) bit, mechanical bit release, head sub, control length drill collar, long top sub, head sub, seven 8-1/4-in. (21.12 cm) drill collars, one cross-over sub (XO), one 7-1/4-in. (18.56 cm) drill collar, and two stands of 5-1/2-in. (14.08 cm) drill pipe.

The core barrel was run with a Smith center bit. After burying the BHA the pump rate was increased to 100 spm and the rotary to 70 rpm, and drilling started. A depth of 385.0 mbsf was reached in 5.17 hr rotating time. After a single core was taken in a critical scientific interval from 385.0 through 394.5 mbsf, drilling continued. The previous depth of Hole 763B (TD = 645 mbsf) was reached in a total rotating time of 11.84 hr (19.5 hr total operational time).

Below 625 mbsf the amount of methane declined as Unit VI (the Barrow Group equivalent) was entered. Core recovery was generally good. A precautionary 10-stand wiper trip was made at 770 mbsf. There was no unusual drag except at 710 mbsf, and 3 m of fill was found at the bottom of the hole. The hole was circulated clean with 2–20-bbl mud sweeps and 234 bbl of seawater. Coring continued for 2 days with nearly 100% recovery. There was no excessive torque, connection fill, or drag, although at times the pump pressure would be as high as several hundred psi. The material in this interval was a silty claystone and sandy silty claystone.

As the hole approached 1000 mbsf, a notation on the Vinck-1 mud log was discovered by a member of the scientific party. A sand at 1157 mbsf (below the approved total depth for Hole 763B) had "kicked" 9.2 ppg mud (i.e., had forced heavy mud back up the drill string). The evidence was that at this hole a total of 127 bbl of salt water with no hydrocarbons had flowed at a rate of 2–3 bbl/min. As the sea water with which we were drilling had a density of only 8.6 ppg, we decided to terminate drilling at 1100 mbsf, which would be at least 60 m above the "water sand." From 700 mbsf to 1000 mbsf the headspace methane had shown a gradual increase to 10,000 ppm. While cutting Core 122-763C-46R the headspace gas in Core 122-763C-45R was being routinely analyzed the methane soared to over 85,000 ppm. Core 122-763C-46R was recovered and its gas was only slightly less than 60,000 ppm, which confirmed that the dramatic gas increase was not an anomaly. After consultation with the co-chief scientists, we decided to end the hole at 1036.6 mbsf because of the high gas content and proximity of the "water sand."

Logging

Prior to running electric logs, a 40-bbl mud sweep was circulated to the seafloor, and a short trip was made to 691 mbsf. Pipe drag was 60,000 lbs pulling out of the hole and 20,000 lbs going down. At least 9 hard bridges were encountered and it was necessary to pick up the top drive and drill them out. A 40-bbl mud sweep was pumped and a second short trip made. Pipe drag was 40,000 lbs and occasionally 80,000 lbs. Four bridges were encountered going down, but the pipe was pushed through them. The bit was released into the bottom of the hole. KCL/Drispac mud was then circulated into the hole, and the bit was pulled up to 225 mbsf. Even

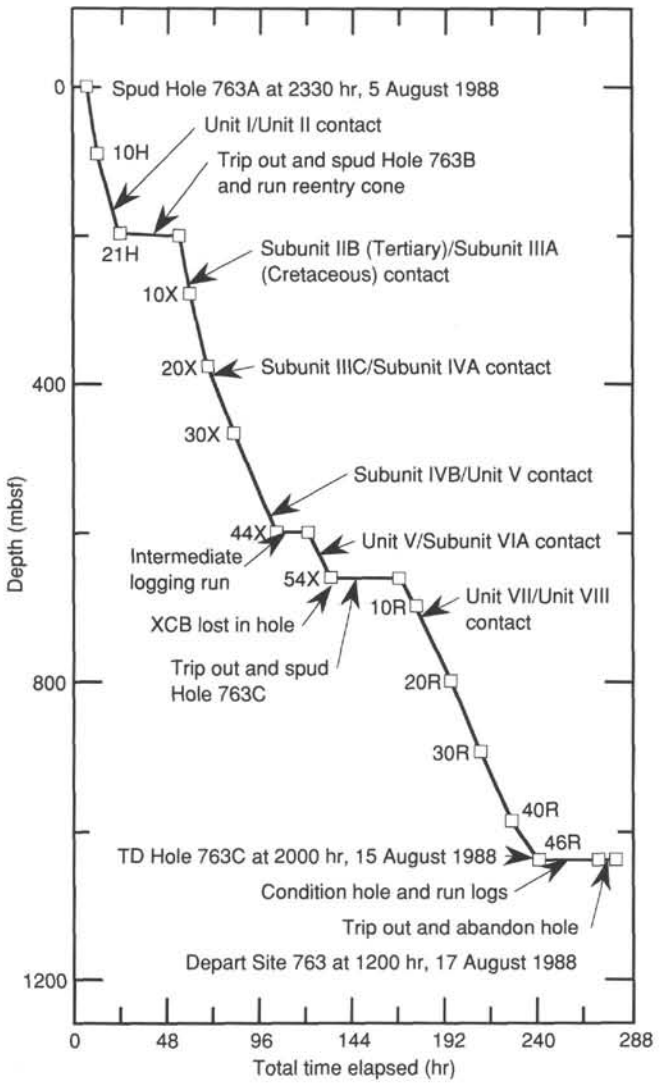

Figure 3. Total time (in hr) elapsed while drilling Site 763. Core numbers are indicated.

without a bit on the end of the BHA the drag was 40,000 lbs down to 759 mbsf, at which depth the drag suddenly disappeared. At 673 mbsf the drill pipe began to flow water; the safety valve was promptly installed, and 150 psi pressure was in the pipe. Heavy mud was pumped into the pipe to control the pressure, and the pipe was pulled to 225 mbsf.

The Schlumberger logging tools were picked up, and the sidewall-entry sub (SES) was installed. The drill pipe was lowered to 710 mbsf, where it struck the bridge that had been encountered every pipe trip. Schlumberger set the logging tool onto the same obstacle, and 3,000 lbs overpull was required to extract the tool. The seismic stratigraphy tool array (LSS/SDT/NGT/MCD) was run between 687 and 200 mbsf.

The prospect of permanently removing the bridge at 710 mbsf and then lowering the logging tools through the sand were meager. Furthermore, the probability of both the drill pipe and logging tools becoming stuck in the silty claystones of Unit VI was substantial. We decided to relinquish further logging efforts, and use the time saved to log at the next site.

The large amount of gas in the hole necessitated that we thoroughly plug it. The drill pipe was run to the bridge at 710 mbsf and 110 bbl of 12.5-ppg mud was circulated into the hole to cover the gassy formation. The drill pipe was pulled to the top of the gassy chalk at 356 mbsf, where 200 sacks of cement were placed on top of the mud.

JOIDES Resolution was underway to Site 764 at 1200 hr (LT), 17 August 1988.

LITHOSTRATIGRAPHY

A 1036-m-thick succession of Quaternary through Berriasian sediments was recovered at Site 763. Hole 763A comprises Quaternary through upper Eocene ooze and semi-indurated chalk, both with clay; Hole 763B recovered upper Eocene to Valanginian chalks with clay and calcareous claystones to claystones; Hole 763C recovered a 1-m-thick black-shale interval close to the Cenomanian/Turonian contact, and Berriasian silty claystones.

The sedimentary succession was subdivided into seven units (Figs. 5 and 6) using visual-description criteria and smear-slide data. Visual criteria include color, induration, sedimentary structures, and percent calcium carbonate (calculated from inorganic carbon measurements; see "Organic Geochemistry," this chapter). Most of the unit boundaries correlate with marked changes in physical properties or with unconformities documented by biostratigraphy. In contrast, subunit boundaries do not necessarily coincide with abrupt changes in physical properties or with unconformities.

The lithologic succession of Site 763 has been tentatively correlated with Site 762 (Fig. 7) on the basis of biostratigraphic zones. Correlation reveals marked differences between the two holes in the Berriasian (the Barrow Group facies are thicker and more proximal than at Site 762), the Albian-Cenomanian (the Gearle Siltstone equivalent is much thicker at Site 763), and in the upper Cretaceous to Paleogene sections (350 m of upper Campanian to early Eocene pelagic sediments in Site 762 that are absent in Site 763). These differences reflect dissimilarity in proximity to the source terrane and perhaps tectonic activity, submarine erosion, and/or basin floor topography.

Unit I (0–141.7 mbsf)

Interval 122-763A-1H-1, 0 cm, through -16H-3, 81 cm; late Miocene to Quaternary in age.

Unit I consists of nannofossil ooze with foraminifers and foraminifer-nannofossil ooze. Because the percentage of foraminifers in smear-slide analysis is most commonly around 20%–35%, and because of the uncertainties in estimating this percentage, the change from nannofossil ooze with foraminifers to foraminifer-nannofossil ooze cannot be used to define subunits. However, in the lower third of Unit I there are commonly <20% foraminifers. Such a change can perhaps be correlated with the relatively low foraminifer content observed in Subunit IB of Site 762. Nannofossils are very abundant throughout Unit I (55%–80%). Sponge spicules are rare (trace to 2%), and rare juvenile brachiopod shells were encountered just below the seafloor (e.g., Section 122-763A-1H-1).

Nonbiogenic constituents are predominantly clay minerals which increase upward from about 5%–10% in the lower third of Unit I to 15% (and exceptionally 20%) above. A few small quartz grains are present in minor amounts (trace to 3%), and do not show any significant variation. Trace amounts of volcanic glass are present. Glauconite is also present in trace amounts in Cores 122A-763A-8H to -10H. Black specks of hydrotroilite are observed intermittently throughout this unit.

Sedimentary structures mainly consist of extensive mottling, except in the lowest cores (i.e., Cores 122-763A-14H to -16H), which are less mottled. Some isolated, spherical, cm-wide burrows are commonly found, marked by a slight

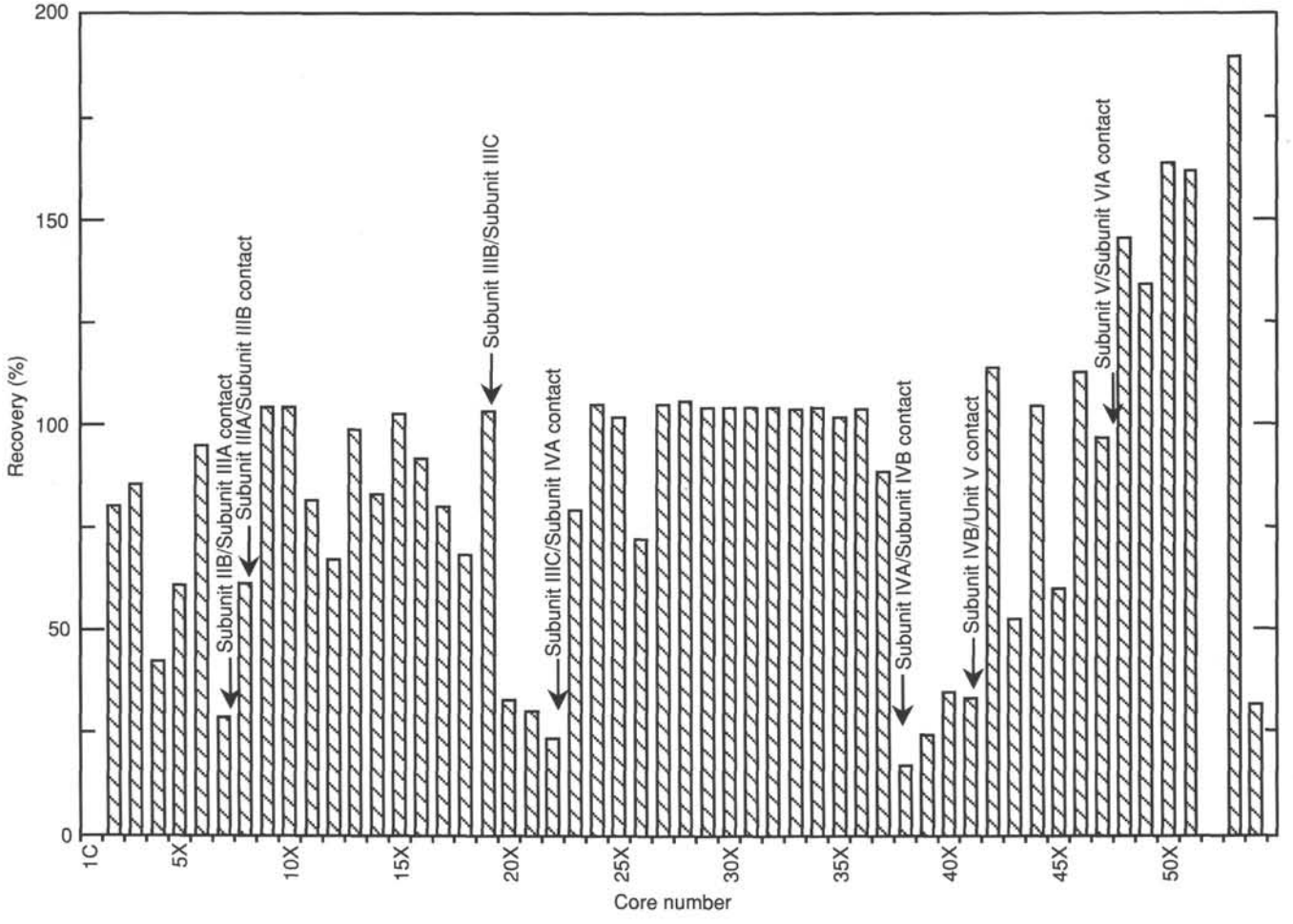

Figure 4. Percent core recovery for Hole 763B, cored with the XCB. Recovery was calculated as the length of sediment in the core barrel, which in the lower siliciclastic sediments may include up to 50% drilling slurry.

color change or halo (pyrite enrichment due to organic matter?). Laminations are generally absent, but some slightly darker, cm-thick layers are common, either gray or rarely green. They may result from a slight enrichment in clay, and do not seem to occur in cycles.

The color is light throughout, ranging downward from light gray (5Y 7/1 in Cores 122-763A-1H to -5H), to light or very light green-gray (10Y 7/1 in Cores 122-763A-6H to -8H, and 10Y 8/1 in Cores 122-763A-9H to -11H), then to white (lighter than 5Y 8/1 in Cores 122A-763A-13H to -15H). Apparently the upward gradation from white to green-gray or gray is linked to the increasing clay content, from <10% to about 15%. Superimposed on the dominant color are some pale brown or pink hues, observed at the very base of Unit I (e.g., very pale brown, 10YR 8/1, grading upward into whiter hues in Sections 122-763A-16H-1 to -16H-3). The near-surface sediments are pink (7.5YR 7/3) as a result of oxidation.

Unit I was fully recovered. Drilling disturbance includes varying degrees of mixing by flowage. The tops of cores are commonly soupy.

Unit I/Unit II Contact (Core 122-763A-16H-3, 81 cm)

The contact between Units I and II is characterized by a change in color and lithology, from semi-indurated white chalk below, to very pale brown ooze above. It is also shown by changes in physical properties and corresponds to an unconformity between lower and upper Miocene.

Unit II (141.7–247.0 mbsf)

Intervals 122-763A-16H-3, 81 cm, through -21H-CC and 122-763B-2X-1, 0 cm, to -7X-CC; middle Eocene to middle Miocene in age.

Unit II shows minor lithologic changes from ooze in the lower half to semilithified chalk in the upper half. Color varies from white to light green-gray and minor olive yellow. We subdivided Unit II into two subunits on the basis of these criteria.

Subunit IIA (141.7–185.4 mbsf)

Interval 122-763A-16H-3, 81 cm, to -20H-CC.

This subunit is composed of (semilithified) foraminifer-nannofossil chalk. Foraminiferal content ranges from 25% to 35%, except in Core 122-763A-20H, where it varies from 10% to 25%. Nannofossils are very abundant. Clay mineral content varies from 10% to 30%, but is generally <15%. Quartz grains are slightly more common in Subunit IIA (around 2%–5%) than in Unit I and in Subunit IIB. Disseminated pyrite specks are more common in the lower part of Subunit IIA. Mottling is unusual (Core 122-763A-20H only), as are distinct burrows. Some darker (gray) layers (2–5 cm-thick) appear in Sections 122-763A-19H-5 to -19H-8, with a frequency of 2 to 3 layers per section. They occur in a slightly grayer background,

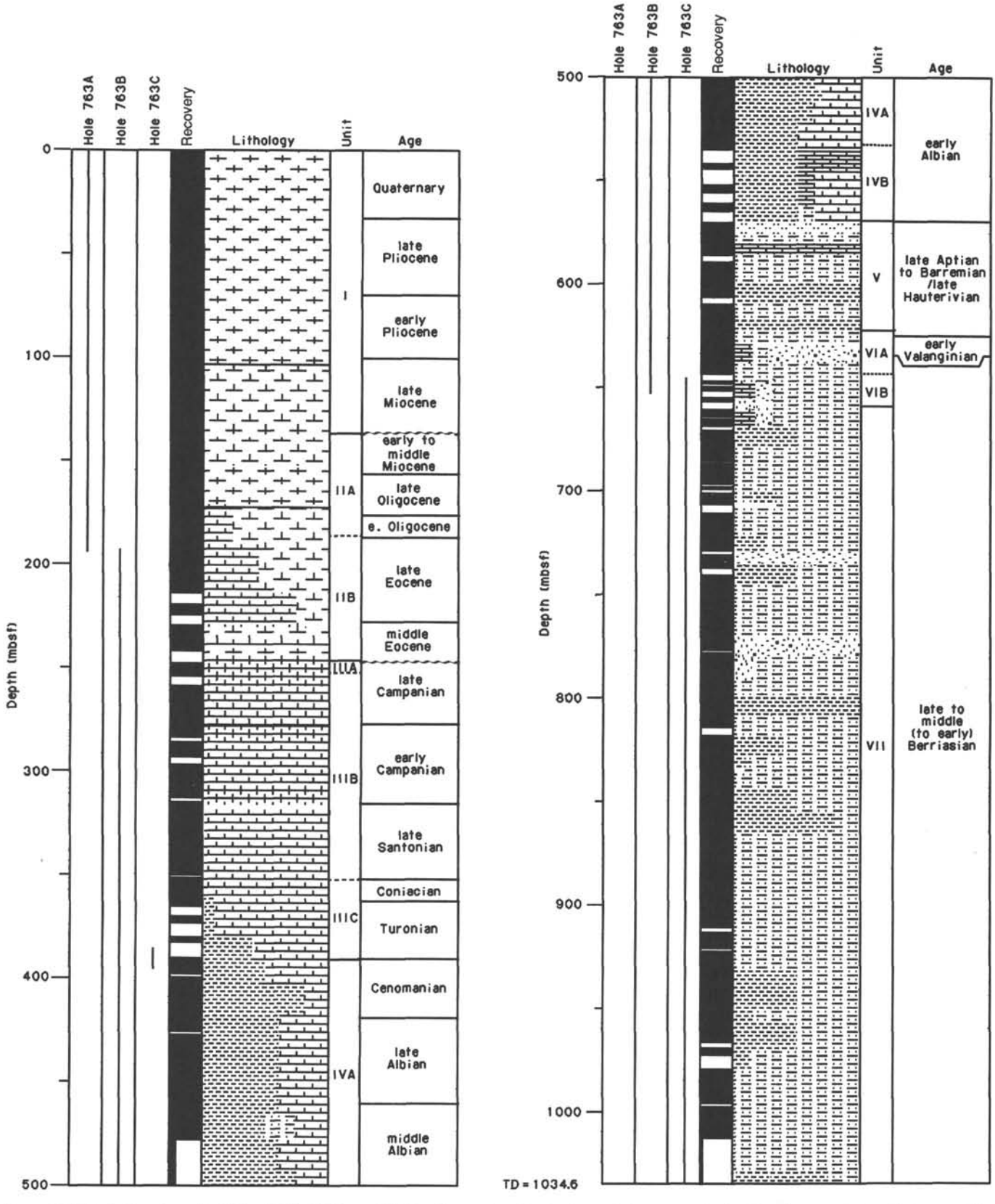

Figure 5. Lithologic column for Holes 763A, 763B, and 763C. A key to the lithologic symbols appears in the "Explanatory Notes" chapter (this volume).

		Depth (mbsf)	Core, section Hole 763A	Hole 763B	Hole 763C	Age	Lithology	Nannofossils (%)	Foraminifers (%)	$CaCO_3$ (%)	Color	Comments
Unit I		0	1H			Quaternary	Ooze (foraminifer-nannofossil)	60-80	20-35	85-90	Gray	Mottling; hydrotroilite.
		141.7	16H-3			late Miocene			15-20		White	
Unit II	A		16H-3			early Miocene	Chalk/ooze (foraminifer-nannofossil)	60-90	25-35	70-90	White	Semilithified; partly oxidized (brown).
		185.4		20H								
	B			21H, 2X		middle Eocene			5-10			
		247.0		7X								
Unit III	A			8X		late Campanian	Chalk (foraminifer-nannofossil)	60-90	25-35	70	Green	Bioturbation; microcycles; *Inoceramus.*
		251.5								80-90		
	B			19X-1								
		353.0		19X-2								
	C					early Turonian			5-25	50-70		
		385.7		22X, 2R								
Unit IV	A			23X, 2R		late Cenomanian	Calcareous (nannofossil) claystone (dolomite)	20-40	<15	20-50	Green/ gray	Zeolites; bioturbation; microcycles.
		532.0		37X								
	B			38X								
		570.0		41X		early Albian						
Unit V				42X		late Aptian to Barremian-late Hauterivian	Silty claystone	20 to rare	Rare or absent	<10	Black	Glauconite; belemnites; pyrite.
		622.5		47X								
Unit VI	A			48X		Hauterivian-early Valanginian	Silty claystone (with sand)	Trace	Rare	<10	Very dark gray (olive)	Glauconite; limestones; sandstones.
		637.0		50X-5								
	B			50X-5		late Berriasian						
		660.6		5R								
Unit VII				6R		late Berriasian	Silty claystone (siderite)	Trace	Rare	<10	Very dark gray	Siderite; plant debris; belemnites.
		1036.6		46R		middle Berriasian						

Figure 6. Summary chart of lithologic units and subunits for Holes 763A (APC cores), 763B (XCB cores), and 763C (RCB cores).

suggesting that they are linked to cyclic(?) variations in the amount of clay minerals.

Colors are generally very light (dominantly white, 10Y 8/1 or 7.5YR 8/0), with two intervals slightly more green-gray: (1) Core 122-763A-20H (partly light green-gray, 10Y 7/2) and Sections 122-763A-19H-4 to -19H-CC, which also show darker cm-thick layers as previously mentioned, and (2) Sections 122-763A-17H-5 to -17H-CC (partly light green-gray, 10Y 7/1 to 10Y 7/2). These slightly darker intervals contain relatively low proportions of calcium carbonate (as low as 70%, determined by calcium carbonate measurements), verifying the positive correlation between darker colors and noncarbonate (clay mineral) content, already noted in Unit I. One thin oxidized interval showing pale yellow (2.5Y 7/4) to olive yellow (2.5Y 6/6) hues occurs in Core 122-763A-17H-4, 0–150 cm, and may correspond to very slow sedimentation rates (consistent with biostratigraphic data).

Recovery was 100%, with drilling disturbance evidenced by rare drilling biscuits.

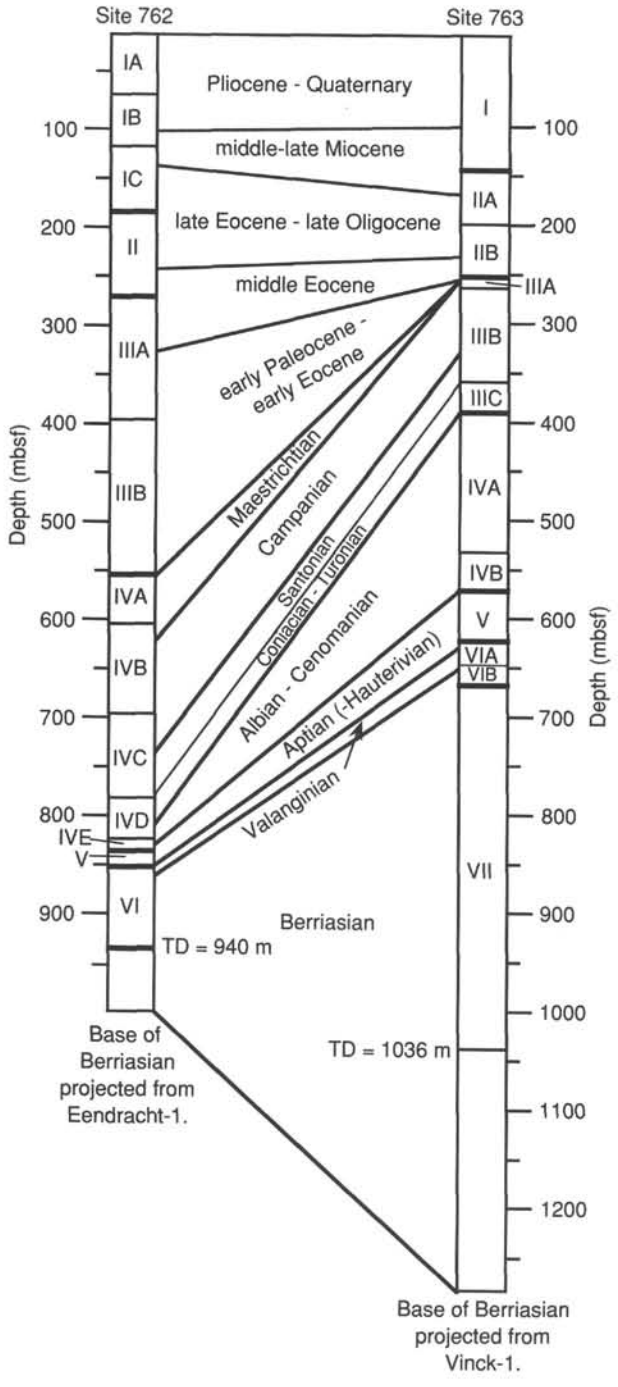

Figure 7. Chart showing correlation between Site 762 and Site 763. The base of the Berriasian (Barrow Group equivalent) is projected from the Eendracht-1 well (near Site 762) and from the Vinck-1 well (near Site 763).

Subunit IIB (185.4–247.0 mbsf)

Cores 122-763A-21H and 122-763B-2X through -7X.

This subunit is composed mainly of weakly indurated (less than Subunit IIA) nannofossil ooze with generally <10% foraminifers. Rare ostracodes are also present. Clay constitutes about 10%–15%, consistent with the white color (10Y 8/1 to 5Y 8/1). Depositional cycles are not visible and quartz grains are rare (trace).

The base of Subunit IIB (Cores 122-763B-6X to -7X) is slightly different from the rest of the subunit, as it is more lithified (similar to Subunit IIA), richer in clay (up to 20%) and in foraminifers (up to 30%), and green-gray (5GY 7/1). These characteristics probably result from the proximity to the Cretaceous/Tertiary boundary interval, a sequence boundary characterized at Site 763 by a long hiatus (around 30 m.y.).

In summary, Subunits IIA and IIB show rather different features, which may be related to the slower rate of accumulation of Subunit IIA (2.1 m/m.y., uncorrected for compaction) than of Subunit IIB (6.1 m/m.y.).

Unit II/Unit III Contact (between Cores 122-763B-7X and -8X)

This contact is a major lithologic change, with the first (downward) appearance of firm chalk, strong green color and abundant bioturbation. The true contact was not recovered, and occurs between Cores 122-763B-7X and -8X. This lithologic change corresponds to a hiatus defined by biostratigraphy, and is clearly visible in physical-properties data (see "Physical Properties," this chapter).

Unit III (247.0–385.72 mbsf)

Interval 122-763B-8X-1 to 763B-22X-CC and 763C-2R-1, 72 cm, early Turonian to late Campanian in age.

Unit III consists of 138.72 m of nannofossil chalk with foraminifers, foraminifer-nannofossil chalk, and nannofossil chalk with clay. Alternating color bands or cycles with abundant bioturbation (including burrows of *Zoophycos*, *Planolites*, and *Chondrites* types) are the most prominent features characterizing Unit III. It has been divided into three subunits on the basis of trends in lithology and calcium carbonate content (calculated from measurements of inorganic carbon; see "Organic Geochemistry," this chapter) and on biostratigraphic data.

Subunit IIIA (247.0–251.5 mbsf)

Interval 122-763B-8X to -8X-3, 150 cm; late Campanian in age.

Subunit III consists of foraminifer-nannofossil chalk grading up to foraminifer-nannofossil chalk with glauconite and quartz. The upper contact is a major unconformity, representing approximately 30 m.y., with middle Eocene chalk overlying upper Campanian chalk (see "Biostratigraphy," this chapter).

Subunit IIIA is 4.5 m thick (247.0–251.5 mbsf) and exhibits an upward-coarsening trend, with increasing proportions of rounded quartz, glauconite, and pyrite grains, and with *Inoceramus* prisms in the upper 25 cm. Subunit IIIA is pale green (5G 7/2) mottled with gray-green (5G 5/2), and is moderately to highly bioturbated. Horizontal and vertical burrows are common, some containing coarser-grained infillings of silt- to sand-sized glauconite, quartz, and pyrite grains (Fig. 8). The lower 50 cm of Section 122-763B-8X-1 (352.5–353.0 mbsf) show a texture that is either brecciated or intensely bioturbated. Calcium carbonate content increases downward from 66.8% to 80.6% in Subunit IIIA. Pyrite and glauconite occur both as disseminated grains and as infillings of foraminiferal tests.

Subunit IIIB (251.5–353.0 mbsf)

Interval 122-763B-8X-4 to 763B-19X-2, late Campanian to early Santonian in age.

Subunit IIIB consists of 100 m of foraminifer nannofossil chalk and nannofossil chalk with foraminifers. Color bands

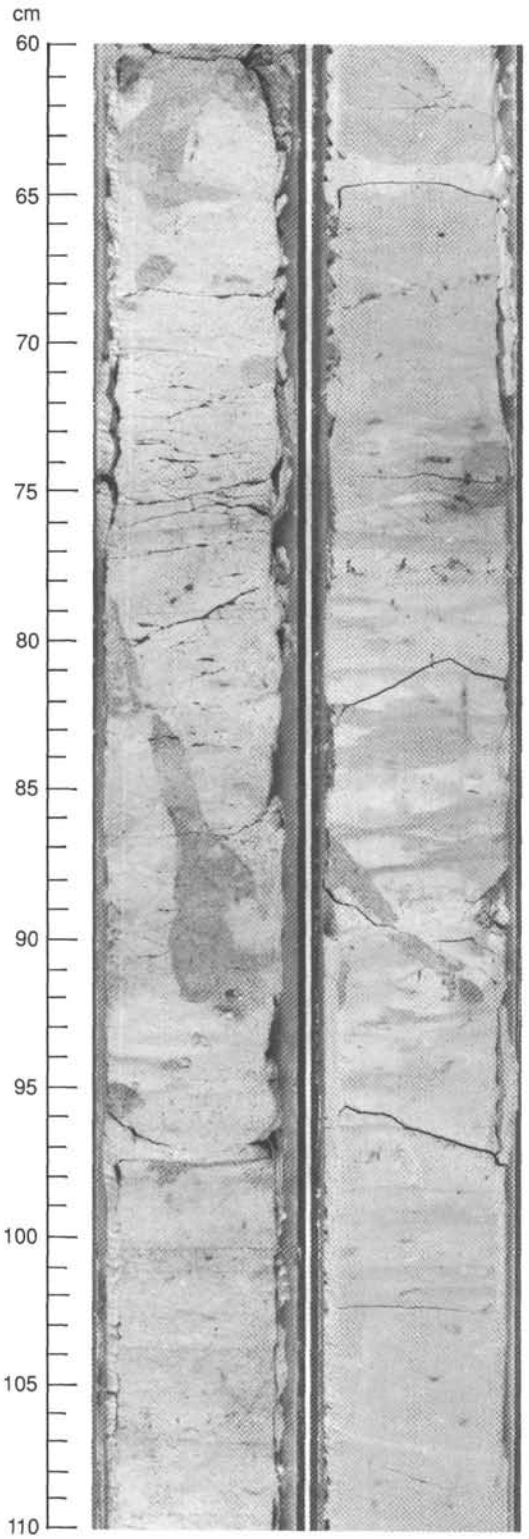

Figure 8. Uppermost part of Subunit IIIA, showing foraminifer-nannofossil chalk with abundant bioturbation. Some large burrows in the center of the picture are infilled with coarser (sandy) material rich in glauconite and quartz grains (Intervals 122-763B-8X-2, 60–110 cm, and -8X-3, 60–110 cm).

and gradually varying colors reflect changes in calcium carbonate content, with darker colors corresponding to lower $CaCO_3$ content. From 251.5 to 313.5 mbsf (Sections 122-763B-8X-4 through -14X-CC), color lightens gradually downward from light green-gray (5G 7/1) and pale green (5G 7/2) hues to white (5G 8/1) and light green-gray (5G 7/1) hues. Calcium carbonate content varies accordingly, increasing from 72.64% to 91.71%. From 313.5 to 351.5 mbsf (Cores 122-763B-15X through -18X), color gradually darkens to green-gray (5G 6/1) and light green-gray (5G 7/1) hues, and $CaCO_3$ content correspondingly decreases (91.71%–86.8%). Variations in foraminiferal content are consistent with those in color and $CaCO_3$ content, reaching a peak in Core 122-763B-14X (35% foraminifers, >90% $CaCO_3$), and decreasing both upward (10%–15% foraminifers and 72% $CaCO_3$ at the top of Subunit IIIB) and downward (6%–12% foraminifers and 86.8% $CaCO_3$ at the base of Subunit IIIB). Within Unit III these peaks in foraminiferal abundance and $CaCO_3$ content correlate with relatively high porosity and velocity values and relatively low wet-bulk density values (see "Physical Properties," this chapter). Foraminiferal sediments are commonly characterized by high porosity and low wet-bulk density values; this correlation is thought to be caused by the numerous hollow chambers contained in foraminifer tests.

Rhythmic alternations between light and dark layers, with correspondingly higher and lower calcium carbonate contents, are superimposed on the more gradual variations in Unit III. Color bands range from well-defined alternating bands, commonly 10–35 cm in thickness, to vague and gradual color changes occurring on the scale of centimeters to several decimeters. Lighter layers are generally more highly fractured than darker layers. Bioturbation commonly obscures color-band boundaries. The 10–35-cm-thick color bands in Subunit IIIB correspond to intervals between 20,000 and 60,000 years duration, assuming uniform sediment accumulation rates in the interval from 275.5 to 353.0 mbsf (122-763B-11X to -19X-2).

Subunit IIIC (353.0–385.72 mbsf)

Interval 122-763B-19X-2 to -22X-CC and 122-763C-2R-1, 72 cm; early Turonian to Coniacian in age.

Color-banded nannofossil chalk with clay and clayey nannofossil chalk make up Subunit IIIC (Fig. 9). This subunit is 32.72 m thick and represents a continuation of the upward-increasing calcium carbonate content and upward-lightening trend observed in the lower part of Subunit IIIB (313.5 to 353.0 mbsf). In Subunit IIIC, darker layers contain <75% calcium carbonate and are classified as clayey nannofossil chalk. The contact between Subunits IIIB and IIIC corresponds approximately to a condensed interval or a hiatus, as determined from calcareous nannoplankton data (see "Biostratigraphy," this chapter).

In Subunit IIIC, the $CaCO_3$ content of both light and dark layers decreases steadily downward, from 86.88% and 73.39% for light and dark layers, respectively, in Core 122-763B-19X to roughly 73% and 50% for light and dark layers at the top of Core 122-763B-22X. The color darkens accordingly, from green-gray (5G 6/1) and light green-gray (5G 7/1) bands at the top of Subunit IIIC, to gray-green (5G 5/2) and green-gray (5G 6/1) dark and light layers, respectively. Foraminifers decline in abundance from 5%–12% to 2%–3%, and both quartz and pyrite decline to trace quantities or disappear at the base of Subunit IIIC. Color bands occur through Subunit IIIC, and are similar to those discussed under Subunit IIIB (Fig. 9). A few circular pyritized burrows are present and contrast with

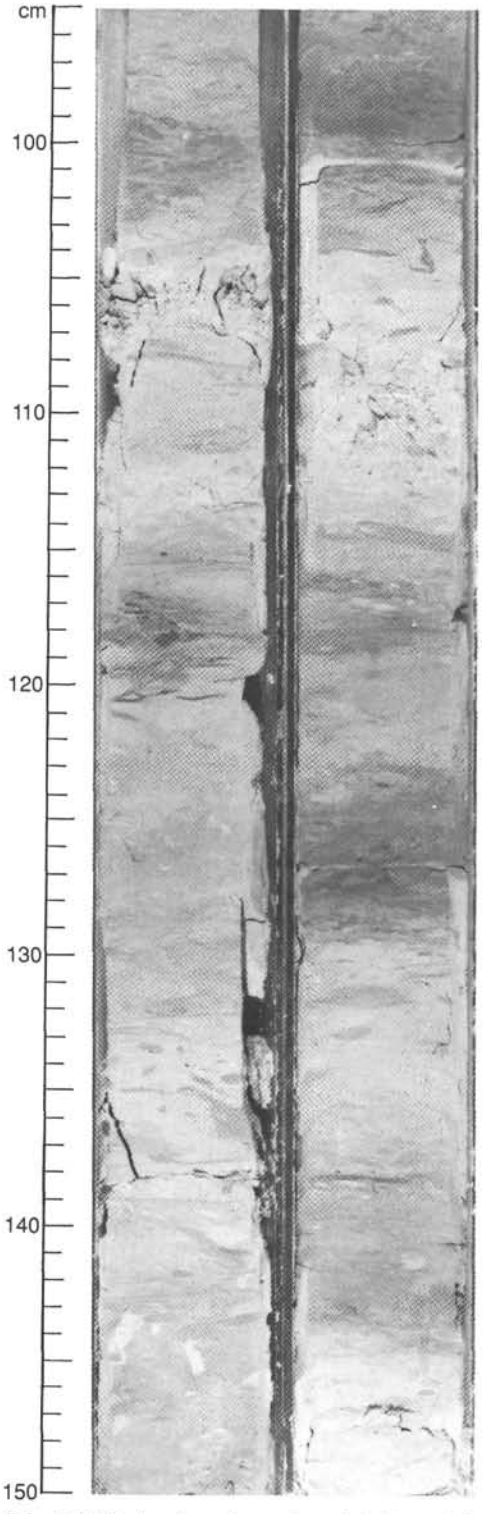

Figure 9. Subunit IIIC, showing color cycles related to variations in clay content (Intervals 122-763B-19X-5, 95–150 cm, and -19X-6, 95–150 cm).

the more common ellipsoidal burrows filled with chalk, suggesting that pyritization occurred early during diagenesis.

Unit III/Unit IV Contact (Cenomanian/Turonian Boundary Event)

The base of Unit III was recovered only in Core 122-763C-2R-1, 0–72 cm, (Fig. 10). Although this 72-cm-thick interval at the top of Core 122-763C-2R has thus far yielded no diagnostic fossils, it separates upper Cenomanian clayey nannofossil chalk and nannofossil claystone (below) from lower Turonian clayey nannofossil chalk (above) and represents a Cenomanian/Turonian boundary sequence (see "Biostratigraphy," this chapter). The boundary sequence consists of dark green-gray (5G 4/1), zeolitic silty claystone that is interbedded with black (N2), carbonaceous claystone with zeolites (Fig. 10). The dark green-gray intervals are in part laminated and in part mottled by bioturbation; they contain varying proportions of silt, and are 10–30 cm thick. The black carbonaceous claystone with zeolites occurs in two beds (4 and 12 cm thick) that are structureless to laminated or bioturbated, and contain 9%–15% organic carbon and about 10% zeolites. The contact with the underlying upper Cenomanian clayey nannofossil chalk is sharp, whereas the contact with the overlying Turonian clayey nannofossil chalk was not recovered. This section was deposited under poorly oxygenated to anoxic conditions, based on the lack of any preserved fauna and the high organic carbon content, and corresponds to a global anoxic event.

Unit IV (385.72–570.0 mbsf)

Interval 122-763B-23X through -41X; (early) Albian to late Cenomanian in age.

Unit IV is composed of nannofossil claystone with zeolite to claystone with nannofossils and zeolite. It has been subdivided into two subunits on the basis of hard carbonate beds that occur only in the lower part of the unit.

The common features of these two subunits are:

1. few foraminifers (<15%) and 20%–40% nannofossils;
2. common authigenic zeolite (probably clinoptilolite; up to 10%–15% according to smear slides) and glauconite;
3. a rather high percentage of clay minerals (noncarbonate material minus zeolites), amounting to about 40%–50%;
4. a great variety of rare detrital minerals, including biotite, muscovite, zircon, feldspar, and kyanite, suggesting a metamorphic source;
5. extensive bioturbation showing various trace fossils such as elliptical (compacted) burrows, *Zoophycos*, *Planolites*, *Teichicnus*, and *Chondrites* (Fig. 11); and
6. dominant green-gray color.

Subunit IVA (385.7–532.0 mbsf)

Cores 122-763B-23X-1 through -37X; early Albian to Cenomanian in age.

Bioclasts are common in Subunit IVA, including pelecypod shell debris (Cores 122-763B-31X to -34X), thick *Inoceramus* shell fragments (Cores 122-763B-23X, and -28X to -36X), and two belemnites (Sections 122-763B-25X-5 and -36X-CC). Rare plant debris is also present, as recognized in smear slides. Abundance of authigenic zeolite crystals (clinoptilolite?) ranges from 5% to 15% (up to 25% in Core 122-763B-32X). The noncarbonate (clay) content is generally about 50% or more, but decreases in the very top of this subunit (30% in Core 122-763B-23X). In some cores, the noncarbonate percentage varies (by up to 30%) between cyclic color bands (e.g., 70% in the dark layers to <40% in the light layers; Cores 122-763B-32X and -35X to -37X). Glauconite (a few percent) is sometimes visible with a hand lens, and quartz grains are rare (trace to 1%). Pyrite and cm-scale marcasite nodules are very common. We also noticed rare dolomite rhombs.

Extensive bioturbation is the main structural characteristic of Subunit IVA, with *Zoophycos*, *Planolites*, *Teichic-*

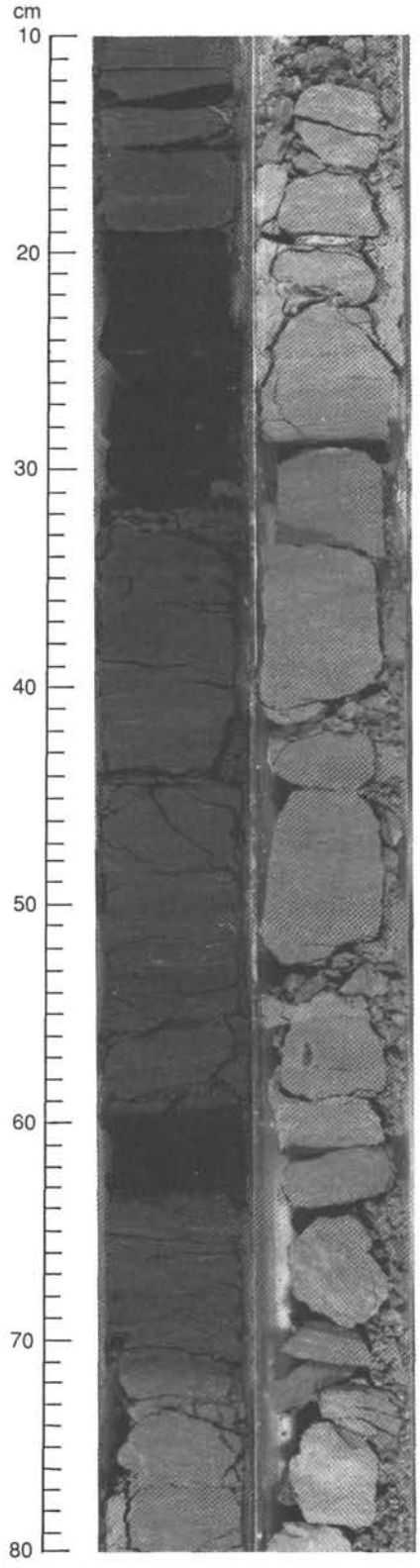

Figure 10. Black shale layers occurring close to the Cenomanian/Turonian contact (Subunit IIIC/IVA contact) marking the global Cenomanian-Turonian Global Event. The lower part (lightest lithology) is dated as Cenomanian. The darkest lithology (with interbedded black shales) is barren (Intervals 122-763C-2R-1, 10–80 cm, and -2R-2, 10–80 cm).

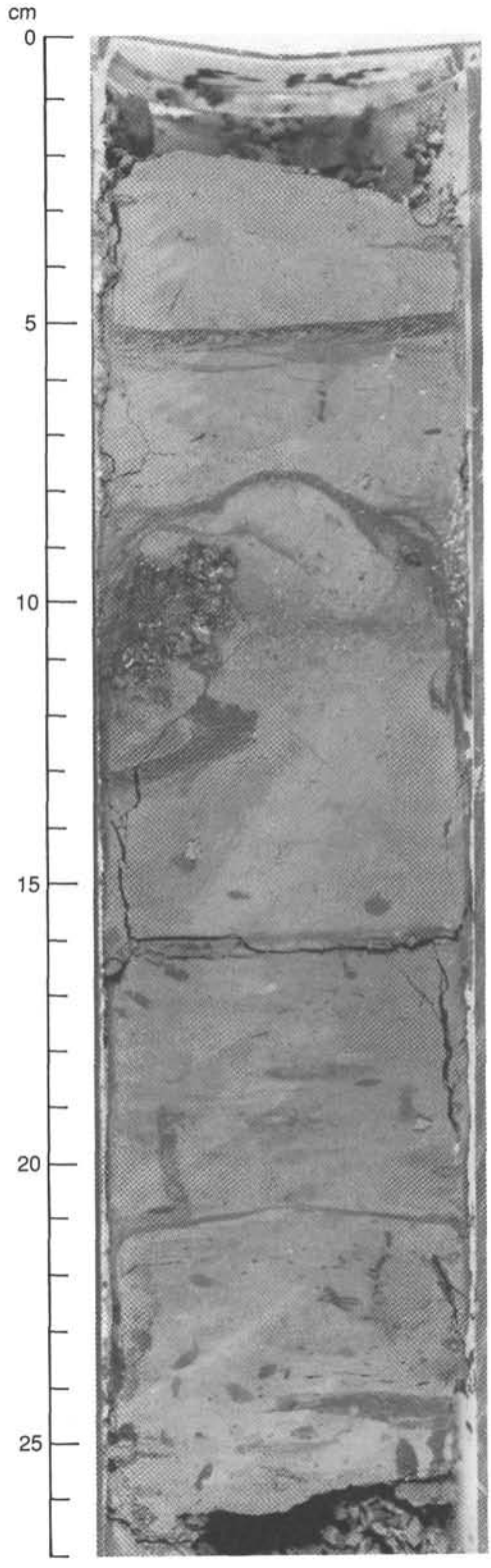

Figure 11. Diverse bioturbation observed in Subunit IVA. Note *Zoophycos* in the upper part, *Teichichnus* between 11 and 14 cm, and *Planolites* at about 19 cm (Interval 122-763B-34X-3, 0–27 cm).

nus, and *Chondrites*. Mottling was only observed in Core 122-763B-23X. Horizontal layering, marked by color changes linked to clay content, was observed in Cores 122-763B-25X, -26X, -33X, and -37X. It consists of darker dm-scale clay-rich layers, more or less regularly interbedded with lighter carbonate-rich layers, with a maximum frequency of 4 to 5 per section (Cores 122-763B-25X and -37X); the boundaries are gradational and do not show erosional contacts. Vertical burrows commonly produce local mixing of colors. Other cores show minor faint color (clay) variations and cycles.

Dominant colors range from light green-gray (5Y 7/1, 5GY 7/1) to green-gray (5Y 6/1 to 5Y 5/1, 5GY 6/1 to 5GY 5/1) with numerous rapid color changes. The upper part shows multiple minor occurrences of darker colors (Cores 122-763B-25X and -26X; 5GY 4/1 and N4). The lowermost part is lighter (Core 122-763B-37X), related to increasing carbonate (i.e., decreasing clay) content.

Recovery was very good, but drilling disturbance includes drill biscuits and extensive fracturing.

Subunit IVB (532.0–570.0 mbsf)

Cores 122-763B-38X through -41X; early Albian to Cenomanian in age.

Subunit IVB is characterized by very-fine-grained hard carbonate layers that are interbedded with claystones and calcareous claystones. These carbonates were very poorly recovered and generally appear as pebbles at the top of the cores (Cores 122-763B-38X to -40X), except for two dm-thick occurrences in Core 122-763B-39X. These appear to be sideritic because $CaCO_3$ analysis gave very low values (15%–30%), though dolomite may also be present. The beds may result from replacement of an initially clayey sediment by secondary carbonate. They have distinct physical-properties characteristics (e.g., much higher velocity values) and are possibly thicker than the sections recovered.

Other distinguishing characteristics of Subunit IVB are the greater clay content compared to overlying sediments (80% versus 40%), quartz grains (up to 15%), and glauconite (up to 10%) near the Unit IV/Unit V contact (the top of the Muderong Shale equivalent). Authigenic zeolites and pyrite-marcasite nodules are rare in Subunit IVB. Bioturbation seems less extensive than in Subunit IVA because parallel laminations highlighted by dark detrital material are more common in Subunit IVB than in Subunit IVA. The extensive drilling disturbance does not permit the identification of cycles. Colors are dominated by darker green-gray (5GY 5/1 to 4/1) in the lower part of section (where clay content is greater), but recrystallized carbonates are lighter (5G 7/1).

In summary, Unit IV exhibits both a gradual variation between detrital and biogenic components and much-higher-frequency, abrupt variations between these components in alternating color bands. These variations probably signal variations in the influx of continental and pelagic material. Calcium carbonate content increases gradationally upward both in Subunit IVB (from 20%–40% to 60%) and in the top of Subunit IVA (from 40%–60% to 70%), indicating a progressive increase in pelagic material (chiefly nannofossils) at the expense of continental material (chiefly clay). Abrupt, higher-frequency variations are expressed as alternating dm-thick color bands. Preliminary calculations for these calcareous claystone/clayey chalk cycles give a time range of 20,000–40,000 years, which is compatible with Milankovitch cycles. Glauconite is common (10%) in the lower part of Subunit IVB but decreases upward, suggesting that sedimentation rates increased over this interval.

Unit V (570.0–622.5 mbsf)

Cores 122-763B-42X through -47X; latest Hauterivian–Barremian to late Albian in age.

Unit V consists of 52.5 m of dark gray (5BG 4/1 to N4) to black (N2) claystone to clayey sandy siltstone, and minor limestone nodules and beds (Fig. 12). Calcareous nannoplankton indicate an early Aptian age for the entire unit. Drilling disturbance was severe throughout the unit, resulting in 2–5-cm-thick drilling biscuits that alternate with 1–3-cm-thick intervals of homogenized "drill slurry" between biscuits.

Dark gray to black claystone to sandy clayey siltstone makes up more than 90% of Unit V. Grain size coarsens downward from claystone with silt at 570.0 mbsf (Section 122-763B-42X-1) to sandy clayey siltstone at about 576.0 mbsf (Section 122-763B-42X-5), then fines downward to claystone (9% silt) at 608.0 mbsf (Section 122-763B-45X-CC). From 608.0 to 622.5 mbsf (Cores 122-763B-46X through -47X), grain size alternates between claystone with silt and silty claystone, but generally coarsens downward. Composition varies with grain size, with silt- to sand-sized grains including quartz (trace to 35%), glauconite (trace to 10%), feldspar grains that are highly altered to clay minerals (0%–30%), zeolites (trace to 28%), and recrystallized carbonate fragments (0%–12%). Glauconite-rich claystone that is speckled with glauconite pellets (up to 10%) occurs near the top and the base of Unit V, in Sections 122-763B-42X-6, -46X-6, and -47X-3.

One 5-cm-thick layer of light-colored clay (100%) of unknown composition occurs in Sample 122-763B-46X-3, 88–93 cm, and may be an altered ash bed. Its base is sharp and contains a 2-mm-thick pyrite concretionary? layer, and its top grades rapidly into silty claystone.

Structureless, bioturbated, and laminated intervals alternate with each other throughout Unit V. Parallel-laminated intervals are variably well developed, partially obscured by bioturbation, or consist of faintly organized, discontinuous stringers of white recrystallized carbonate grains (Fig. 13). Bioturbated intervals are dominated by horizontal burrows including *Planolites* or by tiny (0.5–2.0 mm) elliptical burrows aligned parallel to apparent bedding. This may indicate significant compaction, which tends to exaggerate the parallel lamination by aligning burrows horizontally. Burrows infilled with pyrite occur irregularly, and are spherical and less compacted than elliptical horizontal burrows, indicating early diagenetic pyrite formation. In addition to the bioclastic silt- to sand-sized carbonate grains, two thin-shelled ammonites occur in Unit V, in Samples 122-763B-44X-7, 8 cm, and 122-763B-47X-2, 140 cm (Fig. 14).

Dark gray (5Y 4/1) to light gray (N6 to 5Y 6/1) limestone nodules and one 43-cm-thick limestone bed occur in Unit V. This limestone bed is massive, is recrystallized to calcite and dolomite, and contains glauconite grains (5%) and minor quartz, pyrite, and recrystallized silt- to sand-sized carbonate grains. Grains constitute <25%–30% of the rock, and are matrix (recrystallized calcite and dolomite) supported. A few small limestone nodules/concretions (<5 cm diameter) are scattered through Unit V, and may contain concentric and radial calcite-cemented fractures (Section 122-763B-44X-CC), or may be recrystallized.

Unit V represents the latter stages of dominantly terrigenous sedimentation at Site 763, before the transition (in Subunit IVB, discussed above) to mixed pelagic and terrigenous sedimentation. Unit V accumulated more rapidly (17–18 m/m.y.) than either the underlying Subunit VIA (2.5–5.5 m/m.y., see below), or the overlying Unit IV (10 m/m.y.). Variations in grain size, bioclastic debris, and quartz and

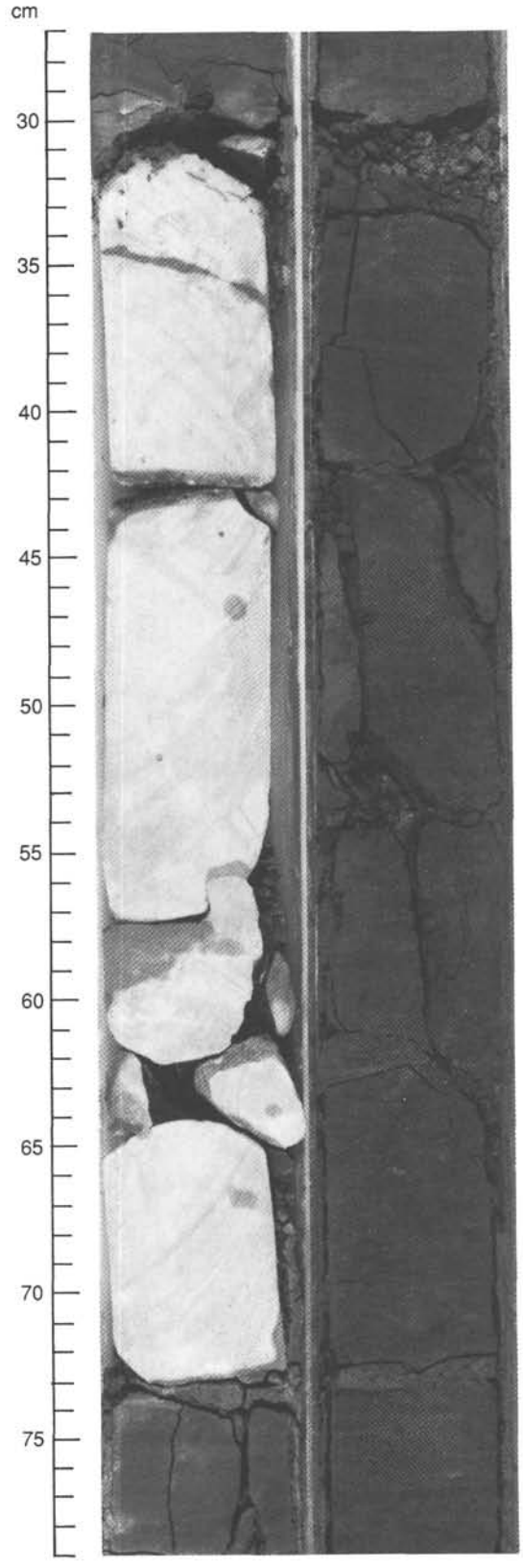

Figure 12. Massive carbonate layer interbedded in silty claystones of Unit V (Intervals 122-763B-43X-2, 27–79 cm, and -43X-3, 27–79 cm).

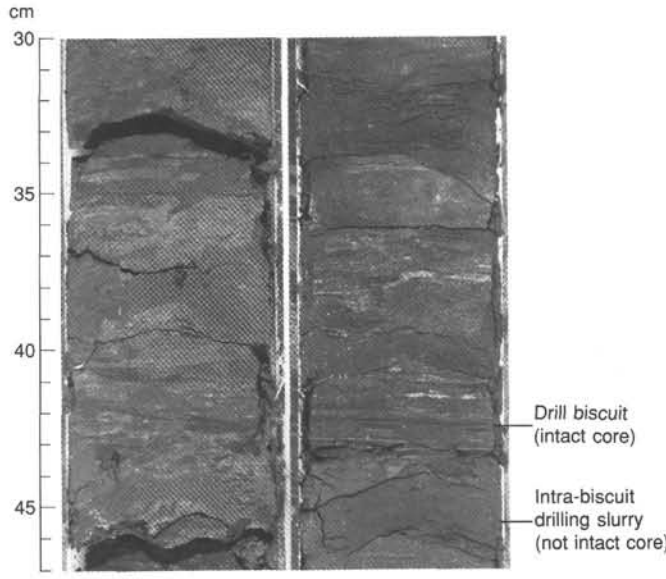

Figure 13. Unit V, showing parallel-laminated intervals with white carbonate grains on the right-hand side (Interval 122-763B-42X-4, 30–47 cm), and bioturbated intervals on the left-hand side (Interval 122-763B-42X-3, 30–47 cm).

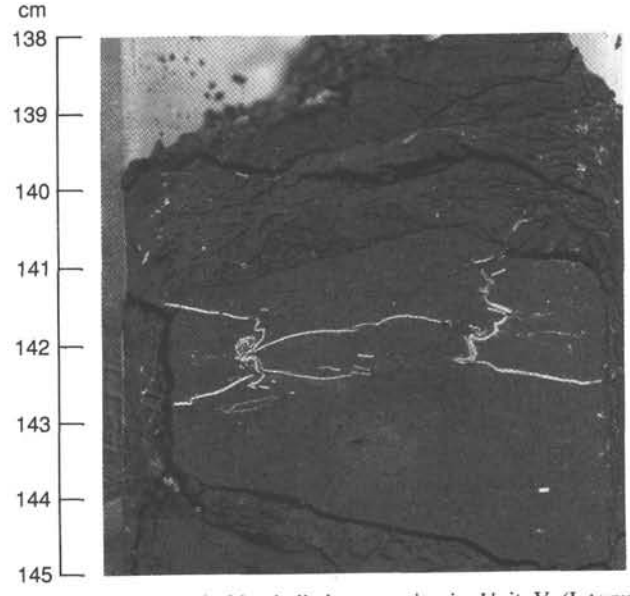

Figure 14. Compacted thin-shelled ammonite in Unit V (Interval 122-763B-47X-2, 138–145 cm).

feldspar grains indicate periodic changes in the flow regime of deposition, perhaps related to transgressive-regressive cycles, distal deposition by mass flow, or tractive transport of coarser grains. Common bioturbation indicates moderately to well-oxygenated bottom-water conditions, a supposition supported by the absence of pyrite. A single layer of light-colored clay (altered ash?) suggests contemporaneous volcanism. This unit was probably deposited under distal shelf conditions, with relative fluctuations in the influx of silt- and sand-sized terrigenous and bioclastic debris.

Unit VI (622.5–660.6 mbsf)

Intervals 122-763B-48X-1 through -54X and 122-763C-4R through -5R; late Berriasian to Hauterivian in age.

Claystone to silty claystone, with lesser siltstone, sandstone, and minor carbonate compose Unit VI. We have divided this unit into two subunits.

Subunit VIA (622.5–637.0 mbsf)

Interval 122-763B-48X-1 to -50X-5, 95 cm; Berriasian to early Valanginian–Hauterivian in age.

Silty claystone to sandy siltstone, with minor recrystallized limestone, makes up Subunit VIA. Although 15.00 m were cored in the interval identified as Subunit VIA, a total of 20.87 m of sediment were recovered in this subunit.

The upper contact is placed at the top of Core 122-763B-48X, above a belemnite- and glauconite-rich silty claystone. The contact lies between a lower Aptian fauna in Section 122-763B-47X-CC, and a lower Valanginian fauna in Sample 122-763B-48X-4, 56–57 cm (see "Biostratigraphy," this chapter). The undated interval between these biostratigraphic markers consists of a 1.0-m-thick, dark gray (2.5Y 4/0) silty claystone speckled with glauconite pellets and disseminated pyrite, overlying a belemnite-, glauconite-, and pyrite-rich silty claystone (Fig. 15). This 5.06-m-thick undated interval is either a hiatus or a condensed sequence encompassing the Hauterivian-Barremian (at least 8 m.y.). The abundance of belemnites (more than one per section) and glauconite supports the interpretation of a condensed sequence. Further biostratigraphic work may refine this interpretation.

In Subunit VIA, lithology gradually coarsens downward, from silty claystone and silty claystone with sand, to sandy clayey siltstone at the base of Subunit VIA. Color also changes downward, from dark gray (2.5Y 4/0) and black (2.5Y 2/0) to more olive hues of dark gray (5Y 4/1) and black (5Y 2.5/1). Drilling biscuits extend through the subunit, and are structureless or rarely faintly laminated. Abundant belemnites and sand-sized glauconite pellets and common disseminated pyrite grains (silt- to fine sand-sized) are the most prominent characteristics of Subunit VIA. Lower in the section, the belemnites decrease in abundance, whereas glauconite pellets and pyrite grains increase slightly in abundance. Quartz (10%–25%), feldspar altered to clay minerals (0%–10%), glauconite (10%–15% in smear slides, though more abundant by visual inspection), and pyrite (5%–12%) are the major constituent grains, with minor (<5%) zeolite, mica, and carbonate grains.

Three limestone interbeds up to 50 cm thick and a few carbonate concretions are scattered through Subunit VIA (Fig. 16). The limestone beds are recrystallized, contain sand-sized glauconite pellets and some calcite veins, and are gray (5Y 6/1) to light gray (10YR 7/1). The concretions are recrystallized, contain shell fragments, and are less than 6 cm in diameter.

Subunit VIB (637.0–660.6 mbsf)

Interval 122-763B-50X-5, 95 cm, through -54X and Cores 122-763C-4R and -5R; late Berriasian in age.

Dark gray (5Y 4/1) to black (5Y 2.5/2) silty claystone to sandy silty claystone, carbonate-cemented quartz sandstone with or without glauconite pellets, and minor recrystallized limestone constitute the recovered lithologies in Subunit VIB. This subunit is differentiated from Subunit VIA in containing only minor glauconite pellets and belemnites, and in containing pyrite nodules up to 1–2 cm diameter, plant debris (2%–3%), and minor bioclastic debris (0%–3%). Gamma-ray and resistivity logs suggest that sandstone and a few thin limestone beds are common in Subunit VIB, but were washed away and mostly not recovered in the core barrels.

The silty claystones of Subunit VIB are generally structureless, with some intervals being faintly laminated. Drilling disturbance is moderate to severe, with drill biscuits developed throughout Cores 122-763B-50X through -54X, and fractured pieces in Cores 122-763C-4R and -5R. Grain size trends are compatible with the gamma-ray log signature in the upper part of Subunit VIB. Grain size decreases slightly with depth in the upper 6.0 m of recovered sediment

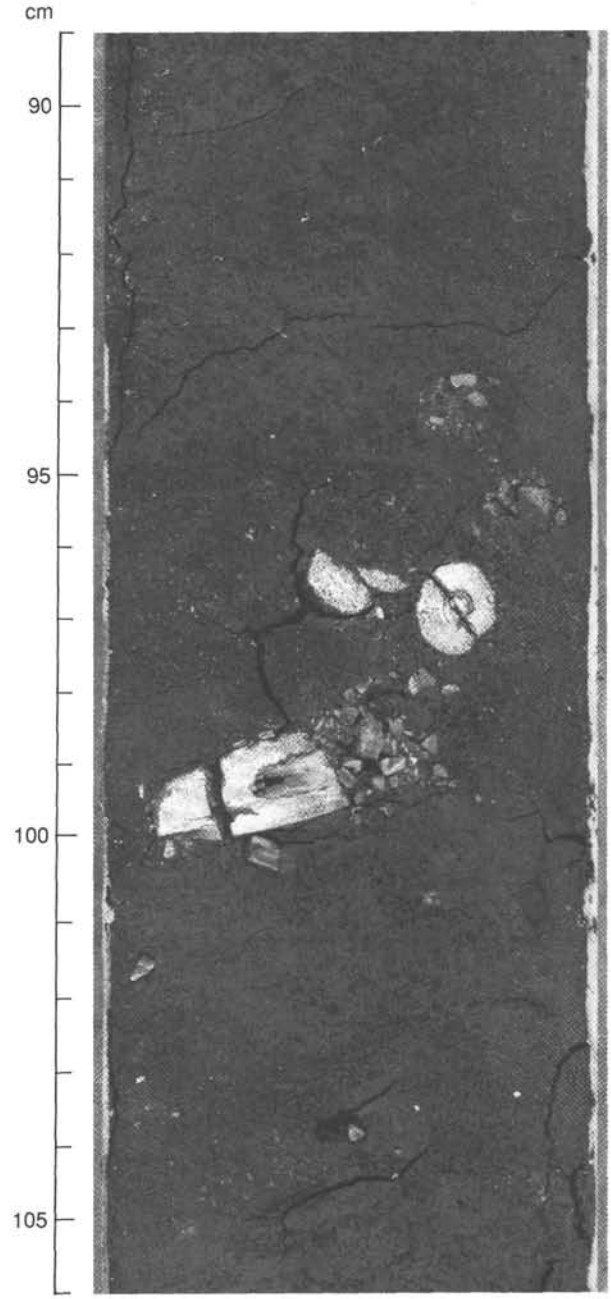

Figure 15. Belemnites recovered in Subunit VIA. Black speckled grains dispersed in the silty claystone are glauconite pellets (Section 122-763B-48X-4, 89–106 cm).

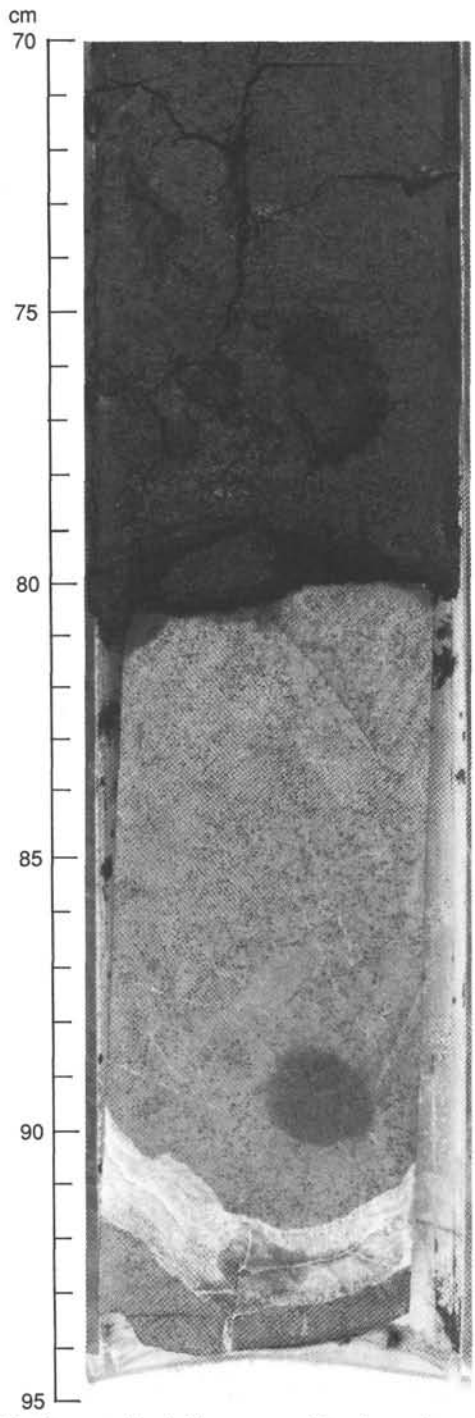

Figure 16. Recrystallized limestone with glauconite pellets, and calcite-filled veins underlying silty claystone. Glauconite pellets appear to increase in abundance upwards (Interval 122-763B-48X-5, 70–95 cm).

from Subunit VIB (20%–25% sand and 35% silt in Section 122-763B-50X-6, to 0%–5% sand and 57%–22% silt in Sample 122-763B-51X-4, 0–75 cm), then increases slightly in the lower part of Core 122-763B-51X. Core 122-763B-52X, in which no sediment was recovered, correlates with a low gamma-ray spike that is probably sand or sandstone (see "Downhole Measurements," this chapter). The lower portion of recovered sediment from Subunit VIB (Cores 122-763B-53X and -54X, and 122-763C-4R and -5R) shows no apparent trend in grain-size variation.

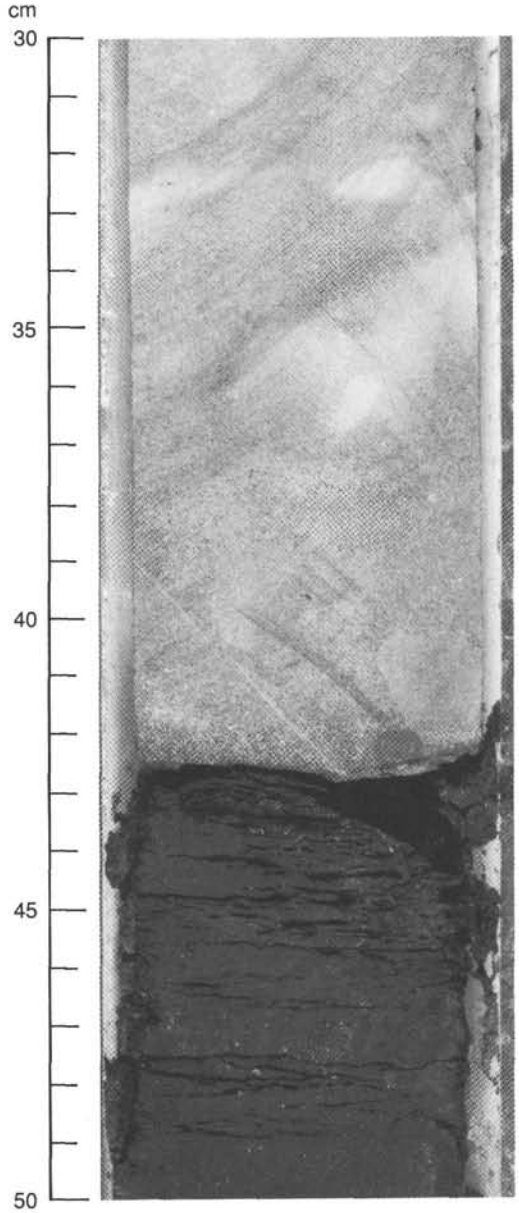

Figure 17. Graded, carbonate-cemented quartz sandstone overlying silty claystone. This is the basal segment of a 42-cm-thick graded layer (Interval 122-763B-54X-1, 30–50 cm).

A few pieces of carbonate-cemented sandstone and limestone, including a 42-cm-thick, graded quartz sandstone with calcite cement (Fig. 17) were recovered in the lower portion of Subunit VIB. Several of the smaller of these pieces occur at the top of Section 122-763B-53X-1, along with a well-preserved ammonite fragment (Fig. 18), and represent downhole contamination from the unrecovered interval above (Core 122-763C-52X). One of these pieces grades from quartz sandstone with glauconite grains at the base to calcite-cemented quartz sandstone with glauconite, and finally to limestone with matrix-supported siliciclastic and glauconite grains at the top. A 13-cm-thick recrystallized limestone bed was also recovered in Subunit VIB.

Unit VI was probably deposited under outer shelf conditions. Subunit VIB contains some graded carbonate-cemented

Figure 18. Ammonite fragment in Subunit VIB. This piece comes from a poorly-recovered interval that appears on the basis of wireline log character, to contain interbedded sandstone and thin limestones (Interval 122-763C-4R-1, 29–32 cm).

sandstone to siltstone beds suggesting deposition by sediment gravity flows (turbidity currents). The presence of quartz grains, plant, and bioclastic debris in Subunit VIB suggests influx from terrigenous (and perhaps reworked shallow marine) sources. Pyrite nodules indicate local reducing conditions during early diagenesis, perhaps induced by the influx of plant debris that was oxidized, depleting the oxygen content of the interstitial pore waters. The upward increase (from Subunit VIB to VIA) of glauconite pellets and belemnite fragments, and the corresponding decrease in plant debris and pyrite nodules, indicates progressive sediment starvation that culminated in a hiatus or condensed sequence (at least 8 m.y.) at the top of Unit VI. This period of sediment starvation apparently reflects a relative rise in base level, induced by accelerated subsidence, sea-level rise, reduced sedimentation rates, or a combination of these factors.

Unit VI/Unit VII Contact

The contact between Units VI and VII occurs in an unrecovered interval between Cores 122-763C-5R and -6R. The contact separates a poorly-recovered interval (Subunit VIB) from an interval with much higher recovery rates (Unit VII). Subunit VIB is characterized by high-amplitude variations in the gamma-ray and resistivity logs, suggesting interbedded sandstone, limestone, and claystone. Unit VII gave much improved recovery rates, with silty claystone being the dominant lithology, indicating that the lithologic break between Unit VI and Unit VII separates thinly interbedded sandstone, limestone, and claystone (above) from silty claystone below.

Unit VII (660.6–1036.6 mbsf)

Cores 122-763C-6R through -46R; middle to late Berriasian in age.

Unit VII is remarkable in its uniformity throughout the 376.0-m-thick recovered succession. Black (5Y 2.5/1) to very dark gray (5Y 3/1) claystone with silt to sandy silty claystone is the dominant lithology, with lesser clayey siltstone to sandy clayey siltstone. This lithology is generally structureless or pseudolaminated, with a bedding-parallel fabric imparted by tiny (1 × 2–3 mm), compacted elliptical burrows or pellets aligned parallel to bedding (Fig. 19). Olive gray (5Y 5/2) to pale yellow (5Y 7/3) siderite(?) nodules and concretionary layers occur throughout Unit VII, with gradational or sharp boundaries and abundant tiny (1 × 2–5 mm) burrows or pellets (Fig. 20). Pyrite abundance is variable throughout Unit VII, where it occurs both as silt- to sand-sized disseminated grains and as pyrite nodules and burrow-fillings in some intervals. Plant debris is also ubiquitous throughout Unit VII, both as microscopic grains (2%–5%), and as rare wood fragments. Glauconite occurs only sporadically in dm- to m-thick intervals with gradational boundaries.

Several other constituents and lithologies are rare but occur within Unit VII. Carbonate-cemented quartz sandstone, with or without glauconite grains, is present in layers up to 35 cm thick. These layers are internally massive or rarely bioturbated and moderately to poorly sorted, with rip-up clasts. Normal grading is common and passes upward through carbonate-cemented sandy siltstone to silty claystone (Fig. 21). We recorded one 55-cm-thick inversely graded carbonate-cemented quartz sandstone bed. The carbonate-cemented sandstones occur most commonly in the upper 125 m of Unit VII. Sand- to granule-sized quartz grains (up to 5 mm diameter and generally subangular) are present as isolated grains dispersed within structureless silty claystone in the upper part of this unit (Cores 122-763C-12R through -18R). Their origin is enigmatic.

Normal and reverse grading also occur intermittently in the clayey lithologies. Two types of graded layers are common in the lower 142.5 m of Unit VII (Cores 122-763C-32R through -46R): (1) normally graded layers with a sharp base, and (2) gradational, inversely to normally graded layers. Silty laminations and parting surfaces are present but rare in the lower 85.5 m of Unit VII (Cores 122-763C-38R through -46R) and indicate deposition by currents.

Fossil debris consists of tiny shell fragments, belemnites, and less common mollusks and ammonites. Belemnites are fairly common between 827 and 1036.6 mbsf (Cores 122-763C-25R through -46R), increasing in abundance in the lower 47.5 m of Unit VII (Cores 122-763C-42R through -46R). Mollusks are rare, and one ammonite was recovered in Core 122-763C-14R. Light gray (5Y 7/1) to gray (5Y 5/1) calcareous carbonate concretions are common and one burrowed limestone bed occurs in the interval from 846.6 to 894.1 mbsf (Cores 122-763C-27R through -31R).

Silt- to sand-sized carbonate (shell?) debris is present as scattered grains in some cm- to dm-thick, lighter colored (gray, 5Y 4/1) intervals that alternate with intervals devoid of shell debris. These grains are faintly organized into discontinuous stringers or small clots, suggesting either disrupted laminations or redistribution by bioturbation. Intervals with shell debris have sustained less drill disturbance than nonshelly intervals (which are often thoroughly biscuited) suggesting more induration, perhaps caused by minor carbonate cementation.

Two thin bentonite layers <10 cm thick are present in the middle of Unit VII (Cores 122-763C-26R and -29R), and represent altered volcanic ash beds. In addition, silt- to sand-sized feldspar grains that are highly altered and pseudomorphed by clay minerals locally compose up to 15% of the silty claystones. These may represent altered phenocrysts

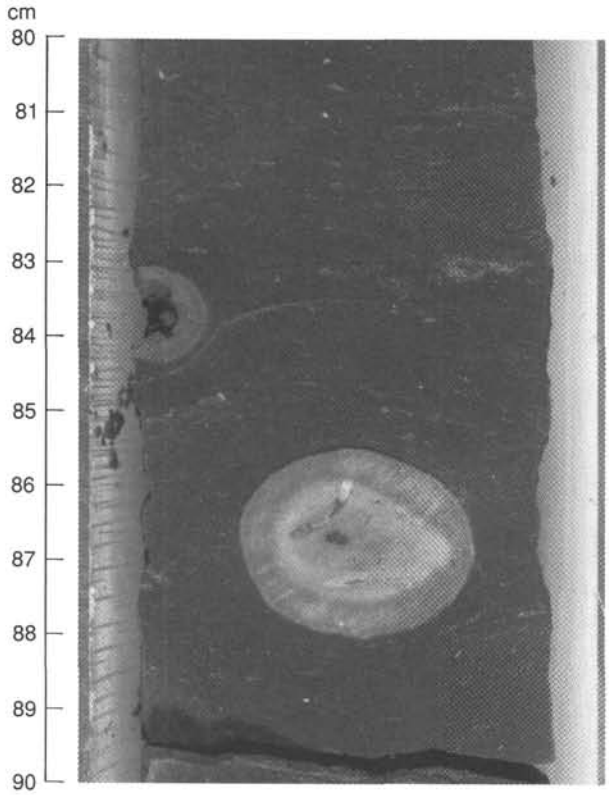

Figure 19. Pseudo-laminations displayed in silty claystone and showing differential compaction around a sideritic belemnite fragment, indicating siderite replacement during early diagenesis (Interval 122-763C-45R-6, 80–90 cm).

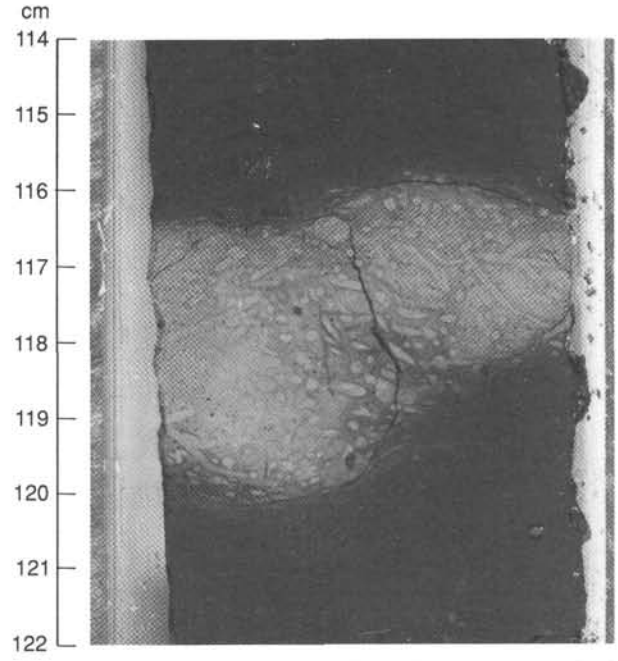

Figure 20. Siderite zone with abundant ellipsoidal and circular, uncompacted burrows (Interval 122-763C-13R-5, 114–122 cm).

from a volcanic source, or weathered crystals from an igneous or sedimentary source.

We have identified several facies in Unit VII, characterized by associations of lithologies and sedimentary structures. From 660.6 to 713.6 mbsf (Cores 122-763C-6R through -12R), carbonate-cemented sandstones are common and are associated with silty claystone to silty sandstone containing sideritic zones and pyrite burrow fillings. Glauconite and fossil fragments are minor constituents. Between 713.6 and 770.6 mbsf, fossil fragments (including an ammonite), tiny shell fragments, glauconite pellets, and granule-sized quartz grains occur scattered through structureless silty claystone to sandy claystone with silt. Pyrite occurs mainly as scattered grains, and burrowed siderite zones and concretions are abundant (generally spaced 1 to 2 m apart). From 770.6 to 827.6 mbsf (Cores 122-763C-19R to -24R), carbonate-cemented quartz sandstones are again common, associated with siderite nodules and minor pyrite and shell debris.

Between 827.6 and 894.1 mbsf (Cores 122-763C-25R to -31R), claystone with silt to silty claystone with sand contains abundant belemnites and shell fragments, calcareous nodules and beds, and pyrite grains and burrow fillings, as well as minor silty laminations and two light-colored clay layers (bentonite). From 894.1 to 951.1 mbsf (Cores 122-763C-32R to -37R), dm- to m-thick intervals of silty claystone that are devoid of shell debris and heavily drill-biscuited alternate with more indurated (sometimes graded) intervals containing tiny shell fragments and occasional belemnites and mollusks. Sideritized burrows and nodules, disseminated and burrow-filling pyrite, and wood fragments are also common. Between 960.6 and 1036.6 mbsf (Cores 122-763C-38R to -46R), silty claystone with common silty laminations and partings is the dominant lithology, associated with common belemnite and mollusk fragments, some scattered tiny shell fragments, and minor wood fragments. Pyrite nodules and burrow fillings, sideritic burrows and concretions, and common quartz (10%–35%) are present throughout this lowermost interval.

Unit VII (the Berriasian sequence, Barrow Group equivalent) accumulated very rapidly at Site 763 (100 to perhaps 300 m/m.y.). Grain size appears to be dominated by silt- and clay-sized material, although grain-size analysis is needed to provide more accurate data on this parameter. The presence of plant debris, quartz and feldspar grains, and intervals with silt- to sand-sized shell debris indicates derivation from a terrigenous source with admixed shallow marine (shelly) debris. Reducing conditions generally prevailed during burial and diagenesis, as shown by the ubiquitous pyritized and sideritized burrows.

The abundance of structureless to pseudolaminated (i.e., the alignment of abundant tiny, elliptical, compacted burrows or pellets) silty claystone suggests deposition by either fine-grained, sand-poor sediment gravity flows, or by fallout from suspension. Suspension fallout may occur by biological flocculation (e.g., excretion of pelletized aggregates of silt and/or clay by pelagic organisms) or by chemical flocculation of fine-grained terrigenous material. Sediment gravity flows (primarily turbidity currents?) deposited the graded, carbonate-cemented sandstones to siltstones that are common in the upper part of the Berriasian sequence (660.6–713.6 mbsf and 770.6–827.6 mbsf). The irregular occurrence of glauconite pellets in such a rapidly deposited succession is surprising, and may represent transport of these pellets into the region of Site 763. Regionally, Unit VII at Site 763 is located north and west of a correlative zone of clinoform reflectors with 150–200 ms (100–200 m) of relief. These clinoform reflectors constitute the basinward edge of a large, prograding clastic wedge that during Berriasian time was being shed north- and northwestward. Such clastic wedges are associated with large suspension clouds of terrigenous clay that extend beyond the limit of tractive deposition, mixing with open-marine waters (e.g., the Amazon River

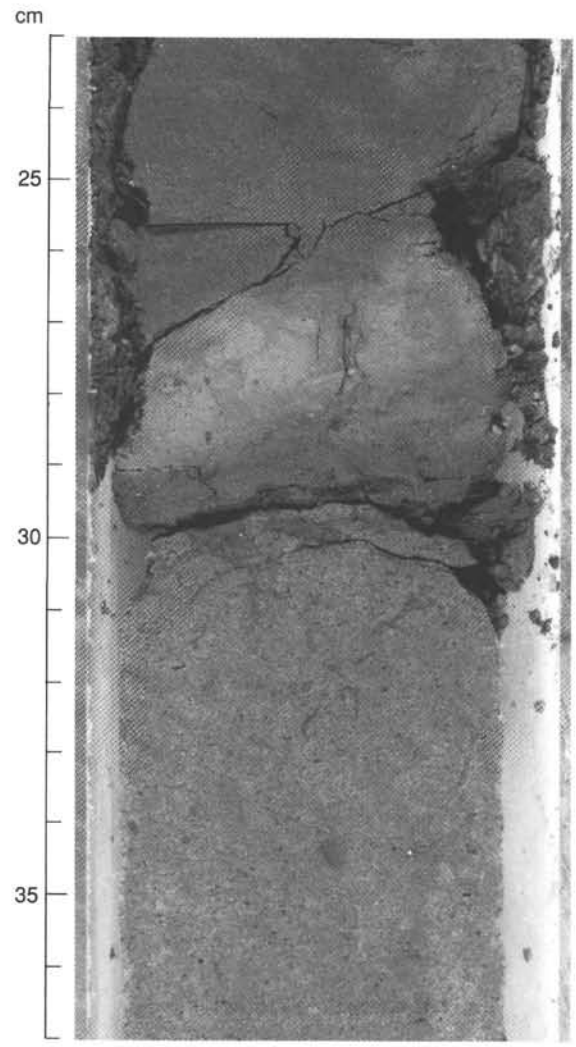

Figure 21. The upper 8 cm of a graded bed of carbonate-cemented sandstone with glauconite. The upper few centimeters of the sand are burrowed and appear to grade upward through a burrowed sideritic zone to silty claystone (Interval 122-763C-23R-2, 23–37 cm).

delta). The location of Site 763 beyond the limit of these clinoforms, coupled with the lithologic characteristics of Unit VII, suggests that Unit VII was deposited as fallout from a suspension cloud, supplemented to some degree by sediment gravity flows derived from the edge of the clinoforms.

BIOSTRATIGRAPHY

Introduction

Site 763 is situated on the central part of the Exmouth Plateau at a water depth of 1368 m. Three holes were drilled to a total depth of 1037 m, recovering sediments that range in age from Berriasian (earliest Cretaceous) to Holocene. As the recovered sediments represent a wide variety of lithologies and sedimentary environments, many different microfossil groups have proven to be effective in dating this sedimentary sequence. Units I to IV, Aptian-Albian to Quaternary chalk, calcareous ooze, and calcareous claystone, were dated using foraminifer and calcareous nannofossil stratigraphy. The age of Unit V, the Muderong Shale equivalent, was determined using nannofossil and dinoflagellate stratigraphy. Units VI and VII, the Barrow Group equivalents, were dated largely using palynomorphs, but in a few samples these ages were supported by nannofossil biostratigraphy. Benthic foraminifers and ostracodes are well preserved in this latter unit and provide important paleoenvironmental control.

The major highlights of this site include the documentation of several dramatic hiatuses which dissect the lithologic column, and the application of precise biostratigraphic ties to sequence stratigraphy. The recovered facies illustrate the complete evolution from a marginal, syn-rift environment to an open-ocean, post-rift setting. Other significant recoveries include a nearly complete Cenomanian/Turonian boundary interval and a thick mid-Cretaceous sequence that will allow detailed biostratigraphic and chemostratigraphic analysis. Finally, extremely well-preserved Neocomian dinoflagellate assemblages will lead to more detailed taxonomic and biostratigraphic studies of this fossil group.

Calcareous Nannofossils

Occurrence and Preservation

The abundance and preservation of calcareous nannofossils at Site 763 corresponds well with the major lithologic units. Unit I, which consists of Miocene to Quaternary ooze, contains abundant, well-preserved nannofossils. Unit II, composed of Eocene to Miocene ooze and chalk, contains abundant, but moderately well-preserved assemblages. Units III and IV, Albian-Cenomanian chalk and calcareous claystone, possesses abundant, exceptionally well-preserved, nannofossils with an interval of moderate to poor preservation extending from the upper Cenomanian to the Santonian. Glauconitic claystone and black shale, recovered at the Cenomanian/Turonian boundary, are virtually barren of nannofossils. The lower Aptian Muderong Shale equivalent strata (Unit V) demonstrate a complete range of nannofossil preservation and abundance, from well-preserved abundant assemblages to poorly preserved sparse ones. Finally, the Barrow Group equivalents (Units VI and VII) are largely barren of nannofossils. However, a few samples contain sparse assemblages with poor to moderate preservation that allow correlation of these units to Berriasian and Valanginian stages.

Cenozoic Biostratigraphy

Holes 763A and 763B recovered a thick Cenozoic section composed predominantly of calcareous ooze whose age can be constrained within narrow limits using nannofossil stratigraphy (Fig. 22). We have applied the zonation of Martini (1971), using in most cases the primary zonal markers. However, in a number of instances where the primary indicators were not observed we relied on secondary markers whose biostratigraphic ranges were summarized by Perch-Nielsen (1985a).

The uppermost part of the sequence in Core 122-763A-1H to Section 122-763-2H-3 contains a late Quaternary assemblage (Zones NN20–NN21) composed of *Emiliania huxleyi* and *Gephyrocapsa oceanica*. Sections 122-763A-2H-4 to -5H-1 are characterized by a mixed Quaternary assemblage, but the presence of *Pseudoemiliania lacunosa* indicates Zone NN19. Sections 122-763A-5H-2 to -5H-CC lie in upper Pliocene Zone NN18 according to the presence of *Discoaster brouweri* and the absence of *Discoaster pentaradiatus*. The interval from Section 122-763A-6H-1 to -8H-CC contains *Discoaster surculus* and *Pseudoemiliania lacunosa*, suggesting a late Pliocene age within Zone NN16. The lower Pliocene also appears to be complete with undifferentiated Zones NN14–15 recovered in Sections 122-763-9H-1 to -9H-4 (suggested by the presence of *Reticulofenestra pseudoumbilica* and the absence of *Amaurolithus delicatus*), Zone NN13

Hole 763A			
Core section		Nanno-fossil zone	Series
1H	1H-CC to 2H-3	NN20-21	Quaternary
2H	2H-3 to 5H-1	NN19	
3H			
4H			
5H	5H-2 to 5H-CC	NN18	upper Pliocene
6H	6H-1 to 8H-CC	NN16	
7H			
8H			
9H	9H-1 to 9H-5	NN14-15	lower Pliocene
	9H-6 to 9H-CC	NN13	
10H	10H-1 to 11H-CC	NN12	
11H			
12H	12H-1 to 14H-CC	NN11	upper Miocene
13H			
14H			
15H	15H-1 to 16H-3	NN10	
16H	16H-3 to 17H-1	NN4-5	middle Miocene
17H	17H-2 to 17H-4	NN3	lower Miocene
	17H-5 to 18h-2	NN1-2	
18H	18H-4 to 18HCC	NP25	upper Oligocene
19H	19H-2 to 19H-4	NP24	
	19H-6 to 20H-2	NP23	lower Oligocene
20H	20H-6	NP22	
21H	20H-CC to 2X-1	NP21	lower Oligocene - upper Eocene

Hole 763B			
Core section		Nanno-fossil zone	Series/Stage
2X	2X-1	NP21	upper Eocene
2X	2X-2 to 3X-CC	NP20	
3X			
4X	4X-1 to 4X-CC	NP19-20	
5X	5X-1 to 4XCC	NP18	
6X	6X-1 to 6X-5	NP15-16	middle Eocene
7X	6X-CC to 7X-CC	NP15	
8X	8X-CC to 10X-CC		upper Campanian

Figure 22. Cenozoic calcareous nannofossil biostratigraphy of Holes 763A and 763B. Zonation is after Martini (1971). Hiatuses are indicated by wavy lines.

recovered in Sections 122-763A 9H-6 to -9H-CC (indicated by the overlapping range of *Ceratolithus rugosus* and *A. delicatus*) and Zone NN12 recovered in Sections 122-763A-10H-1 to -11H-CC (given the absence of *C. rugosus* and *Discoaster quinqueramus* and the presence of *A. delicatus*). The interval from Section 122-763A-12H-1 to -14H-CC is late Miocene in age and lies within the *D. quinqueramus* Total Range Zone (or TRZ; NN11), as indicated by the presence of the nominate species. Sections 122-763A-15H-1 to -16H-3 lie within Zone NN10 as suggested by the occurrence of *Discoaster neohamatus* and the absence of *Discoaster hamatus* and *D. quinqueramus*. Unit I is separated from Unit II by a distinct change in lithology from ooze to chalk in Core 122-763A-16H-3, 82 cm, and this corresponds to a hiatus that represents most of the middle Miocene.

The interval from Section 122-763A-16H-3 to -17H-1 lies within the combined zones NN4 and NN5, between the last occurrence of *Sphenolithus belemnos* at its base and the last occurrence of *Sphenolithus heteromorphus* at its top. The interval could not be subdivided because *Helicosphaera ampliaperta* was not observed. Sections 122-763A-17H-2 to -17H-4 are bounded by the last occurrence of *Triquetrorhabdulus carinatus* at the base and the last occurrence of *Sphenolithus belemnos* at the top, and are therefore correlated to the *Sphenolithus belemnos* Zone (NN3). The underlying Sections 122-763A-17H-5 to -18H-2 lie in undifferentiated Zones NN1–NN2 as suggested by the presence of *Triquetrorhabdus challengeri* and *Sphenolithus conicus* and the absence of *Sphenolithus belemnos*. *Discoaster druggii* was not observed and thus the zones could not be separated.

The Paleogene was recognized in Core 122-763A-18H. Interval 122-763A-18H-4 to -18H-CC lies in the uppermost Oligocene Zone NP25, according to the occurrence of *Sphenolithus ciperoensis* and the absence of *Sphenolithus distentus* and *Sphenolithus predistentus*. Sections 122-763A-19H-2 to -19H-4 lie in Zone NP24 given the combined presence of *S. ciperoensis*, *S. predistentus*, and *S. distentus*, and absence of *Reticulofenestra umbilica*. The interval between Sections 122-763A-19H-6 and -20H-2 is placed in Zone NP23 as suggested by the presence of *S. predistentus* and the absence of *S. ciperoensis*. Zone NP22 was recovered in Section 122-763A-20H-6, according to the presence of *Reticulofenestra umbilica*, *S. predistentus*, and *Helicosphaera reticulata*. The interval from Section 122-763A-20H-CC to -21H-CC corresponds to Zone NP21, as indicated by the occurrence of *Reticulofenestra umbilica* and *Ericsonia formosa* without *Discoaster saipanensis* or *Discoaster barbadiensis*. The position of the Eocene/Oligocene boundary cannot be determined with nannofossils.

The uppermost interval observed in Hole 763B, Section 122-763B-2X-1, also lies in Zone NP21. Sections 122-763B-2X-2 to -3X-CC lie in Zone NP20, given the presence of *D. saipanensis* and *Sphenolithus pseudoradians*. We place Sections 122-763B-4X-1 to -4X-CC within combined Zone NP19/20. Zone NP18 was recovered in Sections 122-763B-5X-1 to -5X-CC according to the occurrence of *Chiasmolithus oamurensis* without *Isthmolithus recurvus*. Sections 122-763B-6X-1 to -6X-5 lie in undifferentiated Zones NP15–NP16 as suggested by the presence of *Chiasmolithus grandis*, *Chiasmolithus expansus* and *D. saipanensis* without *C. oamurensis*. Zone NP15 was recovered in Section 122-763B-6X-CC given the presence of *Chiasmolithus medius* and the absence of *D. saipanensis*. This zone extends down to Section 122-763B-7X-CC, which contains a nannofossil assemblage with elements of Campanian, Maestrichtian, Paleocene, and Eocene floras. This mixed assemblage was formed during the extended episode of erosion, nondeposition, and reworking that created the dramatic unconformity between Sections 122-763B-7X-CC and -8X-1. The latter section contains an upper Campanian assemblage with <1% Tertiary nannofossils, presumably mixed downward from overlying sediments.

Cretaceous Biostratigraphy

The Cretaceous sequence recovered in Hole 763B consists of several complete intervals separated by hiatuses or intervals of very slow sedimentation (Fig. 23). These include an expanded Campanian and Santonian section, a thin Coniacian?-Turonian sequence, an expanded upper Aptian–lower Albian to Cenomanian section, and discrete sequences of lower Aptian, Valanginian, and middle–upper Berriasian. The nature of the boundaries (i.e., erosional, nondepositional, or merely condensed) cannot be determined with certainty at the present time. As in previous sites, the zonations of Sissingh (1977) and Roth (1978) did not work well for the entire Cretaceous interval, and we have therefore relied on individual biohorizons to date the sequence. These allow us to determine combined zonal units of Sissingh (1977) and Roth (1978) (Fig. 23). For the lower Cretaceous we have applied the zonation of Bralower et al. (1989).

An expanded Campanian sequence was obtained at Site 763 and the well-preserved assemblages will allow a detailed biostratigraphy to be developed for this interval. The Santonian/Campanian boundary is recognized by the first occurrence of *Broinsonia parca* in Section 122-763B-15X-2. The Coniacian interval in Sections 122-763B-19X-1 to -19X-CC is probably very condensed. The Cenomanian/Turonian boundary lies in the unrecovered interval between Cores 122-763B-22X and -23X, but was partially recovered in Hole 763C. In Core 122-763C-2R, uppermost Cenomanian nannofossil chalk is overlain by an interval of glauconitic claystone interbedded with two black shale horizons. Sample 122-763C-2R-1, 78–79 cm, represents the last occurrences of the nannofossil species *Axopodorhabdus albianus*, *Corollithion kennedyi*, *Microstaurus chiastius*, and *Lithraphidites acutum*. The extinction levels of these taxa are spaced out over a 5-m interval in sequences from the Western Interior Basin of North America (Bralower, 1988). No true Turonian assemblages were observed in Hole 763C, although the glauconitic claystone contains a very etched nannoflora characteristic of the Cenomanian/Turonian boundary interval. This interval is clearly very condensed at Site 763, although there is no evidence for a break in sedimentation. The Cenomanian/Turonian boundary interval represents a major transgression accompanied by a dramatic rise of the carbonate compensation depth (CCD) resulting in slow sedimentation, erosion, and nondeposition on shelves (Bralower, 1988).

The late Aptian–early Albian to Cenomanian interval is complete and expanded, contains extremely well-preserved nannofossils, and will play an integral role in future attempts to attain high-resolution mid-Cretaceous biostratigraphy. We observed in this interval several events in addition to the zonal markers shown in Figure 23. These include the first occurrences of *Corollithion kennedyi*, *Axopodorhabdus albianus*, *Broinsonia enormis*, *Broinsonia signata*, *Tranolithus orionatus*, and *Cribrosphaerella primitiva*. In addition, the combination of a high sedimentation rate and favorable preservation will allow future detailed morphologic investigations of the evolutionary lineages of *Eiffellithus* and *Tranolithus*.

It is not clear at present whether there is a hiatus between Units IV and V. The base of Unit IV lies within nannofossil Zone NC7 of Roth (1978), which ranges from middle Aptian to lower Albian. The entire Unit V (Muderong Shale equivalent) lies within lower Aptian nannofossil Zone NC6 of Roth (1978). Although the zonal marker *Chiastozygus litterarius* is absent,

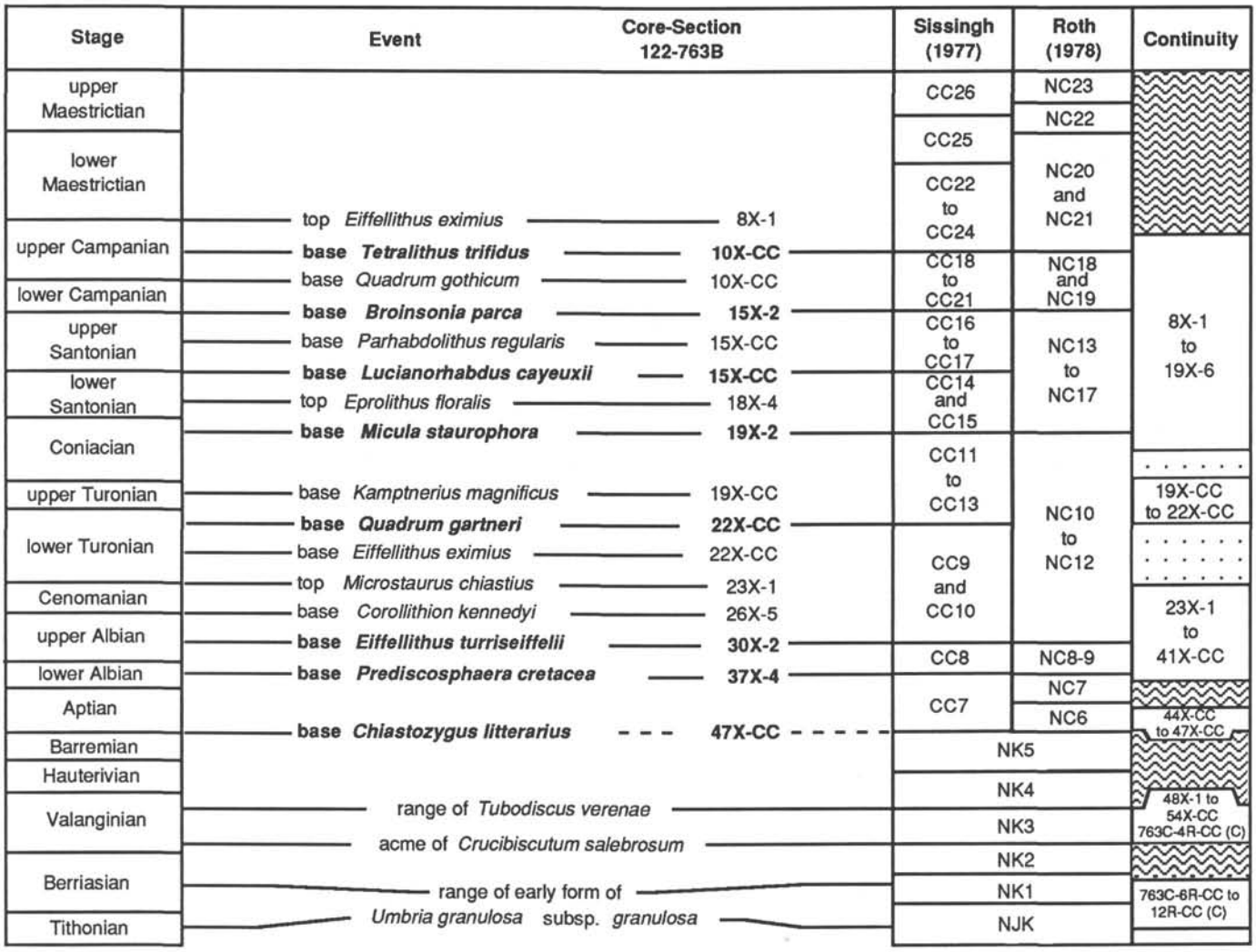

Figure 23. Cretaceous calcareous nannofossil biostratigraphy. All samples are from Hole 763B except where noted as from Hole 763C. Zonal events are shown in bold type. An inferred zonal event is indicated with dashed lines. Lower Cretaceous zonation (NK) is after Bralower (1987) and Bralower et al. (1989). "Continuity" column indicates age of recovered section, hiatuses (wavy pattern), and condensed sections (dotted pattern). See text for details.

Vagalapilla matalosa, whose first occurrence lies within this zone, is found commonly in numerous samples. Additional detailed shore-based work on this interval should help determine the continuity of the sequence.

The upper part of the Barrow Group equivalent (Unit VI) recovered in Sections 122-763B-48X-4 to -54X-CC and in Section 122-763C-4R-CC is Valanginian in age. The age of the former interval is indicated by the occurrence of *Tubodiscus verenae* in Section 122-763B-54X-CC. The age of the latter section is indicated by the combined occurrence of *Cyclagelosphaera deflandrei*, whose range is Tithonian-Valanginian (Thierstein, 1976), and the absence of *Umbria granulosa* subsp. *granulosa*, which is restricted to the Berriasian. A distinct break is observed below the sequence boundary located in Cores 122-763C-5R and -6R and nannofloras in Sections 122-763C-6R-CC to -12R-CC. The latter appear to be late Tithonian to middle Berriasian in age given the occurrence of the early form of *U. granulosa* subsp. *granulosa*, a taxon whose range is limited to this interval (Bralower et al., 1989). *Crucibiscutum salebrosum*, a species whose lowest occurrence was previously thought to be restricted to the uppermost Ryazanian (Jakubowski, 1987; Bralower, unpubl. data), occurs throughout the nannofossiliferous section.

The remainder of Hole 763C below this interval is largely barren of nannofossils, with the exception of the interval between Cores 122-763C-19R and -20R in which we observed some extremely well-preserved assemblages. These lack characteristic Berriasian and Tithonian markers and contain some very rare, and possibly undescribed, forms of the genus *Stradnerlithus*. This interval is characterized by low ratios of *Watznaueria barnesae* to various species of *Ellipsagelosphaera*, which is characteristic of upper Jurassic assemblages. However, as of this writing there is insufficient evidence to ascribe a Tithonian age to this interval. The exotic assemblages observed could instead result from the marginal-marine environmental conditions.

As indicated, the Santonian/Campanian and Cenomanian/Turonian boundaries can be precisely defined in Hole 763B. Other stage boundaries, with the exception of those associated with unconformities, cannot be determined with certainty using nannofossil stratigraphy, and we have relied on the

calibrations summarized by Perch-Nielsen (1985b; Fig. 23; see "Explanatory Notes," this volume).

Foraminifers

Cenozoic Biostratigraphy

Cenozoic foraminifer stratigraphy of Holes 763A and 763B is illustrated in Figure 24.

Neogene

Quaternary planktonic foraminiferal assemblages were recovered from Section 122-763A-1H-CC down to and including Section 122-763A-5H-CC. These all contain *Globorotalia truncatulinoides*, and are dominated by *Globigerinoides sacculifer*, *Pulleniatina obliquiloculata*, and *Globorotalia menardii*, which represent a warm-water fauna. The more temperate form, *Globorotalia inflata*, was also found. Sample 122-763A-5H-CC contains a transitional form between *Globorotalia tosaensis* and *G. truncatulinoides*, indicating the proximity of the Pliocene/Pleistocene boundary.

A Pliocene age was obtained from planktonic assemblages in Sections 122-763A-6H-CC through -10H-CC. The lowest sample containing *G. tosaensis* is Sample 122-763A-8H-CC, marking the base of Zone N21. We place the boundary between lower and upper Pliocene at the highest occurrence of *Globorotalia margaritae*, in Sample 122-763A-9H-1, 78–80 cm. The Miocene/Pliocene boundary is placed at the lowest occurrence of *Globorotalia tumida* (base of Zone N18), in Section 122-763A-10H-CC (Fig. 24). No hiatuses are apparent from the Pliocene succession of faunas.

The combined presence of *Pulleniatina primalis* and *Neogloboquadrina humerosa* and the absence of *G. tumida*, in Samples 122-763A-11H-CC and -12H-CC indicate that these sections belong to uppermost Miocene Zone N17B. The interval from Section 122-763A-13H-CC down to and including Section 122-763A-14H-CC belongs to Zone N17A, as indicated by the presence of *Globorotalia* cf. *plesiotumida*, *Globigerina nepenthes*, and *Globigerinoides bollii* in the absence of *Pulleniatina*. Section 122-763A-15H-CC through Sample 122-763A-16H-3, 52–54 cm, are of early late Miocene age, corresponding to Zone N16, as indicated by the presence of *Orbulina universa*, *Globorotalia acostaensis* and *G. nepenthes*. Immediately below this, in Sample 122-763A-16H-3, 139–141 cm, the faunas are characterized by the presence of *Orbulina suturalis*, *Globorotalia peripheroronda*, and *Globorotalia praemenardii*, indicating Zones N9–N10. Upper middle Miocene sediments appear to be missing in Hole 763A. The lowest sample to contain *Orbulina* is Sample 122-763A-16H-5, 74–76 cm, marking the base of the middle Miocene Zone N9.

Section 122-763A-16H-CC belongs to the uppermost lower Miocene Zone N8, given the presence of *Globigerinoides sicanus*, *Praeorbulina glomerosa*, and *Praeorbulina transitoria*. Samples 122-763A-17H-2, 74–76 cm, and -17H-3, 139–141 cm, contain *Globigerinoides* spp. and *Catapsydrax* spp. including *Catapsydrax dissimilis* and *Catapsydrax unicavus*. In the absence of *Globorotalia kugleri*, this assigns these samples to lower Miocene Zones N5–N6.

Lowermost Miocene Zone N4 was recognized in the lower part of Core 122-763A-17H, given the presence of *G. kugleri*. The Oligocene/Miocene boundary was placed within Zone N4 at the lowest occurrence of *Globoquadrina dehiscens*, in Sample 122-763A-17H-6, 74–76 cm.

Paleogene

Sample 122-763A-17H-CC contains *G. kugleri* and *Globigerinoides primordius* without *G. dehiscens*, indicating uppermost Oligocene Zone N4A. Below this, *Globigerina ciperoensis* and *Globigerina angulisuturalis* indicate the presence of Zone P22 down to the appearance of *Neogloboquadrina opima opima* in Section 122-763A-19H-CC. This taxon marks the top of Zone P21. Sample 122-763A-20H-6, 73–75 cm, is the uppermost sample found to contain *Pseudohastigerina* spp. and marks the top of lower Oligocene Zone P18. As usual, Zones P19 and P20 could not be differentiated; further detailed analysis is needed to establish the planktonic foraminiferal succession in the middle part of the Oligocene. Section 122-763A-20H-CC is assigned to lowest Oligocene Zone P18, given the combined occurrence of *Turborotalia ampliapertura* and *Pseudohastigerina* spp., and the absence of species from the *Turborotalia cerroazulensis* plexus as well as of species belonging to the genus *Hantkenina*. The highest occurrences of *Hantkenina* spp. and the *Turborotalia cerroazulensis* group are in Section 122-763A-21H-CC, and this marks the top of uppermost Eocene Zone P17.

In Hole 763B, an upper Eocene (Zone P17) fauna with *Turborotalia cerroazulensis cocoaensis*, *T. cerroazulensis* s.s., and *Hantkenina* spp. was found in Section 122-763B-2X-CC. Below that, Sections 122-763B-3X-CC down to and including -4X-CC are characterized by the occurrence of the *T. cerroazulensis* group, *Hantkenina* spp., and *Globigerinatheka* spp., indicating that they are late Eocene in age (Zones P15–P17). Section 122-763B-5X-CC contains *T. cerroazulensis* s.s., *Acarinina bullbrooki*, and *Globigerinatheka index*, indicating that it is close to the boundary between Zones P15 and P14.

Section 122-763B-6X-CC contains *Turborotalia frontosa*, *Turborotalia cerroazulensis pomeroli*, and *"Globigerinoides" higginsi*, and therefore is middle Eocene (Zone P12) in age. The highest occurrence of *Morozovella aragonensis* is in Section 122-763A-7X-CC and this marks the top of lower middle Eocene Zone P11.

No *in-situ* older Cenozoic faunas were found above the Cretaceous/Tertiary boundary at Site 763.

Cenozoic Paleoenvironment

Site 763 offered a good upper Paleogene and Neogene planktonic foraminiferal succession in which only one hiatus was found in the middle Miocene. The presence of high planktonic/benthic ratios throughout the Cenozoic succession indicates that deposition took place in an open-marine, pelagic environment.

Middle Eocene sediments unconformably overlie upper Campanian sediments at Site 763. The assemblages just above the unconformity contain up to 50%–60% reworked Campanian, Paleocene, and lower Eocene forms. The middle Eocene faunas are characterized by species belonging to the genera *Acarinina* and *Truncorotaloides* and are typical of temperate austral assemblages. The few warmer-water species that were found, such as *Morozovella aragonensis* and *Hantkenina* spp., occur in very low abundance.

Lower Eocene assemblages have more tropical elements than middle Eocene assemblages (e.g., species belonging to the genera *Globigerinatheka*, *Hantkenina*, and *Turborotalia*). Normal tropical faunas are also found in the Oligocene (to the extent that Oligocene planktonic faunas can be considered normal and tropical).

Lower Miocene faunas are characterized by warm-water species belonging to the genus *Globigerinoides* such as *Globigerinoides primordius*, *Globigerinoides sacculifer*, *Globigerinoides subquadratus*, *Globigerinoides sicanus*, and the *Praeorbulina* group, descendants of the latter species. A hiatus, which corresponds to almost the entire Middle Miocene, was recognized within Core 122-763A-16H. During the late Miocene,

Hole 763A			
Core	Foraminifer zone	Nanno-fossil zone	Series
1H	N22-23	NN20-21	Quaternary
2H	N22	NN19-21	
3H			
4H		NN19	
5H	N21	NN18	upper Pliocene
6H		NN16	
7H			
8H	N19-20		
9H		NN14-15	lower Pliocene
		NN13	
10H	N18	NN12	
11H	N17B		
12H		NN11	upper Miocene
13H	N17A		
14H			
15H	N16	NN10	
16H	N8	NN4-5	middle Miocene
17H	N4	NN3	lower Miocene
		NN1-2	
18H	P22	NP25	upper Oligocene
19H	P21	NP24	
20H	P18	NP23	lower Oligocene
		NP22	
21H	P17	NP21	lower Oligocene - upper Eocene

Hole 763B			
Core	Foraminifer zone	Nanno-fossil zone	Series
2X	P17	NP20	upper Eocene
3X	P16-17		
4X	P15-16	NP19	
5X	P14-15	NP18	
6X	P12	NP15-16	middle Eocene
7X	P11	NP15	
8X	upper Campanian	upper Campanian	upper Campanian

Figure 24. Correlation of foraminifer and nannofossil biostratigraphy of Hole 763A and the upper part of Hole 763B. Series boundaries shown in solid lines are as determined from nannofossil biostratigraphy, the dashed lines are series boundaries from foraminifer biostratigraphy. See text for discussion.

Table 2. Summary of Cretaceous foraminifer biostratigraphy of Hole 763B.

Interval	Age (Zone)
122-763B-	
8X-2 to 11X-CC	Upper Campanian
12X-CC to 14X-CC	Undifferentiated Campanian
15X-CC	Near Campanian/Santonian boundary
16X-CC to 18X-CC	Santonian
19X-CC to 20X-CC	Coniacian–Upper Turonian
21X-CC	Middle Turonian (*Helvetoglobotruncana helvetica* Zone)
22X-CC	Lower Turonian (*Whiteinella archaeocretacea* Zone)
23X-1 to 23X-CC	Upper Cenomanian (*Rotalipora cushmani* Zone)
24X-CC to 25X-CC	Undifferentiated Cenomanian
26X-CC	Indeterminate
27X-CC to 28X-CC	Upper Albian
29X-CC to 36X-CC	Undifferentiated Albian
37X-CC to 39X-CC	Albian-Aptian
40X-CC to 54X-CC	No foraminiferal age data

a large proportion of the fauna were composed of warm, subtropical to tropical forms such as *Globorotalia menardii*, *Globoquadrina altispira*, *Globoquadrina dehiscens*, *Sphaeroidinellopsis seminulina*, and *Globigerinoides sacculifer*.

A complete Pliocene-Quaternary sequence was recovered in Hole 763A. Faunas are dominated by the tropical to warm subtropical species such as *Globorotalia menardii*, *Globorotalia tumida*, *Sphaeroidinella dehiscens*, the *Pulleniatina* complex, *Globigerinella aequilateralis*, and *Globigerinoides sacculifer*. However, it is notable that *Globorotalia inflata*, a more temperate form, occasionally occurs in the upper Pliocene and Quaternary. This indicates a cool-temperate influence in a predominantly tropical pelagic environment during the late Pliocene and Quaternary, very much like present-day conditions on the Exmouth Plateau.

Cretaceous Biostratigraphy

A summary of the Cretaceous foraminifer stratigraphy of Hole 763B is given in Table 2.

Upper Cretaceous

Immediately below the Cretaceous/Tertiary unconformity, we found a planktonic foraminiferal fauna in Sample 122-763B-8X-2, 18–20 cm, with *Rugoglobigerina* spp., *Globotruncana arca*, and *Globotruncana bulloides*, but without *Guembelerina* spp. or any other Maestrichtian markers. We assigned this fauna to the Campanian by correlation with Hole 762C. Down to Section 122-763B-11X-CC, in some intervals the faunas include *Globotruncana linneiana obliqua*, a form which is probably restricted to the upper Campanian. Further down, the Campanian faunas include *G. arca*, *G. linneiana*, *Globotruncana ventricosa*, and *Rosita fornicata*. Normally, such faunas would be assigned to the upper Campanian *G. ventricosa* Zone, but as has been shown elsewhere in this area, *G. ventricosa* has an extended range that prevents us from applying the standard Tethyan zonation. Therefore, an undifferentiated Campanian age is preferred down to and including Section 122-763B-15X-CC, in which *Marginotruncana coronata*, occurring in addition to the previously mentioned taxa, indicates an age close to the Campanian/Santonian boundary.

Santonian *Marginotruncana* assemblages are found from Section 122-763B-16X-CC through -18X-CC. These include *Marginotruncana sinuosa*, *Marginotruncana pseudolinneiana*, and *M. coronata*. *Globotruncanita elevata* is also found in rare numbers. The latter species suggests that these faunas are uppermost Santonian (upper part of the *Dicarinella asymetrica* Zone), but as at Site 761, the Tethyan zonation does not apply. Therefore, an undifferentiated Santonian age is preferred.

The highest occurrence of Coniacian to upper Turonian planktonics was noted in Section 122-763B-19X-CC. These include *Falsotruncana maslakovae*, *Dicarinella imbricata* and *Hedbergella hoelzli*, in addition to *Marginotruncana* spp. The absence of the *Dicarinella concavata* group indicates that this assemblage belongs to either the *Dicarinella primitiva* or the *Marginotruncana sigali* Zone sensu Caron (1985). A similar fauna was found in Section 122-763B-20X-CC.

Section 122-763B-21X-CC belongs to the *Helvetoglobotruncana helvetica* Zone as indicated by the presence of the zonal marker. Section 122-763B-22X-CC, with a similar fauna but without *H. helvetica*, is assigned to the lowest Turonian *Whiteinella archaeocretacea* Zone.

Cenomanian planktonics were first seen in Section 122-763B-23X-CC, where the presence of *Rotalipora cushmani* and *Thalmanninella deeckei* indicate a late Cenomanian age. This was confirmed in Hole 763C, in which Sample 122-763C-2R, 15–16 cm, yielded an identical assemblage immediately below a dark claystone interval thought to mark the Cenomanian/Turonian boundary. Most of the Cenomanian, however, is not developed in a normal pelagic facies. Section 122-763B-24X-CC yielded a predominantly benthic, very diverse fauna; we observed a similar fauna in Section 122-763B-25X-CC. The presence of *Thalmanninella brotzeni* in the latter indicates a broad mid- to early Cenomanian age. Section 122-763B-26X-CC did not yield any foraminifers, probably due to the lithified nature of the rock.

Lower Cretaceous

Sections 122-763B-27X-CC and -28X-CC both contain a double-keeled version of *Planomalina buxtorfi*, as well as the normal single-keeled one which, however, is quite rare. In whatever guise this species may present itself, it is always considered to indicate a latest Albian (Vraconian) age, corresponding to the *Thalmanninella appenninica* Zone.

From Section 122-763B-29X-CC down to Section -36X-CC, abundant but oligospecific *Hedbergella* faunas with *Hedbergella planispira* and *Hedbergella delrioensis* are present, accompanied by diverse benthic faunas including *Osangularia* ex gr. *utaturensis* and less common *Gyroidinoides crassa*. These faunas are not inconsistent with an Albian age, although it may be argued that similar assemblages might be Aptian. Sections 122-763B-37X-CC and -38X-CC are in hard micritic carbonates that did not contain any significant fauna, but Section 122-763B-39X-CC nevertheless contains the abundant *Hedbergella* assemblage of Aptian-Albian age, as seen higher in the section. Sections 122-763B-40X and -41X are in hard micritic limestone that is difficult to process and appeared to be barren.

The break in lithology marking the top of the Muderong Shale equivalent strata is not expressed in the microfaunas because samples at either side of the break are barren of foraminifers. The first sample below the break to contain any microfauna is from Section 122-763B-44X-CC. This contains benthic foraminifers only, including *Gavelinella* ex gr. *intermedia* and *Hoeglundina chapmani*, indicating an age which could range from mid-Albian to Aptian; a hiatus between the Gearle Siltstone and Muderong Shale equivalents can therefore not be demonstrated on the basis of foraminiferal biostratigraphy.

We saw only rather insignificant foraminiferal microfaunas, exclusively benthic, in all the core-catcher samples below (and including) Section 122-763B-45X-CC in Hole 763B. The faunas consist of indeterminate forms belonging to the genera *Haplophragmoides*, *Lenticulina*, *Astacolus*, *Dentalina*, and

(*Eo-*)*Guttulina*. They are of Early Cretaceous aspect but not indicative of any particular age. The lithological boundary between the Muderong Shale equivalent and the Barrow Group is in an interval represented by Cores 122-763B-47X and -48X, both barren of foraminifers.

The foraminifer faunas of the Barrow Group equivalent strata, as seen in Hole 763C, are exclusively benthic. Although present in most of the core-catcher samples studied they are never abundant, and are apparently diluted by the siliciclastic sediment. There are three continuously fossiliferous intervals separated by poor to barren sections. Sections 122-763C-4R-CC through -8R-CC yielded sparse agglutinated assemblages with a few nodosariids and a rare ostracode. A poor to barren interval is represented by Sections 122-763C-9R-CC through -12R-CC; only Section 122-763C-11R-CC contains some indeterminate agglutinating foraminifers and nodosariids.

The second fossiliferous interval is the most diverse. It extends from Section 122-763C-14R-CC to -25R-CC and contains a "background" fauna of agglutinating foraminifers (mainly *Haplophragmoides* and *Trochammina* spp.) and nodosariids. In addition, a few epistominids were seen in Sections 122-763C-14R-CC and -16R-CC. We refer to these as *Epistomina* aff. *E. caracolla*. *E. caracolla* itself would indicate a Valanginian or Berriasian age. Between these two occurrences, a very characteristic ostracode was noted and provisionally recorded as Ostracode 763C-1 in Section 122-763C-15-CC. This form may prove to be of correlative value. Other ostracodes and polymorphinids (*Eoguttulina* sp.) were seen throughout the interval. Sections 122-763C-26R-CC through -28R-CC are barren.

The third fossiliferous interval extends from Section 122-763C-29R-CC to the last core catcher recovered, Section 122-763C-46R-CC. This interval is characterized by regular occurrences of *Ammobaculites* spp., which is more abundant lower in the section. In addition, there are other agglutinating foraminifers, nodosariids, rare polymorphinids, and ostracodes. However, calcareous foraminifers are far less common than agglutinating foraminifers. None of the forms encountered in this interval was age significant.

Cretaceous Paleoenvironments

The Cretaceous of Site 763 offers a wide range of paleoenvironments, from relatively shallow, restricted marine with strong clastic input, to deep, unrestricted, and pelagic marine with very little terrigenous influence. The transition, or break, between these two contrasting extremes is at or near the base of the section equivalent to the Gearle Siltstone.

The microfaunas in Unit VI and VII (Barrow Group equivalent) are doubtlessly marine, but the predominance of relatively primitive agglutinating foraminifers and nodosariids strongly suggests the absence of a good connection with the open sea and the presence of oxygen-deficient seafloor conditions. The lower part of Unit VII contains relatively high abundances of *Ammobaculites*, a genus that in Holocene environments prefers restricted, vegetated, environments (e.g., coastal swamps). We suggest that this abundance reflects a strong restriction of the paleoenvironment (i.e., anoxia and reduced salinity) rather than the paleodepth. Slightly more open marine conditions (yet still restricted) prevailed during the middle fossiliferous part of Unit VII, occasionally allowing such forms as epistominids and ornamented ostracodes to occur. The upper part of Unit VII saw a return to restricted conditions.

The paleoenvironments for the Aptian Unit V (Muderong Shale equivalent) are difficult to assess on the basis of the poor foraminiferal record. Regularly occurring glauconite and pyrite and rare marine foraminiferal faunas (including gavelinellid and epistominid forms) point to a restricted marine environment. The restriction may partly be due to a lack of connections with the open sea, but the open sea was often restricted in Aptian times. The absence of planktonic foraminifers in Unit V, even in the more open marine faunas in Section 122-763C-44R-CC, may point to reduced salinity in the surface waters.

Most of Unit IV (Gearle Siltstone equivalent; Aptian-Albian below the first occurrence of *Planomalina buxtorfi*) must have been deposited in normal open-marine paleoenvironments with strong pelagic influence and strongly reduced terrigenous supply, and at bathyal depths as indicated by the consistent presence of *Osangularia* ex gr. *utaturensis*. It is interesting to note that according to Moullade (1984) there is a difference in abundance of this species group and that of *Gyroidinoides crassa* in the South Atlantic, with the latter species being less abundant in the shallower bathyal environments. *G. crassa* only occurs in small numbers throughout the interval in question. We tentatively suggest upper bathyal depths of deposition during most of the Albian, but outside the reach of low-latitude Tethyan influence, as suggested by the absence of such faunal elements as *Ticinella* spp.

Tethyan planktonic foraminifers first invaded the Site 763 environment in the latest Albian. However, the *Planomalina buxtorfi* faunas are incomplete, with a noticeable lack of rotaliporid species of *Thalmanninella* and *Pseudothalmanninella*, and a predominance of small hedbergellids. These faunas grade into the Cenomanian assemblages with an abundance of outer neritic to upper bathyal benthic foraminifers but relatively few planktonics, indicating a somewhat restricted pelagic environment. Only in the latest Cenomanian *Rotalipora cushmani* Zone did planktonic taxa again become prominent and of Tethyan aspect.

The Cenomanian/Turonian boundary event could not be studied in great detail at Site 763. However, a black shale is present between the *R. cushmani* Zone and the *Whiteinella archaeocretacea* Zone; pending detailed shore-based investigations we conclude that the boundary layers are of the basinal type, reflecting a drastic shallowing of the CCD and deposition of clays in an anoxic environment.

The Turonian to Santonian faunas are dominated by Tethyan forms, with only minor benthic constituents. However, the composition of the planktonic faunas is somewhat different from truly Tethyan ones, with important representatives of *Dicarinella* (the *Dicarinella concavata* group) missing and rather monotonous double-keeled *Marginotruncana* present throughout the Late Turonian to Santonian interval.

These rather restricted Tethyan faunas persisted into the Campanian, although represented by different species. As in all other Leg 122 Campanian sections, *Globotruncana ventricosa* is present throughout the Campanian, and seems to replace the normally quite abundant single-keeled group of *Globotruncanita*. *Rugoglobigerina* is particularly well-represented in the Campanian faunas, but the genus *Rosita* is not. The composition of the faunas strongly suggests deposition of the Campanian pelagic faunas close to the southern limit of the distribution of Tethyan faunas, which, in analogy to the Northern hemisphere, may have been around 45°S.

Radiolarians

Radiolarian recovery from Site 763 was generally poor and extremely sporadic. Most of the faunas are low in abundance and diversity and therefore had to be examined as both wet- and dry-sieved residues instead of as strewn slides. Radiolarian recovery in Hole 763A was particularly poor. Samples 122-763A-2H-2, 60–62 cm, -2H-5, 60–62 cm, and -2H-CC

contain common and well-preserved upper Quaternary radiolarians assignable to the *Collosphaera tuberosa* Zone of Sanfilippo et al. (1985) including *Arcosphaera spinosa*, *Anthrocyrtidium* spp., *Collosphaera tuberosa*, *Didymocyrtis tetrathalamus*, *Lamprocyrtis nigriniae*, *Phormostichoartus corbula*, *Phormostichoartus marylandicus*, and *Stylacontarium acquilonium*. Sample 122-763A-3H-2, 60–62 cm, contains a sparse and mixed mid-Quaternary fauna that contains taxa indicating the *Collosphaera tuberosa* and *Amphirhopalum ypsilon* Zones of Sanfilippo et al. (1985). Sections 122-763A-3H-CC through -21H-CC are barren.

The samples from Hole 763B contain unidentifiable radiolarians, mostly preserved as clear, silica-infilled balls and cones with little or no remaining radiolarian meshwork. Sections 122-763B-2X-CC through -9X-CC are barren. However, Section 122-763B-10X-CC contains poorly preserved forms identifiable to the generic level, including *Artostrobium* sp. and *Phaseliforma* sp. Sections 122-763B-11X-CC through -21X-CC are barren. Sample 122-763B-22X-1, 60–62 cm, contains poorly preserved middle Cretaceous forms assignable to the genera *Dictyomitra* and *Stichomitra*. Section 122-763B-22X-CC contains common but poorly preserved radiolarians assignable to the upper Cenomanian–lower Turonian part of the *Obesacapsula somphedia* Zone of Sanfilippo and Riedel (1985). Identifiable forms include *Alievium* spp., *Pseudoaulophacus* spp., *Pseudodictyomitra pseudomacrocephala*, *Stichomitra communis*, *Stichomitra* spp., and *Thanarla veneta*. The radiolarian fauna from Sample 122-763B-23X-1, 60–62 cm, is sparse but it does contain *Thanarla veneta*, indicative of a probable Cenomanian or Turonian age. Sections 122-763B-24X-CC through -30X-CC contain recrystallized, unidentifiable forms. We identified several radiolarians from Section 122-763B-31X-CC as *Praeconocaryomma* sp. and *Thanarla* sp., whose co-occurrence indicates an undifferentiated Valanginian to Cenomanian age. Sections 122-763B-32X-CC through -36X-CC are all barren.

Common and moderately preserved lower Cretaceous (Albian) radiolarians assignable to the lower part of the *Acaeniotyle umbilicata* Zone of Sanfilippo and Riedel (1985) were found in Section 122-763B-37X-CC. Age-diagnostic forms include *Archaeodictyomitra simplex* and *Thanarla pulchra*. Samples 122-763B-38X-CC, -41X-CC, -42X-2, 57–60 cm, and -42X-CC all contain the long-ranging Cretaceous radiolarian genera *Cryptoamphorella*, *Pantanellium*, *Pseudodictyomitra*, *Stichomitra*, and *Thanarla*. Sample 122-763B-39X-1, 60–62 cm, contains poorly preserved forms assignable to *Acaeniotyle diaphorogona* and *Thanarla* sp.; *A. diaphorogona* has an age range of Berriasian to mid-Albian. Section 122-763B-39X-CC and Sections 122-763B-43X-CC to -54X-CC are all barren with the exception of Samples 122-763B-47X-CC and -48X-1, 60–62 cm, which contain the poorly preserved upper Valanginian to Aptian radiolarians *Cryptoamphorella* sp., *Pseudodictyomitra* aff. *P. leptoconica*, and *Thanarla*(?) *conica*. Sample 122-763B-48X-5, 60–62 cm, contains *Obesacapsula?* sp., *Pseudodictyomitra leptoconica*, *Syringocapsa* sp., and *Thanarla* sp., all of which indicate a questionable Valanginian age. Sections 122-763B-48X-CC through -54X-CC are barren.

In Hole 763C, Sections 122-763C-2R-CC through -46R-CC are all barren of radiolarians with two exceptions. Section 122-763C-22R-CC contains rare and poorly preserved undifferentiated Berriasian to upper Valanginian taxa that include *Archaeodictyomitra apiara* and *Thanarla*(?) *conica*. The radiolarians in Section 122-763C-35R-CC are replaced by pyrite and largely preserved as casts and molds. Unfortunately, the only identifiable taxa include *Mirifusus?* sp., *Parvicingula*(?) *jonesi*, and *Parvicingula* sp., indicating either an early Cretaceous (Berriasian) or late Jurassic (Tithonian) age.

Palynology

All core-catcher samples down through Sample 122-763B-24X-CC are barren of palynomorphs. Sample 122-763B-25X-CC contains few, poorly preserved dinoflagellates. Index species are absent although the presence of *Ascodinium parvum*, *Odontochitina operculata*, *Spiniferites ramosus*, and *Laciniadinium tenuistriatum* points to an age which possibly ranges from late Albian to early Cenomanian. Sample 122-763B-28X-CC contains few, poorly preserved specimens of *Spiniferites ramosus* and *Odontochitina operculata*. All other samples down through Sample 122-763B-38X-CC are barren.

Sample 122-763B-39X-CC contains only moderately to well-preserved dinoflagellates of the *Batiacasphaera* group; we found no other organic remains. This phenomenon could be interpreted as a dinoflagellate bloom or as an extreme marine environment, although not necessarily restricted marine.

The dinoflagellate assemblage from Cores 122-763B-43X through -47X suggests a Barremian to early Aptian age (*Muderongia testudinaria* to lower *Odontochitina operculata* Zone) indicated by *Herendeenia postprojecta*, *Muderongia australis*, *Circulodinium colliveri*, *Dingodinium cerviculum*, and *Epitricysta vinckensis*. The dinoflagellate assemblage of Sample 122-763B-48X-CC contains *Egmontodinium torynum*, *Scriniodinium attadalense*, *Oligosphaeridium* spp., and *Systematophora areolata*. The dominance of *Egmontodinium torynum* in this assemblage suggests that this sample belongs to the top of the *Egmontodinium torynum* Zone (early Valanginian).

Samples 122-763B-50X-CC through -54X-CC contain a palynomorph assemblage of poor to moderate preservation and diversity. Index species are mostly absent, although the presence of the *Meiourogonyaulax/Lithodinia* group, *Rigaudella* spp., and *Leptodinium eumorphum* suggests a late Berriasian to early Valanginian age (*Batioladinium reticulatum* to *Egmontodinium torynum* Zone). This interval is marked by a upward decrease in plant debris (cuticles and wood fragments), spores, and pollen grains.

Terrestrial organic material is likewise dominant in all core-catcher samples of Hole 763C. Dinoflagellate cysts are common, but most of the index species are absent. Although spores and pollen are present in each palynomorph assemblage they belong to a single zone, the *Cicatricosisporites australiensis* Zone (Helby et al., 1987), and are not discussed further. Using dinoflagellates Hole 763C was subdivided into three palynostratigraphic units, mainly on the basis of the occurrence of *Dissimulidinium lobispinosum* (total range from the base of *Dissimulidinium lobispinosum* to the middle *Batioladinium reticulatum* Zone):

1. Samples 122-763C-4R-CC through -9R-CC: *D. lobispinosum* is absent. The presence of *Leptodinium eumorphum*, *Leptodinium ambiguum*, and *Systematophora palmula* suggests that this interval belongs to the upper part of *Batioladinium reticulatum* Zone (late Berriasian).
2. Samples 122-763C-10R-CC through -37R-CC: The presence of *D. lobispinosum* indicates a middle to early late Berriasian age. Samples 122-763C-13R-CC through -16R-CC contain reworked upper Jurassic dinoflagellates (*Wanaea clathrata* and *Gonyaulacysta jurassic*). The palynomorphs of Sample 122-763C-37R-CC are dark colored and do not show fluorescence. Dinoflagellates constitute <1% of the assemblage. This points to restricted-marine and anoxic conditions.
3. Samples 122-763C-38R-CC through -46R-CC: The absence of *Dissimulidinium lobispinosum* suggests that this interval is middle Berriasian in age (*Cassiculosphaeridia del-*

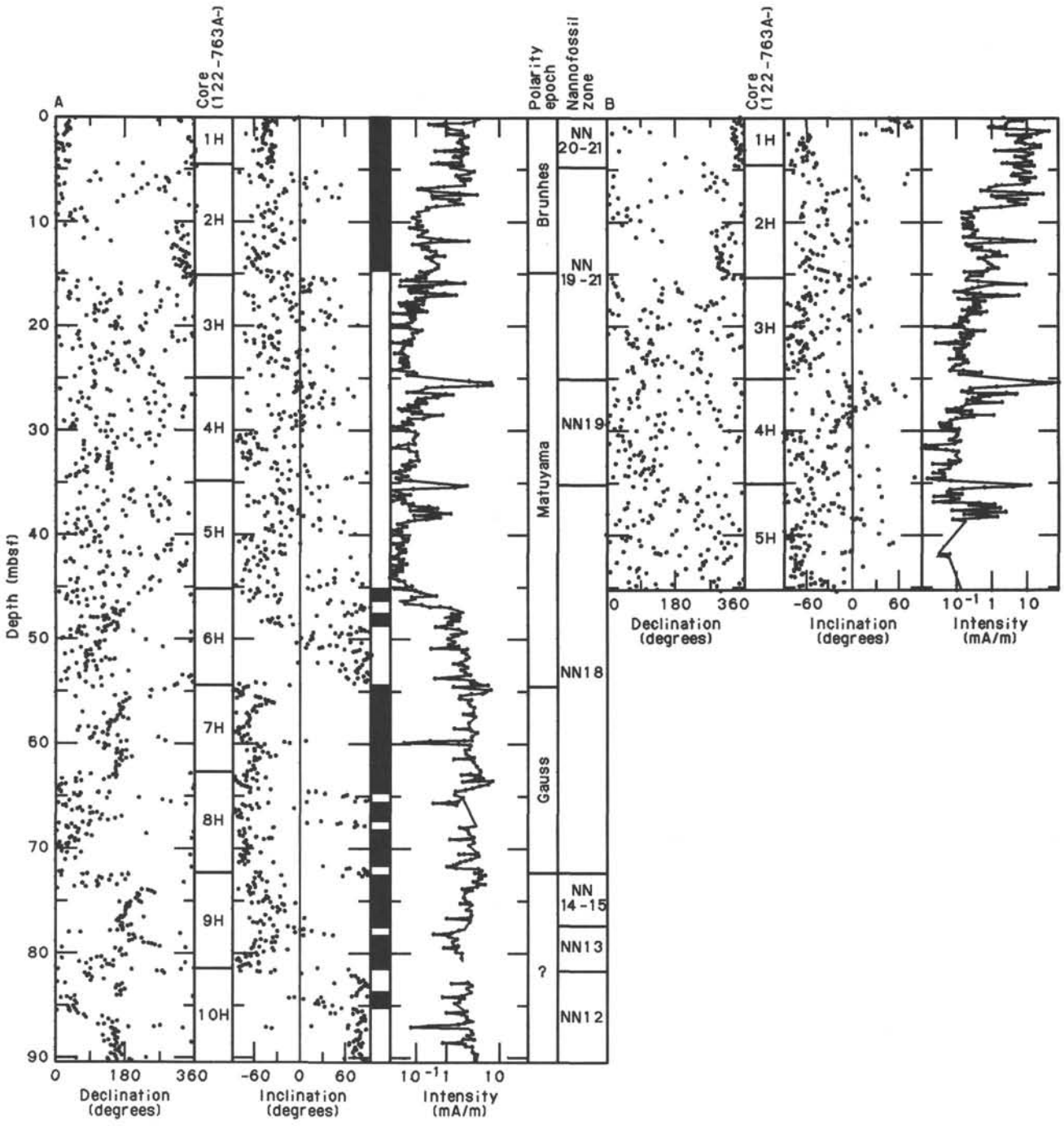

Figure 25. **A.** Paleomagnetic data after 9-mT demagnetization combined with biostratigraphic data for Cores 122-763A-1H through -10H. **B.** Natural remnant magnetism for Cores 122-763A-1H through -5H.

icata Zone). The abundance and diversity of the dinoflagellates are higher than in the interval above, and suggest "more normal marine" conditions.

Discussion

Correlation of Microfossil Ages

Site 763 is a prime example of a site where integrated microfossil biostratigraphy is essential for a number of reasons. The major one is the extremely diverse nature of the facies recovered; the various units contain completely different microfossil assemblages. Composite biostratigraphy is necessary to achieve sufficient stratigraphic resolution to investigate the numerous scientific objectives of the site. The following is a summary of a preliminary comparison of microfossil ages at Site 763.

There is a good agreement between calcareous nannofossil and foraminifer ages for the Cenozoic section of Holes 763A and 763B (Fig. 24). However, the placement of series boundaries determined from the two microfossil groups is quite different in numerous instances. This is probably a result of the preliminary stage of investigation of the two fossil groups, both with a limited sample set. Cretaceous foraminifer and calcareous nannofossil ages agree surprisingly well (compare

Fig. 23 and Table 2). The two microfossil groups appear to complement each other, offering superior resolution in different intervals (foraminifers from the upper Cenomanian to Coniacian and nannofossils in the Aptian-Albian). The use of both fossil groups may also help constrain the position of some of the more elusive stage boundaries, such as the Aptian/Albian and Turonian/Coniacian boundaries.

The age of Unit V (Muderong Shale equivalent) and Units VI and VII (Barrow Group equivalents) has been determined largely using nannofossils and dinoflagellates. Unit V is clearly of early Aptian age and Unit VI is Valanginian or late Berriasian, on the basis of both microfossil groups. Nannofossils, unlike dinoflagellates, indicate a significant stratigraphic break at the sequence boundary in Subunit VIB, and the ages obtained in Unit VII range from late Tithonian–middle Berriasian (calcareous nannofossils) to middle–late Berriasian (dinoflagellates). Because of the diverse and well-preserved nature of this latter group, dinoflagellate ages appear to be more reliable than nannofossil ages for the Barrow Group equivalent units. However, it is clear that other biostratigraphic studies may provide useful subsidiary information.

Summary

1. Site 763 recovered sediments ranging in age from middle Berriasian to Quaternary all of which are datable using microfossil biostratigraphy; different groups proved to be most effective in the various units. We used calcareous nannofossils and foraminifers to date the Aptian to Quaternary calcareous claystone, chalk, and ooze (Units I to IV). Using nannofossils and dinoflagellates we correlated Unit V (Muderong Shale equivalent) to the lower Aptian stage. Dinoflagellates and nannofossils gave age control in Units VI and VII (Barrow Group equivalents), middle Berriasian to Valanginian in age. Rare radiolarians are present throughout the section, but give secondary age control in several intervals.

2. We accurately dated several extensive hiatuses that dissect the lithologic column at Site 763. The major ones are middle Miocene, Campanian–middle Eocene, Hauterivian-Barremian, and late Berriasian in age. We also noted possible breaks in the Coniacian and middle Aptian. Interesting differences between the sedimentation history of Sites 762 and 763 will be investigated in detail during post-cruise studies. We made precise biostratigraphic and paleoenvironmental correlations to sequence stratigraphy.

3. The facies recovered at this site illustrate the complete evolution from a marginal, syn-rift environment to an open-ocean, post-rift setting). Biostratigraphy has enabled us to establish the timing of this evolution; microfossil assemblages (especially foraminifers) reflect the paleoenvironmental changes.

4. We recovered a nearly complete Cenomanian/Turonian boundary interval and a thick mid-Cretaceous sequence that will enable us to conduct detailed biostratigraphic and chemostratigraphic analysis of this interval.

5. Extremely well-preserved Neocomian dinoflagellate assemblages will lead to more detailed taxonomic and biostratigraphic studies of this fossil group.

PALEOMAGNETICS

Remanent Magnetization Measurements

We measured the natural remanent magnetization (NRM) of the archive halves of all cores from Site 763 at 10- or 15-cm intervals using the pass-through cryogenic magnetometer developed by 2-G Enterprises. All core sections underwent alternating-field (AF) demagnetization at 9 mT and were remeasured. The results of paleomagnetic measurements vary substantially for the various lithologies (and chronostratigraphic units) at this site; the following discussion of paleomagnetic results is organized on the basis of chronostratigraphic units.

Quaternary Sediments

Cores 122-763A-1H and -2H have NRM intensities about 1–10 mA/m, which falls to 0.5–1.5 mA/m after 9-mT alternating field treatment (Fig. 25A). These two first cores are of normal polarity and correspond to the upper part of the Brunhes Chronozone. Cores 122-763A-3H through -5H are very weakly magnetized: the NRM intensity ranges about 0.1–1 mA/m (near the noise level of the magnetometer) and the direction measurements are unreliable (Fig. 25B). Thus no magnetic-polarity sequence could be defined from these cores using the whole-core measurements. For this reason, our interpretation identifies the boundary between the Brunhes and Matuyama Chrons (0.73 Ma) only in Section 122-763A-2H-7 (14 mbsf).

Pliocene to Upper Eocene Sediments

Cores 122-763A-6H through 122-763B-7X are somewhat more magnetized, as the NRM intensities range from about 1 to 40 mA/m. The Reunion Subchron (2.01–2.14 Ma) occurs within Core 122-763A-6H (between 42.9 and 46.4 mbsf). We interpreted the Matuyama/Gauss boundary to lie at about 53.3 mbsf, within Section 122-763A-6H-1. According to this paleomagnetic result, the sedimentation rates during the Matuyama Chron would amount to about 22.2 m/m.y. We recognized the Kaena and Mammoth Subchrons within the normal Gauss Chron in Core 122-763A-8H at about 63.2 mbsf and 66.5 mbsf, respectively (Fig. 25A). Although the sediments from Cores 122-763A-9H through -21H provide a good magnetic-polarity sequence, the correlation of the observed polarity record with the geomagnetic reversal time scale (GRTS) (Haq et al., 1987) is difficult, even having the biostratigraphic control. This is because of the geomagnetic reversal frequency in this period and the low sedimentation rate during the Miocene and Oligocene at Site 763.

Upper Campanian Sediments

The upper Campanian chalk (Cores 122-763B-7X through -14X) are very weakly magnetized and it is difficult to recognize reversed or normal directions with the whole-core measurements. Thirty-eight discrete samples from Cores 122-763B-8X through -15X were measured with the Molspin magnetometer; the NRM intensity was low, around 0.1 mA/m. Thus none of these samples were demagnetized, but instead will be analyzed onshore using a cryogenic magnetometer. The NRM intensity was measurable in Core 122-763B-15X, and a transition from a reversed polarity to a normal polarity was observed at the base of this core (between Sections 122-763B-15X-2 and -15X-3). This transition could correspond to the Chron C33/C34 boundary.

Upper Santonian to Lower Cretaceous Sediments

The upper Santonian to upper Albian chalk has an NRM intensity of about 1 mA/m. The 9-mT AF demagnetization had little effect on the magnetization directions; all of this unit is of normal polarity and corresponds obviously to the normal-polarity Chron C34. The lower Albian to lower Cretaceous (upper Jurassic?) claystones have weak NRM intensity, ranging between 0.3 and 1.0 mA/m. We found several reversals in this unit. The first occurs at the base of Core 122-763B-44X (lower Aptian) and probably corresponds to the reversed-polarity zone at the top of Chronozone CM0. Thus, reversals occur until the base of Hole 763C and are part of the lower

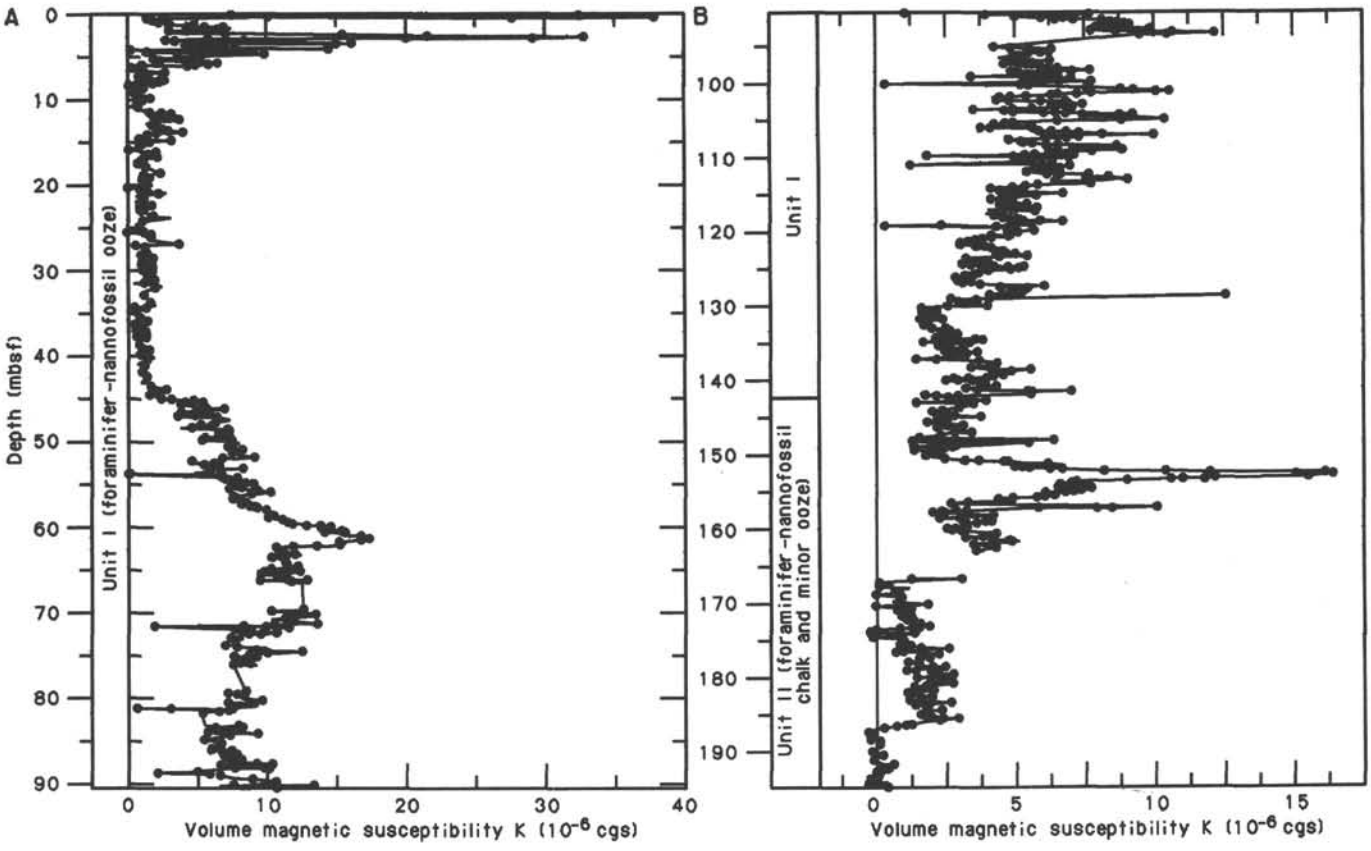

Figure 26. Whole-core-volume magnetic-susceptibility measurements plotted versus depth for Hole 763A. **A.** Cores 122-763A-1H through -10H. **B.** Cores 122-763A-11H through -21H.

Cretaceous–upper Jurassic M-sequence. However, given the poor preliminary shipboard biostratigraphic data from this clastic unit, no assignment to the geomagnetic reversal time scale (Haq et al., 1987) could be made as of this writing. Ninety-six discrete samples from Cores 122-763C-6R through -44R were measured with the Molspin magnetometer. The results agree with those obtained by the whole-core measurements, but given the weakness of NRM intensity, none of these samples was demagnetized. We plan to conduct further post-cruise studies of these samples using a cryogenic magnetometer.

Magnetic Susceptibility Measurements

The volume magnetic susceptibility of Hole 763A sediments was measured on the Bartington Instruments whole-core sensor at 0.1 sensitivity and low-frequency (0.47 kHz) settings. The average amplitude of the Hole 763A susceptibility variability is 2.5 to 15.0 $\times$ 10^{-6} cgs units (Fig. 26). Susceptibility values for the first five meters are very high (about 15.0 $\times$ 10^{-6} cgs). These high values were unexpected and their origin is unclear. They may be due to contamination by rust from the drill pipe. Between 5 and 45 mbsf the data are fairly featureless, with values in the range of 2 $\times$ 10^{-6} cgs units. There is a broad peak in the data extending from 45 to 90 mbsf. Base levels are around 10^{-5} cgs units with a maximum of 1.9 $\times$ 10^{-5} cgs units at 60 mbsf. The general rise in susceptibility parallels a change in color from white to light green-gray, and presumably records an increase in iron oxide content. Below 90 mbsf susceptibility values show many short high-amplitude changes, with an average value of approximately 5 $\times$ 10^{-6} cgs. The high value spikes may correspond to occurrences of pyrite. There is also some fine-scale structure in the record that is difficult to explain.

SEDIMENTATION RATES

Sedimentation rates for the Cenozoic stratigraphic section recovered from Holes 763A, 763B, and 763C are shown in Figure 27. Sedimentation rates of the Mesozoic are illustrated in Figure 28.

The errors involved in calculating sedimentation rates increase gradually with depth in the stratigraphic column. The errors are particularly significant for Unit VI (Barrow Group equivalent), whose position within the Berriasian and Valanginian stages is poorly known. For this unit the following assumptions were made: (1) the age of the base of Subunit VIC approximates the Tithonian/Berriasian boundary (133 Ma); (2) the top of Subunit VIC lies in the middle Berriasian (131.5 Ma); and (3) the age of Subunit VIA is from early to middle Valanginian (125–128 Ma). Even with these rather crude assumptions, obvious trends can be observed in the sedimentation-rate history of Site 763.

The methods used to calculate sedimentation rates are described in the "Explanatory Notes" chapter (this volume), including an extensive discussion of error estimation for the data points.

The highest sedimentation rates observed at Site 763 were within Unit VI (Barrow Group equivalent) where rates were on the order of 10 cm/k.y. (100 m/m.y.) (Fig. 28), and probably between 5 and 50 cm/k.y., allowing for error. Rates fell in Unit V (Muderong Shale equivalent interval) to about 2 cm/k.y. and for much of the middle Cretaceous remained between 1 and 2 cm/k.y., values which are typical for a hemipelagic

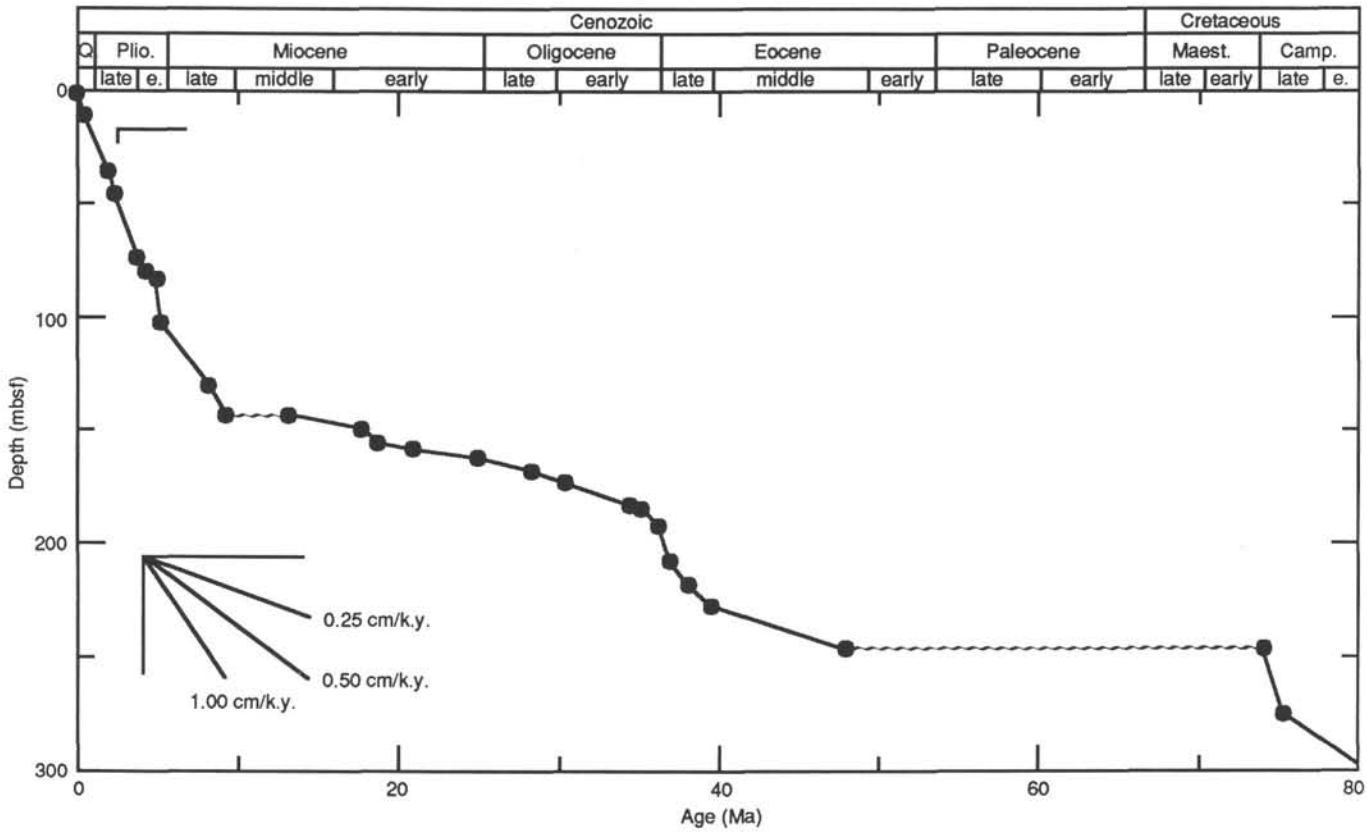

Figure 27. Sedimentation rates for the Cenozoic of Site 763. Hiatuses are indicated by wavy lines. Standard error bars for depth and age are shown at top left. The method of sedimentation-rate calculation is described in the "Explanatory Notes" chapter (this volume).

setting (Fig. 28). Sedimentation rates fell slightly in the Campanian (before the dramatic Cretaceous/Tertiary hiatus) to about 0.8 cm/k.y. The Cretaceous/Tertiary hiatus was followed by an interval of very slow sedimentation (0.1–0.3 cm/k.y.) in the middle Eocene, followed by an interval of more typical pelagic sedimentation rates, on the order of 1 cm/k.y. in the late Eocene (Fig. 27). Sedimentation in the Oligocene and early Miocene was very slow prior to the middle Miocene hiatus, on the order of 0.2 cm/k.y. (Fig. 27). Pelagic sedimentation rates picked up dramatically after the hiatus, rising to 1 cm/k.y. in the late Miocene, and were relatively high from the late Miocene to Quaternary, averaging about 1.5 cm/k.y. These high rates probably reflect the uncompacted nature of the sediment column.

In summary, sedimentation rates fell dramatically from the Berriasian to Aptian. This change is probably the result of subsidence of the Exmouth Plateau and a change in the sediment supply as deposition at Site 763 changed from nearshore continental margin to hemipelagic sedimentation. Hemipelagic sedimentation rates characterized the remainder of the Mesozoic, whereas pelagic rates characterized the Cenozoic. This gradual transition was interrupted by several hiatuses and condensed intervals.

ORGANIC GEOCHEMISTRY

Shipboard organic geochemical analyses at Site 763 consisted of 330 determinations of inorganic carbon, 268 Rock-Eval and total organic carbon (TOC) analyses, 206 measurements of low-molecular-weight hydrocarbons, and 2 determinations of high-molecular-weight hydrocarbons. The procedures used for these determinations are outlined in the "Explanatory Notes" chapter (this volume) and are described in detail by Emeis and Kvenvolden (1986).

Inorganic and Organic Carbon

Results of analyses of inorganic carbon in samples from Holes 763A, 763B, and 763C are listed in Table 3. Calculated estimates of percentages of calcium carbonate are given, assuming that the inorganic carbon is made up totally of calcite. These calcium carbonate estimates are displayed in Figure 29 relative to the lithostratigraphic units for Site 763. The three upper units (0–385 mbsf) are made up of calcareous oozes and chalks. Below ca. 570 mbsf, few carbonate-rich rocks occur in Units V, VI, and VII. Between 385 and 570 mbsf, calcareous claystones containing 30%–40% $CaCO_3$ constitute Unit IV. Organic carbon percentages are low in the carbonate units but increase somewhat in the lower two units (the bottom 465 m of the sequence) to range between 0.2% and 1.5% sample dry weight. Figure 30 shows the distribution of total organic carbon (TOC) in Units IV, V, VI, and VII. The deeper units clearly contain the most organic matter.

Highest concentrations of organic carbon in Site 763 rocks are found in two thin (3 cm and 10 cm) layers of Cenomanian black shale in Section 122-763C-2R-1. Samples from these layers contain ca. 9% and 15% TOC, respectively.

Rock-Eval Pyrolysis

The results of Rock-Eval pyrolysis and TOC analysis of samples from Holes 763A, 763B, and 763C are listed in Table 4. In samples from the uppermost 350 m, pyrolysis yields and TOC contents are very low (generally less than 0.30% and 0.15%, respectively). Because of these low values, all param-

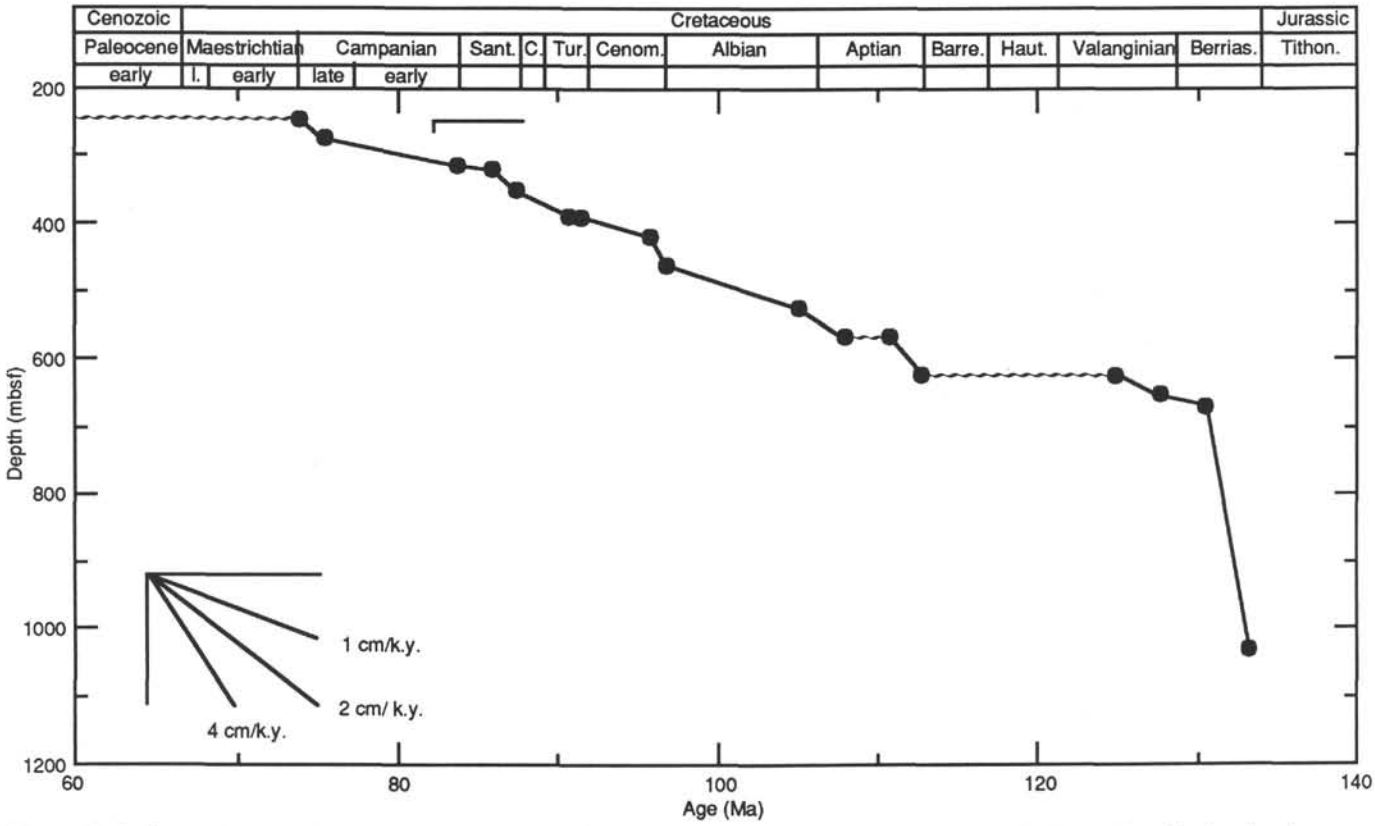

Figure 28. Sedimentation rates for the Mesozoic of Site 763. Hiatuses are indicated by wavy lines. Standard error bars for depth and age are shown at top left. The method of sedimentation-rate calculation is described in the "Explanatory Notes" chapter (this volume).

eters which are derived from them as ratios, such as PI (production index), HI (hydrogen index), and OI (oxygen index), cannot be considered as reliable. Similarly, the pyrolyzable hydrocarbon yield (S_2) is too small and variable to provide a truly meaningful T_{max} determination.

In the clastic-dominated sequences of Hole 763C (below about 350 mbsf), the pyrolysis yields and TOC contents are higher, and we interpret the Rock-Eval results with some confidence. Organic matter from Hole 763C is of type III (Fig. 31) and was probably derived from land plants. These rocks are from distal portions of the Muderong Shale equivalent (Unit V) and the Barrow Group equivalent (Unit VI and VII). Similar results were noted for Site 762 ("Summary and Conclusions," Site 762 chapter, this volume).

Although most of the TOC concentrations in the bottom of Hole 763C are <1% of sample dry weight, many samples, especially from Units V, VI, and VII, have values ranging up to about 1.5% (Fig. 30). The very dark to black color of the cores indicates the presence of relatively large amounts of finely dispersed metal sulfides (e.g., pyrite) rather than the presence of organic matter. Even so, organic carbon concentrations are significantly higher here than in the upper parts of this site.

T_{max} values for Unit V and uppermost Unit VI range from about 415°C to 425°C, whereas there is a clear maturation gradient from about 425°C to 433°C through Units VI and VII (Table 4). These values are equivalent to a vitrinite reflectance range from about 0.4% to 0.5% R_o in Unit V to about the equivalent of 0.65% R_o at the bottom of Hole 763C. This interpreted level of thermal maturation is consistent with the occurrence of higher molecular weight hydrocarbon gases (C_2–C_4) (Powell, 1978) as indigenous products of catagenesis observed in the headspace gas (Table 5). The level of maturity inferred from the Rock-Eval pyrolysis data at Site 763 is somewhat higher than for the approximately equivalent section at Site 762 (Site 762 chapter, this volume). This observation indicates that erosion has occurred and/or the heat flow has been higher at Site 763 than at Site 762.

Low-Molecular-Weight Hydrocarbons

A total of 117 samples from Holes 763A, 763B, and 763C were analyzed for low-molecular-weight hydrocarbons by the headspace procedure. High concentrations of headspace methane (up to 85,000 ppm) were noted over the interval between about 300 and 600 mbsf in Holes 763B and 763C and at around 1030 mbsf in Hole 763C (Table 6). Except for the lowermost samples in Hole 763C (Units VI and VII, equivalent to the Barrow Group just above the Dingo Claystone), the gas was quite dry, with the methane/ethane ratio between 5,000 and 10,000. The cores most rich in gas expanded somewhat after they arrived on deck, developing gas-filled voids. Vacutainer samples taken through the core liner of the gas from the expansion voids yielded from 20% to 90% methane by volume, with very high C_1/C_2 ratios (ca. 10,000). High C_1/C_2 values are usually interpreted as indicative of biogenic gas (cf. Claypool and Kvenvolden, 1983), yet they can equally well indicate a thermogenic origin from gas-prone organic matter (Hunt, 1979, p.438).

Important changes occur in gas concentrations and compositions at ca. 600 mbsf in Hole 763C (Fig. 32). Concentrations start to diminish and ratios of C_1/C_2 begin to drop. Eighty-nine headspace gas samples were analyzed from throughout Holes 763A, 763B, and 763C using the Hewlett-Packard 5890 Natural Gas Analyzer. The results from five of

Table 3. Concentrations of inorganic carbon, calcium carbonate, and total organic carbon (TOC) in samples from Holes 763A, 763B, and 763C. Inorganic carbon concentrations were measured coulometrically. Calcium carbonate percentages were calculated assuming the carbonate contents to be pure calcite. TOC values were determined by Rock-Eval analysis. All percentages are on a whole sediment, dry-weight basis.

Core, section interval (cm)	Depth (mbsf)	Wt. (mg)	Inorganic carbon (%)	$CaCO_3$ (%)	TOC (%)
Unit I: Quaternary to upper Miocene foraminifer-nannofossil ooze					
122-763A-					
1H-1, 7–9	0.07	21.35	9.18	76.4694	
1H-3, 8–10	3.08	23.78	10.34	86.1322	0.06
2H-2, 8–10	6.48	23.47	10.53	87.7149	
2H-4, 8–10	9.48	21.66	10.28	85.6324	
2H-6, 8–10	12.48	20.06	9.88	82.3004	0.04
3H-2, 8–10	15.98	30.16	10.07	83.8831	
3H-4, 8–10	18.98	29.92	9.84	81.9672	
3H-6, 8–10	21.98	22.23	9.67	80.5511	0.02
4H-2, 8–10	25.48	20.48	9.38	78.1354	
4H-4, 56–59	28.96	21.44	10.06	83.7998	
4H-6, 47–49	31.87	24.63	9.93	82.7169	0.19
5H-2, 47–50	35.37	22.18	10.02	83.4666	
5H-4, 36–39	38.26	21.04	10.02	83.4666	
5H-6, 59–62	41.49	23.21	10.03	83.5499	0.05
6H-2, 48–50	44.88	27.81	9.75	81.2175	
6H-4, 52–54	47.92	22.82	10.40	86.6320	
6H-6, 53–55	50.93	31.35	9.85	82.0505	0.05
7H-2, 50–52	54.40	23.03	9.94	82.8002	
7H-4, 50–52	57.40	26.37	10.17	84.7161	
7H-6, 50–52	60.40	20.86	9.58	79.8014	0.02
8H-2, 52–55	63.92	25.83	10.14	84.4662	
8H-4, 58–60	66.98	23.66	9.97	83.0501	
8H-6, 52–55	69.92	25.65	9.87	82.2171	0.01
9H-2, 90–95	73.80	23.32	9.95	82.8835	
9H-4, 93–95	76.83	21.13	10.12	84.2996	
9H-6, 93–95	79.83	21.36	10.30	85.7990	
10H-2, 90–95	83.30	19.13	10.14	84.4662	0.01
10H-4, 91–94	86.31	19.38	10.41	86.7153	
10H-6, 90–93	89.30	19.20	10.24	85.2992	0.04
11H-2, 100–102	92.90	19.39	10.36	86.2988	
11H-4, 93–95	95.83	19.74	10.82	90.1306	
11H-6, 93–95	98.83	19.45	10.64	88.6312	0.05
12H-2, 92–94	102.32	21.10	10.68	88.9644	
12H-4, 93–95	105.33	19.54	11.01	91.7133	
12H-6, 93–95	108.33	22.30	10.22	85.1326	0.03
13H-2, 92–93	111.82	19.98	10.84	90.2972	
13H-4, 92–95	114.82	19.74	10.86	90.4638	
13H-6, 92–95	117.82	26.54	11.05	92.0465	0.03
14H-2, 99–101	121.39	27.46	11.20	93.2960	
14H-4, 7–9	123.47	22.81	10.90	90.7970	
14H-6, 7–9	126.47	20.29	10.91	90.8803	0.01
15H-2, 11–14	130.01	20.08	11.18	93.1294	
15H-4, 6–8	132.96	24.75	11.11	92.5463	
15H-6, 92–94	136.82	20.95	10.83	90.2139	0.00
16H-2, 94–96	140.34	21.39	10.78	89.7974	
Unit II: lower Miocene to middle Eocene foraminifer-nannofossil chalk					
16H-4, 95–97	143.35	23.87	10.52	87.6316	
16H-6, 5–7	145.45	24.44	11.10	92.4630	0.01
17H-2, 81–83	149.71	30.36	10.75	89.5475	
17H-4, 84–86	152.74	33.51	8.01	66.7233	
17H-6, 87–89	155.77	19.98	9.90	82.4670	0.00
18H-2, 89–91	159.29	19.85	10.69	89.0477	
18H-4, 97–99	162.37	19.50	10.60	88.2980	
18H-6, 88–90	165.28	19.62	10.80	89.9640	0.03
19H-2, 52–54	168.42		10.59	88.2147	
19H-4, 69–71	171.59		9.92	82.6336	
19H-6, 103–105	174.93		9.29	77.3857	0.09
20H-2, 48–50	177.88		9.71	80.8843	
20H-4, 24–26	180.64		9.93	82.7169	
20H-6, 56–58	183.96		10.11	84.2163	0.13
21H-2, 55–57	187.45		11.00	91.6300	
21H-4, 55–57	190.45		10.47	87.2151	
21H-6, 53–55	193.43		10.83	90.2139	0.02
122-763B-					
2X-4, 15–17	190.05	19.47	10.79	89.8807	0.00
2X-2, 15–17	191.65	20.71	10.74	89.4642	
3X-2, 10–12	196.50	22.26	10.37	86.3821	
3X-4, 84–86	200.24	20.65	10.54	87.7982	0.00
3X-6, 5–7	202.45	20.40	10.77	89.7141	
4X-2, 106–108	206.96	19.76	10.53	87.7149	
4X-3, 26–28	207.66	20.15	10.66	88.7978	0.02
5X-2, 96–98	216.36	30.31	10.77	89.7141	
5X-4, 16–18	218.56	20.04	10.45	87.0485	0.01
6X-2, 84–87	225.74	20.49	10.19	84.8827	
6X-4, 55–58	228.45	19.69	10.69	89.0477	0.02
6X-6, 27–30	231.17	21.49	10.58	88.1314	
7X-2, 57–54	234.97	20.06	10.65	88.7145	0.01
Unit III: upper Campanian to Turonian greenish chalk					
8X-11, 101–102	243.41	20.20	8.02	66.8066	
8X-1, 102–103	243.42	19.68	9.68	80.6344	
8X-2, 42–44	244.32	21.02	9.04	75.3032	
8X-4, 42–44	247.32	20.88	8.72	72.6376	0.27
8X-11, 101–102	253.60	19.92	9.42	78.4686	
9X-4, 20–22	256.60	19.87	9.40	78.3020	0.03
9X-6, 20–22	259.60	20.74	9.23	76.8859	
10X-2, 24–27	263.14	20.21	10.17	84.7161	
10X-4, 21–24	266.11	30.25	9.84	81.9672	0.02
10X-6, 23–26	269.13	19.16	9.50	79.1350	
11X-2, 21–23	272.61	21.26	10.29	85.7157	
11X-4, 32–34	275.72	22.01	10.73	89.3809	0.04
12X-2, 24–27	282.14	30.80	10.63	88.5479	
12X-4, 23–21	285.13	17.57	10.37	86.3821	0.02
13X-4, 91–93	295.31	20.83	10.26	85.4658	0.03
13X-6, 20–22	297.60	19.10	11.20	93.2960	
14X-2, 89–90	301.79	28.89	10.63	88.5479	
14X-4, 8–10	303.98	17.62	10.91	90.8803	0.01
14X-5, 67–69	306.07	20.04	11.01	91.7133	
15X-2, 85–88	311.25	22.03	10.09	84.0497	
15X-2, 95–97	311.35	30.10	10.76	89.6308	
15X-4, 10–12	313.50	23.03	10.76	89.6308	0.00
15X-6, 132–134	317.72	23.13	10.96	91.2968	
15X-6, 136–138	317.76	27.44	10.97	91.3801	
16X-2, 125–127	321.15	18.85	10.71	89.2143	
16X-4, 72–74	323.62	28.34	10.70	89.1310	
16X-6, 23–25	326.13	23.78	10.50	87.4650	
17X-2, 67–69	330.07	24.38	10.76	89.6308	0.00
17X-5, 96–98	334.86	20.14	9.15	76.2195	
18X-1, 126–128	338.66	18.03	10.15	84.5495	
18X-3, 11–13	340.51	20.07	10.42	86.7986	
18X-5, 17–18	343.57	19.60	8.88	73.9704	0.02
19X-2, 70–72	349.10	19.24	10.05	83.7165	
19X-3, 130–132	351.20	19.87	8.81	73.3873	
19X-4, 67–68	352.07	20.27	10.43	86.8819	
19X-4, 137–140	352.77	18.08	9.89	82.3837	
19X-6, 4–6	354.44	23.92	8.24	68.6392	0.09
20X-1, 2–3	356.42	18.33	7.95	66.2235	
20X-1, 74–76	357.14	24.08	10.01	83.3833	
20X-1, 138–140	357.78	19.50	10.08	83.9664	
20X-3, 2–3	359.42	19.15	10.36	86.2988	
20X-3, 7–9	359.47	18.73	10.21	85.0493	0.06
21X-1, 44–46	366.34	21.20	9.31	77.5523	
21X-3, 8–9	368.98	19.88	6.45	53.7285	
21X-3, 26–28	369.16	22.61	6.03	50.2299	0.03
22X-1, 35–37	375.75	22.75	9.07	75.5531	
22X-3, 34–36	378.74	20.08	6.84	56.9772	0.20
23X-1, 48–50	385.38	27.90	7.36	61.3088	
Unit IV: upper Cenomanian to middle Aptian calcareous claystone					
23X-5, 16–18	391.06	18.69	7.10	59.1430	0.20
24X-2, 40–42	396.30	26.49	6.15	51.2295	
24X-4, 145–147	400.35	21.79	6.10	50.8130	
24X-6, 36–38	402.26	21.86	5.46	45.4818	0.31
25X-3, 105–107	407.95	26.06	3.09	25.7397	
25X-5, 18–19	410.08	17.93	4.01	33.4033	
25X-5, 105–107	410.95	22.73	2.96	24.6568	0.18
26X-1, 20–21	413.60	19.48	3.08	25.6564	
26X-1, 38–40	413.78	38.24	3.63	30.2379	0.26
26X-2, 20–21	415.10	19.86	3.20	26.6560	
26X-3, 38–40	416.78	20.21	5.16	42.9828	
27X-2, 64–66	425.04	37.07	3.89	32.4037	

Table 3 (continued).

Core, section interval (cm)	Depth (mbsf)	Wt. (mg)	Inorganic carbon (%)	$CaCO_3$ (%)	TOC (%)
27X-2, 132–133	425.72	16.52	4.32	35.9856	
27X-4, 7–9	427.47	28.15	4.14	34.4862	0.23
28X-2, 30–32	434.20	18.61	4.85	40.4005	
28X-3, 78–79	436.18	19.37	4.59	38.2347	
28X-3, 144–145	436.84	20.33	5.00	41.6500	
28X-4, 54–56	437.44	27.19	5.34	44.4822	
28X-6, 40–42	440.30	25.35	4.94	41.1502	0.28
29X-2, 86–88	444.26	28.69	4.66	38.8178	
29X-4, 68–70	447.08	21.40	5.36	44.6488	
29X-6, 76–79	450.16	21.51	4.90	40.8170	0.26
30X-2, 10–12	453.00	19.19	4.37	36.4021	
30X-4, 100–103	456.90	22.49	4.43	36.9019	0.17
30X-6, 62–64	459.52	22.26	4.82	40.1506	
31X-1, 65–68	461.55	21.19	3.47	28.9051	
31X-1, 136–137	462.26	20.02	3.78	31.4874	
31X-4, 134–136	466.74	18.89	3.51	29.2383	
31X-6, 42–44	468.82	22.36	3.21	26.7393	0.22
32X-2, 95–97	472.85	19.50	5.01	41.7333	
32X-3, 133–134	474.73	20.21	5.58	46.4814	
32X-4, 46–48	475.36	20.01	6.88	57.3104	0.13
32X-6, 82–84	478.72	32.12	2.95	24.5735	
33X-2, 95–97	482.35	31.08	4.20	34.9860	
33X-4, 80–82	485.20	21.27	3.49	29.0717	0.07
33X-6, 71–73	488.11	23.26	4.10	34.1530	
34X-1, 72–73	490.12	22.56	5.88	48.9804	
34X-3, 120–122	493.60	21.07	4.33	36.0689	
35X-2, 113–115	501.53	20.74	7.14	59.4762	
35X-4, 45–47	503.85	26.24	4.04	33.6532	
35X-6, 22–24	506.62	20.69	3.27	27.2391	0.05
36X-1, 23–25	508.63	22.30	4.11	34.2363	
36X-3, 103–105	512.43	32.35	3.23	26.9059	
36X-5, 67–69	515.07	26.35	5.50	45.8150	0.07
36X-7, 9–11	517.49	20.51	5.21	43.3993	
37X-1, 110–112	519.00	19.50	4.73	39.4009	
37X-3, 135–137	522.25	27.47	8.97	74.7201	
37X-5, 32–34	524.22	23.01	7.68	63.9744	0.07
38X-1, 4–6	527.44	23.87	3.59	29.9047	
38X-1, 79–81	528.19	23.92	6.42	53.4786	0.14
39X-1, 6–7	536.96	20.20	5.28	43.9824	
39X-1, 77–79	537.67	28.45	6.77	56.3941	
39X-2, 7–9	538.47	26.51	1.94	16.1602	0.06
40X-1, 90–91	547.30	20.19	5.34	44.4822	
40X-2, 111–113	549.01	24.11	3.21	26.7393	0.31
41X-1, 55–57	556.45	30.31	0.10	0.8330	0.16
41X-1, 96–97	556.86	27.58	2.09	17.4097	
41X-CC, 38–39	564.01	36.74	4.98	41.4834	
122-763C-					
2R-1, 107–109	386.07	39.36	5.59	46.5647	0.16
2R-3, 76–78	388.76	27.35	5.04	41.9832	0.18
2R-5, 28–30	391.28	21.60	5.38	44.8154	
Unit V: lower Aptian black silty claystone					
122-763B-					
42X-2, 33–35	567.23	23.82	0.05	0.4165	
42X-4, 44–46	570.34	27.38	1.91	15.9103	0.20
42X-6, 35–39	573.25	23.64	0.16	1.3328	0.10
43X-2, 39–41	576.79	37.55	10.41	86.7153	0.08
43X-2, 105–107	577.45	22.26	1.03	8.5799	0.34
44X-2, 34–36	586.24	22.73	0.48	3.9984	0.30
44X-4, 67–68	589.57	20.88	0.74	6.1642	0.54
44X-6, 67–68	592.57	28.29	0.72	5.9976	0.58
45X-1, 59–61	594.49	31.34	0.41	3.4153	1.04
47X-3, 47–49	597.37	29.71	0.39	3.2487	0.82
45X-4, 13–15	598.53	22.37	0.22	1.8326	1.83
49X-1, 94–96	604.84	19.15	8.94	74.4702	0.38
48X-5, 24–25	605.14	23.91	0.09	0.7497	1.23
48X-5, 81–84	605.71	19.63	8.35	69.5555	0.50
49X-3, 108–110	607.98	32.09	0.25	2.0825	0.76
49X-3, 135–137	608.25	25.81	8.33	69.3889	0.60
46X-4, 59–61	608.49	24.71	0.15	1.2495	1.77

Table 3 (continued).

Core, section interval (cm)	Depth (mbsf)	Wt. (mg)	Inorganic carbon (%)	$CaCO_3$ (%)	TOC (%)
49X-4, 61–63	609.01	26.19	0.12	0.9996	1.16
50X-2, 8–10	610.48	23.10	0.32	2.6656	0.90
46X-6, 93–95	611.83	37.56	0.08	0.6664	0.87
51X-2, 66–68	616.06	26.74	0.13	1.0829	0.81
50X-5, 146–148	616.36	43.99	0.24	1.9992	1.02
50X-6, 6–8	616.46	32.72	0.21	1.7493	1.01
51X-4, 66–68	619.06	24.07	0.15	1.2495	0.75
47X-2, 61–63	619.61	20.59	2.57	21.4081	0.96
53X-1, 32–34	647.82	25.25	7.98	66.4734	0.57
54X-1, 39–41	648.89	32.86	7.89	65.7237	0.52
122-763C-					
4R-1, 42–44	645.52	18.99	7.82	65.1406	
5R-1, 53–55	655.13	34.66	0.24	1.9992	0.96
6R-1, 112–114	661.72	41.76	0.10	0.8330	0.84
6R-2, 88–91	662.98	40.50	8.80	73.3040	0.37
6R-3, 23–25	663.83	40.42	0.37	3.0821	0.73
7R-1, 134–136	666.94	47.97	0.19	1.5827	1.07
Unit VII: Berriasian dark gray clayey siltstone					
8R-1, 24–26	670.84	45.81	0.23	1.9159	1.92
8R-1, 64–66	671.24	43.20	7.97	66.3901	0.67
8R-3, 26–28	673.86	49.25	0.38	3.1654	1.57
9R-2, 120–122	678.30	44.08	0.46	3.8318	1.04
9R-4, 64–66	680.74	44.67	0.73	6.0809	0.67
9R-4, 80–82	680.90	44.65	7.86	65.4738	0.37
9R-5, 1–2	681.61	38.21	0.89	7.4137	0.62
10R-2, 128–130	687.88	43.64	0.46	3.8318	0.84
10R-4, 49–51	690.09	45.92	0.56	4.6648	0.80
10R-6, 50–52	693.10	57.74	0.49	4.0817	0.78
10R-7, 65–67	694.75	35.09	7.37	61.3921	0.43
11R-2, 5–7	696.15	53.00	0.09	0.7497	0.89
12R-1, 15–17	704.25	45.93	4.74	39.4842	0.02
12R-2, 14–16	705.74	42.77	0.27	2.2491	0.80
13R-1, 98–100	714.58	45.57	0.99	8.2467	0.74
13R-3, 20–23	716.80	53.08	7.51	62.5583	0.27
13R-5, 47–49	720.07	50.97	0.44	3.6652	0.90
14R-2, 42–44	725.02	43.01	0.60	4.9980	0.90
14R-3, 118–120	727.28	52.38	7.85	65.3905	0.27
14R-4, 24–26	727.84	47.32	0.48	3.9984	0.97
15R-2, 24–26	734.34	58.84	0.64	5.3312	0.76
15R-3, 2–4	735.62	41.98	0.34	2.8322	0.87
16R-2, 46–48	744.06	43.97	0.73	6.0809	0.60
16R-3, 37–39	745.47	41.93	0.21	1.7493	0.90
16R-4, 10–13	746.70	44.51	0.25	2.0825	0.97
16R-5, 10–13	748.20	44.66	0.28	2.3324	0.82
16R-6, 101–103	750.61	57.96	0.50	4.1650	0.78
17R-2, 87–89	753.97	42.47	0.76	6.3308	0.79
17R-4, 6–8	756.16	42.57	1.55	12.9115	0.90
18R-1, 48–52	761.58	42.01	0.59	4.9147	0.63
18R-3, 99–103	765.09	44.96	0.49	4.0817	0.63
18R-4, 109–113	766.69	41.28	0.36	2.9988	0.76
19R-1, 57–59	771.17	44.29	5.96	49.6468	0.33
19R-3, 33–35	773.93	43.85	0.29	2.4157	0.81
19R-5, 13–15	776.73	44.18	0.24	1.9992	0.79
20R-1, 77–79	780.87	48.75	4.56	37.9848	0.01
20R-2, 94–96	782.54	44.63	0.17	1.4161	0.80
20R-4, 101–103	785.61	46.49	0.51	4.2483	0.85
21R-2, 102–104	792.12	45.79	0.65	5.4145	0.86
21R-4, 64–66	794.74	44.37	0.58	4.8314	0.78
21R-6, 28–29	797.38	39.57	0.28	2.3324	
21R-6, 81–83	797.91	42.32	0.32	2.6656	0.61
22R-1, 113–115	800.23	42.25	1.02	8.4966	0.68
22R-3, 28–30	802.38	43.92	0.73	6.0809	0.66
22R-5, 106–108	806.16	35.48	0.52	4.3316	0.65
22R-6, 5–7	806.65	35.76	0.17	1.4161	0.60
23R-2, 42–44	810.52	39.38	0.68	5.6644	0.78
23R-2, 95–97	811.05	62.06	3.83	31.9039	0.03
23R-4, 53–55	813.63	36.67	0.67	5.5811	0.77
23R-5, 27–29	814.87	26.71	0.12	0.9996	0.91
24R-2, 20–22	819.80	26.98	3.06	25.4898	0.75
24R-4, 70–72	823.30	33.09	0.46	3.8318	0.94

Table 3 (continued).

Core, section interval (cm)	Depth (mbsf)	Wt. (mg)	Inorganic carbon (%)	$CaCO_3$ (%)	TOC (%)
24R-6, 60–64	826.20	36.48	0.35	2.9155	0.84
25R-6, 43–45	835.53	26.62	0.23	1.9159	1.32
26R-1, 62–64	837.72	38.77	7.04	58.6432	0.33
26R-3, 54–56	840.64	37.19	0.40	3.3320	1.01
26R-5, 22–25	843.32	37.91	0.50	4.1650	
27R-1, 8–10	846.68	34.68	0.40	3.3320	0.81
27R-3, 90–92	850.50	31.53	0.72	5.9976	0.96
27R-5, 128–130	853.88	29.40	0.25	2.0825	0.84
28R-2, 27–30	857.87	27.36	1.15	9.5795	1.11
28R-4, 7–10	860.67	35.84	0.27	2.2491	1.00
28R-6, 85–87	864.45	41.51	0.41	3.4153	0.98
29R-1, 68–70	866.28	31.58	0.23	1.9159	0.89
29R-3, 37–39	868.97	39.03	0.14	1.1662	0.83
29R-5, 94–97	872.54	30.81	8.06	67.1398	0.29
30R-2, 102–104	877.62	44.99	0.21	1.7493	1.26
30R-4, 134–136	880.94	39.05	0.59	4.9147	0.99
30R-6, 112–114	883.72	40.57	0.57	4.7481	1.06
31R-2, 113–116	887.23	36.79	0.26	2.1658	1.01
31R-4, 70–72	889.80	32.58	0.32	2.6656	0.98
31R-6, 86–88	892.96	32.55	0.48	3.9984	0.93
32R-3, 128–130	898.38	40.26	0.60	4.9980	0.97
32R-5, 44–46	900.54	43.29	0.96	7.9968	1.05
32R-7, 26–28	903.36	46.62	0.14	1.1662	1.09
33R-2, 137–139	906.47	44.19	0.50	4.1650	0.96
33R-4, 87–89	908.97	49.27	0.30	2.4990	1.48
34R-3, 8–10	916.18	37.65	0.18	1.4994	1.23
34R-5, 41–43	919.51	35.08	1.92	15.9936	0.80
35R-1, 24–26	922.84	59.15	0.42	3.4986	1.11
35R-3, 23–25	925.83	54.01	0.96	7.9968	
35R-5, 147–149	930.07	47.70	0.35	2.9155	1.16
36R-3, 117–119	936.27	67.99	0.42	3.4986	1.37
36R-5, 112–114	939.22	70.50	0.33	2.7489	1.33
36R-6, 48–50	940.08	48.13	0.26	2.1658	1.13
37R-1, 142–144	943.02	43.95	0.23	1.9159	0.79
37R-2, 126–128	944.36	53.16	0.38	3.1654	1.36
37R-3, 130–132	945.90	54.78	0.19	1.5827	0.67
37R-6, 63–65	949.73	37.85	0.31	2.5823	0.89
38R-1, 133–135	952.43	52.41	0.51	4.2483	0.82
38R-3, 143–145	955.53	42.31	0.32	2.6656	
38R-5, 55–57	957.65	45.63	0.47	3.9151	
38R-6, 52–54	959.12	39.23	0.49	4.0817	
39R-2, 108–110	963.18	48.09	0.42	3.4986	
39R-4, 22–24	965.32	42.58	0.47	3.9151	1.04
39R-6, 12–14	968.22	41.10	0.56	4.6648	
40R-2, 88–90	972.48	49.51	0.48	3.9984	
41R-2, 108–110	982.18	40.00	0.44	3.6652	
41R-4, 81–83	984.91	48.05	0.53	4.4149	
41R-6, 73–75	987.83	43.30	0.30	2.4990	
42R-1, 39–40	989.49	67.16	0.32	2.6656	
42R-3, 67–70	992.77	47.84	0.30	2.4990	
42R-5, 57–58	995.67	55.82	0.55	4.5815	1.04
43R-2, 72–75	1000.82	60.53	0.23	1.9159	
43R-4, 3–5	1003.13	45.88	0.51	4.2483	0.83
43R-5, 115–118	1005.75	60.92	0.55	4.5815	
44R-2, 95–97	1010.55	40.38	0.54	4.4982	
44R-4, 2–4	1012.62	43.57	0.26	2.1658	0.85
44R-6, 55–57	1016.15	55.77	0.62	5.1646	
45R-2, 138–140	1020.48	59.66	0.27	2.2491	
45R-4, 12–15	1022.22	47.91	0.28	2.3324	1.42
45R-6, 113–115	1026.23	56.31	0.28	2.3324	1.03
46R-2, 60–62	1029.20	66.72	0.50	4.1650	0.90
46R-4, 119–121	1032.79	71.65	0.62	5.2446	1.14

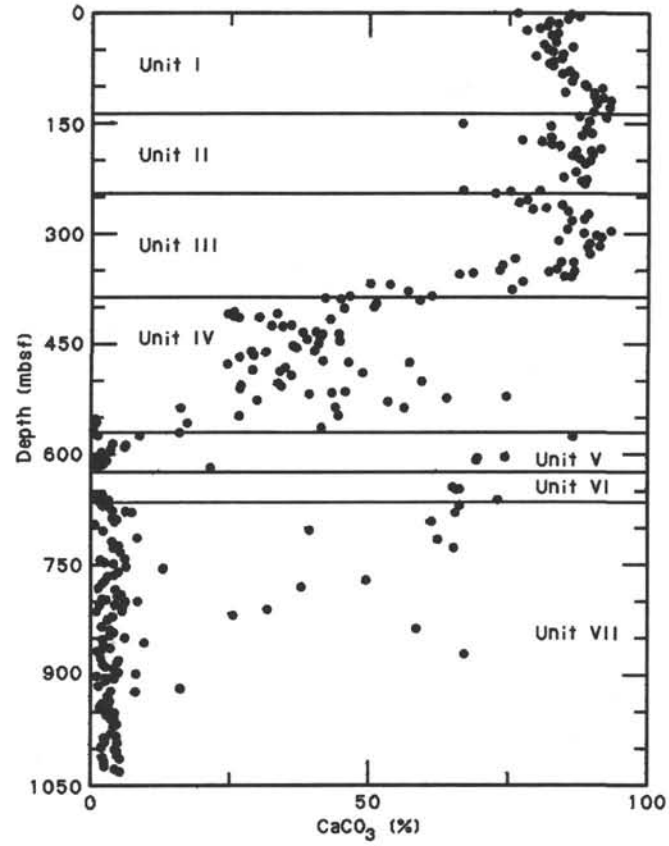

Figure 29. Concentrations of calcium carbonate in sediments and rocks from Site 763. Lithologic units are indicated. Data are from Table 3.

the deeper samples are given in Table 5 and show that higher-molecular-weight gaseous hydrocarbons are important components of these samples. The presence of these constituents suggests that the source of the gases found through much of this hole was being approached at the TD of Hole 763C.

Unlike nearby Site 762, hydrogen sulfide was encountered at this site. Cores from calcareous Units III and IV were malodorous, but measured quantities of hydrogen sulfide remained below 10 ppm in headspace samples and more commonly were below detection limits. This gas was not present in the deeper clastic units of Site 763.

The Natural Gas Analyzer results revealed, predictably, that air is the major fraction of the headspace samples, making up about 90% of their total volumes. The concentrations of CO_2 listed in Table 5, however, are enriched on the order of 100 times over the proportion of this gas in the atmosphere, implying that the sediment gases contain large amounts of CO_2. As further evidence of this, ratios of CO_2 to methane range from ca. 0.7 to 3.7. We could not verify the origin of the CO_2 in these samples without isotopic measurements, yet we assume that postdepositional oxidation of organic matter is involved.

We interpret the high concentrations of gas from this site to have resulted from migrated thermogenic gas derived from a deep-seated source, possibly the Triassic Mungeroo Formation or Jurassic coal seams. Vertical migration is inferred from (1) gas chimneys visible on reflection seismic profiles, (2) the very low concentration of organic carbon over the entire upper portion of the site, and (3) the increase in gas concentrations by about three orders of magnitude over a relatively short depth interval. The high C_1/C_2 ratio is interpreted to have been the product of both the generation from type III (woody or coaly) organic matter and also migration differentiation which favors the movement of methane over heavier gas components (Leythaeuser et al., 1982; 1983). Stable carbon isotopic measurements of the methane were not available on the ship but would almost certainly clarify the nature of the gas source.

The rapid rise in the downhole gas concentration at about 300 mbsf (Fig. 32A) coincides with a lithologic transition with

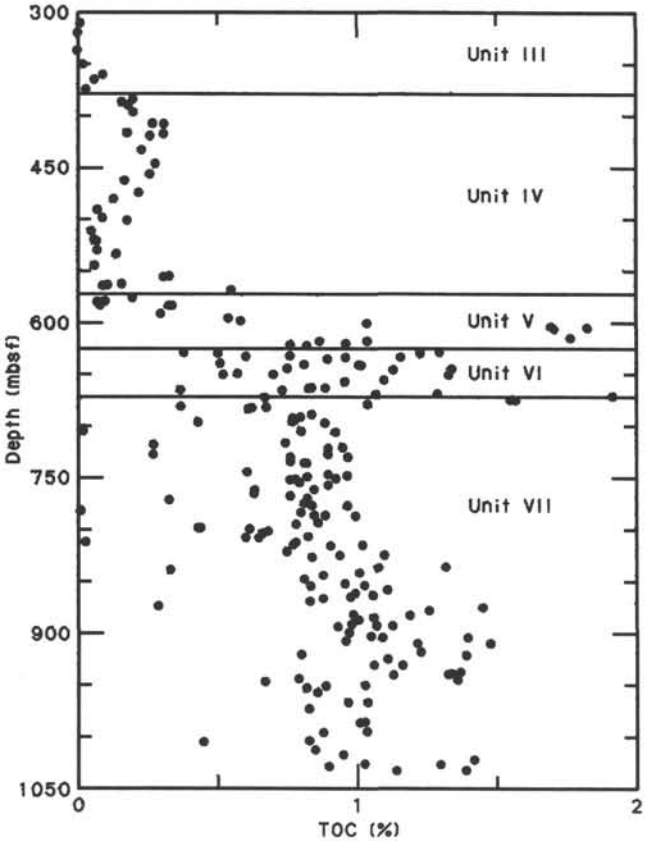

Figure 30. Concentrations of total organic carbon (TOC) rocks from the lower 700 m of Site 763. Percentages are on a whole, dry-weight basis. Lithologic units are indicated. Data are from the Rock-Eval results listed in Table 4.

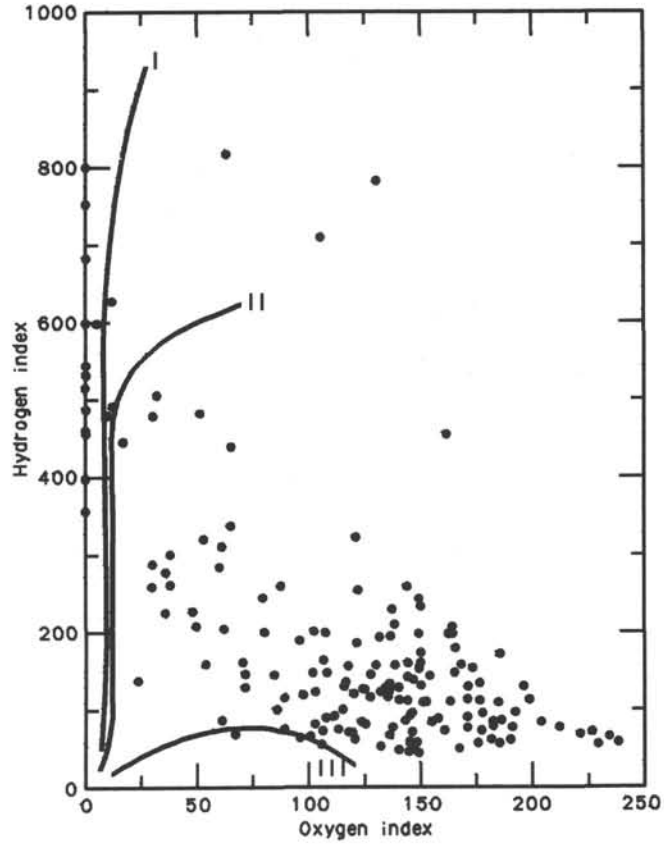

Figure 31. Van Krevelen-type plot of Rock-Eval hydrogen (HI) and oxygen (OI) indexes of samples from Holes 763A, 763B, and 763C. Units for HI are mg total hydrocarbons/g total organic carbon; for OI, mg CO_2/g total organic carbon.

depth from about 85%–90% calcium carbonate to about 35%–50% calcium carbonate. Gas may be trapped due to the establishment of a critical level of lithification and/or change in the effective permeability due to the presence of small amounts of clay. Above about 300 mbsf, there is no seismic expression of gas chimneys, and it appears that gas is dispersed from this zone faster than it can migrate up from the zone below.

Safety Considerations

The decision to continue open-hole drilling at this site despite the presence of relatively large amounts of inferred thermogenic gas was predicated on a number of important factors. The results from the nearby Vinck-1 well, about 12 m structurally higher than Site 763, showed no indication of a free gas phase or overpressures to the targeted drilling depth of 1125 mbsf. The onset of significant amounts of ethane and propane in the headspace gas at about 850 mbsf was similar to the same observation at nearby Site 762, drilled in nearly the same geological setting (Site 762 chapter, this volume). We interpret the increase in concentration of "wet gas" herein to indicate that the level of thermal maturation attained a thresh old level equivalent to a vitrinite reflectance level of about 0.45% R_o (Powell, 1978). Because of the presence of inferred epigenetic gases in the overlying rocks, it must be assumed that some of the gas in the lowermost 250 m of Site 763 is also migrated dry gas. As a result, the C_1/C_2 ratio observed for the bottom of Hole 763C may be somewhat higher than would be expected for a situation in which only syngenetic gases are present.

The last two cores cut from Hole 763C contained elevated concentrations of headspace gas (Fig. 32A) having the same C_1/C_2 ratio (ca. 150) as gas in higher cores. The sudden increase in concentration was not related to any obvious change in the organic or lithologic character and was thus interpreted to indicate that a gas-charged lithologic unit not visible on seismic traces was being approached. Drilling was terminated at this time in order to preclude drilling into a permeable zone with pressures above those controllable with seawater drilling fluid (i.e., hydrostatic pressure).

High-Molecular-Weight Hydrocarbons

Two samples of siltstone, one from Unit V (Muderong Shale equivalent) and one from Unit VI (Barrow Group equivalent), were extracted and analyzed for their contents of high-molecular-weight hydrocarbons. Interstitial-water squeeze cakes from Samples 122-763B-45X-3, 140–150 cm, and 122-763C-6R-1, 140–150 cm, were freeze-dried and ultrasonically extracted with chloroform/methanol (80/20) for 15 min. The extracts were filtered, and the solvent was removed with a rotary evaporator. The saturated hydrocarbon fraction was eluted from a silica gel chromatography column using hexane and analyzed by capillary gas chromatography.

The resulting chromatograms (Fig. 33) show the presence of a relatively larger amount of C_{15}–C_{17} normal alkanes in the shallower, Aptian-age sample, indicating that the precursor organic matter contained a significant amount of algal material. The large odd/even *n*-alkane predominance over this interval and especially from about C_{20} to C_{30} indicates a low level of thermal maturity, consistent with the Rock-Eval

Table 4. Rock-Eval data from samples from Holes 763A, 763B, and 763C. Total organic carbon (TOC) percentages are on a whole sediment, dry-weight basis.

Core, section, interval (cm)	Depth (mbsf)	Wt. (mg)	T_{max} (°C)	S_1	S_2	S_3	PI	S_2/S_3	PC	TOC (%)	HI	OI
122-763A-												
1H-3, 8–10	3.08	101.1	399	0.07	0.09	2.22	0.44	0.04	0.01	0.06	150	3700
2H-6, 8–10	12.48	100.1	317	0.04	0.07	2.08	0.40	0.03	0.00	0.04	175	5200
3H-6, 8–10	21.98	100.2	304	0.04	0.07	2.11	0.40	0.03	0.00	0.02	350	10550
4H-6, 47–49	31.87	100.1	393	0.12	0.23	1.94	0.35	0.11	0.02	0.19	121	1021
5H-6, 59–62	41.49	100.3	384	0.07	0.18	1.81	0.29	0.09	0.02	0.05	360	3620
6H-6, 53–55	50.93	102.5	323	0.06	0.14	1.73	0.30	0.08	0.01	0.05	280	3460
7H-6, 50–52	60.40	100.6	210	0.02	0.00	1.71	1.00	0.00	0.00	0.02	0	8550
8H-6, 52–55	69.92	98.6	304	0.03	0.09	1.52	0.25	0.05	0.01	0.01	900	15200
9H-6, 93–95	79.83	99.9	374	0.04	0.11	1.69	0.29	0.06	0.01	0.01	1100	16900
10H-6, 90–93	89.30	100.0	358	0.06	0.39	1.40	0.14	0.27	0.03	0.04	975	3500
11H-6, 93–95	98.83	100.5	358	0.06	0.34	1.30	0.15	0.26	0.03	0.05	680	2600
12H-6, 93–95	108.33	99.7	354	0.03	0.26	1.17	0.11	0.22	0.02	0.03	866	3900
13H-6, 92–95	117.82	100.7	383	0.00	0.17	1.04	0.00	0.16	0.01	0.03	566	3466
14H-6, 7–9	126.47	100.6	333	0.01	0.11	1.25	0.08	0.08	0.01	0.01	1100	12500
15H-6, 92–94	136.82	99.8	304	0.01	0.01	1.44	0.50	0.00	0.00	0.00	0	0
16H-6, 5–7	145.45	99.8	349	0.00	0.00	1.20		0.00	0.00	0.01	0	12000
17H-6, 87–89	155.77	99.9	412	0.00	0.09	0.99	0.00	0.09	0.00	0.00	0	0
18H-6, 88–90	165.28	100.0	473	0.01	0.37	0.92	0.03	0.40	0.03	0.03	1233	3066
19H-6, 103–105	174.93	99.0	304	0.04	0.04	0.98	0.50	0.04	0.00	0.09	44	1088
20H-6, 56–58	183.96	100.1	379	0.08	0.17	1.02	0.33	0.16	0.02	0.13	130	784
21H-6, 53–55	193.43	101.4	336	0.05	0.21	0.73	0.19	0.28	0.02	0.02	1050	3650
122-763B-												
2X-4, 15–17	194.65	99.9	221	0.00	0.00	0.83		0.00	0.00	0.00	0	0
3X-4, 84–86	204.84	99.9	222	0.00	0.00	0.75		0.00	0.00	0.00	0	0
4X-3, 26–28	212.26	101.0	221	0.00	0.00	0.90		0.00	0.00	0.02	0	4500
5X-4, 16–18	223.16	100.4	371	0.00	0.07	0.75	0.00	0.09	0.00	0.01	700	7500
6X-4, 55–58	233.05	100.6	348	0.01	0.21	0.70	0.05	0.30	0.01	0.02	1050	3500
7X-2, 51–54	239.51	99.2	346	0.02	0.11	0.72	0.17	0.15	0.01	0.01	1100	7200
8X-4, 42–44	251.92	100.6	283	0.03	0.14	1.31	0.19	0.10	0.01	0.27	51	485
9X-4, 20–22	261.20	99.8	390	0.02	0.16	0.99	0.11	0.16	0.01	0.03	533	3300
10X-4, 21–24	270.71	98.5	363	0.01	0.17	0.87	0.06	0.19	0.01	0.02	850	4350
11X-4, 32–34	280.32	99.6	380	0.02	0.19	0.83	0.10	0.22	0.01	0.04	475	2075
12X-4, 21–23	289.71	100.5	343	0.00	0.17	0.75	0.00	0.22	0.01	0.02	850	3750
13X-4, 91–93	299.91	100.7	402	0.00	0.15	0.87	0.00	0.17	0.01	0.03	500	2900
14X-4, 8–10	308.58	99.3	298	0.00	0.00	0.75		0.00	0.00	0.01	0	7500
15X-4, 10–12	318.10	99.7	304	0.00	0.00	0.62		0.00	0.00	0.00	0	0
17X-2, 67–69	334.67	99.4	396	0.00	0.00	0.72		0.00	0.00	0.00	0	0
18X-5, 17–18	348.17	99.3	304	0.00	0.00	0.97		0.00	0.00	0.02	0	4850
19X-6, 4–6	359.04	100.5	401	0.00	0.01	1.26		0.00	0.00	0.09	11	1400
20X-3, 7–9	364.07	103.3	298	0.00	0.00	0.89		0.00	0.00	0.06	0	1483
21X-3, 26–28	373.76	99.6	387	0.01	0.01	0.79	0.50	0.01	0.00	0.03	33	2633
22X-3, 34–36	383.34	105.4	367	0.01	0.13	0.88	0.07	0.14	0.01	0.20	65	440
23X-5, 16–18	395.66	97.7	304	0.00	0.00	1.37		0.00	0.00	0.20	0	685
24X-5, 140–150	406.40	100.3	430	0.00	0.00	0.97		0.00	0.00	0.27	0	359
24X-6, 36–38	406.86	98.9	360	0.01	0.00	1.52		0.00	0.00	0.31	0	490
25X-5, 105–107	415.55	103.8	299	0.00	0.00	1.08		0.00	0.00	0.18	0	600
25X-6, 0–2	416.00	102.1	394	0.01	0.10	1.57	0.10	0.06	0.00	0.31	32	506
26X-1, 38–40	418.38	100.7	281	0.05	0.08	1.25	0.42	0.06	0.01	0.26	30	480
27X-4, 7–9	432.07	101.7	226	0.00	0.00	1.26		0.00	0.00	0.23	0	547
28X-6, 40–42	444.90	100.3	277	0.03	0.05	1.25	0.37	0.04	0.00	0.28	17	446
29X-6, 76–79	454.76	102.4	231	0.00	0.00	1.19		0.00	0.00	0.26	0	457
30X-4, 100–103	461.50	99.7	278	0.07	0.18	1.21	0.29	0.14	0.02	0.17	105	711
31X-6, 42–44	473.42	101.1	268	0.03	0.14	1.80	0.19	0.07	0.01	0.22	63	818
32X-4, 46–48	479.96	100.7	224	0.00	0.00	0.98		0.00	0.00	0.13	0	753
33X-4, 80–82	489.80	100.5	269	0.00	0.00	1.22		0.00	0.00	0.07	0	1742
34X-3, 120–122	498.20	101.4	220	0.00	0.00	0.00			0.00	0.09	0	0
34X-5, 0–2	500.00	100.9	346	0.00	0.01	1.08		0.00	0.00	0.18	5	600
35X-6, 22–24	511.22	100.9	278	0.00	0.00	0.00			0.00	0.05	0	0
36X-4, 140–150	518.90	99.8	222	0.01	0.00	1.04		0.00	0.00	0.06	0	1733
36X-5, 67–69	519.67	97.9	247	0.00	0.00	0.00			0.00	0.07	0	0
37X-5, 32–34	528.82	101.4	220	0.00	0.00	0.00			0.00	0.07	0	0
38X-1, 79–81	532.79	99.6	425	0.03	0.11	1.86	0.21	0.05	0.01	0.14	78	1328
39X-2, 7–9	543.07	97.8	234	0.01	0.00	1.77		0.00	0.00	0.06	0	2950
40X-2, 0–2	552.50	100.4	331	0.00	0.04	1.63	0.00	0.02	0.00	0.33	12	493
40X-2, 111–113	553.61	100.6	266	0.02	0.04	1.95	0.33	0.02	0.00	0.31	12	629
41X-1, 55–57	561.05	101.4	404	0.00	0.14	0.42	0.00	0.33	0.01	0.16	87	262
41X-2, 0–2	562.00	100.1	252	0.00	0.00	1.14		0.00	0.00	0.11	0	1036
41X-2, 33–35	562.33	100.8	304	0.00	0.00	0.36		0.00	0.00	0.09	0	400
41X-5, 0–2	566.50	101.5	417	0.00	0.30	0.89	0.00	0.33	0.02	0.55	54	161
42X-4, 44–46	574.94	100.1	375	0.00	0.00	1.07		0.00	0.00	0.20	0	535
42X-6, 35–39	577.85	100.7	304	0.00	0.00	0.46		0.00	0.00	0.10	0	460
42X-7, 0–2	579.00	100.3	235	0.00	0.00	0.22	0.00	0.00	0.00	0.07	0	31442
43X-2, 39–41	581.39	99.6	290	0.00	0.00	0.64		0.00	0.00	0.08	0	800

Table 4 (continued).

Core, section, interval (cm)	Depth (mbsf)	Wt. (mg)	T_{max} (°C)	S_1	S_2	S_3	PI	S_2/S_3	PC	TOC (%)	HI	OI
43X-2, 105–107	582.05	100.3	345	0.02	0.13	1.03	0.14	0.12	0.01	0.34	38	302
43X-3, 0–2	582.50	101.0	354	0.00	0.08	0.46	0.00	0.17	0.00	0.33	24	139
44X-2, 34–36	590.84	100.9	325	0.01	0.11	0.84	0.08	0.13	0.01	0.30	36	280
44X-4, 67–68	594.17	100.9	402	0.01	0.26	1.23	0.04	0.21	0.02	0.54	48	227
44X-6, 67–68	597.17	100.6	402	0.03	0.29	1.22	0.09	0.23	0.02	0.58	50	210
45X-1, 59–61	599.09	100.6	413	0.06	0.89	1.04	0.06	0.85	0.07	1.04	85	100
45X-3, 140–150	602.90	99.7	431	0.06	2.84	0.87	0.02	3.26	0.24	1.70	167	51
45X-4, 13–15	603.13	100.9	423	0.11	2.42	0.97	0.04	2.49	0.21	1.83	132	53
45X-5, 0–2	604.50	99.8	429	0.06	2.62	0.89	0.02	2.94	0.22	1.71	153	52
46X-4, 59–61	613.09	101.0	427	0.07	2.95	0.71	0.02	4.15	0.25	1.77	166	40
46X-6, 93–95	616.43	99.8	410	0.05	0.59	0.62	0.08	0.95	0.05	0.87	67	71
46X-7, 0–2	617.00	100.8	422	0.01	0.93	0.83	0.01	1.12	0.07	1.04	89	79
47X-2, 61–63	619.61	100.4	414	0.03	0.69	1.42	0.04	0.48	0.06	0.96	71	147
47X-3, 0–2	620.50	100.5	425	0.00	0.68	0.89	0.00	0.76	0.05	0.76	89	117
47X-3, 47–49	620.97	100.8	412	0.03	0.59	1.08	0.05	0.54	0.05	0.82	71	131
48X-4, 0–2	627.00	101.6	423	0.08	1.38	0.75	0.05	1.84	0.12	1.30	106	57
48X-5, 24–25	628.74	100.4	414	0.15	1.23	0.84	0.11	1.46	0.11	1.23	100	68
48X-5, 81–84	629.31	100.0	343	0.06	0.15	1.30	0.30	0.11	0.01	0.50	30	260
49X-1, 94–96	628.44	99.8	374	0.04	0.25	1.29	0.14	0.19	0.02	0.38	65	339
49X-3, 108–110	631.58	100.7	477	0.10	1.03	0.90	0.09	1.14	0.09	0.76	135	118
49X-3, 135–137	631.85	99.8	367	0.07	0.23	1.58	0.23	0.14	0.02	0.60	38	263
49X-4, 0–2	632.00	102.2	424	0.15	1.32	0.77	0.10	1.71	0.12	0.96	137	80
49X-4, 61–63	632.61	100.3	412	0.12	1.45	0.90	0.08	1.61	0.13	1.16	125	77
50X-2, 8–10	634.08	100.2	420	0.05	1.26	1.03	0.04	1.22	0.10	0.90	140	114
50X-5, 0–2	638.50	99.9	422	0.02	0.71	0.82	0.03	0.86	0.06	0.51	139	160
50X-5, 146–148	639.96	102.3	422	0.02	1.54	0.73	0.01	2.10	0.13	1.02	150	71
50X-6, 6–8	640.06	101.3	422	0.05	1.62	0.77	0.03	2.10	0.13	1.01	160	76
51X-2, 66–68	639.66	99.5	415	0.10	1.48	0.71	0.06	2.08	0.13	0.81	182	87
51X-4, 66–68	642.66	100.2	413	0.05	1.16	0.66	0.04	1.75	0.10	0.75	154	88
51X-5, 0–2	643.50	101.3	427	0.06	2.97	0.94	0.02	3.15	0.25	1.34	221	70
53X-1, 32–34	647.82	100.5	414	0.04	0.61	1.15	0.06	0.53	0.05	0.57	107	201
53X-2, 0–2	649.00	100.1	425	0.03	1.35	0.70	0.02	1.92	0.11	0.70	192	100
54X-1, 39–41	648.89	100.8	420	0.06	0.89	0.69	0.06	1.28	0.07	0.52	171	132
54X-1, 128–130	649.78	100.5	423	0.15	2.82	1.07	0.05	2.63	0.24	1.33	212	80
122-763C-												
2R-1, 22–24	385.22	99.7	404	1.39	36.71	2.39	0.04	15.35	3.17	8.94	410	26
2R-1, 22–24	385.22	102.1	406	1.51	36.78	2.57	0.04	14.31	3.19	7.42	495	34
2R-1, 63–65	385.63	99.1	410	1.45	63.61	4.64	0.02	13.70	5.42	11.86	536	39
2R-1, 63–65	385.63	99.9	413	1.79	64.98	4.32	0.03	15.04	5.56	15.00	433	28
2R-1, 107–109	386.07	99.6	437	0.00	0.00	0.83	0.00	0.00	0.00	0.16	0	518
2R-3, 76–78	388.76	102.7	267	0.00	0.00	0.88	0.00	0.00	0.00	0.18	0	488
4R-1, 0–5	645.10	100.5	424	0.10	2.56	0.84	0.04	3.04	0.22	1.13	226	74
5R-1, 0–5	654.60	99.5	424	0.04	1.16	0.63	0.03	1.84	0.10	1.10	105	57
5R-1, 53–55	655.13	100.7	428	0.03	2.25	0.66	0.01	3.40	0.19	0.96	234	68
6R-1, 112–114	661.72	101.0	427	0.01	2.00	0.50	0.00	4.00	0.16	0.84	238	59
6R-1, 140–150	662.00	101.0	424	0.00	1.29	0.41	0.00	3.14	0.10	0.89	144	46
6R-2, 0–2	662.10	99.5	424	0.01	2.06	0.48	0.00	4.29	0.17	0.83	248	57
6R-2, 88–91	662.98	99.4	421	0.00	0.60	0.75	0.00	0.80	0.05	0.37	162	202
6R-3, 23–25	663.83	101.1	429	0.00	1.25	0.78	0.00	1.60	0.10	0.73	171	106
7R-1, 134–136	666.94	98.7	427	0.00	1.94	0.70	0.00	2.77	0.16	1.07	181	65
7R-2, 0–2	667.10	100.5	428	0.00	2.39	0.78	0.00	3.06	0.19	1.29	185	60
8R-1, 24–26	670.84	100.2	429	0.03	4.41	1.12	0.01	3.93	0.37	1.92	229	58
8R-1, 64–66	671.24	100.8	426	0.00	0.54	1.36	0.00	0.39	0.04	0.67	80	202
8R-3, 0–2	673.60	99.9	430	0.03	3.17	1.32	0.01	2.40	0.26	1.56	203	84
8R-3, 0–2	673.60	100.7	429	0.00	2.83	1.31	0.00	2.16	0.23	1.55	182	84
8R-3, 26–28	673.86	100.3	430	0.02	2.79	1.19	0.01	2.34	0.23	1.57	177	75
9R-2, 120–122	678.30	100.0	429	0.00	1.85	1.04	0.00	1.77	0.15	1.04	177	100
9R-4, 64–66	680.74	99.5	479	0.00	0.79	1.07	0.00	0.73	0.06	0.67	117	159
9R-4, 80–82	680.90	100.5	353	0.00	0.04	1.78	0.00	0.02	0.00	0.37	10	481
9R-5, 0–2	681.60	99.6	421	0.00	0.22	1.38	0.00	0.15	0.01	0.61	36	226
9R-5, 1–2	681.61	100.8	421	0.00	0.49	1.53	0.00	0.32	0.04	0.62	79	246
10R-2, 128–130	687.88	100.6	426	0.00	1.07	1.24	0.00	0.86	0.08	0.84	127	147
10R-4, 49–51	690.09	100.2	427	0.00	0.89	1.23	0.00	0.72	0.07	0.80	111	153
10R-5, 0–2	691.10	99.7	429	0.00	1.12	1.03	0.00	1.08	0.09	0.80	140	128
10R-5, 0–2	691.10	100.4	426	0.00	1.03	1.18	0.00	0.87	0.08	0.77	133	153
10R-6, 50–52	693.10	101.3	424	0.00	1.13	1.27	0.00	0.88	0.09	0.78	144	162
10R-7, 65–67	694.75	99.5	415	0.00	0.23	1.39	0.00	0.16	0.01	0.43	53	323
11R-1, 0–2	694.60	100.1	429	0.00	0.82	1.02	0.00	0.80	0.06	0.77	106	132
11R-1, 0–2	694.60	100.9	425	0.00	1.28	0.50	0.00	2.56	0.10	0.86	148	58
11R-2, 5–7	696.15	101.0	423	0.01	1.29	0.56	0.01	2.30	0.10	0.89	144	62
12R-1, 15–17	704.25	101.4	327	0.00	0.00	0.32		0.00	0.00	0.02	0	1600
12R-2, 0–2	705.60	100.4	429	0.00	1.78	0.75	0.00	2.37	0.14	0.93	191	80
12R-2, 14–16	705.74	100.6	427	0.00	1.16	0.77	0.00	1.50	0.09	0.80	145	96
13R-1, 98–100	714.58	99.8	428	0.01	1.07	1.08	0.01	0.99	0.09	0.74	144	145
13R-3, 20–23	716.80	100.8	345	0.00	0.07	4.62	0.00	0.01	0.00	0.27	25	1711
13R-5, 0–2	719.60	100.7	432	0.00	2.35	1.07	0.00	2.19	0.19	0.95	247	112

Table 4 (continued).

Core, section, interval (cm)	Depth (mbsf)	Wt. (mg)	T_{max} (°C)	S_1	S_2	S_3	PI	S_2/S_3	PC	TOC (%)	HI	OI
13R-5, 47–49	720.07	100.2	430	0.00	1.32	0.80	0.00	1.65	0.11	0.90	146	88
14R-2, 42–44	725.02	99.8	431	0.02	1.37	1.02	0.01	1.34	0.11	0.90	152	113
14R-3, 118–120	727.28	101.0	430	0.00	0.16	5.32	0.00	0.03	0.01	0.27	59	1970
14R-4, 24–26	727.84	99.8	432	0.00	1.43	0.87	0.00	1.64	0.11	0.97	147	89
14R-5, 0–2	729.10	100.8	426	0.00	0.68	0.88	0.00	0.77	0.05	0.76	89	115
15R-2, 24–26	734.34	100.5	429	0.00	0.95	0.98	0.00	0.96	0.07	0.76	125	128
15R-3, 0–2	735.60	101.1	427	0.00	1.02	1.06	0.00	0.96	0.08	0.82	124	129
15R-3, 0–2	735.60	101.2	430	0.01	0.92	0.63	0.01	1.46	0.07	0.81	113	77
15R-3, 2–4	735.62	101.6	428	0.04	1.37	0.80	0.03	1.71	0.11	0.87	157	91
16R-2, 46–48	744.06	100.7	424	0.00	0.70	0.83	0.00	0.84	0.05	0.60	116	138
16R-3, 37–39	745.47	99.9	429	0.00	0.96	0.66	0.00	1.45	0.08	0.90	106	73
16R-4, 10–13	746.70	100.4	430	0.07	1.74	0.66	0.04	2.63	0.15	0.97	179	68
16R-5, 10–13	748.20	100.7	431	0.01	1.10	0.64	0.01	1.71	0.09	0.82	134	78
16R-5, 140–150	749.50	100.6	431	0.01	1.36	0.69	0.01	1.97	0.11	0.93	146	74
16R-6, 101–103	750.61	100.2	429	0.02	1.18	0.88	0.02	1.34	0.10	0.78	151	112
16R-7, 0–2	751.10	101.3	431	0.02	0.98	0.89	0.02	1.10	0.08	0.76	128	117
17R-2, 87–89	753.97	101.2	431	0.00	0.95	0.98	0.00	0.96	0.07	0.79	120	124
17R-4, 6–8	756.16	100.5	430	0.00	0.63	1.46	0.00	0.43	0.05	0.90	70	162
17R-6, 28–29	759.38	101.1	429	0.00	1.19	0.75	0.00	1.58	0.09	0.83	143	90
17R-7, 0–2	760.60	101.0	430	0.00	1.30	0.63	0.00	2.06	0.10	0.85	152	74
18R-1, 48–52	761.58	100.1	427	0.00	0.64	0.95	0.00	0.67	0.05	0.63	101	150
18R-3, 99–103	765.09	100.7	426	0.00	0.73	0.85	0.00	0.85	0.06	0.63	115	134
18R-4, 109–113	766.69	99.9	430	0.00	0.85	0.70	0.00	1.21	0.07	0.76	111	92
18R-6, 0–2	768.60	99.9	428	0.00	0.98	0.59	0.00	1.66	0.08	0.82	119	71
19R-1, 57–59	771.17	100.6	364	0.00	0.10	0.96	0.00	0.10	0.00	0.33	30	290
19R-3, 33–35	773.93	99.3	426	0.01	0.87	0.75	0.01	1.16	0.07	0.81	107	92
19R-4, 140–150	776.50	99.5	430	0.00	1.15	0.59	0.00	1.94	0.09	0.84	136	70
19R-5, 0–2	776.60	99.7	427	0.00	0.81	0.66	0.00	1.22	0.06	0.79	102	83
19R-5, 0–2	776.60	100.1	429	0.00	1.22	0.80	0.00	1.52	0.10	0.97	125	82
19R-5, 13–15	776.73	100.3	432	0.00	1.16	0.66	0.00	1.75	0.09	0.79	146	83
20R-1, 77–79	780.87	99.1	224	0.00	0.00	0.32		0.00	0.00	0.01	0	3200
20R-2, 94–96	782.54	101.0	426	0.00	0.96	0.50	0.00	1.92	0.08	0.80	120	62
20R-4, 101–103	785.61	101.1	431	0.00	0.98	0.87	0.00	1.12	0.08	0.85	115	102
20R-5, 0–2	786.10	99.9	431	0.01	1.35	0.74	0.01	1.82	0.11	0.89	151	83
20R-5, 0–2	786.10	101.2	428	0.00	1.49	0.46	0.00	3.23	0.12	1.00	149	46
21R-2, 102–104	792.12	101.0	431	0.00	1.20	0.88	0.00	1.36	0.10	0.86	139	102
21R-4, 64–66	794.74	100.4	432	0.00	1.13	0.90	0.00	1.25	0.09	0.78	144	115
21R-6, 0–2	797.10	100.6	430	0.00	0.26	1.24	0.00	0.20	0.02	0.43	60	288
21R-6, 0–2	797.10	100.9	429	0.00	0.27	1.38	0.00	0.19	0.02	0.44	61	313
21R-6, 81–83	797.91	100.5	425	0.00	0.82	0.81	0.00	1.01	0.07	0.61	134	132
22R-1, 113–115	800.23	101.2	429	0.00	0.70	1.39	0.00	0.50	0.05	0.68	102	204
22R-3, 28–30	802.38	100.7	428	0.00	0.56	0.97	0.00	0.57	0.04	0.66	84	146
22R-5, 0–2	805.10	101.2	432	0.00	1.12	1.11	0.00	1.00	0.09	0.82	136	135
22R-5, 106–108	806.16	100.8	425	0.00	0.62	1.25	0.00	0.49	0.05	0.65	95	192
22R-6, 5–7	806.65	99.3	426	0.00	0.71	0.63	0.00	1.12	0.05	0.60	118	105
23R-2, 42–44	810.52	99.5	429	0.00	0.80	0.99	0.00	0.80	0.06	0.78	102	126
23R-2, 95–97	811.05	99.7	304	0.00	0.00	0.31		0.00	0.00	0.03	0	1033
23R-4, 0–2	813.10	100.2	435	0.00	1.20	0.75	0.00	1.60	0.10	1.02	117	73
23R-4, 53–55	813.63	99.1	429	0.01	0.82	1.28	0.01	0.64	0.06	0.77	106	166
23R-5, 27–29	814.87	99.3	425	0.00	0.87	0.59	0.00	1.47	0.07	0.91	95	64
24R-2, 20–22	819.80	100.7	429	0.00	0.47	1.55	0.00	0.30	0.03	0.75	62	206
24R-4, 70–72	823.30	100.9	434	0.00	1.45	1.38	0.00	1.05	0.12	0.94	154	146
24R-5, 0–2	824.10	99.6	434	0.00	1.82	2.01	0.00	0.90	0.15	1.10	165	182
24R-6, 60–64	826.20	101.3	430	0.00	1.15	1.22	0.00	0.94	0.09	0.84	136	145
25R-6, 0–2	835.10	100.9	431	0.00	1.63	2.56	0.00	0.63	0.13	1.08	150	237
25R-6, 43–45	835.53	101.6	430	0.02	1.94	1.88	0.01	1.03	0.16	1.32	146	142
26R-1, 62–64	837.72	99.9	448	0.00	0.40	3.74	0.00	0.10	0.03	0.33	121	1133
26R-3, 54–56	840.64	101.2	430	0.04	1.66	2.04	0.02	0.81	0.14	1.01	164	201
26R-5, 0–2	843.10	101.1	430	0.00	1.42	4.03	0.00	0.35	0.11	0.88	161	457
26R-5, 22–25	843.32	100.5	432	0.00	1.23	2.22	0.00	0.55	0.10	0.85	144	261
27R-1, 8–10	846.68	100.6	430	0.02	1.11	1.87	0.02	0.59	0.09	0.81	137	230
27R-3, 90–92	850.50	100.5	432	0.05	1.59	1.44	0.03	1.10	0.13	0.96	165	150
27R-5, 0–2	852.60	100.2	432	0.00	1.27	0.90	0.00	1.41	0.10	1.03	123	87
27R-5, 128–130	853.88	100.6	423	0.03	1.25	0.77	0.02	1.62	0.10	0.84	148	91
28R-2, 27–30	857.87	100.9	430	0.05	1.83	2.35	0.03	0.77	0.15	1.11	164	211
28R-4, 7–10	860.67	100.1	429	0.03	1.37	1.64	0.02	0.83	0.11	1.00	137	164
28R-5, 0–2	862.10	101.4	432	0.00	1.37	1.22	0.00	1.12	0.11	1.06	129	115
28R-6, 85–87	864.45	100.7	425	0.02	1.29	1.93	0.02	0.66	0.10	0.98	131	196
29R-1, 68–70	866.28	100.8	421	0.01	0.87	1.08	0.01	0.80	0.07	0.89	97	121
29R-3, 37–39	868.97	100.7	415	0.01	0.51	0.74	0.02	0.68	0.04	0.83	61	89
29R-5, 94–97	872.54	99.8	392	0.00	0.25	3.60	0.00	0.06	0.02	0.29	86	1241
29R-6, 0–2	873.10	101.7	433	0.00	2.76	0.92	0.00	3.00	0.23	1.45	190	63
30R-2, 102–104	877.62	100.6	435	0.00	1.85	0.75	0.00	2.46	0.15	1.26	146	59
30R-4, 134–136	880.94	101.3	432	0.02	1.70	0.80	0.01	2.12	0.14	0.99	171	80
30R-6, 0–2	882.60	100.3	432	0.00	1.62	1.51	0.00	1.07	0.13	1.19	136	126
30R-6, 112–114	883.72	100.8	432	0.00	1.59	1.87	0.00	0.85	0.13	1.06	150	176
31R-2, 113–116	887.23	100.7	433	0.00	1.30	1.30	0.00	1.00	0.10	1.01	128	128

Table 4 (continued).

Core, section, interval (cm)	Depth (mbsf)	Wt. (mg)	T_{max} (°C)	S_1	S_2	S_3	PI	S_2/S_3	PC	TOC (%)	HI	OI
31R-4, 70–72	889.80	100.3	430	0.00	1.47	1.60	0.00	0.91	0.12	0.98	150	163
31R-5, 140–150	892.00	99.0	434	0.00	1.65	1.11	0.00	1.48	0.13	1.13	146	98
31R-6, 0–2	892.10	100.6	434	0.00	1.61	1.43	0.00	1.12	0.13	1.07	150	133
31R-6, 86–88	892.96	100.2	425	0.01	1.27	1.84	0.01	0.69	0.10	0.93	136	197
32R-3, 128–130	898.38	100.3	435	0.00	1.59	1.21	0.00	1.31	0.13	0.97	163	124
32R-5, 44–46	900.54	100.9	432	0.00	1.79	1.46	0.00	1.22	0.14	1.05	170	139
32R-7, 26–28	903.36	99.8	430	0.00	1.61	0.59	0.00	2.72	0.13	1.09	147	54
32R-7, 49–51	903.59	100.8	433	0.00	2.42	1.04	0.00	2.32	0.20	1.40	172	74
33R-2, 137–139	906.47	99.3	433	0.01	1.62	1.55	0.01	1.04	0.13	0.96	168	161
33R-4, 87–89	908.97	100.2	430	0.03	2.39	1.44	0.01	1.65	0.20	1.48	161	97
33R-5, 0–2	909.60	99.9	434	0.00	1.90	1.05	0.00	1.80	0.15	1.22	155	86
34R-3, 8–10	916.18	100.3	433	0.00	2.16	0.73	0.00	2.95	0.18	1.23	175	59
34R-5, 41–43	919.51	100.6	431	0.00	1.11	1.71	0.00	0.64	0.09	0.80	138	213
34R-6, 0–2	920.60	100.0	434	0.00	2.41	1.42	0.00	1.69	0.20	1.39	173	102
35R-1, 24–26	922.84	99.1	422	0.04	1.66	2.72	0.02	0.61	0.14	1.11	149	245
35R-5, 147–149	930.07	99.1	429	0.02	1.70	1.63	0.01	1.04	0.14	1.16	146	140
35R-6, 0–2	930.10	102.0	433	0.00	1.73	1.20	0.00	1.44	0.14	1.06	163	113
36R-3, 117–119	936.27	99.9	431	0.03	2.42	1.88	0.01	1.28	0.20	1.37	176	137
36R-5, 0–2	938.10	99.6	431	0.01	2.24	2.08	0.00	1.07	0.18	1.34	167	155
36R-5, 112–114	939.22	99.8	428	0.02	2.28	1.20	0.01	1.90	0.19	1.33	171	90
36R-6, 48–50	940.08	98.9	431	0.02	1.72	1.08	0.01	1.59	0.14	1.13	152	95
37R-1, 142–144	943.02	99.6	426	0.01	1.05	1.00	0.01	1.05	0.08	0.79	132	126
37R-2, 126–128	944.36	100.9	431	0.02	2.53	1.19	0.01	2.12	0.21	1.36	186	87
37R-3, 130–132	945.90	100.3	421	0.00	0.79	1.10	0.00	0.71	0.06	0.67	117	164
37R-6, 0–2	949.10	100.5	431	0.00	1.25	1.95	0.00	0.64	0.10	1.03	121	189
37R-6, 63–65	949.73	101.3	429	0.00	1.16	1.43	0.00	0.81	0.09	0.89	130	160
38R-1, 133–135	952.43	98.3	427	0.01	1.00	2.67	0.01	0.37	0.08	0.82	121	325
38R-5, 0–2	957.10	100.3	433	0.00	1.49	1.35	0.00	1.10	0.12	0.86	173	156
39R-4, 22–24	965.32	100.5	431	0.00	1.55	2.11	0.00	0.73	0.12	1.04	149	202
39R-5, 0–2	966.60	100.4	431	0.00	1.60	1.67	0.00	0.95	0.13	0.97	164	172
40R-2, 0–2	971.60	101.3	427	0.00	0.90	1.24	0.00	0.72	0.07	0.83	108	149
41R-5, 0–2	985.60	100.2	431	0.00	1.55	0.88	0.00	1.76	0.12	1.01	153	87
42R-5, 0–2	995.10	100.5	435	0.00	1.63	0.98	0.00	1.66	0.13	0.88	185	111
42R-5, 57–58	995.67	99.7	434	0.06	2.04	1.39	0.03	1.46	0.17	1.04	196	133
43R-4, 3–5	1003.13	101.0	430	0.02	1.24	1.28	0.02	0.96	0.10	0.83	149	154
43R-5, 0–2	1004.60	100.5	432	0.00	0.55	1.16	0.00	0.47	0.04	0.45	122	257
44R-4, 2–4	1012.62	100.0	432	0.03	1.46	0.98	0.02	1.48	0.12	0.85	171	115
44R-7, 0–2	1017.10	101.1	434	0.00	1.68	1.10	0.00	1.52	0.14	0.95	176	115
45R-4, 12–15	1022.22	100.7	435	0.03	3.48	0.87	0.01	4.00	0.29	1.42	245	61
45R-6, 113–115	1026.23	100.6	434	0.00	2.11	0.88	0.00	2.39	0.17	1.03	204	85
45R-7, 0–2	1026.60	100.7	429	0.00	1.83	0.64	0.00	2.85	0.15	1.30	140	49
46R-2, 60–62	1029.20	100.8	432	0.00	1.77	1.53	0.00	1.15	0.14	0.90	196	170
46R-4, 119–121	1032.79	100.7	432	0.02	2.12	2.00	0.01	1.06	0.17	1.14	185	175
46R-5, 0–2	1033.10	99.2	434	0.02	2.76	1.64	0.01	1.68	0.23	1.39	198	117

Table 5. Concentrations and compositions of low-molecular-weight hydrocarbons of selected samples from Hole 763C. Analyses were done with the Hewlett-Packard 5890 Natural Gas Analyzer. Data from both flame ionization detection (FID) and thermal conductivity detection (TCD) of gas components are given. Concentrations are in ppm of headspace volume.

	Sample 122-763B-	Sample 122-763C-			
	45X-5, 0–2 cm	30R-6, 0–2 cm	44R-7, 0–2 cm	45R-7, 0–2 cm	46R-5, 0–2 cm
Depth (mbsf)	609.5	882.6	1017.1	1026.6	1033.1
FID:					
methane	9818	6642	6711	28658	10543
ethane	24	33	95	168	148
propane	12	6	12	12	8
n-butane	4	4	6	6	4
i-butane	7	0	0	2	3
n-pentane	8	7	7	3	5
n-hexane	4	8	6	5	0
TCD:					
methane	11305	6974	7447	30719	11373
ethane	26	37	104	228	163
CO_2	8035	25963	24793	24399	30997
C_1/C_2 ratio:					
FID	409	189	71	171	71
TCD	434	203	72	135	70

Table 6. Concentrations of low-molecular-weight hydrocarbons of samples from Holes 763A, 763B, and 763C. Analyses were done with the Carle gas chromatograph. Data are from headspace samples. Concentrations are given in ppm of headspace volume.

Core, section, interval (cm)	Depth (mbsf)	C_1 (ppm)	C_2 (ppm)	C_1/C_2
122-763A-				
1H-3, 0–5	3.0	1.8	0.0	
2H-5, 0–5	10.9	2.1	0.0	
3H-5, 0–5	20.4	3.0	0.0	
4H-5, 0–5	29.9	2.5	0.0	
5H-5, 0–5	39.4	2.8	0.0	
6H-5, 0–5	48.9	3.0	0.0	
7H-5, 0–5	58.4	2.5	0.0	
8H-5, 0–5	67.9	2.2	0.0	
9H-5, 0–5	77.4	5.2	0.0	
10H-5, 0–5	86.9	8.6	0.0	
11H-5, 0–5	96.4	8.0	0.0	
12H-5, 0–5	105.9	8.6	0.0	
13H-5, 0–5	115.4	6.3	0.0	
14H-5, 0–5	124.9	10.9	0.0	
15H-5, 0–5	134.4	9.0	0.0	
16H-5, 0–5	143.9	11.1	0.0	
17H-6, 0–5	154.9	28.3	0.0	
18H-6, 0–5	164.4	210.7	1.0	210.7
19H-5, 0–5	172.4	528.7	1.2	440.5
20H-5, 0–5	181.9	1373.0	2.7	508.5
21H-6, 0–5	192.9	1652.0	2.9	569.6
122-763B-				
2X-5, 0–5	196.0	891.4	1.3	685.6
3X-5, 0–5	205.5	2016.0	3.0	672.0
4X-2, 0–5	210.5	1242.0	1.9	653.6
5X-3, 0–5	221.5	1606.0	2.4	669.1
6X-5, 0–5	234.0	1500.0	1.8	833.3
7X-2, 0–5	239.0	3266.0	3.1	1053.5
8X-3, 0–5	250.0	3350.0	2.8	1196.4
9X-5, 0–5	262.5	1951.0	1.9	1026.8
10X-4, 0–5	270.5	5250.0	3.5	1500.0
11X-5, 0–2	281.5	8919.0	5.9	1511.6
12X-4, 0–2	289.5	7414.0	4.5	1647.5
13X-5, 0–2	300.5	8491.0	4.9	1732.8
14X-5, 0–2	310.0	9805.0	8.2	1195.7
15X-5, 0–2	319.5	9808.0	5.9	1662.3
16X-5, 0–2	329.0	21206.0	7.6	2790.2
17X-5, 0–2	338.5	2946.0	1.5	1964.0
18X-4, 0–2	346.5	40894.0	8.6	4755.1
19X-5, 0–2	357.5	5074.0	2.2	2306.3
20X-2, 0–5	362.5	33472.0	9.1	3678.2
21X-2, 0–5	372.0	9122.0	7.1	1284.7
22X-1, 0–5	380.0	9051.0	20.8	435.1
23X-5, 0–5	400.5	34356.0	37.0	928.5
24X-6, 0–2	411.5	43043.0	38.0	1132.7
25X-6, 0–2	421.0	43165.0	36.2	1192.4
26X-4, 0–2	427.5	70005.0	26.4	2651.7
27X-5, 0–2	438.5	7719.0	18.1	426.4
28X-5, 0–2	448.0	41222.0	27.4	1504.4
29X-5, 0–2	457.5	58222.0	29.8	1953.7
30X-5, 0–2	467.0	9452.0	28.5	331.6
31X-5, 0–2	476.5	65450.0	31.7	2064.6
32X-5, 0–2	486.0	13938.0	33.3	418.5
33X-6, 0–2	497.0	52959.0	32.3	1639.5
34X-5, 0–2	505.0	82435.0	44.6	1848.3
35X-5, 0–2	514.5	44107.0	24.8	1778.5
36X-5, 0–2	524.0	7920.0	18.8	421.2
37X-5, 0–2	533.5	66908.0	32.5	2058.7
38X-1, 0–2	537.0	63351.0	6.9	9181.3
39X-1, 0–2	546.5	43129.0	3.8	11349.7
40X-2, 0–2	557.5	7667.0	4.3	1783.0
41X-2, 0–2	567.0	6865.0	19.2	357.5
42X-7, 0–2	584.0	9159.0	26.6	344.3
43X-3, 0–2	587.5	28262.0	11.1	2546.1
44X-5, 0–2	600.0	14477.0	18.8	770.0
45X-5, 0–2	609.5	62157.0	73.0	851.4
46X-7, 0–2	622.0	41121.0	17.3	2376.9
47X-3, 0–2	625.5	9266.0	7.1	1305.0
48X-4, 0–2	627.0	1103.0	2.6	424.2
49X-4, 0–2	632.0	3252.0	5.8	560.6
50X-5, 0–2	638.5	2478.0	2.7	917.7
51X-5, 0–2	643.5	1247.0	3.9	319.7
53X-2, 0–2	649.0	6023.0	3.1	1942.9
54X-1, 128–130	649.8	1353.0	3.5	386.5
122-763C-				
2R-4, 0–2	389.5	47612.0	27.9	1706.5
4R-1, 0–5	645.1	8817.0	4.9	1799.3
5R-1, 0–5	654.6	16826.0	14.0	1201.8
6R-2, 0–2	662.1	3887.0	208.0	18.6
7R-2, 0–2	667.1	2831.0	4.4	643.4
8R-3, 0–2	673.6	1701.0	4.6	369.7
9R-5, 0–2	681.6	3998.0	1.2	3331.6
10R-5, 0–2	691.1	1083.0	1.7	637.0
11R-1, 0–2	694.6	1149.0	1.9	604.7
12R-2, 0–2	705.6	2280.0	3.7	616.2
13R-5, 0–2	719.6	1232.0	1.2	1026.6
14R-5, 0–2	729.1	2909.0	4.0	727.2
15R-3, 0–2	735.6	1707.0	3.4	502.0
16R-7, 0–2	751.1	574.0	1.8	318.8
17R-7, 0–2	760.6	6770.0	6.6	1025.7
18R-6, 0–2	768.6	9021.0	7.6	1186.9
19R-5, 0–2	776.6	7546.0	7.5	1006.1
20R-5, 0–2	786.1	5433.0	10.1	537.9
21R-6, 0–2	797.1	7821.0	6.8	1150.1
22R-5, 0–2	805.1	3503.0	3.8	921.8
23R-4, 0–2	813.1	4150.0	6.7	619.4
24R-5, 0–2	824.1	4503.0	7.3	616.8
28R-6, 0–2	835.1	3914.0	9.1	430.1
26R-5, 0–2	843.1	3730.0	7.6	490.7
27R-5, 0–2	852.6	1437.0	7.6	189.0
28R-5, 0–2	862.1	4345.0	13.5	321.8
29R-6, 0–2	873.1	5719.0	30.1	190.0
30R-6, 0–2	882.6	8237.0	43.6	188.9
31R-6, 0–2	892.1	7910.0	42.9	184.3
32R-7, 49–51	903.6	11463.0	56.2	203.9
33R-5, 0–2	909.6	7698.0	45.1	170.6
34R-6, 0–2	920.6	6776.0	48.1	140.8
35R-6, 0–2	930.1	7889.0	33.9	232.7
36R-5, 0–2	938.1	4347.0	31.3	138.8
37R-6, 0–2	949.1	6502.0	39.6	164.1
38R-5, 0–2	957.1	5535.0	38.5	143.7
39R-5, 0–2	966.6	4699.0	27.8	169.0
40R-2, 0–2	971.6	5416.0	33.4	162.1
41R-5, 0–2	985.6	8066.0	59.2	136.2
42R-5, 0–2	995.1	14554.0	61.3	237.4
43R-5, 0–2	1004.6	16395.0	73.8	222.1
44R-7, 0–2	1017.1	9964.0	169.0	58.9
45R-7, 0–2	1026.6	85144.0	274.9	309.7
46R-5, 0–2	1033.1	57380.0	305.8	187.6

results. The level of maturity is probably too low to reliably interpret the pristane/phytane ratio of about 1.3. A minor discrepancy exists between the organic matter type as inferred from the Rock-Eval results (continental source) and the shipboard extract data (marine source). This probably relates to the level of thermal maturity, which is just sufficient to yield a small amount of bitumen from the most reactive phase (that is, the lipid-rich material), but a much smaller relative amount from the Type III organic matter. An additional factor which may help to explain the discrepancy in organic-matter character is the possibility of an analytical artifact. Selective loss of the higher molecular weight components of the hydrocarbon fractions was observed during gas chromatography of standard mixtures. This possibility was not quantitatively evaluated in the shipboard laboratory. Subsequent shore-based gas chromatography confirmed that the shipboard instrument discriminated in favor of low-molecular-weight hydrocarbons and against high-molecular-weight (terrigenous) compounds

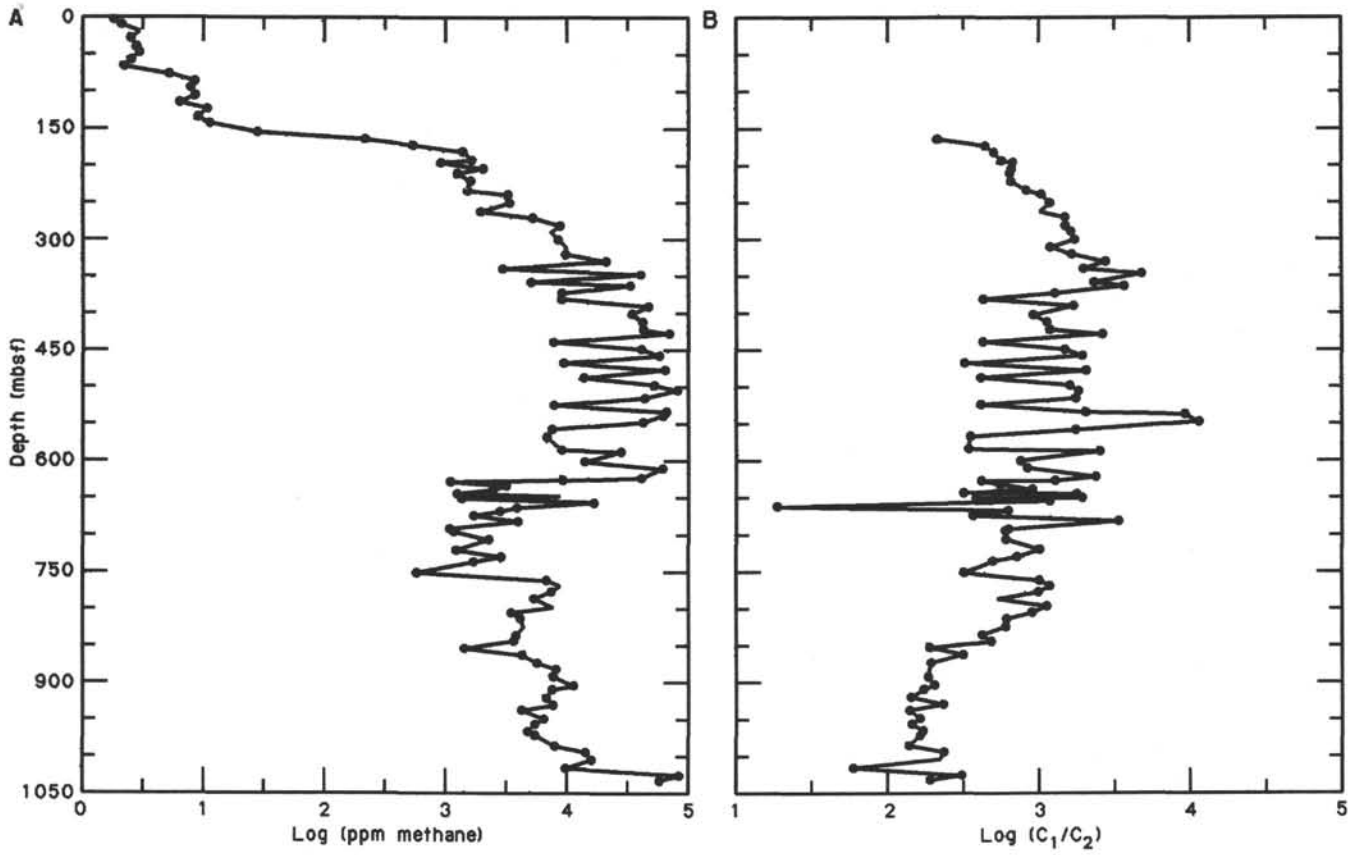

Figure 32. **A.** Downhole concentrations of methane, in log ppm of headspace volume, from Holes 763A, 763B, and 763C. **B.** C_1/C_2 ratios of headspace samples from Hole 763A, also in logarithmic notation (data appears in Table 6).

(Meyers and Snowdon, unpubl. data to appear in the Leg 122 *Scientific Results*).

The second chromatogram (Sample 122-763C-6R-1, 140–150 cm, Fig. 33) has a much higher proportion of higher-molecular-weight *n*-alkanes, as would be expected from land-plant debris, and is interpreted to contain a smaller amount of lipid-rich algal material than present in Sample 122-763C-45X-3, 140–150 cm. It, too, shows a relatively low degree of diagenetic alteration of the odd-to-even predominance of the original source material. In addition, indications of diterpenoid hydrocarbons are given by the group of small peaks between the C_{20} and C_{21} *n*-alkanes (Fig. 33). The precursors of these diagenetic products are believed to be contained in the saps and resins of continental woody plants.

INORGANIC GEOCHEMISTRY

Introduction

Only chemical analyses of interstitial waters were carried out at Site 763 (Fig. 34, Table 7). The X-ray diffractometer was not available for solid-phase studies during operations at Site 763 because of continued problems with the shipboard regulated power. Consequently, these analyses were performed during the transit to Singapore; the resulting data table appears in the Site 762 chapter (this volume). Three *in-situ* pore-water samples were obtained during downhole heat-flow measurements, one sample of surface seawater was collected, and 42 whole-round (5- or 10-cm-long) cores were squeezed for interstitial waters. One of the whole-round cores (Sample 122-763C-37R-5, 140–150 cm) did not yield any pore water; several others (Samples 122-763B-42X-6, 140–150 cm, and 122-763C-10R-4, 140–150 cm, -13R-4, 140–150 cm, -25R-5, 140–150 cm, -34R-5, 140–150 cm, and -41R-5, 140–150 cm) yielded only enough fluid to permit limited shipboard analyses. The low-volume pore-water samples all came from the bottom of Hole 763B or from Hole 763C within the sediments of Unit V (Muderong Shale equivalent) or Subunits VIIA and VIIC (Barrow Group equivalent).

Site 763 is characterized by steep concentration gradients for Mg^{2+}, SO_4^{2-}, and salinity in the upper 250–300 m of the sediments; all these constituents appear to have been strongly affected by diffusion processes. Below this depth, major elements demonstrate a more complicated and variable behavior.

Interstitial Waters

Magnesium (Mg^{2+}) and Calcium (Ca^{2+})

The dissolved Mg^{2+} profile at Site 763 is characterized by large concentration gradients in the first 350 m (Fig. 34) of the sediments. The steepest gradient (−17.7 mM/100 m) occurs in the first 67.9 m of Hole 763A, where the concentration drops from 54.2 to 42.2 mM; it then decreases to 38.0 mM by 124.9 mbsf, representing more than a two-fold decrease in the gradient (−7.4 mM/100 m) relative to the uppermost section. From 124.9 to 346.4 mbsf the concentration of Mg^{2+} decreases further to 25.7 mM but at a reduced rate. The gradient over this interval is −5.6 mM/100 m. Below 346.4 mbsf Mg^{2+} decreases only slightly with depth from a concentration of 25.7 to 17.5 mM by 776.5 mbsf (gradient = −1.9 mM/100 m). A slight increase is then observed at 814.5 mbsf, beyond which Mg^{2+} concentrations remain nearly constant (Table 7).

Data from *in-situ* samples agree well with the corresponding interstitial waters except for Sample 122-763A-17X-1, 0–10 cm, which shows evidence of seawater contamination in

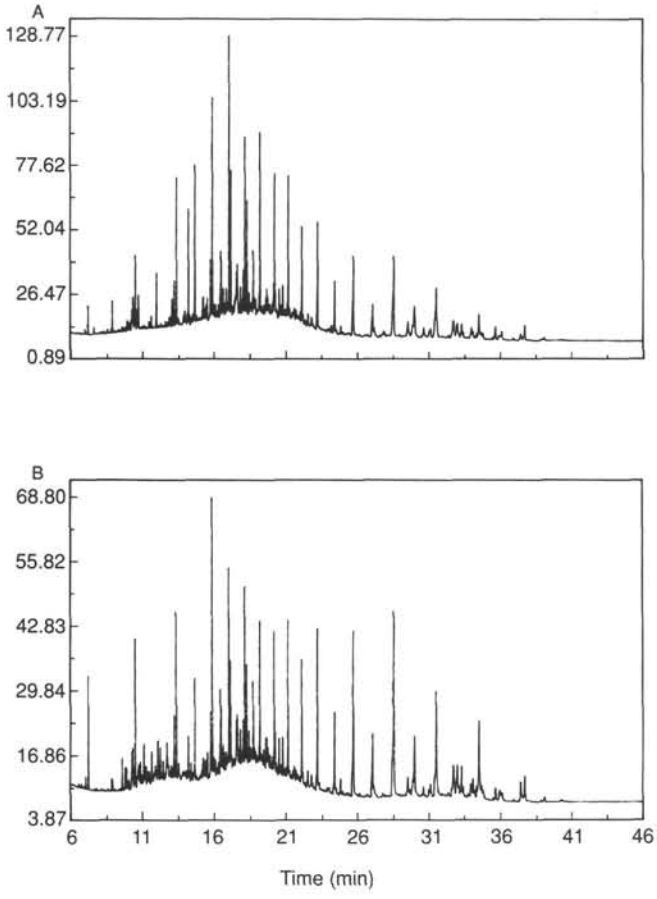

Figure 33. Chromatograms of saturated hydrocarbon fractions extracted from Site 763 samples. **A.** Sample 122-763B-45X-3, 140–150 cm, Unit V (Muderong Shale equivalent). **B.** Sample 122-763C-6R-1, 140–150 cm, Unit VI (Barrow Group equivalent). Straight-chain components are identified by the number of their carbon atoms. Vertical axis is flame ionization detector (FID) response. Horizontal axis is chromatographic retention time (increasing to the right).

its significantly higher Mg^{2+} concentration. We anticipated this result because as we recovered the water sampler we noticed that its overflow was quite full; this situation typically arises when the sampler triggers before complete penetration into the sediment.

The Ca^{2+} profile in the upper 200 m of the sediments (Fig. 34) differs from that normally observed at deep-sea drill sites but the profile from the uppermost 50 m of Hole 763A bears some resemblance to that from Site 762. An unexpected decrease in the concentration of Ca^{2+} occurs down to 48.9 mbsf. In this interval the concentration drops from the near-seawater value of 10.8 mM to 8.9 mM. The concentration decrease in the first 50 m of Hole 763A is at least twice as large as that observed at Site 762. Between 48.9 and 124.9 mbsf Ca^{2+} remains constant; it is followed by a further decrease to the minimum concentration (7.4 mM at 181.9 mbsf) observed at Site 763.

Under normal carbonate diagenesis conditions an exchange of Ca^{2+} for Mg^{2+} occurs, which results in an increase in the concentration of Ca^{2+} and a decrease in that of Mg^{2+}. The pattern anticipated for Mg^{2+} is observed at Site 763, whereas the corresponding Ca^{2+} trend is not. Thus some other process occurring in the interstitial waters of this site results in the removal of dissolved Ca^{2+} from solution. From 205.5 to 491.9 mbsf the expected Ca^{2+} increase is observed with the concentration rising back to the original near-seawater value of 10.8 mM. A relatively large increase occurs between 518.9 and 578.9 mbsf, below which Ca^{2+} exhibits a gradual downhole increase to 15.9 mM. Excluding the increase between 518.9 and 578.9 mbsf, the Ca^{2+}, the gradient between 205.5 and 930.0 mbsf averages 0.63 mM/100 m.

Variations in Mg^{2+} and Ca^{2+} at Site 763 cannot be explained solely by carbonate diagenesis in the upper 300 m of the sediments. However, below this depth there is approximately a one-to-one correspondence in the average increases and decreases of Ca^{2+} and Mg^{2+} respectively. The unusual behavior observed at Site 763 is reflected in the Mg^{2+}/Ca^{2+} ratio (Fig. 34), which displays three major regions. The first is a slight decrease in the ratio down to 124.9 mbsf; this is followed by an increase from 124.9 to 181.9 mbsf. Although the seawater-contaminated *in-situ* sample is within this interval, it does not represent either of the extremes of the range of Mg^{2+}/Ca^{2+} observed. Below 181.9 mbsf, the smooth linear decrease in the ratio down to 346.4 mbsf constitutes the third region. From the latter depth to the bottom of the hole there is only a slight further decrease in the Mg^{2+}/Ca^{2+} that corresponds approximately to the region of possible one-to-one ion exchange.

Sulfate (SO_4^{2-})

Sulfate is rapidly removed from the sediments of Site 763, reaching a nearly depleted concentration of 1.41 mM at 319.4 mbsf (Fig. 34). Below 346.4 mbsf, SO_4^{2-} remains low and ranges between 0.78 and 9.30 mM, exhibiting a series of downhole oscillations with a slight increasing trend. The concentration reversal that occurs at 156.9 mbsf is due to the previously discussed seawater contamination of the *in-situ* sampler.

The sharp gradient of −8.84 mM/100 m observed in the upper 320 m of the sediment of Site 763 results from the oxidation of organic matter by SO_4^{2-} coincidentally this is also the zone of greatest Mg^{2+} depletion (Fig. 34). The mechanism of reduction of SO_4^{2-} to S^{2-} is supported by the observation of the alkalinity (e.g., HCO_3^-) maximum, which is also produced by the oxidation of organic matter (see following discussion of alkalinity and Fig. 34).

Silica (SiO_2)

The SiO_2 concentration profile at Site 763 displays considerable variation with depth (Fig. 34) but is similar to that observed within the upper 200 m of the sediments at other Leg 122 sites. A striking resemblance exists between the profiles from Sites 762 and 763 (see "Inorganic Geochemistry," Site 762 chapter, this volume) and extends approximately to 500 mbsf. This observation is not entirely surprising because both sites have similar lithologies within the specified depth interval (see "Lithostratigraphy," this chapter). A significant difference arises, however, in the greater maximum SiO_2 concentration observed at Site 762 relative to Site 763.

Concentrations of SiO_2 in the near-surface-sediment pore waters range between 1.0 and 1.2 mM, drop steadily to approximately 0.4 mM by 67.9 mbsf, and remain between 0.3 and 0.5 mM down to 153.4 mbsf. An increase is then observed and a first maximum of 1.29 mM occurs at 205.5 mbsf. This SiO_2 maximum, although smaller by nearly 25%, corresponds remarkably well to that of Site 762 (1.79 mM at 193.5 mbsf). Between 234.0 and 346.4 mbsf somewhat lower concentrations (0.72–0.91 mM) are maintained before another broad maximum (1.51–1.70 mM) occurs from 406.4 and 491.9 mbsf. A general agreement again exists between Sites 762 and 763 within this depth range, although the maximum concentration

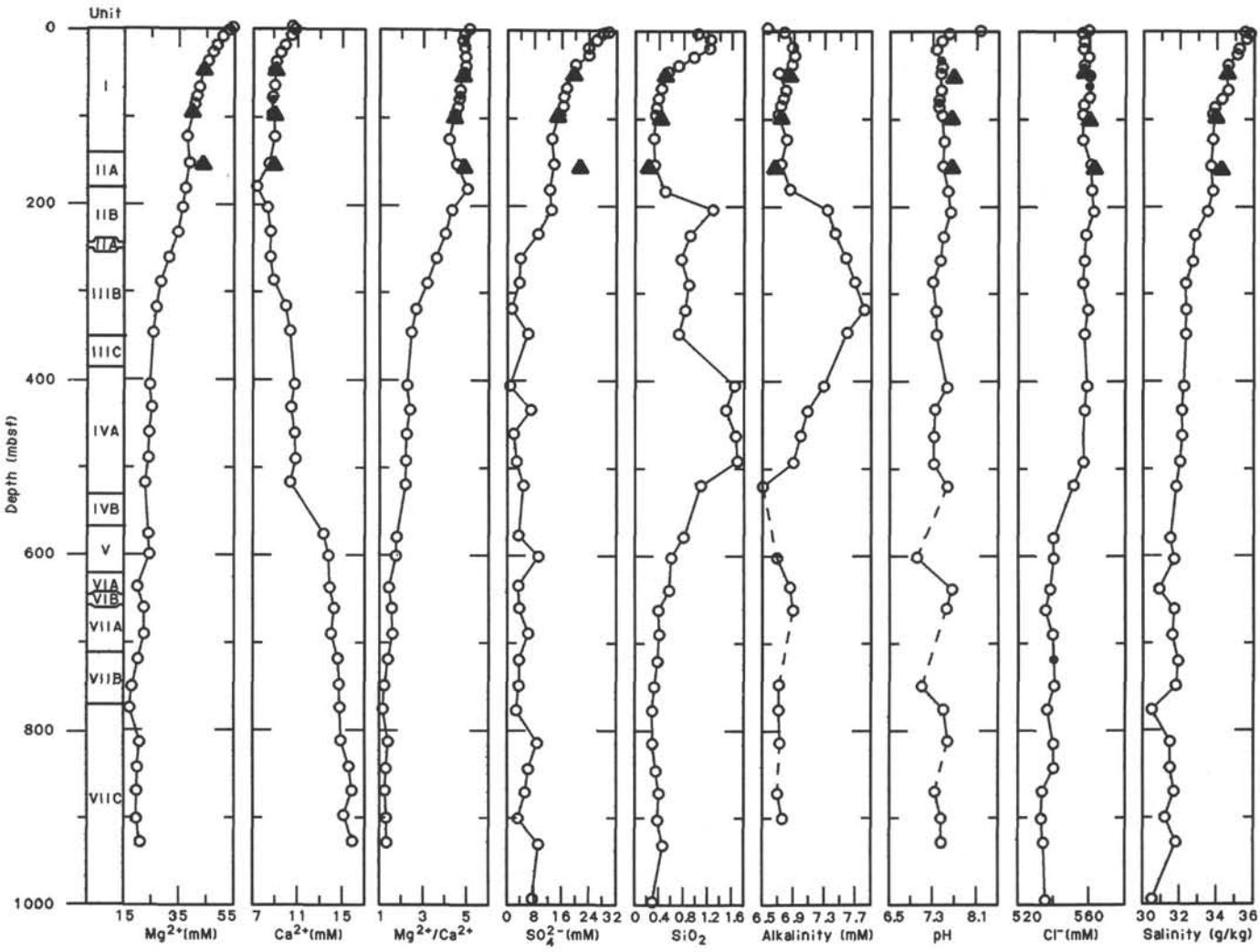

Figure 34. Interstitial water analyses, Site 763. Triangles represent *in-situ* pore-water samples obtained during downhole heat-flow measurements.

of 2.43 mM (403.9 mbsf) observed at Site 762 is considerably larger. From 518.9 to 662.0 mbsf, SiO_2 concentrations decrease sharply to 0.39 mM and then remain in the range of 0.29–0.47 mM down to 995.0 mbsf.

The SiO_2 profile obtained through the detailed sampling in the first 100 m clearly reveals the early diagenetic dissolution of opaline silica in unconsolidated oozes and reflects the disappearance of radiolarians over this depth range (see "Biostratigraphy," this chapter). Downhole variations may be due to mobilization of SiO_2 associated with the conversion of opaline silica to opal-CT. The presence of completely infilled radiolarians in the intervals where SiO_2 concentrations fluctuate but remain high supports this hypothesis (see "Biostratigraphy," this chapter). Below 578.9 mbsf, a return to concentrations <1 mM and eventually near 0.4 mM corresponds to the transition from the calcareous, nannofossil, and glauconitic claystones of Subunit IVB, through black restricted-marine silty claystones of Unit V (Muderong Shale equivalent), to the black prodelta silty clay and siltstones of Units VI and VII (Barrow Group equivalent) (see "Lithostratigraphy," this chapter).

Alkalinity and pH

Except for the interval between 205.5 and 433.4 mbsf the alkalinity at Site 763 remains in a narrow range of 2.75–4.50 mM (Table 7 and Fig. 34). The zone in the sediments where the alkalinity reaches 8.57 mM corresponds to the interval in which relatively high concentrations of H_2S were observed. The H_2S results from the protonation of S^{2-} produced by the reduction of SO_4^{2-} during the decomposition of organic matter. Deeper in the hole the precipitation of pyrite consumed much of the S^{2-} produced, and little or no H_2S was detected. Pyrite precipitation requires the presence of dissolved iron, which apparently was not available in the sediments between 205.5 and 433.4 mbsf.

The pH of interstitial waters at Site 763 remains within a narrow range of 7.3–7.7 (Fig. 34), except for two occurrences where we observed values of 7.0 (602.9 mbsf) and 7.1 (749.5 mbsf). Neither of these appear to correspond to any unusual variations in any other constituents although they occur in black prodelta silty claystones of Unit V and Subunit VIIB respectively. A slight local minimum in the pH also appears in the region of high alkalinity.

Table 7. Composition of interstitial waters, Site 763.

Core, section, interval (cm)	Depth (mbsf)	Vol. (cm^3)	pH	Alkalinity (mM)	Salinity (g/kg)	Mg^{2+} (mM)	Ca^{2+} (mM)	Mg^{2+}/Ca^{2+}	Cl^- (mM)	SO_4^{2-} (mM)	SiO_2 (mM)
122-763A-											
Surface seawater	0.0	100	8.16	2.281	35.5	54.2	10.5	5.16	559	29.63	0.004
1H-2, 145–150	3.0	50	7.59	3.364	35.8	52.9	10.8	4.92	556	28.01	1.041
2H-4, 145–150	10.9	54	7.46	3.766	35.6	50.7	10.5	4.84	557	25.94	1.248
3H-4, 145–150	20.4	49	7.36	3.895	35.2	48.5	9.9	4.91	556	23.68	1.231
4H-4, 145–150	29.9	47	7.45	4.049	35.1	47.0	9.5	4.96	559	23.81	0.970
5H-4, 145–150	39.4	50	7.46	3.856	34.6	45.2	9.1	4.97	557	19.94	0.713
6H-4, 145–150	48.9	40	7.44	3.021	34.5	43.5	8.9	4.90	556	18.95	0.545
7H-1, 0–10[a]	52.4	55	7.66	3.657	34.5	43.4	9.0	4.81	560	19.05	0.489
7H-4, 145–150	58.4	40	7.44	3.441	34.6	42.2	8.9	4.72	560	17.37	0.435
8H-4, 145–150	67.9	40	7.41	3.334	34.3	41.3	8.8	4.70	560	16.66	0.388
9H-4, 145–150	77.4	38	7.41	3.149	33.9	40.6	8.8	4.62	557	16.43	0.360
10H-4, 145–150	86.9	37	7.46	2.995	33.8	39.4	8.8	4.50	556	15.37	0.343
11H-1, 0–10[a]	90.4	65	7.63	3.126	33.9	39.8	9.0	4.44	559	14.76	0.422
13H-4, 145–150	115.4	36	7.50	3.534	33.8	38.0	9.0	4.22	556	13.17	0.313
16H-4, 145–150	143.9	33	7.48	3.179	33.7	38.6	8.5	4.56	561	13.71	0.325
17H-1, 0–10[a]	147.4	60	7.63	2.735	34.2	43.1	8.9	4.87	562	20.93	0.211
19H-4, 145–150	172.4	25	7.57	3.756	33.8	37.2	7.4	5.06	561	12.48	0.498
122-763B-											
3X-4, 145–150	205.5	35	7.62	6.169	33.5	36.1	8.3	4.34	562	12.89	1.289
6X-4, 145–150	234.0	21	7.49	6.654	32.8	34.5	8.6	4.02	558	9.00	0.905
9X-4, 145–150	262.5	24	7.44	7.374	32.7	31.3	8.6	3.63	557	3.95	0.767
12X-3, 140–150	289.4	36	7.30	7.946	32.3	28.5	8.9	3.20	556	3.65	0.892
15X-4, 140–150	319.4	41	7.36	8.548	32.3	26.8	10.0	2.69	559	1.41	0.825
18X-3, 140–150	346.4	21	7.36	7.424	32.3	25.7	10.4	2.48	557	6.16	0.722
24X-5, 140–150	406.4	43	7.56	5.947	32.2	24.4	10.7	2.28	559	0.78	1.647
27X-4, 140–150	433.4	20	7.34	4.913	32.1	25.3	10.4	2.42	557	7.13	1.509
30X-4, 140–150	461.9	22	7.32	4.464	32.1	24.2	10.8	2.25	557	1.93	1.668
33X-5, 140–150	491.9	15	7.32	4.007	32.0	24.0	10.8	2.21	557	2.83	1.696
36X-4, 140–150	518.9	22	7.57	2.028	31.8	22.8	10.4	2.20	551	4.85	1.088
42X-6, 140–150	578.9	5			31.5	23.9	13.4	1.79	540	3.42	0.806
45X-3, 140–150	602.9	7	7.01	2.961	31.7	24.4	13.8	1.77	540	9.30	0.601
50X-4, 140–150	638.4	7	7.66	3.793	30.9	20.1	13.9	1.44	538	3.33	0.565
122-763C-											
6R-1, 140–150	662.0	7	7.55	3.996	31.7	22.5	14.3	1.57	535	3.61	0.390
10R-4, 140–150	691.0	10			31.6	22.5	14.0	1.60	539	6.23	0.403
13R-4, 140–150	719.5	5			31.9	20.3	14.6	1.39	540	3.59	0.377
16R-5, 140–150	749.5	9	7.10	3.083	31.8	18.2	14.7	1.24	540	3.61	0.328
19R-4, 140–150	776.5	10	7.50	3.066	30.5	17.5	14.8	1.18	536	2.82	0.291
22R-4, 140–150	805.1	12	7.58	3.136	31.5	21.0	14.9	1.41	540	8.90	0.295
25R-5, 140–150	835.1	2			31.5	20.2	15.6	1.29	540	6.20	0.349
28R-4, 140–150	862.1	7	7.34	2.955	31.7	19.9	15.8	1.25	533	5.30	0.403
31R-5, 140–150	892.1	9	7.45	3.278	31.2	19.8	15.1	1.31	533	3.22	0.377
34R-5, 140–150	920.6	2	7.46		31.8	21.4	15.9	1.34	534	9.27	0.466
41R-4, 140–150	985.6	1			30.5				535	7.41	0.295

[a] *In-situ* pore-water sample obtained during heat-flow measurements.

Salinity and Chlorinity

Chloride concentrations at Site 763 remain nearly constant (557–561 mM) to a depth of 491.9 mbsf (Fig. 34). A decrease in Cl^- to 540 mM occurs between 518.9 and 578.9 mbsf, below which slight fluctuations in the range 533–540 mM are observed to 995.0 mbsf. The lower Cl^- concentrations occur within the terrigenous sediments of Units VI and VII (Barrow Group equivalent see "Lithostratigraphy," this chapter) and could be related to the lower-salinity waters of the shelf prodeltaic environment. It is somewhat surprising that Cl^--concentrations at this site did not decrease further. Chloride concentrations at Site 762 (see "Inorganic Geochemistry," Site 762 chapter, this volume) reached a minimum value of 491 mM within the Barrow Group equivalent, yet are 10% greater here in sediments deemed more proximal to the source than those of Site 762. It is possible that horizontal advection of low-salinity water from the Australian continent through porous sediment layers occurred at the latter site but not at Site 763, and that the Cl^- minimum is not representative of bottom currents from nearshore environments.

The initial salinity gradient at Site 763 (Fig. 34) is primarily due to the sharp decreases in Mg^{2+} and SO_4^{2-} between 3.0 and 289.4 mbsf. A more subdued and steady decrease in salinity is observed from 289.4 and 578.9 mbsf. Further downhole variations in the salinity are slight except for three minima of approximately 30.5–30.9 g/kg at 638.4, 776.5, and 995.0 mbsf. Again these occur within the silty claystones of Subunits VIA, and VIIC (see "Lithostratigraphy," this chapter), and salinities are all considerably higher than the minimum (28.2 g/kg) observed at Site 762 (see "Inorganic Geochemistry," Site 762 chapter, this volume).

Conclusions

The chemistry of interstitial waters from Site 763 is characterized by large concentration gradients, particularly for Mg^{2+}, SO_4^{2-}, and salinity in the upper 200 m of the sediments. The concentration profile for Ca^{2+} exhibits an unusual subsurface decrease before resuming the normal increase with depth. Evidence of early and intermediate silica diagenesis is present in the upper 520 m of Site 763 and resembles that observed at

Table 8. Physical-property data, Hole 763A.

Core, section, interval (cm)	Depth (mbsf)	V_{ph} (km/s)	Wet-bulk density (g/cm^3)	Porosity (%)	Water content (%)	Grain density (g/cm^3)	Formation factor		Shear strength (kPa)
							Horizontal	Vertical	
122-763A-									
1H-1, 10	0.10	1.52	1.47	76.3	53.2	2.75	2.06	1.78	6.1
1H-3, 10	3.10	1.56	1.56	70.5	46.4	2.64	2.91	2.34	10.6
2H-2, 10	6.50	1.54	1.55	71.1	47.0	2.63	4.15	3.34	
2H-4, 10	9.50	1.54	1.57	70.1	45.8	2.68	3.76	3.22	
2H-6, 10	12.50	1.55	1.60	68.3	43.8	2.67	3.35	2.66	
3H-2, 10	16.00	1.54	1.59	69.2	44.6	2.66	3.65	2.63	
3H-4, 10	19.00	1.54	1.55	70.1	46.4	2.62	3.09	2.41	
3H-6, 10	22.00	1.54	1.57	69.1	45.2	2.66	3.19	2.34	10.8
4H-2, 8	25.48	1.55	1.59	69.5	44.8	2.66	3.34	2.81	
4H-4, 60	29.00	1.57	1.65	67.2	41.8	2.58	2.61	3.17	
4H-6, 50	31.90	1.57	1.75	68.2	40.0	2.78	2.75	2.49	16.8
5H-2, 50	35.40	1.59	1.69	69.7	42.2	2.78	3.31	2.66	8.8
5H-4, 40	38.30	1.55	1.71	67.5	40.6	2.67	2.35	2.26	13.5
5H-6, 50	41.40	1.55	1.75	68.9	40.4	2.86	2.39	2.22	
6H-2, 50	44.90	1.57	1.75	68.1	39.8	2.50	2.52	2.32	24.7
6H-4, 50	47.90	1.59	1.80	65.0	36.9	2.66	3.00	2.82	17.3
6H-6, 50	50.90	1.57	1.75	65.7	38.5	2.75	2.85	3.24	18.0
7H-2, 50	54.40	1.56	1.73	64.8	38.4	2.60	2.92	2.55	19.1
7H-4, 50	57.40	1.57	1.76	65.2	38.0	2.65	2.78	2.80	16.8
7H-6, 50	60.40	1.58	1.81	66.4	37.6	2.66	3.09	2.94	11.2
8H-2, 50	63.90	1.55	1.73	63.8	37.8	2.52	2.95	2.65	11.2
8H-4, 50	66.90	1.59	1.72	61.7	36.7	2.59	3.26	2.88	18.0
8H-6, 50	69.90	1.60	1.80	65.4	37.2	2.84	3.65	3.01	14.6
9H-2, 90	73.80	1.56	1.72	64.2	38.2	2.70	3.09	2.68	13.5
9H-4, 93	76.83	1.54	1.67	63.0	38.7	2.61	2.88	2.81	15.7
9H-6, 93	79.83	1.53	1.71	63.9	38.2	2.65	2.53	2.42	16.8
10H-2, 90	83.30	1.54	1.76	65.0	37.9	3.01	2.78	2.55	15.7
10H-4, 90	86.30	1.57	1.73	63.7	37.8	2.71	3.09	2.84	18.0
10H-6, 90	89.30	1.56	1.73	62.0	36.8	2.70	3.13	2.81	19.1
11H-2, 100	92.90	1.54	1.77	62.5	36.3	2.75	3.09	2.84	11.4
11H-4, 90	95.80	1.55	1.73	61.1	36.1	2.65	2.99	2.71	20.2
11H-6, 90	98.80	1.56	1.74	61.0	36.0	2.72	3.02	2.94	15.7
12H-2, 90	102.30	1.56	1.77	60.9	35.3	2.79	3.01	2.81	20.2
12H-4, 90	105.30	1.55	1.74	61.9	36.5	2.76	2.88	2.61	16.6
12H-6, 90	108.30	1.57	1.76	60.3	35.0	2.70	3.16	2.91	16.8
13H-2, 92	111.82	1.56	1.75	59.2	34.7	2.69	3.16	2.84	19.5
13H-4, 92	114.82	1.56	1.73	58.9	34.9	2.65	3.58	3.17	16.2
13H-6, 92	117.82	1.56	1.76	59.0	34.3	2.73	3.09	2.81	12.8
14H-2, 92	121.32	1.56	1.80	58.6	33.4	2.73	2.99	2.91	3.3
14H-4, 8	123.48	1.56	1.77	60.6	35.1	2.73	3.16	2.78	13.2
14H-6, 8	126.48	1.56	1.77	59.1	34.2	2.72	2.91	2.69	10.3
15H-2, 8	129.98	1.62	1.78	57.9	33.3	2.69	3.48	3.42	4.5
15H-4, 8	132.98	1.62	1.76	58.3	33.9	2.71	3.61	3.33	3.4
15H-6, 90	136.80	1.63	1.71	60.7	36.3	2.63	4.06	6.97	47.1
16H-2, 90	140.30	1.60	1.69	64.3	39.0	2.72	3.24	3.06	5.4
16H-4, 90	143.30	1.70	1.69	63.8	38.7	2.68	3.61	6.67	20.2
16H-6, 8	145.48	1.59	1.65	64.7	40.2	2.69	3.42	3.47	8.8
17H-2, 90	149.80	1.62	1.66	61.3	37.9	2.68	3.94	3.39	
17H-4, 90	152.80	1.68	1.74	58.2	34.2	2.67			98.8
17H-6, 90	155.80	1.65	1.60	62.9	40.3	2.62	3.21	3.20	
18H-2, 88	159.28	1.61	1.72	62.6	37.3	2.68	3.35	3.62	13.5
18H-4, 98	162.38	1.64	1.70	63.9	38.6	2.74	2.82	3.06	
18H-6, 88	165.28	1.62	1.66	65.4	40.3	2.76	3.21	2.79	9.0
19H-2, 50	168.40	1.57	1.76	63.7	37.0	2.59	2.94	2.64	15.7
19H-4, 66	171.56	1.59	1.72	64.6	38.6	2.67	2.79	2.85	
19H-6, 106	174.96	1.59	1.79	65.9	37.7	2.77	2.94	2.70	22.4
20H-2, 50	177.90	1.59	1.72	63.8	37.9	2.65	3.18	3.03	18.0
20H-4, 20	180.60	1.62	1.81	59.4	33.7	2.63	3.38	3.24	89.8
20H-6, 50	183.90	1.61	1.89	50.8	27.5	3.01	3.65	3.65	74.1
21H-2, 50	187.40	1.56	1.81	57.9	32.9	2.81	2.26	2.37	18.0
21H-4, 50	190.40	1.60	1.93	61.1	32.4	2.82	2.97	3.71	58.4
21H-6, 50	193.40		1.83	59.3	33.2	2.73	2.18	2.18	15.7

Site 762. The broad alkalinity maximum between 205.5 and 433.4 mbsf corresponds to a zone of H_2S production associated with the oxidation of organic matter by SO_4^{2-}.

PHYSICAL PROPERTIES

Introduction

The physical properties determined from sediments of Site 763 on the Exmouth Plateau include compressional wave velocity, velocity anisotropy, thermal conductivity, and the index properties (wet-bulk density, grain density, porosity, and water content) (see "Explanatory Notes," this volume). It was possible to conduct all physical-properties measurements to the bottom of Hole 763A. Shear-strength measurements were not performed below 230.34 mbsf (Section 122-763B-6X-4) because at this depth the material began to show brittle failure. The last resistivity measurement was made at 239.5 mbsf (Section 122-763B-7X-2) after which the instru-

Table 9. Physical-property data, Hole 763B.

Core, section, interval (cm)	Depth (mbsf)	V_{ph} (km/s)	V_{pv} (km/s)	Anisotropy (%)	Bulk density (g/cm^3)	Porosity (%)	Water content (%)	Grain density (g/cm^3)	Formation factor		Shear strength (kPa)
									Horizontal	Vertical	
122-763B-											
2X-2, 18	191.68	1.54			1.72	59.8	35.7	2.68	2.20	2.19	11.20
2X-4, 18	194.68	1.57			1.73	59.2	35.1	2.64	2.94	3.22	22.40
3X-2, 10	201.10	1.57			1.79	58.6	33.5	2.69	2.54	2.33	15.70
3X-4, 84	204.84	1.57			1.77	58.0	33.6	2.58	2.57	2.39	18.40
3X-6, 8	207.08	1.57			1.78	58.4	33.7	2.71	2.71	2.89	24.70
4X-2, 106	211.56	1.57			1.80	58.1	33.1	2.68	2.77	3.08	26.90
4X-3, 26	212.26	1.56			1.77	58.9	34.2	2.71	2.83	3.36	33.70
5X-2, 100	221.00	1.57			1.82	57.6	32.5	2.73	2.77	2.58	11.20
5X-4, 16	223.16	1.58			1.80	55.5	31.6	2.64	2.80	2.81	28.10
6X-2, 84	230.34	1.68			1.84	54.4	30.4	2.68	3.82	2.97	25.80
6X-4, 60	233.10	1.62			1.85	56.6	31.4	2.65	3.35	2.84	
6X-6, 30	235.80				1.87	57.2	31.3	2.71			
7X-2, 50	239.50	1.62			1.79	59.3	33.9	2.71	2.99	2.86	
8X-2, 40	248.90	1.84			1.92	50.4	26.9	2.65			
8X-4, 40	251.90	1.78			2.03	52.3	26.4	2.77			
9X-2, 20	258.20	1.75			2.05	47.6	23.7	2.67			
9X-4, 20	261.20	1.85			1.99	47.8	24.6	2.71			
9X-6, 20	264.20	1.76			2.14	51.2	24.5	2.78			
10X-2, 20	267.70	1.66			2.04	52.0	26.1	2.82			
10X-4, 20	270.70	1.85			2.04	48.2	24.3	2.69			
10X-6, 20	273.70	1.85			1.98	51.6	26.7	2.76			
11X-2, 20	277.20	1.74			1.98	52.4	27.1	2.72			
11X-4, 20	280.20	1.72			1.91	49.0	26.3	2.57			
12X-2, 20	286.70	1.74			1.94	52.6	27.8	2.76			
12X-4, 20	289.70	1.82			2.03	51.2	25.8	2.90			
13X-2, 85	296.85	1.71			1.92	48.2	25.8	2.67			
13X-4, 85	299.85	1.76									
13X-4, 91	299.91	1.73	1.79	−3.63	1.95	48.6	25.6	2.72			
13X-7, 21	303.71	1.77			1.87	53.7	29.5	2.73			
14X-2, 89	306.39	1.69			1.90	53.0	28.6	2.79			
14X-4, 8	308.58	1.67			1.84	55.7	31.0	2.71			
14X-5, 66	310.66	1.74	1.78	−2.10	1.85	55.0	30.4	2.73			
15X-2, 95	315.95	2.06	2.06	−0.05	1.92	49.2	26.3	2.72			
15X-4, 10	318.10	2.08	2.11	−1.43	1.83	52.4	29.3	2.73			
15X-6, 132	322.32	2.03	2.00	1.39	1.93	47.9	25.4	2.74			
15X-6, 136	322.36	2.03	2.02	0.40	1.87	50.5	27.6	2.71			
16X-2, 126	325.76	1.92	1.88	2.27	1.96	48.3	25.2	2.75			
16X-4, 73	328.23	2.04	1.99	2.98	1.95	47.5	24.9	2.74			
16X-6, 23	330.73	1.89	1.88	0.74	2.01	43.9	22.4	2.72			
17X-2, 68	334.68	1.97	1.88	4.94	1.99	45.5	23.4	2.73			
17X-5, 96	339.46	1.93			2.12	37.2	18.0	2.74			
18X-1, 126	343.26	2.04			2.06	41.2	20.5	2.71			
18X-3, 9	345.09	1.99	1.92	3.69	2.09	40.4	19.8	2.71			
18X-5, 11	348.11	2.00	1.82	9.27	2.06	41.6	20.7	2.74			
19X-2, 70	353.70	2.13	2.08	2.23	2.16	38.2	18.1	2.73			
19X-4, 137	357.37	2.04	1.93	5.58	2.17	36.4	17.2	2.72			
19X-6, 4	359.04	1.87	1.80	3.60	2.19	36.2	17.0	2.73			
20X-1, 74	361.74	1.91	1.87	1.96	2.11	39.1	19.0	2.71			
20X-1, 137	362.37	1.94			2.13	39.4	19.0	2.73			
20X-3, 7	364.07				2.08	40.8	20.1	2.72			
21X-1, 44	370.94	1.91			2.22	39.0	18.0	2.72			
21X-3, 26	373.76	1.71			2.23	39.6	18.2	2.91			
22X-1, 34	380.34	1.74			2.29	62.5	27.9	2.70			
22X-CC, 34	389.84				2.01	43.3	22.0	2.56			
23X-1, 48	389.98	1.88			2.01	40.4	20.6	2.58			
23X-3, 50	393.00	1.88									
23X-5, 16	395.66		1.75		1.96	46.9	24.5	2.64			
24X-2, 39	400.89				1.82	55.2	31.0	2.64			
24X-4, 143	404.93		1.65		1.82	57.0	32.1	2.64			
24X-6, 37	406.87				1.79	54.7	31.3	2.54			
25X-2, 18	410.18	1.67	1.75	−4.44							
25X-3, 105	412.55	1.62	1.76	−8.06	1.86	52.1	28.7	2.55			
25X-5, 105	415.55	1.72	1.75	−1.96	1.81	51.4	29.2	2.47			
26X-1, 40	418.40				1.71	56.3	33.8	2.23			
26X-3, 40	421.40				1.81	53.8	30.5	2.47			
27X-2, 50	429.50				1.87	54.2	29.7	2.47			
27X-4, 10	432.10				1.91	52.3	28.0	2.64			
28X-2, 30	438.80				1.85	52.6	29.0	2.70			
28X-4, 54	442.04				1.88	53.8	29.3	2.61			
28X-CC, 40	446.90				1.91	56.1	30.1	2.70			
29X-2, 86	448.86	1.64			1.93	51.5	27.4	2.51			
29X-4, 68	451.68				1.94	51.2	27.0	2.49			
29X-6, 80	454.80				1.86	52.8	29.1	2.49			
30X-2, 10	457.60				1.91	51.5	27.7	2.61			

Table 9 (continued).

Core, section, interval (cm)	Depth (mbsf)	V_{ph} (km/s)	V_{pv} (km/s)	Anisotropy (%)	Bulk density (g/cm^3)	Porosity (%)	Water content (%)	Grain density (g/cm^3)	Formation factor		Shear strength (kPa)
									Horizontal	Vertical	
30X-4, 98	461.48	1.80	1.72	4.59	1.82	50.0	28.2	2.49			
30X-6, 63	464.13	1.81	1.73	4.41	1.82	48.6	27.3	2.53			
31X-1, 65	466.15	1.78	1.66	6.93	1.82	50.6	28.5	2.46			
31X-4, 134	471.34	1.79	1.68	6.17	1.85	52.0	28.8	2.50			
31X-6, 42	473.42	1.76			1.84	52.3	29.1	2.50			
32X-2, 94	477.44	1.89	1.73	8.85	1.90	47.3	25.5	2.57			
32X-4, 47	479.97	1.91	1.83	4.13	1.96	44.3	23.2	2.64			
32X-6, 83	483.33	1.79	1.67	6.47	1.86	51.2	28.2	2.57			
33X-2, 94	486.94	1.76	1.72	2.30	1.81	52.4	29.6	2.53			
33X-4, 79	489.79	1.83	1.74	5.03	1.81	49.7	28.1	2.47			
33X-6, 70	492.70				1.89	67.2	36.4	2.20			
34X-1, 72	494.72	1.78	1.66	7.14	1.92	49.8	26.5	2.62			
34X-3, 120	498.20	1.45	1.59	−9.08	1.90	52.0	28.1	2.61			
34X-6, 4	501.54	1.85	1.74	6.18	1.90	50.7	27.3	2.58			
35X-2, 113	506.13	1.99	1.89	5.21	2.04	43.6	21.8	2.64			
35X-4, 45	509.00	1.83	1.83	−0.05	1.95	49.5	26.0	2.58			
35X-6, 21	511.21	1.91	1.77	7.83	1.97	47.1	24.5	2.62			
36X-1, 23	513.23				1.90	51.1	27.5	2.63			
36X-3, 103	517.03		1.71		2.10	53.0	25.8	2.59			
36X-5, 67	519.67	1.89	1.74	8.26	1.97	45.5	23.7	2.61			
36X-7, 9	522.09	2.00	1.86	7.59	2.05	40.4	20.3	2.63			
37X-1, 110	523.60	2.02	1.90	6.58	2.03	42.6	21.5	2.63			
37X-3, 135	526.85	1.92	1.87	2.70	2.00	43.8	22.5	2.67			
37X-5, 32	528.82	2.02	1.98	2.30	2.06	38.5	19.1	2.63			
38X-1, 4	532.04	2.88	2.69	6.69	1.99	25.5	13.1	2.27			
38X-1, 79	532.79	1.94	1.78	8.28	1.97	48.3	25.1	2.75			
39X-1, 77	542.27		1.82		1.97	48.4	25.2	2.72			
39X-2, 7	543.07	2.74	2.66	3.00	1.95	26.7	14.0	2.26			
40X-1, 90	551.90	2.01			1.95	47.4	24.9	2.60			
40X-2, 111	553.61	1.92			1.90	50.9	27.4	2.57			
41X-1, 55	561.05	2.21			2.06	40.1	19.9	2.59			
42X-2, 63	572.13				2.06	47.2	23.5	2.73			
42X-4, 44	574.94	1.46			2.04	46.7	23.5	2.72			
42X-6, 38	577.88				2.00	46.6	23.8	2.56			
43X-2, 39	581.39	5.02	5.00	0.58	2.69	2.2	0.8	2.67			
43X-2, 105	582.05	1.92	1.88	2.00	2.00	43.2	22.1	2.60			
44X-2, 34	590.84	1.48	1.72	−15.57	1.95	42.9	22.5	2.56			
44X-4, 66	594.16	1.40	1.73	−21.31	1.95	48.6	25.5	2.61			
44X-6, 65	597.15	1.58	1.62	−2.93	1.98	43.4	22.5	2.60			
45X-1, 58	599.08	1.63	1.61	1.24	1.95	46.0	24.1	2.59			
45X-4, 13	603.13	1.30			1.94	46.9	24.8	2.48			
46X-4, 59	613.09	1.48	1.44	3.09	1.96	43.3	22.6	2.60			
46X-6, 93	616.43	1.44	1.32	8.53	1.98	46.1	23.8	2.72			
47X-2, 61	619.61	1.65	1.56	5.62	2.08	43.6	21.5	2.73			
47X-3, 47	620.97	1.51	1.47	3.16	2.12	51.2	24.7	2.76			
48X-5, 74	628.24				2.05	45.3	22.7	2.75			
48X-6, 81	628.31	4.70	4.62	1.70	2.66	2.7	1.0	2.64			
49X-1, 94	628.44	4.29	4.55		2.61	3.0	1.2	2.65			
49X-3, 108	631.58				2.03	44.1	22.3	2.84			
49X-3, 135	631.85	3.99	3.99	0.00	2.54	8.0	3.2	2.54			
49X-4, 61	632.61		1.62		1.91	38.5	20.6	2.72			
50X-2, 8	634.08				2.13	41.3	19.9	2.74			
50X-5, 146	636.96				2.25	39.1	17.8	2.71			
50X-CC, 6	639.06				2.16	38.0	18.0	2.67			
51X-2, 67	639.67				2.17	38.5	18.2	2.61			
51X-4, 67	642.67				2.20	39.1	18.2	2.95			
53X-1, 32	647.82	3.71	3.64	1.74	2.54	15.8	6.3	2.76			
54X-1, 39	648.89	4.12	4.20	−1.85	2.67	8.2	3.2	2.69			

ment failed to register meaningful values. Thermal conductivity determinations were not carried out below 617.50 mbsf (Core 122-763B-46X-7) because the drilling biscuits became too thin to give accurate values. Velocity and index properties were measured in all of the cores. In Tables 8–12 the values of the various physical property measurements are listed and in Figures 35–39 the variations of these properties with depth are illustrated.

Velocity

The mean compressional velocity data from Site 763, as determined with the Hamilton Frame (Fig. 35) show a range from 1.52 km/s (oozes, Core 122-763A-1H) to 5.41 km/s (carbonate-cemented claystone, Section 122-763C-12R-1). Most of the materials (oozes, chalks, and claystones) show low velocities (<2.0 km/s). High-velocity samples consisting of minor amounts of carbonate-cemented claystones and sandstones are restricted to an interval that lies between 581.39 mbsf (Section 122-763B-43X-2) and 872.55 mbsf (Section 122-763C-29R-5). This interval corresponds to Units V and VI (see "Lithostratigraphy," this chapter) and is composed of mainly dark silty claystone. High attenuation in the horizontal direction, possibly due to microfracturing, was observed in many of the claystone samples and may be responsible for underestimating velocity by a few hundred

Table 10. Physical-property data, Hole 763C.

Core, section, interval (cm)	Depth (mbsf)	V_{ph} (km/s)	V_{pv} (km/s)	Anisotropy (%)	Bulk density (g/cm^3)	Porosity (%)	Water content (%)	Grain density (g/cm^3)
122-763C-								
2R-1, 107	386.07	1.97			1.87	51.7	28.4	2.61
2R-3, 76	388.76	1.77			1.90	50.4	27.2	2.55
2R-5, 28	391.28	1.83	1.73	5.55	1.87	49.1	26.9	2.52
4R-1, 44	645.54	3.29	3.47	−5.36	2.74	8.7	3.2	2.78
5R-1, 53	655.13				2.19	33.1	15.5	2.70
6R-1, 112	661.72		1.67		2.19	39.0	18.2	2.71
6R-2, 88	662.98	4.79	4.77	0.40	2.67	2.5	1.3	2.66
6R-3, 22	663.82				2.17	38.4	18.1	2.73
7R-1, 134	666.94	1.64	1.69	−3.42	2.23	37.7	17.3	2.70
8R-1, 24	671.24	3.81	3.86	−1.28	2.57	11.2	4.5	2.63
8R-3, 26	673.86		1.60		2.07	40.0	19.8	2.61
9R-2, 120	678.30		1.56		2.16	36.2	17.2	2.69
9R-4, 64	680.74				2.15	39.1	18.6	2.74
9R-4, 80	680.90	3.96	4.23	−6.52	2.58	7.2	2.9	2.40
9R-5, 1	681.61	1.66	1.69	−1.61	2.15	41.4	19.8	2.78
10R-2, 128	687.88				2.18	41.3	19.4	2.71
10R-4, 49	690.09				2.10	41.8	20.4	2.76
10R-6, 50	693.10		1.65		2.16	38.5	18.2	2.73
10R-7, 65	694.75	3.48	3.45	0.81	2.52	13.5	5.5	2.70
11R-2, 6	696.16		1.61		2.23	37.7	17.3	2.70
12R-1, 15	704.25	5.41	5.41	−0.06	2.70	0.2	0.1	2.69
12R-2, 15	705.75		1.61		2.15	38.5	18.3	2.73
13R-1, 98	714.58		1.64		2.17	34.5	16.3	2.65
13R-3, 20	716.80	3.38	3.36	0.83	2.82	16.0	5.8	3.13
13R-5, 47	720.07		1.76		2.16	36.8	17.4	2.69
14R-2, 42	725.02				2.11	50.6	24.5	2.71
14R-3, 118	727.28		3.79		2.94	13.7	4.8	3.19
14R-4, 24	727.84				2.20	43.1	20.1	2.71
15R-2, 24	734.34				2.29	36.6	16.4	2.76
15R-3, 10	735.70				2.17	38.9	18.4	2.68
16R-2, 42	744.02				2.21	37.3	17.3	2.73
16R-3, 32	745.42				2.18	40.7	19.2	2.73
16R-4, 10	746.70	1.46			2.22	38.0	17.5	2.75
16R-5, 12	748.22				2.16	40.8	19.4	2.71
16R-6, 100	750.60	1.79			2.19	37.4	17.5	2.72
17R-2, 88	753.98	1.30			2.28	38.6	17.3	2.81
17R-4, 8	756.18	1.31			2.11	46.4	22.5	2.68
17R-6, 24	759.34	1.34			2.23	37.2	17.1	2.71
18R-1, 48	761.58				2.18	35.5	16.7	2.69
18R-3, 100	765.10	1.45			2.19	36.6	17.1	2.70
18R-4, 108	766.68	1.35			2.24	35.4	16.2	2.69
19R-1, 57	771.17	3.58	3.23	10.08	2.55	11.3	4.5	2.69
19R-3, 33	773.93	1.26			2.12	38.3	18.5	2.65
19R-5, 13	776.73	1.26			2.16	37.0	17.6	2.67
20R-1, 77	780.87	5.07	5.14	−1.39	2.69	0.4	0.2	2.68
20R-2, 94	782.54	1.69	1.79	−5.51	2.17	35.4	16.7	2.69
20R-4, 101	785.61	1.69	1.81	−6.81	2.20	34.1	15.9	2.71
21R-2, 102	792.12	1.72	1.68	2.24	2.20	34.2	16.0	2.72
21R-4, 64	794.74	1.76	1.77	−0.57	2.20	35.1	16.3	2.72
21R-6, 81	797.91	1.75	1.85	−5.84	2.19	33.9	15.9	2.69
22R-1, 113	800.23	1.58	1.87	−16.50	2.24	32.1	14.7	2.71
22R-3, 28	802.38	1.78	1.85	−3.69	2.24	32.6	14.9	2.74
22R-5, 106	806.16	1.39	1.72	−20.99	2.22	35.6	16.4	2.72
22R-6, 5	806.65	1.65	1.84	−10.43	2.23	32.9	15.1	2.67
23R-2, 42	810.52	4.00	4.11	−2.71	2.67	2.1	0.8	2.67
23R-2, 95	811.05	1.38	1.75	−23.56	2.21	35.0	16.2	2.73
23R-4, 55	813.65	1.50	1.81	−18.46	2.31	29.0	12.8	2.65
23R-5, 27	814.87	1.51	1.80	−17.16	2.24	30.1	13.7	2.68
24R-2, 20	819.80	1.89	1.84	2.14	2.58	51.7	20.6	2.76
24R-4, 69	823.29	1.70	1.89	−10.63	2.23	31.6	14.5	2.68
24R-6, 62	826.22	1.74	1.90	−8.81	2.21	31.4	14.5	2.66
25R-2, 125	830.35	2.87	2.67	7.34	2.70			2.67
25R-4, 2	832.12	1.85	1.82	1.20	2.33			2.73
25R-6, 43	835.53	1.88	1.84	2.21	2.19	30.0	14.0	2.61
26R-1, 62	837.72	3.35	3.19	5.11	2.90	15.4	5.4	3.19
26R-3, 54	840.64	1.39			2.23	37.6	17.3	2.70
26R-5, 22	843.32	1.33			2.25	35.7	16.2	2.74
27R-1, 10	846.70	1.38			2.23	35.6	16.4	2.67
27R-3, 90	850.50				2.24	33.8	15.4	2.72
27R-5, 128	853.88	1.38			2.26	33.8	15.3	2.74
28R-2, 28	857.88	1.34			2.25	34.3	15.6	2.75
28R-4, 9	860.69				2.26	33.8	15.4	2.74
28R-6, 85	864.45	1.95			2.30	35.9	16.0	2.82
29R-1, 67	866.27	1.55			2.27	34.7	15.7	2.80
29R-3, 37	868.97	1.67	1.85	−10.51	2.29	36.0	16.1	2.74

Table 10 (continued).

Core, section, interval (cm)	Depth (mbsf)	V_{ph} (km/s)	V_{pv} (km/s)	Anisotropy (%)	Bulk density (g/cm^3)	Porosity (%)	Water content (%)	Grain density (g/cm^3)
29R-5, 95	872.55	4.45	3.73	17.57	2.98	4.3	1.5	3.00
30R-2, 100	877.60	1.32			2.25	37.2	16.9	2.75
30R-4, 134	880.94	2.75			2.25	38.7	17.6	2.81
30R-6, 112	883.72				2.24	34.8	15.9	2.71
31R-2, 112	887.22	1.73	1.78	−2.79	2.22	32.2	14.9	2.68
31R-4, 70	889.80	1.77	1.78	−0.45	2.22	32.4	14.9	2.66
31R-6, 86	892.96	2.03	2.00	1.54	2.25	30.6	14.0	2.70
32R-3, 128	898.38	1.81	1.87	−2.88	2.23	31.9	14.7	2.72
32R-5, 44	900.54	1.86	1.92	−2.81	2.25	32.7	14.9	2.73
32R-7, 26	903.36	1.89	1.97	−3.94	2.22	34.9	16.1	2.62
33R-2, 138	906.48	1.88	1.90	−0.90	2.30	33.5	14.9	2.71
33R-4, 87	908.97	1.66	1.87	−11.72	2.23	35.7	16.4	2.72
34R-3, 8	916.18		1.57		2.25	31.6	14.4	2.64
34R-5, 41	919.51	1.62			2.33	30.2	13.3	2.76
35R-1, 24	922.84	1.85	1.98	−6.64	2.25	28.7	13.0	2.65
35R-3, 23	925.83	1.78	1.94	−8.40	2.27	30.2	13.7	2.72
35R-5, 147	930.07	1.82	1.98	−8.31	2.24	29.9	13.7	2.67
36R-3, 117	936.27	1.88	1.82	3.18	2.31	28.5	12.6	2.65
36R-5, 112	939.22	1.83	2.02	−10.23	2.34	30.7	13.5	2.64
36R-6, 48	940.08	2.14	2.01	6.21	2.29	27.0	12.1	2.63
37R-1, 142	943.02	1.92	1.91	0.37	2.27	27.5	12.4	2.67
37R-2, 126	944.36	1.92	1.99	−3.22	2.27	27.6	12.5	2.60
37R-3, 130	945.90	1.91	2.00	−4.77	2.29	26.7	11.9	2.62
37R-6, 63	949.73	2.13	1.98	7.39	2.36	31.1	13.5	2.67
38R-1, 133	952.43	1.96			2.26	33.5	15.2	2.71
38R-3, 143	955.53	1.85	1.89	−2.03	2.28	32.5	14.6	2.72
38R-5, 58	957.68	1.69			2.28	30.3	13.6	2.70
38R-6, 52	959.12	2.02			2.31	31.7	14.1	2.71
39R-2, 108	963.18				2.32	36.8	16.2	2.72
39R-4, 22	965.32				2.21	33.8	15.7	2.71
39R-6, 12	968.22				2.19	33.1	15.5	2.63
40R-2, 88	972.48	1.82			2.28	30.7	13.8	2.72
41R-2, 108	982.18	1.70			2.23	33.6	15.4	2.75
41R-4, 82	984.92	1.57			2.32	33.9	15.0	2.77
41R-6, 73	987.83	1.66			2.22	33.0	15.2	2.66
42R-1, 38	989.48	1.63			2.25	31.6	14.4	2.82
42R-3, 68	992.78				2.16	40.0	19.0	2.71
42R-5, 57	995.67				2.31	30.2	13.4	2.87
43R-2, 77	1000.87	1.78			2.32	30.2	13.3	2.70
43R-4, 4	1003.14				2.34	29.9	13.1	2.76
43R-5, 114	1005.74	2.20	2.12	3.76	2.31	29.3	13.0	2.74
44R-2, 95	1010.55	1.77	1.85	−4.75	2.27	30.7	13.9	2.70
44R-4, 2	1012.62	2.06	2.10	−1.59	2.28	28.6	12.9	2.69
44R-6, 56	1016.16	2.30	2.11	8.80	2.30	27.1	12.1	2.70
45R-2, 138	1020.48	1.81	1.83	−1.05	2.28	30.7	13.8	2.68
45R-4, 12	1022.22	2.16	2.12	1.50	2.27	27.7	12.5	2.69
45R-6, 113	1026.23	2.22	2.07	7.03	2.31	24.5	10.8	2.69
46R-2, 60	1029.20	2.19	2.16	1.52	2.29	25.9	11.6	2.67
46R-4, 119	1032.79	2.22	2.08	6.56	2.29	26.8	12.0	2.69

meters per second (e.g., Section 122-763C-17R-2, 754.0 mbsf, to Section 122-763C-30R-2, 878.0 mbsf).

On the basis of an increase in velocity we place the beginning of the ooze/chalk transition at approximately 223.0 mbsf (Section 122-763B-5X-4), about 24 m above the Cretaceous/Tertiary boundary. Anisotropy in the velocity measurements (Fig. 35) is mostly positive for the samples taken from Hole 763B and scattered for Hole 763C, generally showing no consistent trend with depth.

Physical-Properties Units and Index Properties

Grain densities (Fig. 35) fall into three distinct units. Between the seafloor and the Cenomanian/Turonian boundary at 385.7 mbsf (between the bottom of Core 122-763B-22X and the top of Core 122-763B-23X) the grain densities are on average between 2.6–2.7 g/cm^3 (carbonate oozes and chalks). Below approximately 625.0 mbsf (Core 122-763B-48X) grain densities are similar, about 2.65 g/cm^3 (claystones). Between these two units there is a region with low grain densities of about 2.2–2.5 g/cm^3 (calcareous claystones). The density of opal-CT is approximately 2.2 g/cm^3, and in this interval the relative abundance of silica increases (see "Inorganic Geochemistry," this chapter). Zeolites were described in this unit as well (see "Lithostratigraphy," this chapter), and can have low densities similar to opal-CT (Deer et al., 1978).

Wet-bulk densities (Fig. 35) in the oozes increase irregularly with depth until the ooze/chalk transition. The most marked features are the rapid increase of the bulk density with depth between the seafloor (1.47 g/cm^3) and about 50 mbsf (1.75 g/cm^3 in Core 122-763A-6H), a change not correlative with the velocity data or any of the other index properties. At about 150 mbsf (Core 122-763A-17H) bulk densities show a relative minimum of 1.6 g/cm^3 that is correlative with a locally high porosity of 61% (Fig. 35) and a high water content of 38% (Fig. 35). Between the bottom of Core 122-763A-21H and the top of Core 122-763B-2X there is a decrease of about 0.1 g/cm^3 in the bulk densities, much more abrupt than the previous minimum. A sharp decrease in water content is also measured in this precinct. In previous sites such large variations in index

Table 11. Thermal-conductivity data, Holes 763A and 763B.

Core, section, interval (cm)	Depth (mbsf)	Thermal conductivity (W/m·K)
122-763A-		
3H-2, 60	16.50	1.27
3H-3, 60	18.00	1.27
3H-4, 60	19.50	1.27
3H-5, 60	21.00	1.26
3H-6, 60	22.50	1.21
4H-2, 60	26.00	1.31
4H-3, 60	27.50	1.23
4H-4, 60	29.00	1.25
4H-5, 60	30.50	1.22
4H-6, 60	32.00	1.05
5H-2, 60	35.50	1.26
5H-3, 60	37.00	1.32
5H-4, 60	38.50	1.28
5H-5, 60	40.00	1.25
5H-6, 60	41.50	1.28
6H-2, 60	45.00	1.38
6H-3, 60	46.50	1.38
6H-4, 60	48.00	1.31
6H-5, 60	49.50	1.41
7H-2, 60	54.50	1.39
7H-3, 60	56.00	1.37
7H-4, 60	57.50	1.41
7H-5, 60	59.00	1.26
8H-2, 60	64.00	1.41
8H-3, 60	65.50	1.37
8H-4, 60	67.00	1.43
8H-5, 60	68.50	1.36
9H-2, 60	73.50	1.46
9H-4, 60	76.70	1.41
9H-5, 60	78.00	1.38
9H-6, 60	79.50	1.36
10H-2, 60	83.00	1.45
10H-4, 60	86.00	1.39
10H-6, 60	89.00	1.32
10H-7, 40	90.30	1.40
11H-2, 60	92.50	1.40
11H-4, 60	95.50	1.41
11H-6, 60	98.50	1.53
12H-2, 60	102.00	1.38
12H-4, 60	105.00	1.46
12H-6, 60	108.00	1.42
13H-2, 60	111.50	1.50
13H-4, 60	114.50	1.46
13H-6, 60	117.50	1.47
14H-2, 60	121.00	1.62
14H-4, 60	124.00	1.51
14H-6, 60	127.00	1.47
15H-2, 60	130.50	1.39
15H-4, 60	133.50	1.51
15H-6, 60	136.50	1.48
16H-2, 60	140.00	1.38
16H-4, 60	143.00	1.38
16H-6, 60	146.00	1.37
17H-2, 60	149.50	1.43
17H-4, 60	152.50	1.51
17H-6, 70	155.60	1.42
18H-2, 70	159.10	1.42
18H-4, 70	162.10	1.44
18H-6, 70	165.10	1.41
19H-2, 65	168.55	1.43
19H-5, 79	173.19	1.53
20H-2, 69	178.09	1.53
20H-4, 69	181.09	1.44
20H-6, 64	184.04	1.47
21H-2, 59	187.49	1.61
21H-4, 61	190.51	1.65
21H-6, 63	193.53	1.48
122-763B-		
3X-4, 45	204.45	1.44
3X-5, 45	205.95	1.47
4X-2, 45	210.95	1.57
5X-1, 60	219.10	1.45
5X-2, 60	220.60	1.44

Table 11 (continued).

Core, section, interval (cm)	Depth (mbsf)	Thermal conductivity (W/m·K)
5X-3, 60	222.10	1.47
6X-2, 60	230.10	1.57
6X-4, 70	233.20	1.49
6X-5, 70	234.70	1.60
6X-6, 70	236.20	1.52
7X-1, 60	238.10	1.52
7X-2, 60	239.60	1.44
8X-2, 60	249.10	1.61
8X-3, 60	250.60	1.60
10X-4, 40	270.90	1.65
10X-6, 30	273.80	1.69
10X-7, 25	275.25	1.74
11X-4, 60	280.60	1.72
11X-5, 60	282.10	1.68
12X-2, 20	286.70	1.58
12X-4, 20	289.70	1.48
13X-2, 60	296.60	1.14
13X-4, 105	300.05	1.64
13X-6, 70	302.70	1.67
13X-7, 10	303.60	1.76
14X-4, 54	309.04	1.55
15X-2, 66	315.66	2.20
15X-4, 42	318.42	1.64
15X-6, 69	321.69	1.72
16X-2, 31	324.81	1.68
16X-4, 31	327.81	1.70
16X-6, 26	330.76	1.71
17X-4, 49	337.49	1.92
18X-2, 49	343.99	1.77
18X-4, 50	347.00	1.63
19X-4, 50	356.50	1.76
19X-6, 66	359.66	1.88
20X-2, 51	363.01	1.72
21X-1, 48	370.98	1.82
22X-1, 54	380.54	1.35
24X-2, 54	401.04	1.36
24X-4, 29	403.79	1.34
25X-2, 65	410.65	1.10
25X-4, 37	413.37	1.20
25X-6, 29	416.29	1.25
26X-4, 36	422.86	1.26
27X-2, 58	429.58	1.35
27X-4, 73	432.73	1.26
28X-2, 60	439.10	1.24
28X-4, 60	442.10	1.44
28X-6, 60	445.10	1.34
29X-2, 60	448.60	1.41
29X-4, 60	451.60	1.36
29X-6, 60	454.60	1.42
30X-2, 60	458.10	1.35
30X-4, 60	461.10	1.13
30X-6, 60	464.10	1.37
31X-2, 60	467.60	1.42
31X-4, 60	470.60	1.36
31X-6, 60	473.60	1.13
32X-2, 60	477.10	1.38
32X-4, 60	480.10	1.55
32X-6, 60	483.10	1.28
33X-4, 60	489.60	1.23
34X-2, 60	496.10	1.41
34X-4, 60	499.10	1.36
34X-6, 60	502.10	1.23
35X-2, 60	505.60	1.41
35X-4, 60	508.60	1.19
35X-6, 60	511.60	1.38
36X-2, 38	514.88	1.37
36X-4, 28	517.78	1.23
36X-6, 14	520.64	1.46
37X-4, 34	527.34	1.67
37X-6, 22	530.22	1.48
38X-1, 33	532.33	1.54
39X-1, 39	541.89	1.46
40X-1, 60	551.60	1.15
40X-2, 60	553.10	1.33
41X-1, 84	561.34	1.20
41X-2, 76	562.76	1.34
42X-2, 68	572.18	1.35

Table 11 (continued).

Core, section, interval (cm)	Depth (mbsf)	Thermal conductivity (W/m·K)
42X-4, 68	575.18	1.46
42X-6, 68	578.18	1.54
42X-7, 68	579.68	1.53
43X-1, 60	580.10	1.53
43X-3, 60	583.10	1.40
44X-2, 60	591.10	1.34
44X-4, 60	594.10	1.25
44X-5, 60	595.60	1.27
44X-6, 60	597.10	1.35
45X-1, 60	599.10	1.26
45X-3, 60	602.10	1.26
46X-3, 45	611.45	1.32
46X-5, 39	614.39	1.34
46X-7, 50	617.50	1.40

properties have been attributed to large changes in the sedimentation rate.

Wet-bulk density, porosity, water content, and velocity measurements allow us to subdivide the grain-density units proposed above and to make a correlation with the lithostratigraphic units for this site (see "Lithostratigraphy," this chapter). We consider that there are four major physical-properties units: (1) the first unit consists of oozes down to 223 mbsf and corresponds approximately to Units I and II; (2) chalk constitutes the second unit down to 385 mbsf (Units III and IV, from the Cretaceous/Tertiary boundary to the Cenomanian/Turonian boundary); (3) calcareous claystone makes up the third unit down to 625 mbsf (low grain densities, Unit IV to the top of Unit V); and (4) silty claystone composes the fourth unit, from about 625 mbsf to the bottom of the hole (Unit V and VI).

Chalk ranges in velocity from 1.66 km/s to 2.1 km/s. Across the Cretaceous/Tertiary unconformity velocities increase downward by about 0.2 km/s, the wet-bulk density increases by about 0.1 g/cm^3 to 1.92 g/cm^3 (e.g., Section 122-763B-7X-2), the porosity decreases by about 10%, and the water content decreases by about 7%. Two major physical-properties trends are noticeable within the chalk. Wet-bulk densities decrease fairly linearly from the top of the chalk (223 mbsf) to 310–320 mbsf (1.83 g/cm^3, Section 122-763B-15X-4) and then increase linearly until 380.34 mbsf (2.29 g/cm^3, Section 122-763B-22X-1). In the upper region of this unit the porosity and water content show a linear increase to 310–320 mbsf. Below 310–320 mbsf both properties linearly decrease to the bottom of the chalk. In the upper region of the chalk, the calcium carbonate content (see "Organic Geochemistry," this chapter) also shows an increase approaching 310–320 mbsf and a linear decrease to the bottom of the unit. As suggested for Site 762 data, a maximum in porosity, minimum in wet-bulk density, and maximum in carbonate content may be related to a maximum in the abundance of hollow biogenic grains in the sediment. There does appear to be a maximum in the foraminiferal content at the point where these physical properties trends change sign (Core 122-763B-14X, see "Lithostratigraphy," this chapter). Within the chalk unit, the velocities remain relatively constant except for an abrupt 0.3 km/s increase over a 5-m interval between Sections 122-763B-14X-5 and -15X-2 due to increased competence of the stratigraphically lower material.

The transition from the chalk unit into the calcareous claystone unit (385.7 mbsf, Core 122-763B-22X) is marked by a decrease in the wet-bulk density of about 0.5 g/cm^3 over a two-core span, from 2.29 g/cm^3, 5 m (Section 122-763B-22X-1, 380 mbsf) above the Cenomanian/Turonian boundary to 1.82 g/cm^3 (Section 122-763B-24X-2, 401.0 mbsf), 16 m below the boundary. Within the unit, the wet-bulk density increases to about 2.29 g/cm^3 at its base (Section 122-763B-48X-5, 628 mbsf).

Table 12. Summary of temperature measurements taken on Leg 122.

Hole	Depth (mbsf)	Temperature (°C) Bottom	Temperature (°C) Sediment	Thermal conductivity (W/m·K)	Heat flow (mW/m^2)	Data
760A	74.2	10.7	12.7	—	—	N
761B	32.7	3.2	10.9	1.37	42.8	N
761B	89.7	2.8	5.6	1.37	42.8	Y
762B	99.4	4.8	14.5	1.33	129.8	?
762B	156.4	4.0	15.4	1.33	96.9	Y
763A	52.4	4.1	7.0	1.35	74.7	Y
763A	90.4	4.4	10.0	1.35	74.7	Y
763A	147.4	4.4	12.0	1.35	74.7	?

Note: Data quality indicated by Y = yes, N = no, ? = uncertain.

The lowermost unit (silty claystone) is defined by a slight average increase in the wet-bulk density of about 0.1 g/cm^3 with respect to the overlying unit. The dominant lithology (silty claystone) shows a general linear increase with depth in wet-bulk density from about 2.1 g/cm^3 to 2.3 g/cm^3 at the bottom (Section 122-763C-46R-4). Porosity and water content values (Fig. 35) show good correlation throughout and an inverse correlation with velocity. Porosities start at about 40%–50% and water content at about 25% at the top of the unit, and decrease linearly to about half their values at the bottom of Hole 763C. An important but minor fraction of the claystones and some sandstones are carbonate-cemented and have high velocity and wet-bulk density, and low porosity and water content values. Depending on the degree of cementation the range of physical-property values for these cemented materials is quite variable. Velocities can range from 2.5–5.4 km/s, porosities can be as low as 0.2% and water content as low as 0.1%. This lithology forms a small percentage of the cores but extends over a broad region that spans from the base of the previous unit (Section 122-763B-38X-1, 532.0 mbsf) to about 873 mbsf (in Section 122-763C-29R-5).

Formation Factor and Shear Strength

The formation factor (Fig. 36) measured horizontally (perpendicular to the core axis) is generally higher than the formation factor measured vertically (parallel to the core axis). Values of formation factor appear to be approximately constant. Shear strengths (Fig. 36) show a slight increase with depth from 6.1 kPa (Section 122-763A-1H-1, 0.1 mbsf) to 25.8 kPa (Section 122-763B-6X-2, 230.34 mbsf). Several large increases in the shear strength cause a departure from the general trend.

Thermal Conductivity

Thermal conductivity (Fig. 35, Table 11) values display a general trend of increasing conductivity with depth from 0.0 to 372.0 mbsf, ranging from 1.27 W/m·K at the top of the hole to about 1.82 W/m·K at 372.0 mbsf. A significant drop starts to occur at this depth. In the next lower core, the conductivity decreases to 1.35 W/m·K (Section 122-763B-22X-1, 380.54 mbsf). Conductivity values remain relatively low below this point and average about 1.4 W/m·K. This marked decrease in the thermal conductivity is possibly related to the change in lithology from chalk to calcareous siltstone (Sydney, 1966) across the Cenomanian/Turonian boundary, which occurs at 385 mbsf.

GRAPE and *P*-wave Logger

GRAPE density measurements and *P*-wave logging (Fig. 37) were stopped at 194.9 mbsf (in ooze) with the last piston

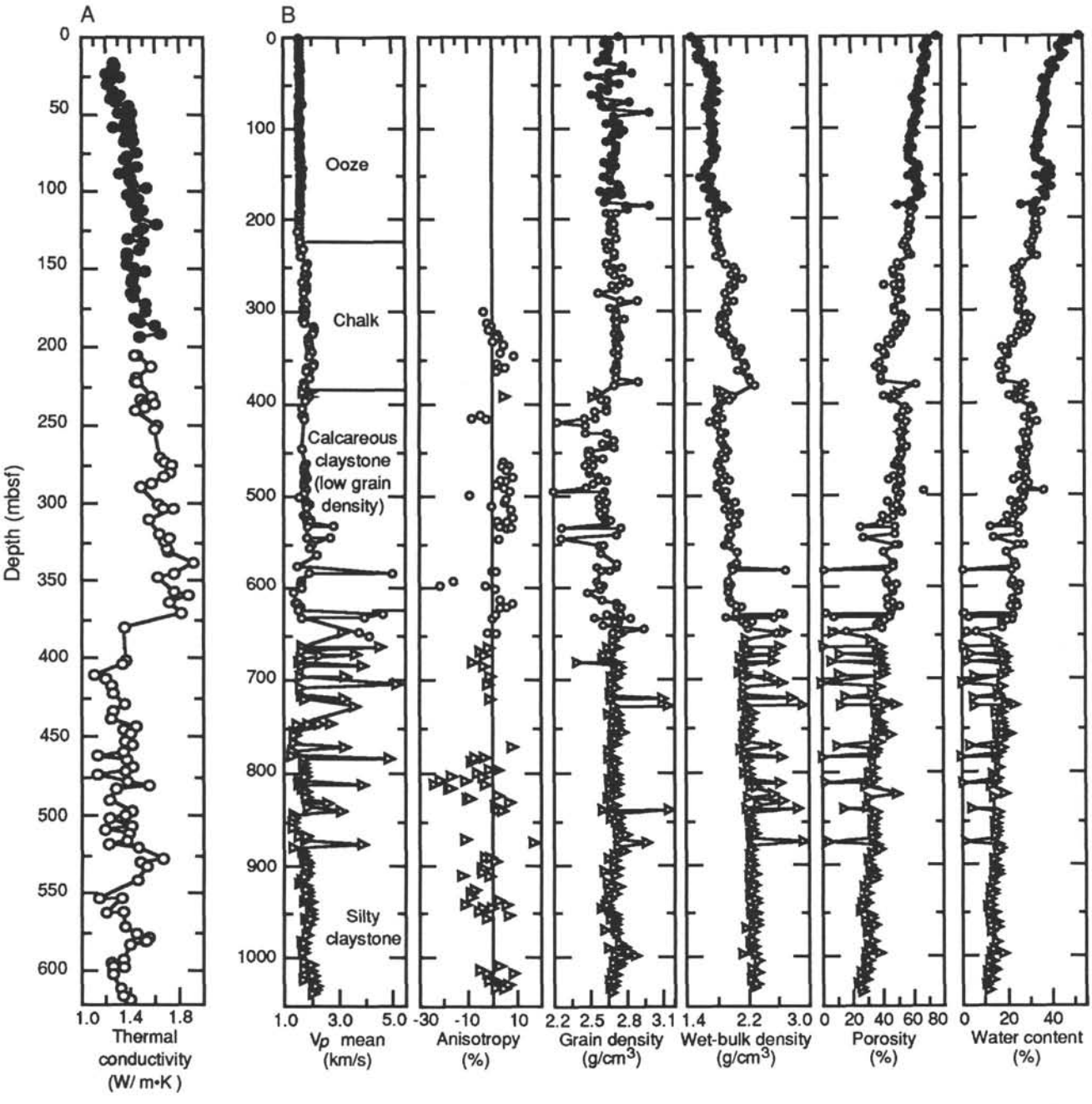

Figure 35. Physical-property data from Site 763. **A.** Thermal conductivity measured through the core liner (upper part of section only). **B.** Horizontal compressional velocity (from Hamilton Frame measurements), velocity anisotropy, grain density, wet-bulk density, porosity, and water content. Solid circles = measurements from Hole 763A; open circles = measurements from Hole 763B; triangles = measurements from Hole 763C.

core (Core 122-763A-21H). GRAPE wet-bulk density estimates agree well with the gravimetric wet-bulk-density values. However, GRAPE data define better the oscillatory nature of the wet-bulk density and show a smaller increase of the wet-bulk density within the first 50 m than do the gravimetric density data. *P*-wave-logger velocities are consistently lower than the Hamilton Frame calibration estimates by about 0.1 km/s. Accurate results on the Hamilton Frame require daily calibration due to instrument drift. Variable equipment delays in the *P*-wave logger could explain the apparent shifts in the two velocity data sets.

Heat Flow

The present-day heat flow pattern on the Exmouth Plateau appears to be dominated by a pore-fluid convection cell (M. Swift, pers. comm., 1988). We developed this hypothesis on the basis of measured surface heat flow values and thermal geohistory analysis of oil exploration wells. Downhole temperature data collected at Sites 762 and 763 were designed to constrain thermal geohistory analyses, especially those from the adjacent industry wells Eendracht-1 and Vinck-1, and to provide data for temperature studies in oil maturation. Three

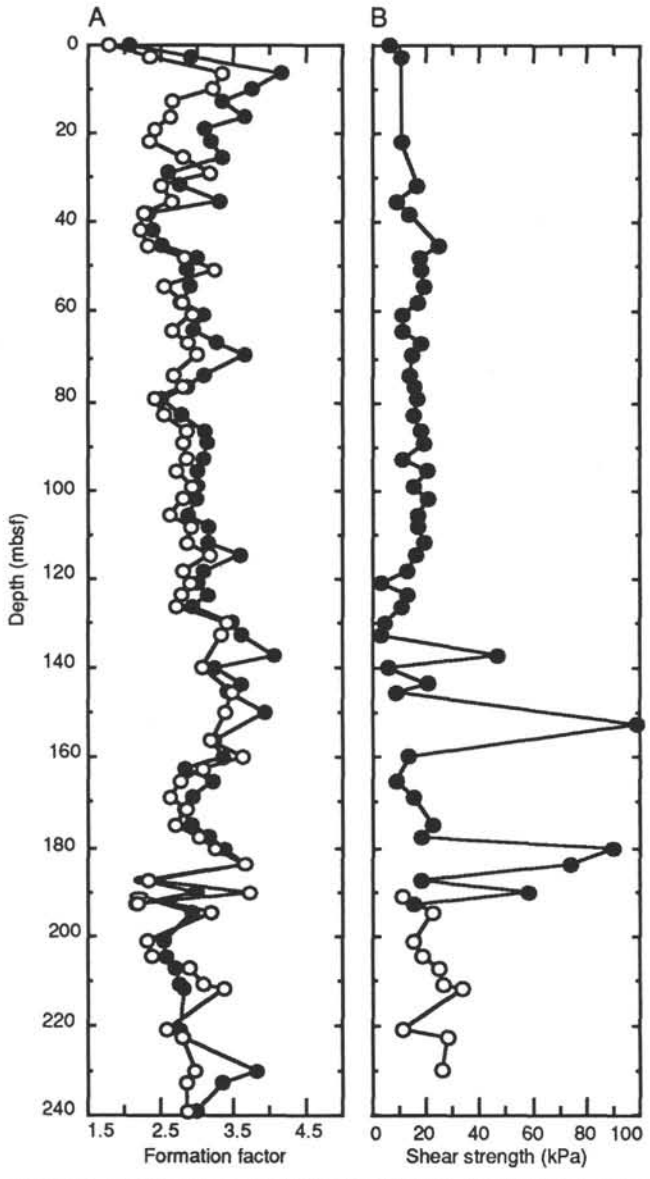

Figure 36. Physical-property data from Site 763. **A.** Formation factor: solid circles = measurements taken horizontally, perpendicular to the core axis, open circles = measurements taken vertically, parallel to the core axis. **B.** Shear strength: solid circles = measurements from Hole 763A; open circles = measurements from Hole 763B.

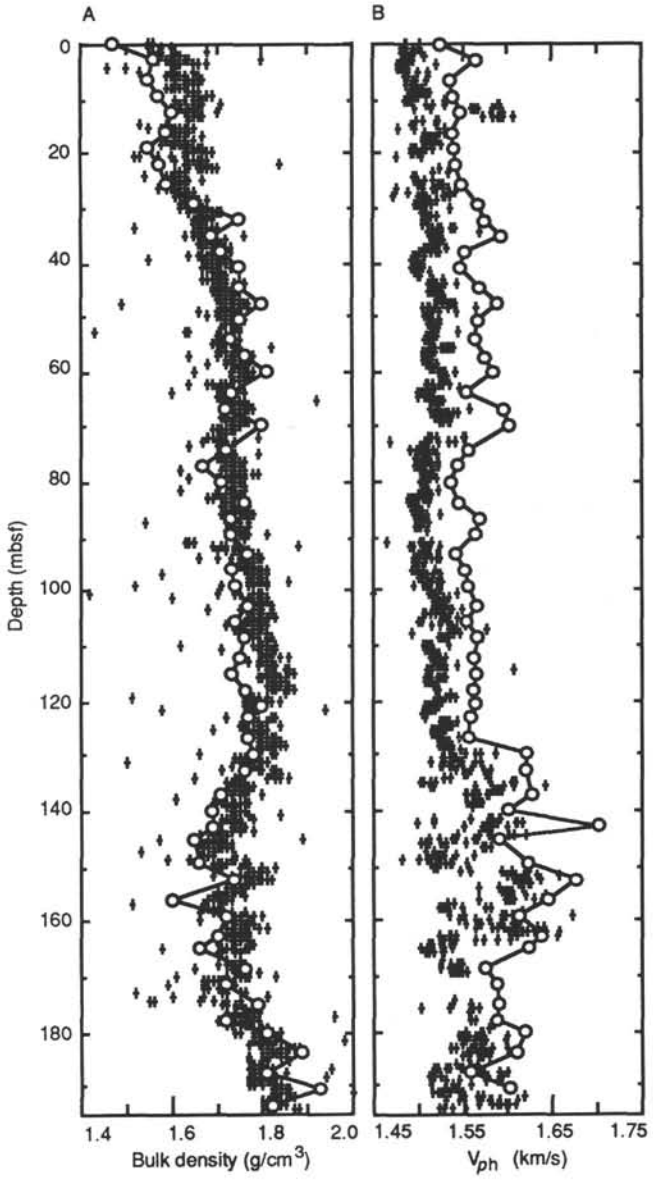

Figure 37. Physical-property data from Site 763. **A.** GRAPE wet-bulk density estimates (small crosses) plotted with the gravimetric wet-bulk density index property values (open circles connected by lines). **B.** *P*-wave velocity measurements from the *P*-wave logger (crosses) plotted with velocities derived from Hamilton Frame measurements (open circles connected by lines).

temperature probe measurements were taken in Hole 763A. The measurements were performed at 52.4, 90.4, and 147.4 mbsf, and the sea state was calm. At 52.4 mbsf, the probe stayed at the mudline for 5 min on both the ascent and descent, and remained on the bottom for 18 min. At 90.4 mbsf, the probe stayed at the mudline for 5 min on both the ascent and descent, and remained on the bottom for 26 min. At 147.4 mbsf, the probe stayed at the mudline for 5–7 min on both the ascent and descent, and remained on the bottom for 30 min.

The bottom temperature at 52.4 mbsf was 7.0°C, at 90.4 mbsf 10.0°C, and at 147.4 mbsf 12.0°C. The upper two temperature values were characterized by flat plateaus in the temperature versus time plots while the third value shows several noise spikes followed by a short plateau (Fig. 38). The plateaus were used to derive the temperature values and these values were plotted against depth to determine a temperature gradient of 55.3°C/km (Fig. 39). Using thermal conductivity measurements of 1.35 W/m·K, averaged over the upper 150 m of Hole 763A, heat flow was calculated (Garland, 1979) as 74.7 mW/m^2. This value is slightly higher than those for sediments above stable continental crust or Mesozoic ocean crust (Sclater et al., 1981) and is intermediate between the low heat-flow values collected on the Wombat Plateau (Site 761) and the high heat-flow values collected nearby at Site 762 (Table 12). Further work is required to determine if these heat-flow values confirm the existence of a pore-fluid convection cell on the southern Exmouth Plateau.

Summary

Compressional-wave-velocity, index-property, and thermal-conductivity values allow us to characterize the sediments at Site 763 into four physical-property units that corre-

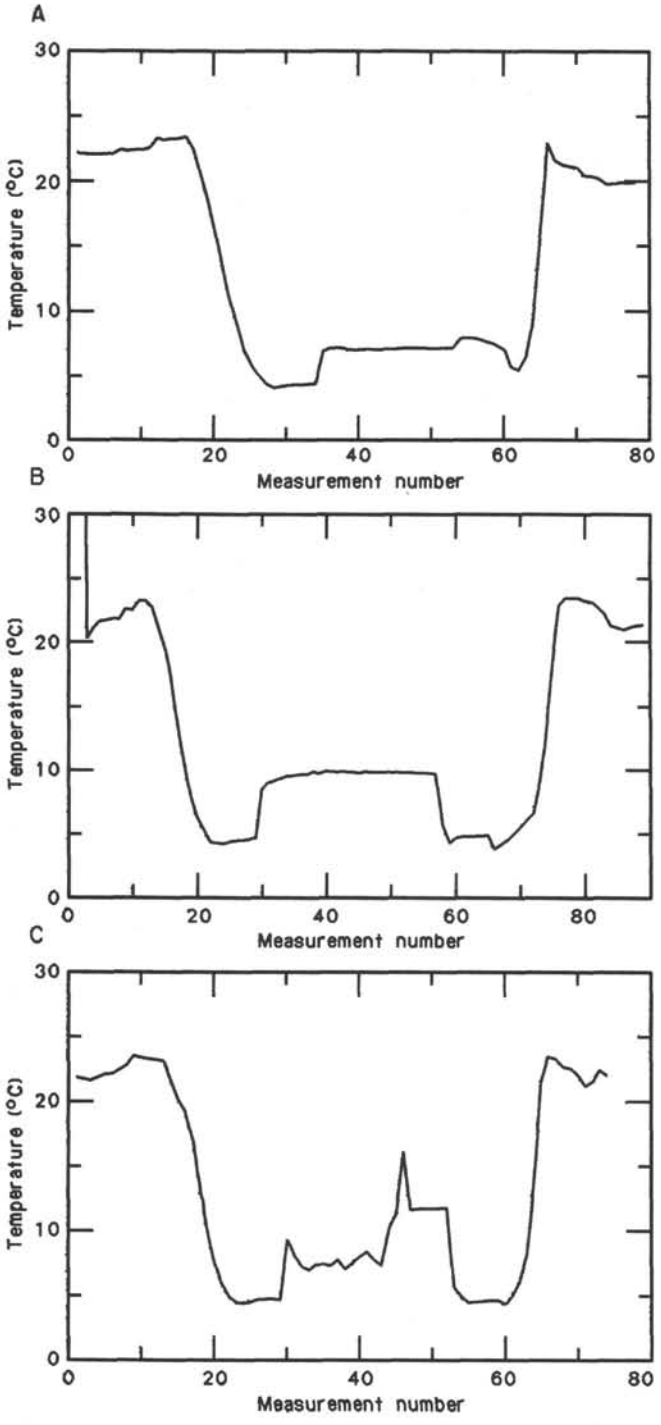

Figure 38. A. Temperature-versus-time records obtained with the temperature probe, Hole 763A. **A.** 52.4 mbsf. **B.** 90.4 mbsf. **C.** 147.4 mbsf.

spond approximately to the lithostratigraphic units (see "Lithostratigraphy," this chapter). From top to bottom, the first unit consists of oozes (seafloor to 223 mbsf), the second of chalk (to the Cenomanian/Turonian boundary at 385 mbsf), the third of calcareous claystone (to about 625 mbsf), and the fourth of siltstone. A sharp increase in velocity characterizes the ooze-to-chalk transition. Low grain density and a noticeable decrease in bulk density and thermal conductivity possibly associated with the increase in water content and lithological change characterizes the third unit.

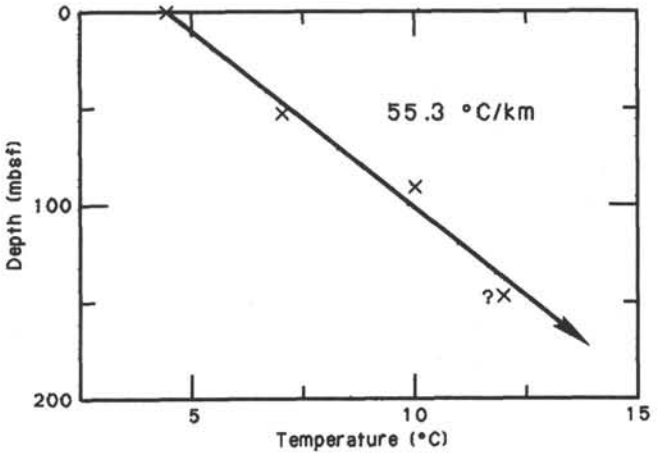

Figure 39. Temperature gradient in Hole 763A.

SEISMIC STRATIGRAPHY

Site 763 was located using petroleum industry multichannel seismic reflection data that was collected in 1978 and used in locating the Vinck-1 well. As with Site 762, the detailed industry seismic reflection data were used in defining the site location because of safety concerns regarding scientific drilling in a region of known gas occurrence. The proposed location of Site 763 was on Line X78A-272 near shotpoint 3508. The quality of the data was good, and strong regional reflectors were recorded in the Tertiary and Cretaceous section to be drilled at Site 763. Site 763 was located on the southeastern Exmouth Plateau in an area of Tertiary and Cretaceous marine calcilutites and chalks, overlying a well-developed distal section of the Late Jurassic to Early Cretaceous Barrow Group. The Barrow Group overlies the Jurassic Dingo Claystone, which drapes the tilted and eroded rift-faulted blocks of the Triassic Mungaroo Formation. Minor reactivation of rift faulting extends into the Cretaceous strata near Site 763.

Radio navigation was used during collection of the industry seismic reflection data and consequently locations along Line X78A-272 are accurately known. The early component of site survey seismic reflection Line 122-5 collected to locate Site 763 was obtained while GPS navigation was available. This component consists of the line segment through the Vinck-1 well and the proposed site location duplicating part of Line X78A-272. GPS navigation coverage was lost during the turn onto the perpendicular line through the proposed site location, required by the JOIDES Pollution Prevention and Safety Panel. We shot the perpendicular line to ensure that the site location was in a structurally low position on both the north-south and east-west profiles and that the site was at least 10 m lower than the Vinck-1 well at the level of any potential reservoir sand at the top of the Barrow Group.

Line 122-5 was thus accurately navigated until beyond the proposed location of Site 763 (including the beacon drop), but locations on the north-south component of that line should be treated with caution. Features on the part of Line 122-5 that duplicates part of Line X78A-272 correspond reasonably well with equivalent features on Line X78A-272. Site 763 was located at shotpoint 218.705 on Line 122-5 at a position 0.8 km east of the Vinck-1 well, at a water depth of 1367.5 m.

Structure

Site 763 is located in a region where the trends of the Triassic and Jurassic rift faults change from mainly north-

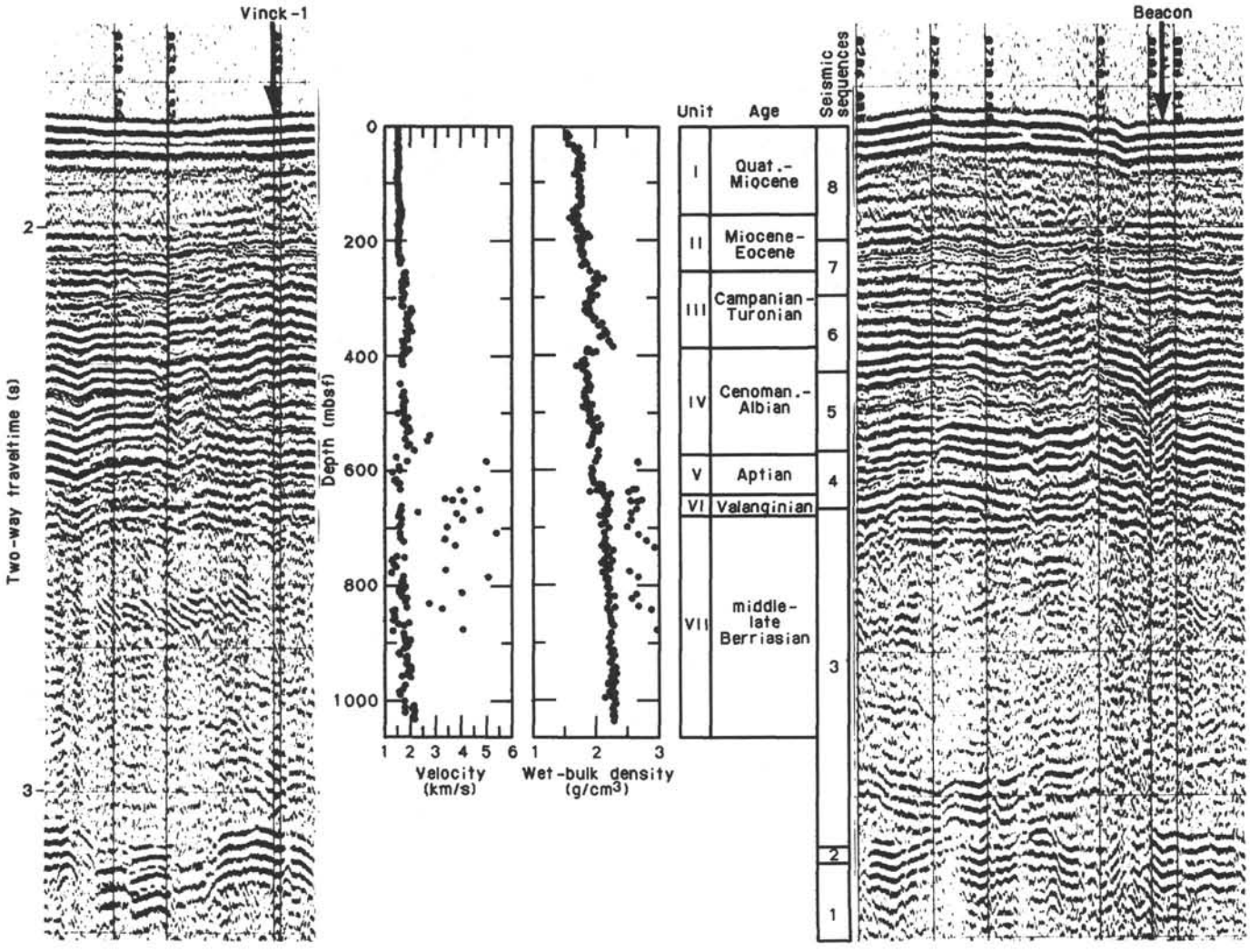

Figure 40. Correspondence between seismic sequences, seismic reflectors, velocity, wet-bulk density, and stratigraphy, Site 763.

south to the north of the site, to mainly northwest-southeast to the south of the site (Exon and Willcox, 1978; Barber, 1982). The structure on which the Vinck-1 well and Site 763 are located is a faulted anticline developed in the zone where the directions of the rift faults change. Horst and graben structures in the region are developed by faults that dip both seaward and landward. The faults are approximately normal at the Jurassic-Triassic level.

Faulting associated with the Triassic and Jurassic rifting has throws on the order of hundreds of meters. The faulting is reactivated and displaces the overlying Jurassic and lower Cretaceous strata with fault throws on the order of tens of meters. Fault throws decrease progressively within the upper Cretaceous, however, so that little displacement and minor fault-associated drape are observed for the seismic horizon corresponding to the top of the Cretaceous.

Sequence Stratigraphy

Figure 40 shows the correspondence between the seismic data and physical-properties measurements at Site 763 and seismic sequences. The seismic sequences distinguished at Site 762 using methods outlined in Vail et al. (1977) were also identified at Site 763. Analysis of these sequences allows an interpretation of the seismic structure and seismic stratigraphy at Site 763, correlation with other data sets from the site (such as wireline logs), and enables a preliminary understanding of seismic facies and relative sea level in that area. Figure 41 shows correlation of seismic sequences between Sites 763 and 762, and between the sites along seismic Line 122-6, and facilitates analysis of the sequence variations between these sites.

Seismic Sequences

Sequence 1

This is the basal sequence at Site 763 (Fig. 40) and lies below approximately 3.14 s two-way traveltime (TWT). It is also identified at Site 762. The upper sequence boundary corresponds to the prominent unconformity near the top of the series of tilted fault blocks found throughout the Exmouth Plateau. Although not drilled at Sites 763 and 762, the sequence can be correlated to the Triassic Mungaroo Formation (e.g., Barber 1982; Wright and Wheatley, 1979).

Sequence 2

This thin sequence lies approximately between 3.10 and 3.14 s (TWT) below sea level. As at Site 762, it displays a conformable to onlapping relationship with the underlying Sequence 1. Drilling at Site 763 terminated around 300 m above the top of Sequence 2, but correlation to other seismic

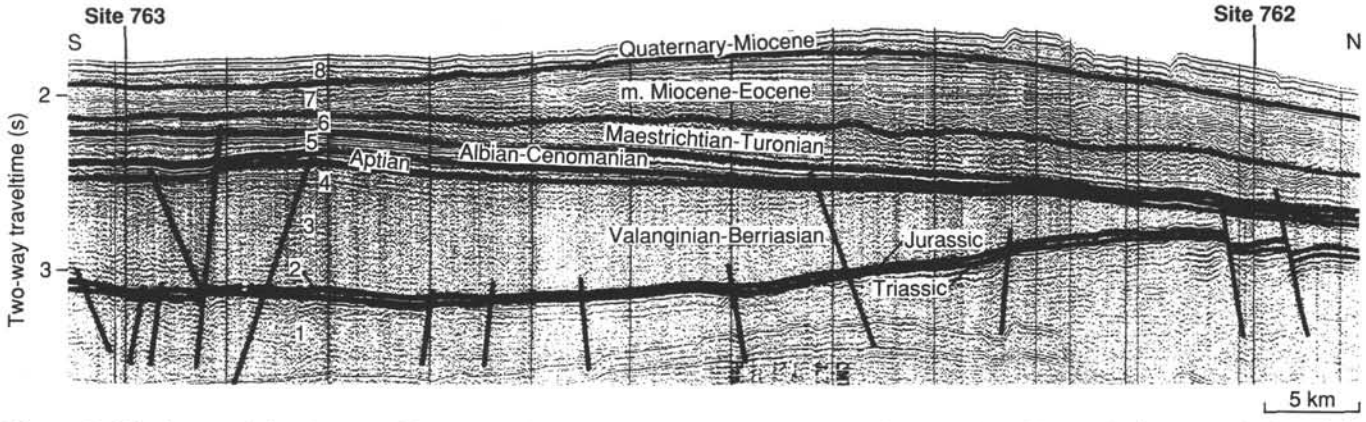

Figure 41. Seismic correlation between Sites 763 and 762. Note the northward thinning of the clastic sediments in Sequences 3–5, and the northward thickening of deep-water carbonate sediments in Sequences 6–8.

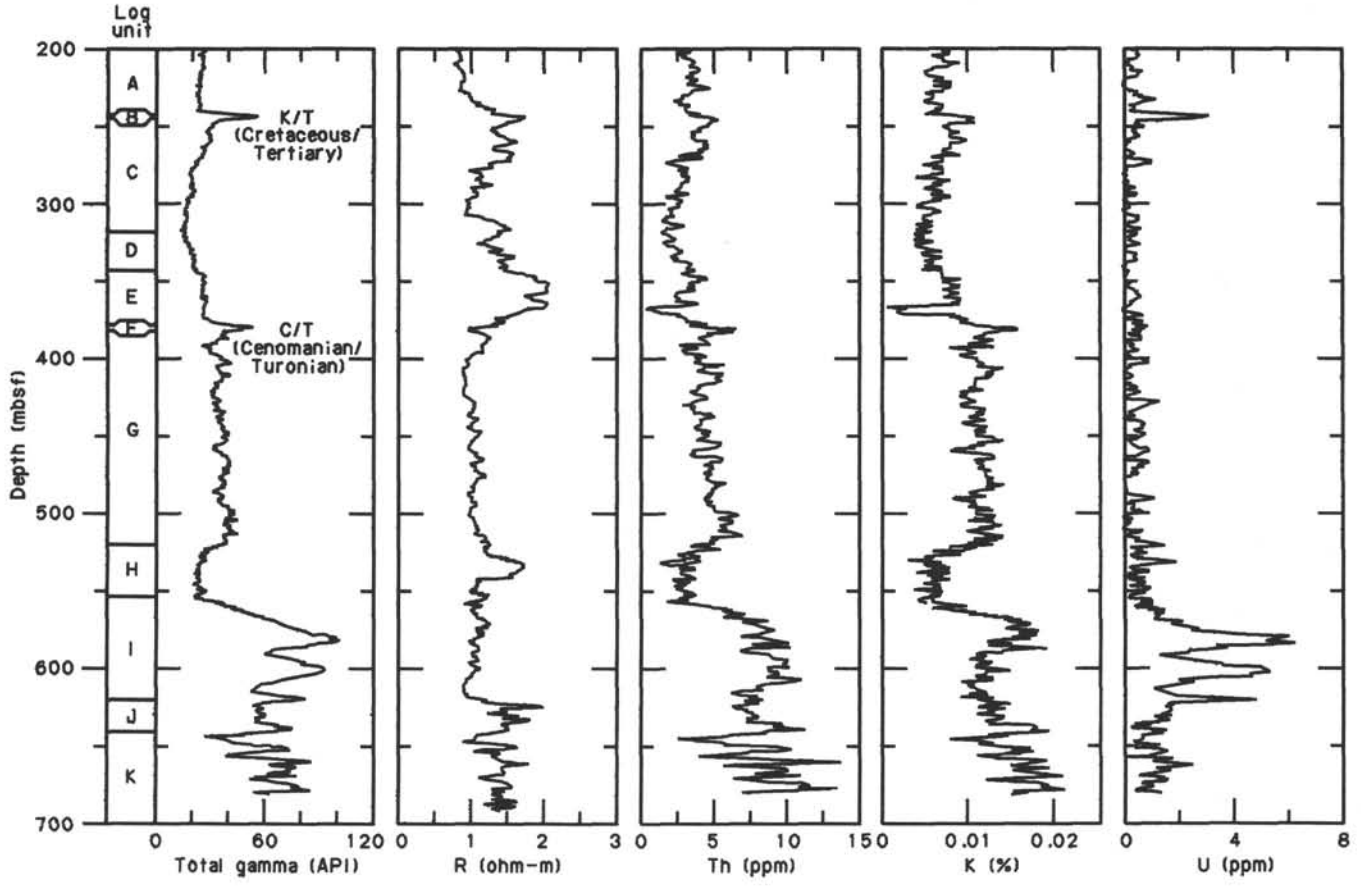

Figure 42. Total gamma-ray activity, electrical-resistivity, and spectral gamma-ray logs (U, K, and Th) from Site 763. Units are discussed in text.

studies on the Exmouth Plateau (e.g., Barber, 1982; Wright and Wheatley, 1979) suggests that it is the Dingo Claystone of early to late Jurassic age. The top of Sequence 2 is often an erosional unconformity related to fault-block tilting and exposure.

Sequence 3

This sequence lies between 2.49 (644 mbsf from corrected log picks) and 3.10 s (TWT) and occupies a northward-thinning wedge considerably thicker at Site 763 than at Site 762. This sequence has similar seismic characteristics to (and correlates with) the black claystones drilled at Site 762, and identified as the Barrow Group equivalent of Berriasian to Valanginian age. As at Site 762, thin limestones at the top of the Barrow Group appear to generate the strong seismic event that marks the top of Sequence 3. Within Sequence 3 we recognize two units. The lowermost of these occurs below 3.96 s (TWT; 1157 mbsf). This reflector is a regional high-amplitude event conformable locally with the lower boundary of Sequence 3, and is identified from industry log analysis as a water-charged sand. The upper unit is only 20 ms thick at Site 763, but increases to over 100 ms thick 6 km farther to the east. Within this package reflectors downlap to the west and toplap against the upper boundary. Between

these units from 2.51 to 2.96 s reflectors are of low amplitude and are conformable, continuous, and subhorizontal.

Sequence 4

This sequence occurs from 2.405 to 2.49 s (TWT), or 563–644 mbsf. It is conformable with Sequence 3 at Site 763 but appears to onlap Sequence 3 further toward the southeast. Correlation with Site 763 drilling results indicates that Sequence 4 consists of the Muderong Shale equivalent sediments of Aptian age. Its upper boundary is a velocity decrease from chalk downward into mudstone.

Sequence 5

This sequence is much thicker at Site 763 than at Site 762 and occurs from 2.24 to 2.405 s below sea level (TWT), or 382–563 mbsf. The upper sequence boundary is a prominent erosional unconformity. This unconformity marks a change in seismic style from several high-amplitude parallel reflectors below, each of which are sequence boundaries, to overlying sequences of lower-amplitude, less-continuous reflectors. This transition corresponds to the Turonian/Cenomanian boundary and may also mark the transition to a deep-water marine depositional environment with reduced clastic input. Sequence 5 at Site 763 corresponds to the Gearle Siltstone equivalent strata of Cenomanian to Albian age, characterized by a prominent decrease in velocity and a local peak in the gamma-ray content at the top.

Sequence 6

The upper and lower boundaries of this sequence occur at 2.09 and 2.24 s (TWT), or 248–382 mbsf. The top of the sequence is an erosional unconformity and corresponds to the Cretaceous/Tertiary boundary. Reflectors at the base of the sequence onlap the underlying Cenomanian/Turonian sequence boundary. The age of Sequence 6 is thus Maestrichtian to Turonian and includes the Toolonga Calcilutite equivalent.

Sequence 7

Above the Cretaceous/Tertiary boundary the sequence is dissimilar to that encountered at Site 762. Sequences 7, 8, and 9 identified at Site 762 are combined into Sequence 7 at Site 763. Extensive onlap of Sequence 7 onto the Cretaceous/Tertiary boundary results in the Paleocene and much of the Eocene being absent at Site 763. The top of Sequence 7 occurs at 2.005 s (TWT) and the base at 2.09 s, corresponding to 152–248 mbsf.

Sequence 8

This sequence can be differentiated from those below by relatively low-amplitude internal reflectors that display high continuity and have a high frequency content. This change in reflector character correlates well with a lithological change at Site 763 from green chalk/ooze with clay to overlying white foraminifer-nannofossil ooze. Sequence boundaries occur at 1.840 and 2.005 s (TWT), or 0–142 mbsf. The upper boundary of Sequence 8 is the seafloor and the lower boundary is Middle Miocene age, and hence Sequence 8 extends from Quaternary to Middle Miocene.

DOWNHOLE MEASUREMENTS

Operations

A single logging run was made with the seismic stratigraphic tool string (LSS, DIT-E, and NGT) between 200 and 678 mbsf. The compressional wave velocity tool (LSS, or long spaced sonic) failed to pick traveltimes downhole. This discussion will be limited to the results of the spectral gamma-ray and electrical resistivity logs.

The first of a dozen bridges noted by the drillers during hole conditioning prior to logging halted the drill pipe while attempting to use the sidewall entry sub-assembly (SES) to advance the logging tool string to the bottom of the hole. The decision to log only the upper part of Hole 763C made on the basis of assessment by the rig-floor personnel that both the drill pipe and the logging tools would be in severe danger in the lower portions of the hole due to bridging. An additional consideration was that the well logs from the Vinck-1 well, less than 1 km from Site 763, were now public domain information and as such were available to the Leg 122 scientists. We decided not to run the geochemical tool string in order to save time for logging Site 764, the last site of Leg 122.

Lithology

For purposes of the present discussion we have placed the data into log units lettered A to K from the top to the bottom of the logged interval. These divisions correspond to changes noted in the lithostratigraphic description (see "Lithostratigraphy," this chapter). No attempt has been made to group the units into any sort of hierarchical order (unit, subunit, etc.). Log Units A through K are identified on a plot of natural gamma-ray intensity and electrical resistivity in Figure 42. The divisions include two thin zones of anomalous behavior associated with major stratigraphic boundaries (log Unit B, the Cretaceous/Tertiary boundary; log Unit F, the Cenomanian/Turonian boundary) and nine zones identified by the uniformity of their log characteristics or by the uniformity of trends seen in these values.

Log Unit A, extending from the top of the logged interval to 241.5 mbsf, is characterized by pelagic oozes and chalks; it exhibits very low gamma-ray activity (25–30 API) and low electrical resistivity (0.75–1.00 ohm-m). Electrical resistivity increases at the base of log Unit A (230 mbsf) and trends into a broad maximum in resistivity (up to 1.75 ohm-m) that extends to almost 270 mbsf. A similar resistivity maximum zone (up to 2.1 ohm-m) occurs between 308 mbsf and 396 mbsf. These resistivity maxima and the minimum between them correspond to changes seen in porosity measurements of physical-property samples measured from Site 763 cores. Higher porosities translate directly into decreased electrical resistivity in sediments of relatively uniform composition. The changes in porosity are probably the result of subtle changes in the microfabrics of the sediment due to changing ratios of clay to carbonate constituents as well as a change in the nature of the calcitic component.

The Cretaceous/Tertiary boundary is characterized, as at other Leg 122 sites, by a local maximum in gamma-ray flux (55 API). In Hole 763C it is represented by a 3.8-m-thick zone of particularly abundant uraniferous materials as seen in the spectral gamma-ray log presentation in Figure 42. The increased gamma-ray activity is probably the result of a concentration of clay at the boundary, but as none of the interval seen in the logs was recovered during coring its precise nature is not known.

From 245.3 to 378.5 mbsf, the nannofossil chalks seen in the core can be broken into three distinct units based on the trends in the gamma-ray log. From the top of this interval to 317.5 mbsf, log Unit C is defined by a steadily decreasing gamma-ray count log (35–14 API). This decrease appears to be the result of a decreasing amount of clay in the sediments with depth and a corresponding increase in the carbonate content (see "Inorganic Geochemistry," this chapter). Below 317.5 mbsf the trend reverses, with increasing gamma-ray activity (14–22 API, increasing clay content) to the boundary between

Units D and E. Unit E (346.3–378.5 mbsf) is characterized by a stable gamma-ray value (27–28 API).

The Cenomanian/Turonian boundary appears in the logging record as a gamma-ray peak which is designated log Unit F. It is 3.8 m thick and extends from 378.5 to 382.3 mbsf. This unit was poorly sampled (i.e., it is represented by approximately 30 cm of black claystone in Core 122-763C-2R). The relatively high gamma-ray count (50 API) is the result of clay enrichment, although it is worthwhile to note that the composition of the materials are different than those at the Cretaceous/Tertiary boundary. Spectral gamma-ray logs indicate that the Cenomanian/Turonian boundary interval exhibits an enrichment in potassium and thorium whereas the Cretaceous/Tertiary boundary interval was enriched primarily in uranium (Fig. 42).

The interval from 382.3 mbsf to 521.5 mbsf (Unit G) is uniform in its electrical resistivity and gamma-ray properties (1 ohm-m, 30 API). Small-scale changes in the logs appear to reflect the presence of short-term cycles in the sediments, seen in the core as rhythmic color changes. The generally higher level of gamma-ray activity reflects the larger overall percentage of detrital elements in the sediments than were observed in younger sections. At the base of log Unit G (521.5 mbsf) there is a shift in the gamma-ray log to values near 20 API. This shift extends to 556.0 mbsf and defines log Unit H as a relatively clay-poor interval. The peak in electrical resistivity (2.75 ohm-m) covering the upper half of log Unit H corresponds to the first occurrence of limestone- and siderite-cemented claystones in the core.

A major shift in gamma-ray activity occurs below 556.0 mbsf as the log values increase from 20 API to near 100 API at 585 mbsf. Log Unit I extends to 621.5 mbsf, encompassing three peaks in the gamma-ray log. In the core descriptions the intervals of highest gamma-ray activity correspond to finer-grained detrital sediments; the lower gamma-ray intervals to coarser-grained material.

Log Unit J (621.5–640.5 mbsf) is defined by moderate gamma-ray log values (50 API) and relatively high electrical resistivity (1.5 ohm-m). Particular peaks in the resistivity log at 626 and 635 mbsf suggest the clayey limestones recovered in the core. Between the limestones are sandy siltstones which include potassium- and thorium-rich glauconite (Fig. 42).

The final log unit (K) begins at 640.5 mbsf and continues to the bottom of the logged interval. It is characterized by three major sand or silty sand intervals at 644–650 mbsf, 655–658 mbsf, and 669–675 mbsf. Small relative resistivity maxima may indicate the presence of thin marly limestones seen in the recovered core.

SUMMARY AND CONCLUSIONS

Introduction

Site 763 (latitude 20°35.19′S, longitude 112°12.52′E, water depth 1367.5 m; proposed Site EP7V) is located about 84 km south of Site 762 on the western part of central Exmouth Plateau. The site is about 1.2 km east of the Vinck-1 commercial well site. Because of safety considerations, Site 763 was designed to duplicate the upper part of the Vinck-1 well to a maximum total depth (TD) of 1125 mbsf. Hole 763A was continuously cored using the APC to a depth of 194.9 mbsf with 100% recovery. We then set the large reentry cone, entered Hole 763B, washed to 190 mbsf, and continuously cored with the XCB to 653.5 mbsf. At a depth of 590 mbsf we ran an intermediate logging program (570–375 mbsf), to compare precisely the level of stratigraphic boundaries at this site with the Vinck-1 well, as requested by the JOIDES Pollution Prevention and Safety Panel. This was done to ascertain that the boundaries occur at the same level or lower at Site 763 than in Vinck-1.

At 653.5 mbsf, the bottom part of the core barrel was lost in the hole and the hole had to be abandoned. The RCB system was used in Hole 763C, which was washed to a depth of 385 mbsf. A core was taken between 385.0 and 394.5 mbsf to re-core the Cenomanian/Turonian boundary interval. The hole was again washed to 645 mbsf and continuously cored thereafter to the TD of 1036.6 mbsf. The recovery rate of rotary-cored Hole 763C was approximately 83% (332.8 m out of 401.0 m penetrated), a superior result compared to 81% recovery with the XCB at Hole 763B, which penetrated the less-lithified upper two thirds of the section. Coring with a single rotary bit to more than 1000 mbsf posed no problems, and recovery rate was ideal in the lower Cretaceous claystones. Coring at Hole 763C was stopped at 1036.6 mbsf (about 81 m less than the originally planned TD) due to the unpredicted sudden increase in hydrocarbon gas contents (see "Organic Geochemistry," this chapter). Logging with the NGT and Dual Induction-LSS-NGT tools was only possible between 690 and 200 mbsf because we encountered severe bridging and rapidly deteriorating hole conditions due to caving of lower Cretaceous claystones.

The main objectives of Sites 762 and 763 were to provide a transect of sites on the central Exmouth Plateau, where Site 762 is located distally and Site 763 more proximally to the terrigenous source of sediments being shed from the southern hinterland during Triassic through early Cretaceous times. Extensive seismic data in the area shows a thinner Cenozoic, but considerably expanded and hence stratigraphically important early to mid-Cretaceous section at Site 763 compared to that at Site 762. The major objectives of Site 763 were documenting Cretaceous depositional sequences (and dating hiatuses and sequence boundaries) and testing sequence-stratigraphic and eustatic models.

The pre-site information available from the Esso well Vinck-1 was helpful in planning this site, not only for predictions of the expected stratigraphy, but also for predictions of the gas content of various formations as a safeguard against drilling hazards in an area of known substantial gas occurrence.

Stratigraphy, Paleoenvironment, and Sedimentation History

The stratigraphic results of Site 763 and some preliminary paleoenvironmental interpretations are summarized in Figure 2E of the "Summary and Highlights" chapter, this volume (in back pocket). The units have been discussed and interpreted in the "Lithostratigraphy" section (this chapter) and in the "Summary and Conclusions" section, Site 762 chapter (this volume). In the following discussions we highlight some of the stratigraphic findings.

Berriasian to Valanginian Restricted Shelf Margin Prodeltaic Environment (Barrow Formation equivalent, Units VI and VII, 1036.6–622.5 mbsf)

In the Vinck-1 well the Barrow Formation equivalent strata (Berriasian to Valanginian), which overlie the upper Jurassic Dingo Claystone equivalent sediments, are 424 m thick and divided into three informal subunits. At Site 763, we recovered a very similar sequence which belongs to the major "syn-rift" continental margin progradational wedge system, as described from Site 762 (see "Summary and Conclusions," Site 762 chapter, this volume). Site 763 is considerably more proximal to the terrigenous source area (which shed sediments to the west, north, and northwest) than the more distally located Site 762. Therefore, it is not surprising that the Barrow

Formation equivalent is about three times thicker at Site 763 than at Site 762.

In our discussion of the Site 763 lithological units (see "Lithostratigraphy," this chapter) we designated the thin Valanginian units of the upper Barrow equivalent as Subunits VIA and VIB, and the underlying rapidly deposited Berriasian prodelta mudstone facies of the lower Barrow equivalent as Unit VII. The oldest sediments recovered at Site 763 are structureless, homogeneous, very dark gray, silty prodelta claystones (Subunit VIIC) that were rapidly deposited (60 to >100 m/m.y.) on a prodelta slope at a few hundred meters water depth. Higher in the section, the occurrence of siderite beds, siderite concretions and/or sideritized burrows increases, as does the content of glauconite and pyrite (Subunit VIIB). Subunit VIIA is characterized by the alternation of black, silty claystone with a few calcite-cemented sandstone interbeds.

In Sections 122-763C-26R-4 and -29R-4 we recovered smectite (bentonite) layers of middle Berriasian age that may correlate with the bentonite layers of Site 761. Strongly coalified palynomorphs occur in Section 122-763C-37R-CC and might indicate a secondary heating or anoxic event (see "Biostratigraphy," this chapter).

According to foraminiferal faunas, the environment was a restricted (variably oxygen depleted) shelf with water depths of less than a few hundred meters. The water depth increases upsection from Core 122-763C-30R. Well-preserved dinoflagellates might provide better age and paleoenvironmental control after more detailed studies.

The overlying Subunit VIB consists of 17.1 m of well-sorted medium-grained sand which was only recovered in trace amounts, but whose presence is clearly demonstrated by the logging results (Fig. 2E of the "Summary and Highlights" chapter, this volume, in back pocket). This quartz sand may represent a basin-floor fan deposit that documents the major late Berriasian–early Valanginian sea-level lowstand and its underlying sequence boundary (126 Ma). The sand is interbedded with structureless to weakly laminated silty claystone with pyrite nodules, plant debris, and pelecypods, but with little glauconite. No belemnites were found in this interval. Alternatively, the sand may also represent channel fill within the lowstand systems tracts.

The youngest Barrow Group sequence (Subunit VIA) is a black, organic-rich (0.8%–1.0% C_{org}) sandy/silty claystone to clayey siltstone with a few glauconitic limestone interbeds. This subunit may represent a 21-m-thick condensed section that is marked by the abundance of belemnites in its upper part (middle Valanginian according to palynomorphs; Cores 122-763B-48X to -49X). Glauconite, pyrite, shell fragments, belemnites, quartz, and calcareous concretions are abundant in this sequence, which was deposited during a sea-level rise (transgressive systems tracts).

The Hauterivian is represented by a hiatus that marks the post-Hauterivian and pre-Barremian erosional event following the breakup of the western margin of the plateau ("breakup unconformity"). The onset of seafloor spreading in the oldest part of Gascoyne Abyssal Plain was dated at Site 766 as being of latest Valanginian to Hauterivian age (Leg 123 Shipboard Scientific Party, in press).

Early Aptian Black, Silty Claystone (Muderong Shale Equivalent, Unit V, 622.5–570.0 mbsf)

This unit consists of a 52.5-m-thick section of dark to black, organic-rich claystone to clayey sandy siltstone with minor limestone nodules and interbeds. This is a considerably expanded early Aptian transgressive section, if compared with the equivalent Unit V of Site 762 (only 10 m thick). Glauconite pellets are abundant, as are terrigenous grains such as silt- to sand-sized quartz and altered feldspar. Secondary minerals include pyrite, a typical early diagenetic mineral in oxygen-depleted environments, and zeolites (probably clinoptilolite), which commonly occur in carbonaceous mid-Cretaceous claystones. Organic carbon contents range from 0.3% to 1.8%. Thin-shelled ammonites are also present in this unit. The foraminiferal record is poor, but the few gavelinellid and epistominid benthic foraminifers suggest a restricted-marine environment, most probably a poorly aerated, middle to inner(?) shelf environment with strong terrigenous influx. The absence of planktonic foraminifers and the rare occurrence of calcareous nannoplankton may indicate a semienclosed marginal-sea environment, possibly with reduced salinity.

In Section 122-763B-46X-3 we recovered a 5-cm-thick light-colored "waxy" clay layer that appears to be disordered smectite-illite with a sharp basal boundary. This clay might correspond to the smectite layers noted in the lower Cretaceous Subunit IIC of Site 761, where they were thought to be bentonites (altered ash beds).

The claystones show strong signs of compaction, such as horizontally aligned burrows deformed to ellipsoids. Limestone nodules and beds are rare and recrystallized to macrocrystalline calcite or to dolomite and possibly siderite/ankerite(?). Claystones also contain recrystallized carbonate fragments.

Palynomorph flora suggests a possible sea-level lowstand in the earliest Aptian (Core 122-763B-45X), indicated by large terrigenous content, spores, and wood, followed by a normal marine (transgressive? and highstand) period in Core 122-763B-49X. Downhole logs show three gamma-ray (clay) peaks in this unit. The uppermost 4.5 m are upward fining.

Mid-Aptian to Late Cenomanian Hemipelagic Marl Sedimentation (Gearle Siltstone Equivalent, Unit IV, 570.0–385.7 mbsf)

As at Site 762, the first hemipelagic sediments deposited after early Aptian times are upper Aptian–lower Albian, greenish gray, zeolitic nannofossil marlstones (calcareous claystones). They mark the onset of the "juvenile ocean" stage, following the breakup of the central Exmouth Plateau area. According to foraminiferal faunas (see "Biostratigraphy," this chapter), most of this 184.3-m-thick, expanded sequence (equivalent to the Gearle Siltstone on land, and about 10 times thicker than the equivalent section at Site 762) was deposited in an open-marine paleoenvironment at bathyal water depths. Terrigenous supply was reduced, possibly derived from a source dominated by metamorphic rocks. According to foraminiferal faunas, however, most of the Cenomanian section was not developed in a normal pelagic facies.

The hemipelagic nature of the calcareous claystone (marl) is characterized by biogenic contents of <50% (about 20%–40% nannofossils, <15% foraminifers), the presence of quartz and feldspar, mica, heavy minerals, and glauconite (<10%), and a upward decrease of clay content. Bioclasts include *Inoceramus* prisms, other pelecypods, and belemnites. Bioturbation is extensive, with distinct individual trace fossils (*Zoophycos*, *Planolites*, *Teichichnus*, and *Chondrites*) present. Authigenic zeolites are common (10%–15%) in these marlstones, as are hard interbeds of recrystallized carbonate (dolomite or siderite?) that occur in the lower part of the unit (Subunit IVB). Color cycles ($CaCO_3$ = 40% in dark layers, 70% in light layers) occur at a maximum of 4–5 cycles per 1.5-m section, corresponding to about 20–40 k.y./cycle. With the exception of the lowermost two cores of the hole, this unit has the highest content of thermogenic methane (and ethane) experienced at Site 763.

Turonian to Late Campanian Eupelagic Chalk Deposition (Toolonga Calcilutite Equivalent, Unit III, 385.7–247.0 mbsf)

Slow, ongoing subsidence of the Exmouth Plateau during the middle Late Cretaceous and the removal of a sediment-shedding southern source area (in the area of the present Cuvier Abyssal Plain) due to northwest-ward drift of this continental fragment, gradually changed the environment from a hemipelagic setting with considerable terrigenous supply (Unit IV) to an eupelagic, carbonate-dominated milieu in Unit III, the "mature ocean stage" (see carbonate contents and gamma-ray log in Fig. 2E of the "Summary and Highlights" chapter, this volume, in back pocket). Unit III is represented by a 138.7-m-thick sequence of Turonian to upper Campanian light greenish gray nannofossil chalk with foraminifers with alternating color bands or cycles, and abundant bioturbation (including *Zoophycos*-, *Planolites*-, and *Chondrites*-type burrows).

At the base of this unit, we recovered two thin black shale intervals, marking the global "Cenomanian/Turonian Boundary Anoxic Event" and separating upper Cenomanian clayey nannofossil chalk and marl from lower to mid-Turonian nannofossil marl. The contact with the overlying Turonian chalk was not recovered. The zeolitic black claystone is structureless to laminated or bioturbated, contains 9%–15% organic carbon, and was probably deposited during conditions of complete to partial bottom water stagnation.

The $CaCO_3$ content in Unit III gradually increases upsection, coinciding with an upward trend toward lighter colors (i.e., decreasing clay content). As at Site 762, rhythmic alternations between light-colored (85%–90% $CaCO_3$) and darker-colored (70%–75% $CaCO_3$) intervals are common, and correspond to cycles with a duration of 20–60 k.y. A condensed sequence or a hiatus (covering most of the Coniacian to Santonian) marks the boundary between Subunits IIIB and IIIC (353 mbsf). The upper part of the thin (4.5 m) Subunit IIIA shows an upward-coarsening trend with increasing proportions of rounded quartz, glauconite, pyrite, and *Inoceramus* prisms (especially in the upper 25 cm). The major ooze/chalk boundary at Site 763 coincides with the boundary between Units III and II.

Mid-Eocene to Early Miocene Chalk Deposition (Unit II, 247.0–141.7 mbsf)

Approximately 348 m of upper Campanian to middle Eocene sediments recovered at Site 762, including the Cretaceous/Tertiary boundary interval, were eroded at Site 763 as evidenced by middle Eocene white chalks directly overlying upper Campanian pale green chalk at Site 763. The foraminiferal assemblages just above the unconformity contain up to 60% reworked Campanian, Paleocene, and lower Eocene foraminifers. This dramatic 30-m.y. hiatus might either be explained by increased bottom-water circulation or by tectonic uplift of the southern hinterland and its immediate foreland, which caused widespread erosion of pelagic sediments at Site 763 but not at Site 762, and their subsequent deposition in a deeper margin environment, possibly during Paleogene times. This unexpected finding suggests vertical tectonics and/or enhanced bottom current circulation for extended periods during late Cretaceous to Paleogene times.

Deposition of the middle Eocene chalks took place in an open-marine, pelagic environment. The lower part of this unit (Subunit IIB) is composed of white nannofossil ooze that is less indurated than the overlying sequence of white, semi-lithified foraminifer-nannofossil chalk to ooze (Subunit IIA). This inversion of the normal trend might be due to comparatively high contents of H_2S in Subunit IIB which might inhibit the ooze/chalk transformation. Subunit IIB shows only minor contents of finely disseminated pyrite, whereas the underlying Unit III contains abundant pyrite, indicating the presence of Fe^{2+} in the pore waters, necessary for the formation of pyrite in S^{2-}-rich interstitial waters. Below the Unit II/III contact (and increasing in Unit IV), large contents of methane were found, and take the place of the disappearing H_2S (see Fig. 2E of the "Summary and Highlights" chapter, this volume, in back pocket).

Sedimentation rates decrease drastically during the deposition of the carbonate sediments of Unit II, from 10 m/m.y. during middle Eocene to late Oligocene times (Subunit IIB) to about 2 m/m.y. from late Oligocene to middle Miocene times (condensed section, Subunit IIA). The lower sedimentation rates might also have been the reason for the somewhat higher degree of induration of Subunit IIA (i.e., oozes exposed longer at the sediment/seawater interface).

Late Miocene to Quaternary Pelagic Ooze Deposition (Unit I, 147.7–0 mbsf)

Unit I is characterized by a comparatively high (15 m/m.y.) homogeneous rate of sedimentation of eupelagic nannofossil oozes with abundant foraminifers and very small contents of terrigenous quartz and clay minerals. The color grades from white at the base of the unit to gray at its top, correlated with an upward increase of the clay content to about 15%. Nannofossils and foraminifers (increasing in abundance upwards) are well preserved.

Biostratigraphy

Site 763 recovered sediments ranging in age from middle Berriasian to Quaternary. All sediments can be dated using microfossil biostratigraphy and different groups have proven to be effective in the different lithologic units. Calcareous nannofossils and foraminifers have been used to date the Aptian to Quaternary calcareous claystone, chalk, and ooze (Units I–IV) nannofossils and dinoflagellates have correlated the Unit V (Muderong Shale equivalent) to the lower Aptian; dinoflagellates and nannofossils (down to Core 122-763C-21R) give age control to the Unit VI (Barrow Group equivalent), which ranges from Berriasian to Valanginian in age. Radiolarians are present irregularly throughout the section and give secondary age control in several intervals.

Several extensive hiatuses dissecting the lithologic column have been accurately dated. The major ones are middle Miocene, Campanian–middle Eocene, and intra-Hauterivian or Hauterivian-Barremian in age. Possible breaks in the Coniacian and middle Aptian have also been noted. Interesting differences in sedimentation history between Sites 762 and 763 will be investigated in detail during post-cruise studies. Precise biostratigraphic ties have been made to sequence stratigraphy.

The facies recovered at this site illustrate the complete evolution from a marginal, syn-rift environment to an open ocean, post-rift setting. Biostratigraphy has allowed us to establish the timing of this evolution, and microfossil assemblages, especially foraminifers, reflect the changing paleoenvironment.

A nearly complete Cenomanian/Turonian boundary interval and a thick mid-Cretaceous sequence have been recovered and will allow detailed biostratigraphic and chemostratigraphic analysis. Extremely well-preserved Neocomian dinoflagellate assemblages will lead to more detailed taxonomic and biostratigraphic studies of this fossil group.

Magnetostratigraphy

Good results were obtained in the Pliocene-Pleistocene parts of the section at Site 763. Preliminary shipboard work also revealed that the resolution of magnetic chron boundaries was possible in the latest Cretaceous (Chron 33–34). Another minor reversal (probably corresponding to Chron M0) was seen in the mid-Cretaceous part of the section. Detailed studies may also resolve at least some of the M-sequence (Late Jurassic–early Cretaceous) anomaly boundaries.

Organic Geochemistry

Total organic carbon percentages are low in the carbonate units at Site 763, rising somewhat in the lower 465 m of the section (Barrow Group equivalent) where they range from 0.2% to 1.5%. The highest concentrations of organic carbon occur in two thin layers of Cenomanian black shales (9% and 15%). Rock-Eval pyrolysis results suggest that the organic matter type in the clastic dominated section is type III (from land plants).

Hydrogen sulfide was encountered in Units III and IV, but the quantities remained below 10 ppm (in headspace samples). High concentrations of methane (up to 85,000 ppm in headspace samples) were encountered between 300 and 600 mbsf and below 1030 mbsf. With the exception of the interval below 1030 mbsf the gas was quite dry, with methane/ethane ratios remaining between 5000 and 10,000. Below 1030 mbsf, however, not only was the gas concentration high, but higher-molecular-weight gaseous hydrocarbons occurred in significant amounts, which led to the decision to stop drilling at 1036 mbsf.

Inorganic Geochemistry

The chemistry of interstitial waters from Site 763 is characterized by large concentration gradients particularly for Mg^{2+}, SO_4^{2-}, and salinity in the upper 200 m of the sediments. The concentration profile for Ca^{2+} exhibits an unusual subsurface decrease before resuming the expected slight increase with depth. Evidence of early and intermediate silica diagenesis is present in the upper 520 m of Site 763 and resembles that observed at Site 762. The broad alkalinity maximum between 205.5 and 433.4 mbsf corresponds to a zone of H_2S production associated with the oxidation of organic matter by SO_4^{2-}.

Physical Properties

We used compressional-wave velocities, index properties, and thermal-conductivity values to divide the Site 763 sediments into four physical-properties units that correspond approximately to lithostratigraphic subdivisions. From top to bottom, the first unit consists of oozes (seafloor to 223 mbsf), the second of chalk (to the Cenomanian/Turonian boundary at 385 mbsf), the third of calcareous claystone (to about 625 mbsf), and the last of siltstone. A sharp increase in velocity characterizes the ooze-to-chalk transition. Low grain density and a noticeable decrease in wet-bulk density and thermal conductivity possibly associated with the increase in water content and lithological change characterizes the third unit.

Downhole Measurements

The logs show that the entire progression of the logged interval is one of increasing sea level and a reduction in the influx of continentally derived sediments. The sands and limestones of Units VI and VII (Barrow Group equivalent strata) represent several transgressive-regressive cycles of changing shallow-water depositional environments. The overlying clayey limestones and claystones of Unit V (Muderong Shale equivalent) sediments suggest some deepening. The relative clay-rich to clay-poor cycles of the unit between 555 and 625 mbsf record changes in a more distal environment than the underlying sedimentary units.

The log response suggests that a major transgression must have been responsible for the pelagic nature of the overlying unit. It consists of a thick section of almost uniform sedimentation in an environment influenced by detrital sedimentation. Above the Cenomanian/Turonian boundary interval the record shows pelagic sedimentation interrupted only by the Cretaceous/Tertiary boundary event.

Seismic Stratigraphy

Site 763 lies on a faulted anticline where the trends of the Triassic and Jurassic rift faults change from predominantly north (to the north of the site) to predominantly northwest (to the south) (Exon and Willcox, 1978; Barber, 1982). This change implies an extensional component for both the southern transform margin and the western rifted margin of the Exmouth Plateau during Triassic and Jurassic rifting.

Eight seismic sequences were identified at Site 763 using methods outlined in Vail et al. (1977). Prograding clinoforms at the top of Sequence 3 indicate north to northwestward sediment dispersal from a source along the southern margin of the Exmouth Plateau or from the adjacent southern block, onto a northward prograding continental margin/slope (Sangree and Widmier, 1977). Sequences 4 and 5 are considerably expanded at Site 763, indicating closer proximity to a southern clastic source. Upper Cretaceous–Tertiary chalks and oozes thicken northward from Site 763 toward Site 762. Much of this increase in thickness occurs adjacent to the Cretaceous/Tertiary and Turonian/Cenomanian erosional unconformities. Deep-water carbonate deposition began in the distal part of the basin after each erosional event, onlapping the southern margin as subsidence continued. This explains the thicker Upper Cretaceous to Tertiary section at Site 762 and indicates that the southern margin of the Exmouth Plateau remained a topographic high into the Tertiary. Above Sequence 5, sediments were deposited primarily in a pelagic environment.

REFERENCES

Barber, P. M., 1982. Paleotectonic evolution and hydrocarbon genesis of the Central Exmouth Plateau. *APEA J.*, 22:134–44.

Bralower, T. J., 1987. Valanginian to Aptian calcareous nannofossil stratigraphy and correlation with the upper M-sequence magnetic anomalies. *Mar. Micropaleontol.*, 11:293–310.

_____, 1988. Calcareous nannofossil biostratigraphy of the Cenomanian-Turonian boundary interval and the origin and timing of oceanic anoxia. *Paleoceanography*, 3:275–316.

Bralower, T. J., Monechi, S., and Thierstein, H. R., 1989. Calcareous nannofossil zonation of the Jurassic-Cretaceous boundary interval and correlation with the geomagnetic polarity timescale. *Mar. Micropaleontol.*, 14:153–235.

Caron, M., 1985. Cretaceous planktonic foraminifera. *In* Bolli, H. M., Saunders, J. B., and Perch-Nielsen, K. (Eds.), *Planktonic Stratigraphy:* Cambridge (Cambridge Univ. Press), 17–86.

Claypool, G. A., and Kvenvolden, K. A., 1983. Methane and other hydrocarbon gases in marine sediment. *Ann. Rev. Earth Planet. Sci.*, 11:299–327.

Deer, W. A., Howie, R. A., and Zussman, J., 1978. *An Introduction to the Rock-Forming Minerals.* London (Longman).

Emeis, K.-C., and Kvenvolden, K. K., 1986. *Shipboard Organic Geochemistry on JOIDES Resolution.* ODP Tech. Note, 7.

Exon, N. F., and Willcox, J. B., 1978. Geology and petroleum potential of the Exmouth Plateau area off Western Australia. *AAPG Bull.*, 62:40–72.

Garland, G. D., 1979. *Introduction to Geophysics:* Philadelphia (Saunders).

Haq, B. U., Hardenbol, J., and Vail, P. R., 1987. Chronology of fluctuating sea levels since the Triassic. *Science*, 235:1156–1167.

Helby, R., Morgan, R., and Partridge, A. D., 1987. A palynological zonation of the Australian Mesozoic. *Mem. Ass. Australas. Paleontol.*, 4:1–94.

Hunt, J. M., 1979. *Petroleum Geochemistry and Geology:* San Francisco (W. H. Freeman).

Jakubowski, M., 1987. Lower Cretaceous calcareous nannofossil zonation of the North Sea. *Abh. Geol. Bundesanst. Austria,* 39:100–119.

Leg 123 Shipboard Scientific Party, in press. Site 766: *In* Gradstein, F., Ludden, J., et al., *Proc. ODP, Init. Repts.*, 123: College Station, TX (Ocean Drilling Program), 000–000.

Leythaeuser, D., Schaefer, R. G., and Yükler, A., 1982. Role of diffusion in primary migration of hydrocarbons. *AAPG Bull.,* 66: '08–429.

Leythaeuser, D., Schaefer, R. G., and Pooch, H., 1983. Diffusion of light hydrocarbons in subsurface sedimentary rocks. *AAPG Bull.,* 67:889–895.

Martini, E., 1971. Standard Tertiary and Quaternary nannoplankton zonation. *In* Farinacci, A. (Ed.), *Proc. II Planktonic Conf.* (Vol. 2): Rome (Ed. Tecnoscienza), 739–785.

Moullade, M., 1984. Intérêt des petits foraminiferes benthiques "profonds" pour la biostratigraphie et l'analyse des paleoenvironnements oceaniques Mésozoiques. *In* Oertli, H. J. (Ed.), *IId Int. Symp. Benth. Foraminifera,* "Benthos '83," Pau 1983, 429–464.

Perch-Nielsen, K., 1985a. Cenozoic calcareous nannofossils. *In* Bolli, H. M., Saunders, J. B., and Perch-Nielsen, K. (Eds.), *Plankton Stratigraphy:* Cambridge (Cambridge Univ. Press), 427–554.

_____, 1985b. Mesozoic calcareous nannofossils. *In* Bolli, H. M., Saunders, J. B., and Perch-Nielsen, K. (Eds.), *Plankton Stratigraphy:* Cambridge (Cambridge Univ. Press), 329–426.

Powell, T. G., 1978. *An assessment of the hydrocarbon source rock potential of the Canadian Arctic Islands.* Geol. Surv. Canada Paper, 78–12.

Roth, P. H., 1978. Cretaceous nannoplankton biostratigraphy and oceanography of the Northwestern Atlantic Ocean. *In* Benson, W. E., Sheridan, R. E., et al., *Init. Repts. DSDP,* 44: Washington (U.S. Govt. Printing Office), 731–759.

Sanfilippo, A., and Riedel, W. R., 1985, Cretaceous Radiolaria. *In* Bolli, H. M., Saunders, J. B., and Perch-Nielsen, K. (Eds.), *Plankton Stratigraphy:* Cambridge (Cambridge Univ. Press), 573–630.

Sanfilippo, A., Westberg-Smith, M. J., and Riedel, W. R., 1985. Cenozoic radiolaria. *In* Bolli, H. M., Saunders, J. B., and Perch-Nielsen, K. (Eds.), *Plankton Stratigraphy:* Cambridge (Cambridge Univ. Press), 631–712.

Sangree, J. B., and Widmier, J. M., 1977. Seismic interpretation of clastic depositional facies. *In* Payton, C. E. (Ed.), *Seismic Stratigraphy—Applications to Hydrocarbon Exploration.* AAPG Memior, 26:165–184.

Sclater, J. G., Parsons, B., and Jaupart, C., 1981. Oceans and continents: similarities and differences in the mechanisms of heat loss. *J. Geophys. Res.,* 86(B12):11535–11552.

Sissingh, W., 1977. Biostratigraphy of Cretaceous calcareous nannoplankton. *Geol. Mijnbouw,* 56:37–65.

Sydney, C., 1966. *Handbook of Physical Constants.* Geological Society of America Memoir, 97.

Thierstein, H. R., 1976. Mesozoic calcareous nannoplankton biostratigraphy of marine sediments. *Mar. Micropaleontol.,* 1:325–362.

Vail, P. R., Mitchum, R. M., Jr., Todd, R. G., Widmier, J. M., Thompson, S., III, Sangree, J. B., Bubb, J. N., and Hatlelid, W. G., 1977. Seismic stratigraphy and global changes in sea level. *In* Payton, C. E. (Ed.), *Seismic Stratigraphy—Applications to Hydrocarbon Exploration.* AAPG Memoir, 26:49–212.

Wright, A. J., and Wheatley, T. J., 1979. Trapping mechanisms and hydrocarbon potential of the Exmouth Plateau, Western Australia. *APEA J.,* 19:19–29.

Ms 122A-109

NOTE: All core description forms ("barrel sheets") and core photographs have been printed on coated paper and bound as Section 3, near the back of the book, beginning on page 387.